Université de Montréal

Evaluating the Predictive Potential of a Micro-Dissected Tissue Model

Par

Kayla Simeone

Département de Biologie Moléculaire

Faculté de Médicine

Thèse présentée en vue de l'obtention du grade de doctorat en biologie moléculaire,

Option générale

Décembre 2021 du dépôt finale

Université de Montréal

Unité Académique : Département de Biologie Moléculaire, Université de Montréal, CRCHUM,

Faculté de Médicine

Cette thèse intitulée

Evaluating the Predictive Potential of Micro-Dissected Tissue Model

Présenté par

Kayla Simeone

Cette thèse a été évalué par un jury composé des personnes suivantes

Richard Bertrand

Président

Anne-Marie Mes-Masson

Directrice de recherche

Fred Saad

Co-Directeur

Gerardo Ferbeyre

Membre du jury

Mark Basik

Examinateur externe (pour une thèse)

Résumé de Thèse

Un défi majeur en oncologie clinique est de caractériser avec précision la réponse des patients aux agents thérapeutiques. Actuellement, il n'existe pas de modèles et de tests fiables capable de reproduire précisément une tumeur primaire dans toute sa complexité. Or, ce paramètre est essentiel pour mettre en œuvre une stratégie de médecine personnalisée capable d'identifier le régime de traitement le plus approprié pour un patient particulier dans un délai cliniquement pertinent. Pour répondre à ce besoin, notre groupe a développé un nouveau modèle 3D *ex vivo* qui repose sur la micro-dissection d'un échantillon de tumeur (MDT) d'un patient et l'utilisation de technologies microfluidiques pour maintenir la viabilité du tissu et le microenvironnement tumoral naturel afin d'évaluer la sensibilité aux traitements dans un délai adapté à la prise de décision clinique. Cette approche permettrait de sélectionner les thérapies les plus efficaces tout en réduisant l'administration de traitements inefficaces associés à des effets secondaires indésirables, ainsi que les coûts de prise en charge des patients.

Des travaux précédemment publiés par notre équipe ont montré que la viabilité des cellules cancéreuses situées dans notre modèle de tumeur *ex vivo* pouvait être caractérisée par microscopie confocale sur l'intégralité du MDT ou par cytométrie de flux sur les MDTs après dissociation enzymatique des cellules. Cependant, ces techniques présentent des limitations en termes de résolution visuelle pour la microscopie confocale et de sensibilité et information spatiale pour la cytométrie de flux. Nous proposons ici d'associer notre modèle 3D de MDTs en microfluidiques à des techniques d'immuno-histopathologie, dans le but d'offrir une évaluation moléculaire, spatiale et quantitative de la réponse de la tumeur au traitement. Pour cela, nous avons optimisé une procédure de lithographie en paraffine de nos systèmes microfluidiques, permettant la production de blocs de micro-étalages micro-réseaux de tissus micro-disséqués (MDTMA). afin de permettre une coloration morphologique du tissu et un marquage de protéines spécifiques pour analyser l'architecture tissulaire, la prolifération et l'apoptose cellulaire au sein des échantillons traités. En outre, nous avons montré que le modèle *ex vivo* est comparable et corrélé au système de modèle de souris

in vivo de référence pour l'essai de chimio-sensibilité. Suite à l'optimisation de ce modèle, nous avons collecté 25 échantillons de tumeurs de patientes atteintes de cancer de l'ovaire, pour réaliser des MDTs et des cultures de cellules primaires afin de comparer les profils transcriptomiques de ces deux modèles avec celui de la tumeur d'origine, et d'analyser les réponses aux traitements et le microenvironnement tumoral. Les données transcriptomiques obtenues par micropuces ARN nous ont permis d'effectuer une analyse bio-informatique des voies de signalisation incluant un groupement hiérarchique non supervisé. Nos résultats montrent que les MDT à chaque point de temps (jour 0, 8 et 15) sont génétiquement similaires à la tumeur primaire par opposition aux cultures cellulaires primaires, et que les principales voies dérégulées sont impliquées dans la réponse cellulaire au stress. Nous avons observé une viabilité élevée des cellules au sein des MDT sur une période de culture de 15 jours. En outre, nous avons déterminé qu'un régime de chimiothérapie (carboplatine et paclitaxel) consistant en une induction thérapeutique de 10 heures suivie d'une période de récupération de 14 heures était idéal pour caractériser la réponse au traitement. Notre analyse de prédiction de la réponse des patients montre que nous avons une corrélation positive élevée d'une efficacité de 95 % entre la réponse *ex vivo* et la réponse clinique pour les patients appariés. En général, nos résultats suggèrent que notre technique fournit un modèle plus sophistiqué et précis pour récapituler la réponse de la tumeur primaire dans un laps de temps cliniquement adapté, et pourrait servir de plateforme pour tester de nouvelles thérapeutiques, et d'outil d'orientation clinique pour la réponse des patients.

Mots-clés : modèle *ex vivo*, microfluidique, réponse clinique du patient, prédiction, chimiothérapie, comparaison des systèmes de modèles, preuve de principe.

Thesis Abstract

A major challenge in clinical oncology is the inability to accurately predict the patients' response to therapeutic agents. Currently, there are no reliable models and assays available that reiterate the immense complexity of a primary tumor. These factors are important to implement a personalized medicine strategy capable of identifying the most suitable treatment regimen for a particular patient in a clinically relevant timeframe. To answer this need, our group has developed a novel *ex vivo* 3D model that relies on the micro-dissection of a patient's tumor specimen and the utilization of microfluidic technologies to monitor drug sensitivity within a time-frame suitable for clinical decision-making. This approach would allow for better selection of effective therapies and limit the administration of ineffective treatments, further improving treatment outcome of patients while reducing cost and drug-induced toxicities.

Previously published work studied that the viability of cancer cells located within the tumor was characterized using two imaging modalities: confocal microscopy and flow cytometry. However, each technique has its own disadvantage, limiting their ability to molecularly characterize the effect of therapeutic agents on cancer cells. Thus, we hypothesize that our 3D *ex vivo* tumor-derived model coupled to a pathology-like tool would allow for a more comprehensive approach to evaluate tumor response to treatment, providing a readout system to closely mirror the patient's response, and evaluating molecular mechanisms involved in response to drugs. To address this hypothesis, we optimized a paraffin-embedding lithography procedure allowing the production of micro-dissected tissue micro-array (MDTMA) block to allow morphological and protein-specific staining to analyze the cellular integrity and tissue architecture of treated samples. In addition, we showed that *ex vivo* model is comparable and correlated to the gold standard *in vivo* mouse model system for chemosensitivity assay. Moreover, we collected, following informed consent, 25 post-surgical OC patient tumor samples, to form micro-dissected tissues (MDTs), and primary cell cultures for micro-array analysis and characterization of the TME and response prediction.

The micro-array data allowed us to perform unsupervised hierarchical clustering and pathway analysis showing that the MDTs at each time-point (day 0, 8 and 15) are genetically similar to the primary tumor as opposed to the primary cell cultures and that main deregulated pathways are involved in cellular response to stress. We observed a high viability of cells within MDTs over a culture period of 15 days. In addition, we determined that a treatment regimen consisting of a 10-hour therapy induction followed by a 14-hour recovery period was ideal for characterizing carboplatin treatment response. Our response prediction analysis of patients shows that we have a high positive correlation of 95% efficiency between *ex vivo* and clinical response for matched patients. In general, our results suggest that our *ex vivo* drug response model provides a more sophisticated model to recapitulate primary tumor response in a clinically suitable timeframe that can be exploited further serving, in part, as a platform to test new therapeutics and as a clinical guidance tool for patient response.

Keywords: *ex vivo* model, microfluidics, patient clinical response, prediction, chemotherapy, model system comparison, proof of principal.

Table of Content

List of Tables

List of Figures

List of Abbreviations

2D	Two-dimensional
3D	Three-dimensional
ADT	Androgen deprivation therapy
ALT	Alternative lengthening of telomeres
AR	Androgen receptor
BRCA1/2	Breast cancer genes 1 or 2
CA-125	Cancer antigen 125
CA9	Carbonic anhydrase 9
C/P	Carboplatin/paclitaxel
CAF	Cancer-associated fibroblast
CC3	Cleaved caspase-3
CCRC	Clear cell renal carcinoma
CIPA	Comité institutionnel de protection des animaux
CRCHUM	Centre de recherche du centre hospitalier de l'Université de Montréal
CRPC	Castrate-resistant prostate cancer
CSRA	Chemotherapy sensitivity and resistance assay
CT	Computed tomography
CTRNet	Canadian Tumor Repository Network
CYP	Cytochrome P450
DC	Dendritic cell
DHT	Dihydrotestosterone
ECM	Extracellular matrix
EMT	Epithelial-mesenchymal transition

EOC	Epithelial ovarian cancer
ER	Estrogen receptor
FBS	Fetal boivine serum
FDA	Food and Drug Administration
FFPE	Formalin-fixed paraffin-embedding
FOV	Field-of-view
FRQS	Fonds de recherche du Québec Santé
GCIC	Gynecological Cancer Intergroup
H&E	Hematoxylin and Eosin
HBOC	Hereditary breast ovarian cancer syndrome
HBSS	Hank's balances salt solution
HER2	Human epidermal growth factor receptor 2
HGS	High-grade serous
HGSC	High-grade serous carcinoma
HGSOC	High-grade serous ovarian cancer
HP	Histopathology
HR	Homologous recombination
IC_{50}	Half-maximal inhibition concentration
ICM	Institut du Cancer de Montréal
IF	Immunofluorescence
IHC	Immunohistochemistry
IMI	Innovation Medicines Initiatives
IP	Intraperitoneal
LGS	Low-grade serous
LH	Luteinizing hormone

MAPK	Mitogen-activated protein kinase
MCM	Minichromosomal maintenance
MDTMA	Micro-dissected tissue micro-array
MDT	Micro-dissected tissue
MeV	Multi-experiment Viewer
MRI	Magnetic resonance imaging
OC	Ovarian cancer
PARP	Poly (ADP-ribose) polymerase
PARPi	Poly (ADP-ribose) polymerase inhibitor
PBS	Phosphate buffered saline
PC	Prostate cancer
PCA	Principal component analysis
PCC	Primary cancer cell
PCNA	Proliferating cell nuclear antigen
PCWG	Prostate cancer working group
PDMS	Poly di-methyl siloxane
PDX	Patient-derived xenograft
PEL	Paraffin-embedding lithography
PI3K	Phosphoinositide 3-kinase
PR	Progesterone receptor
PSA	Prostate-specific antigen
PT	Primary tumor
RECIST	Response Evaluation Criteria in Solid Tumors
ROC	Receiver operating characteristics
SASP	Senescence-associated secretory phenotypes

SEM	Standard error of the mean
TAC	Transcriptome Analysis Console
TMA	Tumor micro-array
TME	Tumor microenvironment
TNF	Tumor necrosis factor
TNM	Tumor, Nodules, Metastatic lesion
TSP-1	Thrombospondin-1
TURP	Transurethral resection of the prostate
UHC	Unsupervised hierarchical clustering
VEGF-A	Vascular endothelial growth factor-A
WHO	World Health Organization

This thesis is dedicated to my family and my loving fiancée for always having my back and pushing me to reach my dreams.

This thesis is also dedicated to my grandparents and late great uncle, Valentino, for they are/were my greatest supporters and motivators. The smiles that extended from one end to another and the stars that sparkled in their eyes when they would express their interest in my academic career gave me the courage to bring this thesis to an end. I am their golden child, but they are my shooting stars.

Love you all so much!

Acknowledgement

I would like to thank my supervisors, Dr Anne-Marie Mes-Masson and Dr Fred Saad, for their support, and encouragement, for without whom this thesis would not be possible. Thank you for giving me a chance and allowing me to evolve in your laboratories. Your immense support has allowed me to grow scientifically, critically, and personally, to become an independent, educated young lady. No words can describe the gratitude I feel for you both for allowing me to complete this chapter in my life. I would also like to thank Benjamin Péant and Euridice Carmona for your support, ideas and advice that have allowed my projects to grow. A big thanks to all my dear colleagues (Adriana, Sylvie, Dina, Maxime, Laudine, Melica, Alex, Kishanda, Amelia, Anne-Marie Demers, Pamela, Hubert, Sophie, Véronique Barrès, Liliane, Zied, Amine, Lise, Manon, Kim, Gabriela, Jennifer, Lateef and Robin) for making this journey easy, joyful and fun. For all we've been through together, I am honoured to think of you all as family. We've made so many memories and inside jokes to last a lifetime. A special thanks to Adriana, Sylvie, Melica, Laudine and Pamela, for whom without their support, great friendship and guidance, life as a PhD student would have been long and overwhelming. Thank you for standing by my side, putting up with me and joking around with me throughout the years. Thank you for being my shoulder to lean on and for motivating me to get through hard times. Lastly, I would like to thank my parents Mary and Sam, my brother, Christopher, my sister-in-law, Jessie, my grandparents, Sonia, Denio and Elvira and my in-laws, Fulvio, Mary, Carlo, Vanessa and Frankie for always believing in me, for supporting me in every way possible and for being there whenever I needed you. Thank you to my amazing fiancée, Joseph, who has always had my back throughout this journey, who has never stopped believing in me and continuously pushes me to succeed and reach my goals and for your patience during hard times and crazy work hours to bring this chapter to an end.

1 INTRODUCTION

Cancer is one of the most lethal diseases worldwide. In Canada, approximately one in two Canadians (45% of men and 43% of women) will develop cancer in their lifetime, and about one in four Canadians (26% of men and 23% of women) diagnosed with cancer will die each year[1]. Cancer is defined as an abnormal proliferation of cells that can originate in almost any tissue within the body[1]. Development of a tumor is a multistep process, in which cells gradually become malignant through a series of genetic alterations that lead to uncontrolled proliferation. As cells acquire successive mutations that advance tumor progression, an outgrowth of clonal selection creates a mixed population of cells characterized by different phenotypic and genotypic features[2,3]. The immense complexity and evolving nature of this disease remains the core challenge in developing potential curative drugs.

The most commonly used systemic treatments targeting the proliferation of cancer cells are cytotoxic drugs, which include various chemotherapy-based agents. However, these drugs will also interrupt the cell cycle of all rapidly growing normal cells, including hematopoietic cells in the bone marrow, hair follicles, and the cells that line the mouth, digestive tract and reproductive system[4]. As a result, patients can experience extremely harsh side effects including fatigue, hair loss, vomiting and anemia. Furthermore, these conventional drugs are not 100% efficient and often result in the development of resistance phenotypes. These phenotypes may in part be explained by the heterogeneity of the tumor, accompanied by clonal selection resulting in an innate resistance mechanism response from diagnosis. In addition, following treatment administration[5] some cancer cells can acquire resistance mechanisms, that can in part, explain why individuals fail to respond to same therapeutic agents over time. To address this complexity there is a need for models that represent patient-specific tumor characteristics in order to predict drug response.

There exists a wide range of research models from *in vitro* 2D monolayer cell cultures to 3D cell aggregate spheroids and organoids as well as *in vivo* models including cell line xenografts and patient-derived xenografts (PDX). More recent innovation include *ex vivo* models based on tissue slices. However,

not all models recreate the phenotypic and genotypic heterogeneity or tumor microenvironment (TME) characteristics seen in tumors to fully mirror treatment efficacy. Organoids, PDX and tissue slice models have gained interest as they have the capacity to maintain patient-specific characteristics predicting response to drugs. The demand for more predictive models is driven in part by a greater understanding of cancer hallmarks and the importance of modulating the TME resulted as well as the creation of an ever-expanding number of new drugs. With this, the cancer therapeutic field is currently evolving from a conventional one-drug-fits-all to a more personalized targeted medicine approach. Ideally, this approach allows for each cancer patient to receive the most appropriate treatment, which would not only deliver superior medical care tailored to the individual while minimizing toxicities but would also directly impact health economics and patient quality of life.

This thesis is centred on developing an *ex vivo* model to monitor therapeutic response. It is based on published data of our novel tumor-derived model[6], which utilizes microfluidic technologies, and several improvements were applied, such as modifications in the microfluidic culture platform, the read-out system and the treatment strategies to better represent patient-specific clinical responses to chemotherapeutics. Clinically, there is an uncertainty in patient-specific response to drugs resulting in random selection of potentially effective therapeutic agents. The validation of this model system might help dictate personalized treatment regimen according to patient-specific tumor characteristics. It might also provide insight on drug efficacy in patient model during pre-clinical drug development setting and lastly aid answering biological questions including drug resistance mechanisms. The practicality and adaptability of this *ex vivo* model system for different solid tumors is described here through the use of distinct cancers: ovarian cancer (OC) and prostate cancer (PC).

1.1 Cancer Biology

1.1.1 Tumorigenesis and Hallmarks of Cancer

1.1.1.1 Tumor Development

The abnormal proliferation of cells that give rise to neoplastic disease can occur in different organs of the body, each of which have inherent characteristics that dictate the cancers type, aggressivity, response rate and metastatic potential[3]. Cancer development is a multistep process, largely initiated when a single cell undergoes permanent genetic change that is passed on to the progenitor cells upon division. This first mutation renders the cells susceptible to accumulating more genetic modifications that selectively increase the capacity to proliferate and disrupt regulatory mechanisms. As the progenitor cells continue to acquire mutations that advance tumor progression, an outgrowth of clonal selection occurs (Figure 1) resulting in the clonal expansion of a sub-population of mutated cancer cells that can dictate the tumor growth rate and drives the acquisition of cancer hallmarks, increasing its malignancy potential[2]. Hence, understanding tumor development and progression is key to identifying regulatory mechanisms that can be targeted to inhibit the function and growth of the cancer cells.

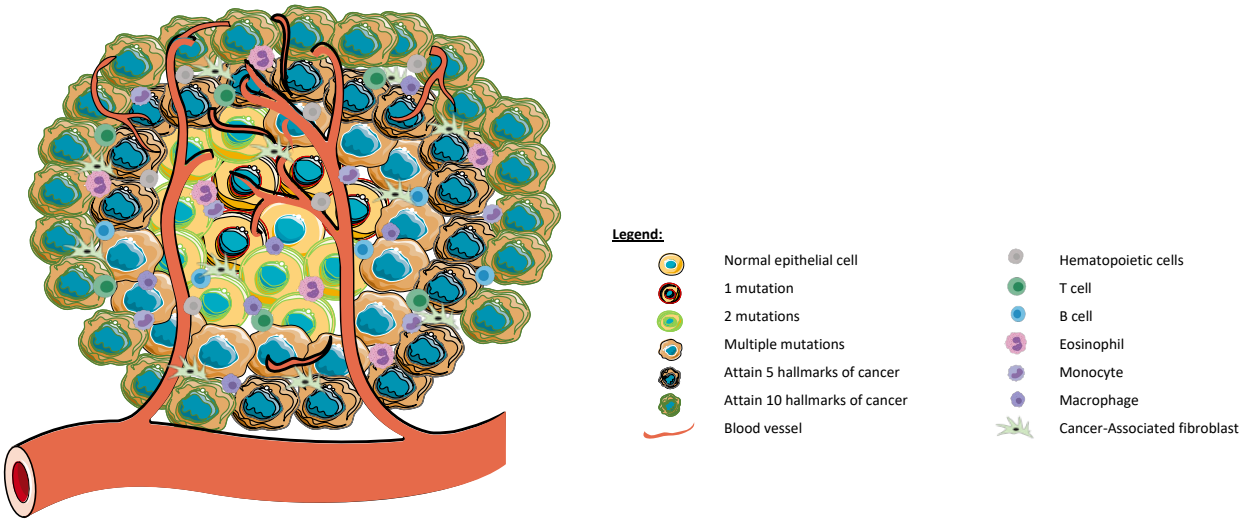

Figure 1. – Characteristics of the tumor and its microenvironment. A legend of the various cell lineages and tumorigenic cells of a variety of mutagenic levels are found within the figure. The combination of all these variables creates a microenvironment that favours cancer cell growth and progression.

The classification of solid tumors is based on the cell and site of origin that the cancer cell arose from. There are two main groups of solid tumors, carcinomas, and sarcomas. Carcinomas are related to a malignancy originating from epithelial cells and account for 90% of all solid tumors. Sarcomas, on the other hand, are less common and originate from connective tissues including muscle, bone, cartilage or fibrous tissue[2]. On rare occasions patients can develop carcinosarcomas, a highly malignant tumor that consists of a mixture of both carcinomas and sarcomas. Often these patients are diagnosed with late-stage disease and face limited therapeutic options.

1.1.1.2 Tumor Characteristics

Formation of tumors and its gain in malignancy depends on the acquisition of key characteristics for adaptation and survival. Over the past decades, studies in cancer development have revealed ten hallmarks of cancer contributing to the clonal expansion theory[7,8]. These includes sustaining proliferative signalling, evading growth suppressors, resisting cell death, enabling replicative immortality, inducing angiogenesis, activating invasion and metastasis, evading immune destruction, reprograming energy metabolism, initiating tumor-promoting inflammation and inducing genomic instability (Figure 2)[7,8]. These distinct and complementary capabilities are the foundation to better understanding cancer cell biology.

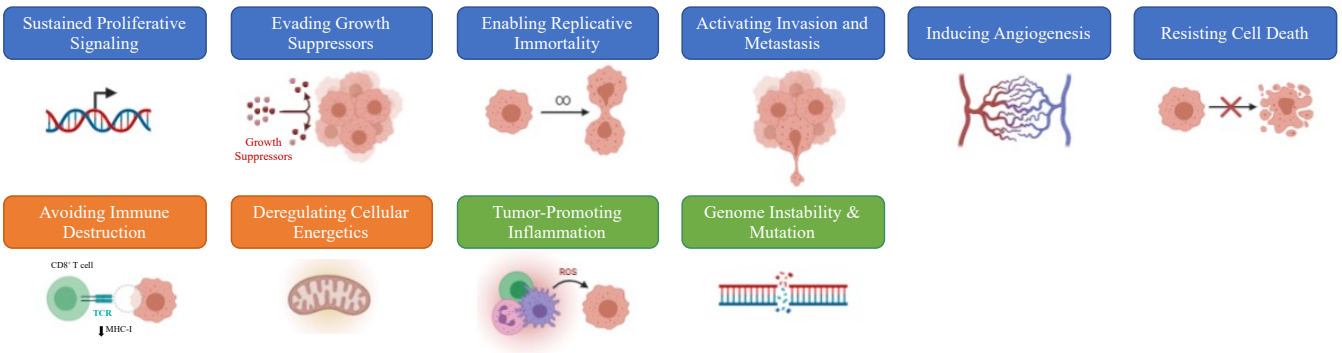

Figure 2. – Hallmarks of cancer. Original biological capabilities acquired in blue, new emerging hallmarks in orange and enablers in green. Image was adapted with permission from "Hallmarks of Cancer: The Next Generation" by Hanahan D and Weinberg RA, 2011, Cell, 144(5): 646-674.

Cancer cells must initially sustain a chronic proliferation by deregulating growth-promoting signals and enabling replicative immortality. To attain this goal, cancer cells produce their own growth factor ligands that control cell cycle entry; increase production of receptor proteins at the cellular surface, allowing a hyper-response to limiting amounts of growth factor ligands; or manipulate surrounding normal cells to supply necessary growth factors[7]. Somatic mutations and defects in feedback mechanisms involved in signalling circuits, such as mitogen-activated protein kinase (MAPK)[9] and phosphoinositide 3-kinase (PI3K)[10,11] pathways, also play a role in cell cycle checkpoints that regulate proliferation[8]. In contrast, normal cells have a limited number of successive cell division cycles dictated by the telomeric ends of each chromosome, which shortens after every replication cycle and eventually activates senescence, cellular arrest, apoptotic and cellular death pathways[12,13]. However, cancer cells express significant levels of telomerase (found in ~85% of tumors), a DNA polymerase that adds telomeric repeated segments to telomeric ends[7], as well as activation of alternative lengthening of telomeres (ALT) (in ~15% of tumors), a telomerase-independent telomere maintenance through DNA homologous recombination (HR) repair pathway[14,15], which counteracts telomere erosion and extends their lifespan.

Cancer cells also circumvent programs that negatively regulate cell proliferation by preventing the activation of growth suppressors and resisting cell arrest mechanisms[7]. In the presence of cellular stress or excessive genomic damage, these programs depend on tumor suppressor genes such as *RB* and *TP53*[16] to govern cell fate decisions such as proliferation, senescence and apoptosis as well as the lack of proliferative contact inhibition antigens. Contact inhibition antigens are present in noncancerous cells such that when in contact with one another a signal is sent to cease proliferation and cell growth[17]. It has been shown that in malignant transformation, cells lose contact antigens such as proteins linked to the Hippo pathway[18] or integral membrane proteins including JAM-A and Claudin-15[19]. A defect in *RB* and *TP53* gatekeeper genes contributes to persistent cell division. By losing cell-cell adhesion properties, cancer cells continue to proliferate and grow regardless of contact with surrounding cells. In addition, cancer cells are able to resist cell death in the presence of cellular stress or therapeutic agents by stimulating anti-apoptotic proteins such as BCL-2 family members[20,21] and suppressing pro-apoptotic triggering proteins such as Bax and Bak[8]. By

bypassing these normal cellular functions, cancer cells maintain their proliferation, advancing tumor development.

Cancer cells are often characterized by their high mutational burden reflecting an underlying genomic instability[7,8]. Normal cells can detect and resolve DNA defects, however cancer cells from a malignant tumor have acquired several mutations compromising the normal monitoring rate of genomic integrity. The alterations amid increasing spontaneous mutations gives rise to genomic instability[22], specifically by destabilizing gene copy numbers and nucleotide sequences. These defects accumulate favoring those that selectively become advantageous for cancerous cells driving tumor evolution and malignancy.

As tumors evolve, their cells gain the ability to reprogram their energy metabolism[7,8]. Due to their increased proliferation, cancer cells have a higher demand for energy and undergo a metabolic switch by up-regulating glycolytic pathways to increase the production of ATP through the mitochondria[23,24]. This is achieved through the activation of oncogenes (such as Ras)[25] and the hypoxia response pathway by upregulating glucose transporters, glycolic enzymes and HIF transcription factors[26]. Some tumors have subpopulations of cancer cells that depend on different energy-generating pathways. This includes glucose-dependent cells that secrete lactate and hypoxic cells that utilize lactate produced by neighbouring cells as a main energy source. These cells function symbiotically to thoroughly fuel tumor growth.

Tumors progress to higher pathological grades by inducing angiogenesis and manifest characteristics to locally invade the tissue and attain distant metastatic potential[7]. As cancer cells aggregate into a solid tumor, they can activate the angiogenic switch by stimulating vascular endothelial growth factor-A (VEGF-A) and inhibiting thrombospondin-1 (TSP-1) signalling proteins, which causes the normal quiescent vasculature to generate new vessels[27]. This phenomenon allows the tumor to gain increased access to nutrients and oxygen as well as evacuate metabolic waste and carbon dioxide[8]. These processes help sustain the growth of neoplastic tumors transforming premalignant and non-invasive lesions into *in situ* carcinomas. At this stage, cells may undergo a multistep invasion and migration process involving epithelial-mesenchymal transition (EMT) that results in the down-regulation of cell adhesion proteins such

as E-cadherin, and up-regulation of cell migration proteins such as N-cadherin[8,28]. Tumor cells can then locally invade the primary organ and migrate to nearby blood and lymphatic vessels, enter the circulatory system by intravasation to reach distant tissues. These circulating tumor cells enter distant tissues through an extravasation process, where they can form a metastatic niche, colonize the tissue, and develop into a macroscopic tumor[7,8,29].

Cancer cells can communicate with the surrounding cells in the TME, creating a microenvironment that benefits tumor progression and evade immune destruction[8]. Cancer-associated fibroblasts (CAFs) have been shown to modulate cancer cell metastatic events through the synthesis and remodeling of the extracellular matrix surrounding the cancer cells. Their implication involves the production of growth factors that influence angiogenesis[8]. Several studies have shown that CAFs originate from various cellular lineages including stromal cells through the process of stromagenesis[30] as well as from conversion of adipocytes[31-33], pericytes[31], and bone marrow-derived mesenchymal stem cells[34]. However, the conversion of adipocytes, pericytes, endothelial cells and bone marrow-derived mesenchymal stem cells[34] into CAFs is not applicable across different tumor types or evidence is sparse. These interactions convert surrounding stromal fibroblasts into cancer-associated fibroblasts (CAFs) that will supply cancer cells with various growth factors. In addition, these CAFs and tumor cells present tumor antigens that are detected by dendritic cells (DCs), which induces the anti-tumor immunity by attracting immune cells such as macrophages, monocytes and lymphocytes to the primary site[8]. However, cancer cells rapidly adapt to their environment to escape immune recognition by expressing tumor-derived factors including IL-6, IL-10 and VEGF to maintain DCs in an immature state or by adopting normal presentation antigens such as PD-L1 and CTLA-4 to suppress T cell activity[35,36]. This capability to evade the immune system supports cancer cell survival.

To conclude, a better understanding of how cancer cells manipulate surrounding neoplastic cells to evade normal cell arrest pathways has led to the important development of inhibitor-based drugs to elucidate cancer response as well as attenuate cancer cell growth. Moreover, strategies to modulate the TME have generated a new era of cancer therapeutics of emerging targeted therapies.

1.1.2 Cancer Therapeutics

1.1.2.1 Surgical Resection

For local tumor ablation, primary treatment for many solid tumors includes surgical resection. This strategy is intended to remove all of tumor content while sparing the unaffected normal tissue. To confirm that the tumor has been completely removed without positive surgical margins, a pathologist analyzes the resected tumor through cryostat procedures and hematoxylin and eosin (H&E) staining. The detection of positive surgical margins through the presence of cancer cells at the edge of the resected tissue reflect incomplete surgical removal. To reduce the presence of positive margins, fluorescence imaging used during *in situ* surgical procedures can be used to better visualize and compare between normal and cancerous tissue[37]. This type of cancer treatment has shown to be potentially curative in early-stage disease, however in late-stage disease it is used to reduce tumor burden[38].

1.1.2.2 Radiotherapy

Radiotherapy is also used as a local tumor ablation therapy that consists of various types of external beam radiation (x-ray) and internal radiation (brachytherapy, radioactive iodine and targeted radionuclide therapy)[39]. This type of therapy is often used in a neoadjuvant setting, prior to surgical excision to reduce the size of the tumor, or after surgical resection to kill residual cancer cells and as palliative treatment to relieve cancer-associated symptoms. Radiotherapy damages the DNA of cells to inhibit cellular division and cell growth. However, this treatment affects cancer cells as well as normal cells and current studies have shown that the TME is also affected by radiotherapy[40].

1.1.2.3 Cancer Therapeutics

Cancer therapeutics has evolved over the last century based on important discoveries and novel understanding of biological and pathological features of cancer. The nature of these drugs can be categorized into two distinct mechanisms of action: chemotherapy and targeted therapies[41-43].

Chemotherapy agents were among the first type of drugs discovered to treat cancers. These drugs are often nonselective and are toxic to all types of rapidly dividing cells, including those of healthy tissues[1]. Consequently, these agents are often associated with severe side effects including hair loss and nausea. Their main mode of action is to prevent cellular replication and growth[43]. Standard chemotherapeutics, including taxane[44] and platinum[45]-based chemotherapies, are among some of the most common chemotherapeutic drugs used to treat various cancers. Taxane drugs are microtubule inhibitors that interfere with normal mitotic and interphase functions. Taxanes block the cell cycle progression through centrosome impairment, induction of abnormal spindles and suppression of spindle microtubule dynamics. This inhibition further triggers cell death by activating the apoptosis pathway[44] (Figure 3A). Alternatively, platinum-based chemotherapies are known as alkylating agents that possess anticancer activity by disrupting DNA function and inducing cell death. They can have three distinct mechanisms that will directly arrest DNA synthesis or transcription: direct interaction with DNA strands preventing them from uncoiling and separating, interaction with DNA bases resulting in DNA fragmentation, or interaction of alkyl groups with nucleotides inducing DNA mispairing[45] (Figure 3B). These drugs can be used to reduce tumor burden in a neoadjuvant (systemic treatment prior to surgical procedures) setting, however, they are widely used in an adjuvant setting (after surgical resection procedure) to eliminate any residual disease.

Among the emerging discoveries of tumor biology, cancer therapeutics is moving towards the use of targeted therapies. These agents are developed to block cellular growth of cancer cells by either influencing cell signaling pathways or blocking their ability to replicate their DNA, taking advantage of cancer cell vulnerabilities that have been created from genetic and epigenetic dysfunction. In addition, their effect on normal cells is less pronounced, resulting in fewer side effects while decreasing tumor burden[43,46]. There exist various targeted therapies that target individual specific proteins that are highly expressed on cancer cells such as tamoxifen[47] and tratuzumab[48] used in breast cancer expressing estrogen/progesterone receptors (ER/PR) (Figure 3C) and HER2+ cells, respectively. In this example, cancer cells that present ER/PR or HER2 depend on hormones to sustain their growth and proliferation and tamoxifen and tratuzumab prevent the interaction between the normal ligand and their receptors to inhibit cell proliferation

and growth. In addition, targeted therapies are also produced to attack proteins that are mutated such as Vemurafenib[49] targeting mutated BRAF V600E kinase in melanoma, which reduces the signalling of MAPK pathway (Figure 3D). In leukemia, BCR-ABL fusion is targeted by Gleevec[50], a tyrosine kinase inhibitor of this chromosomal abnormality. Furthermore, poly (ADP-ribose) polymerase (PARP) inhibitors (PARPi), which include Olaparib, Niraparib and Talazoparib, have recently been approved in ovarian and breast cancer and Olaparib has currently been approved around the world (including Canada) for patients with prostate cancer and cancers having a homologous recombination repair mutation/deficiency. They rely on synthetic lethality mechanism[42,51] to stop the growth of cancer cells (Figure 3E). This is based on targeting cancer cells having a deficiency in a protein of DNA repair mechanism that comes from a gene/protein alteration[52,53] within the tumor cell. These crippled cells are more susceptible to PARPi therapeutics, which inhibits a second protein in DNA repair, such that the combination of both deficiencies are lethal for the cancer cells[54,55]. These various strategies targeting cancer cell vulnerabilities are dependent on a better stratification of patients based on tumor characteristics.

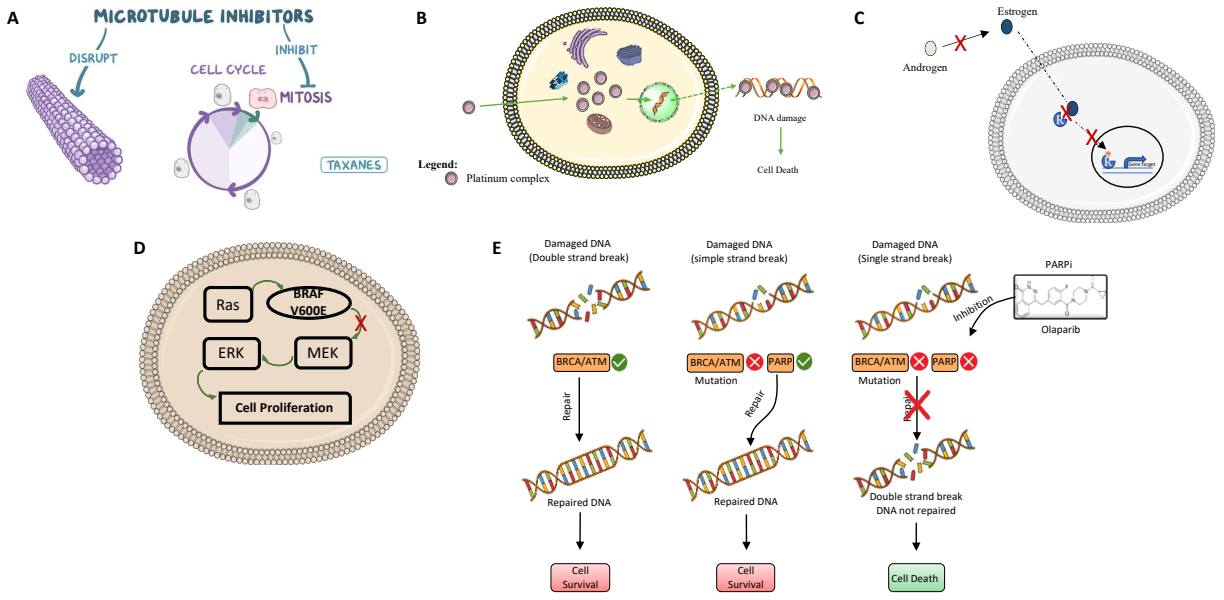

Figure 3. – Mechanism of action of cancer drugs. A. Taxol-based agents are microtubule inhibitors. B. Platinum-based agents induce DNA damage by adding alkyl groups. C. Various hormone therapy mechanism of action. D. Inhibitor of mutated BRAF V600E kinase. E. PARP inhibitors induce synthetic lethality by inhibiting PARP proteins and reducing its capacity to repair single strand DNA breaks. If the cell is deficient in genes involved in repair of double-strand DNA breaks, the prediction is the cell will die.

1.1.2.4 Cell Fate Decisions

The goal when using an anticancer agent is to induce cellular arrest and/or cell death[56]. However, cancer cells respond quickly to selective pressures induced by treatment, which can lead to various therapy-induced cell fates including apoptosis and senescence amongst others, as well as allow resistant populations to emerge[56,57].

When exposed to therapeutic agents, cells often are subject to cellular death by inducing the intrinsic apoptosis pathway[56] (Figure 4A). DNA damage induced by the drug will activate a death signal, activating the pro-apoptotic protein in the BCL-2 family, BH3. Activated BH3 oligomerizes Bax and Bak proteins in the mitochondrial outer membrane, which will permeabilize and release the apoptogenic factor, cytochrome c. This in turn interacts with an adaptor protein, Apaf-1, to further recruit and activate caspase-9 that will cleave the downstream effectors caspase-3 and caspase-7[58]. The activation of these effector proteins results in cell size reduction, cytoplasm condensation, membrane blebbing, chromatin collapse and DNA fragmentation[59].

Exposure to treatment may also trigger a transient or prolonged cellular arrest in cancer cells, characterized by senescence phenotypes[60,61]. DNA damages can also activate p531/p21 and/or $p16^{INK4a}$ to initiate a senescence phenotype (Figure 4B)[62]. Recently, a study from our laboratory showed that PARPi maintenance therapy may lead to therapy-induced senescence in cancer cells, which allows them to bypass the anticancer effects of PARPi and allows a resistant population that is not eliminated by therapy to emerge over time and continue its malignancy course[61]. A better understanding of the factors that drive therapy-induced cell fates can aid in the development of novel therapies or approaches that exploit therapy-induced senescence for enhanced killing of cancer cells. This strategy has been shown through an initial treatment of epithelial ovarian cancer (EOC) cells with PARPi, which induced cellular senescence, followed by treatment with a senolytic, a drug that specifically targets senescent cells, resulting in the elimination of senescent cancer cell[61] and potentially reducing recurrence rates of patients.

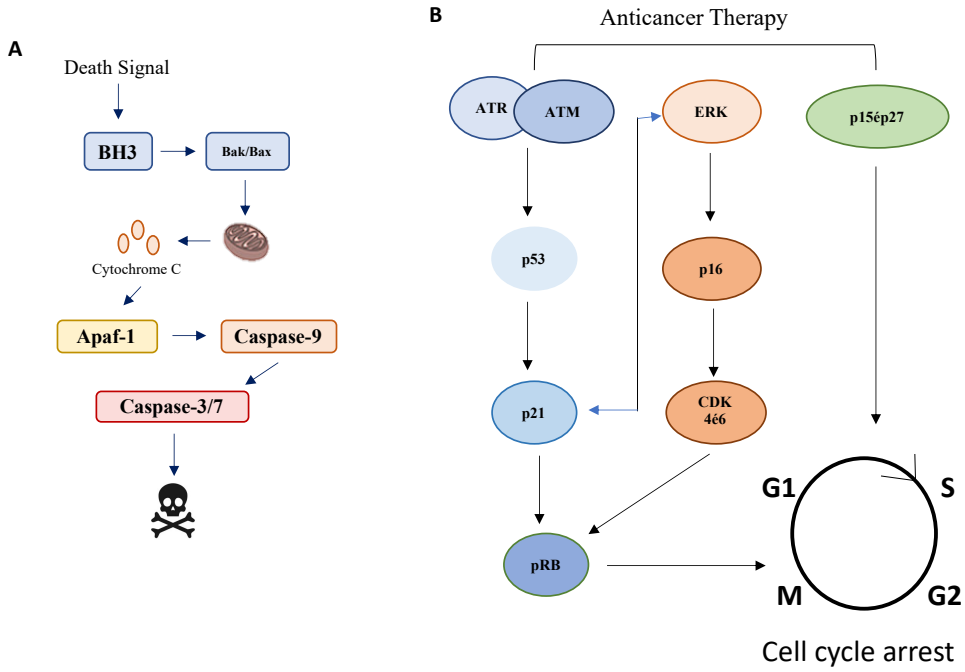

Figure 4. – Therapy-induced cellular apoptosis and senescence. A. Intrinsic apoptosis pathway activated by death signal initiated in response to anticancer agent. B. Cell cycle arrest initiation induced by anticancer therapy bringing forward senescence phenotypes.

1.1.2.5 Patient Stratification for Treatment

Individual cancers display significant variability at a clinical, histopathological and molecular level such that the same cancer type may respond differently to the same treatment[63]. Therefore, risk stratification systems are used to estimate patient outcome as well as facilitate clinical decision making and treatment selection[8]. Patient stratification includes clinical staging, tumor grading, and predictive (therapeutic response) and prognostic (overall outcome) biomarkers.

Staging and grading of tumors estimate the potential spread of the cancer within the body and severity of the disease and is based on a numerical classification to select the treatment plan that best suits the tumors' location and aggressiveness[64,65]. Clinical staging uses imaging modalities and surgical examination to estimate the extent and spread of the cancer. Pathological staging is based on the examination of the resected specimen to characterize the margins (i.e is there disease at the edge of the resected specimen). Together the clinical and pathological information is incorporated in TNM classification of

malignant tumors before or following surgical resection of the tumor. Clinicians assess the size of the tumor (T), number of lymph nodes infected (N) and presence of metastatic lesions (M). On the other hand, the grading is determined by a pathologist through the assessment of cancer cell morphology, histopathology and organization within the tissue[66]. As the numerical value of the clinical staging or grading increases, the patient prognosis and outcome worsen. This system is an essential component to determine the appropriate treatment regimen and patient outcome[67].

At the molecular level, predictive and prognostic biomarkers help stratify patients according to their susceptibility to respond to targeted therapeutic options and the likelihood of disease progression. Different strategies exist for biomarker development depend on the role of the biomarker, including a single biomarker that is directly associated to a therapeutic target or a robust multiple-biomarker signature of target activities using genomic or proteomic analyses[68]. The major bottleneck in biomarker discovery is the extensive work needed to validate its predictive and prognostic potential[69]. Biomarker assessment is quantitative and uses expression levels or signal strength to help define patient categories for stratification. Examples of validated predictive biomarkers include those used for breast cancer therapeutics. The expression levels of biomarker receptor proteins at the cellular surface of cancer cells, such as ER/ PR, and human epidermal growth factor receptor 2 (HER2), help select patients for treatment using targeted therapies, such as tamoxifen and Herceptin, respectively[70]. However, the use of predictive biomarkers is still limited and only available for a small subset of cancer types.

Even current therapeutic recommendations are often based on the one-size-fits-all approach. However, our understanding of the various molecular mechanisms implicated in cancer progression and the global utilization of large cohort data, the development of novel targeted therapies has accelerated. These therapies target a specific population of patients with specific genetic alterations. Ultimately, more than 80% of new treatments in clinical phase studies fail to show clinically significant efficacy during phase 2 trials[69,71]. Many of these trials show a few particularly good responders although the use of the drug in the general population is not warranted. As such, being able to predict these responses would help rescue some

of these drugs. This highlights the need to refine patient stratification for more accurate assessment and to optimize patient selection.

1.1.2.6 How Resistance Impacts Treatment Management?

Resistance to treatment can be categorized as either innate or acquired resistance[5,55,72]. Innate resistance indicates that resistance phenotypes already exist in cancer cells prior to therapy[72]. The genetic makeup of the major tumor population gives rise to innate resistance to drugs through inherent genetic mutations in intrinsic cell growth and cell apoptosis pathways[5]. However, in acquired resistance, cancer cells develop resistance after therapy, reducing the anticancer efficacy of the given drugs[72]. Here, the tumor heterogeneity allows minor subpopulations to be selected over the treatment course or the genomic instability of the cancer creates the selective pressure to permit the emergence of acquired resistance. Drugs can sometimes stimulate the activation of proto-oncogenes that become new driver genes to facilitate tumor survival throughout treatment[8,73]. In addition, drugs can induce mutations or alter target proteins or modify the TME to create a barrier against treatments reducing their efficacy over time[5]. With the lack of predictive and prognostic biomarkers available to help determine patient response to novel therapies, along with the rise in treatment resistance, different approaches to personalized medicine are urgently needed to address these challenges.

1.1.3 Ovarian Cancer

Ovarian cancer is a gynecological cancer that affects approximately 3,100 women yearly with an overall low incidence rate of 2.8% in Canada. However, ovarian cancer has a high mortality rate. It is ranked as the fifth cause of cancer-related deaths and the first cause of death among gynecological malignancies in North American women[1]. The high mortality rate is, in part, due to the lack of early detection and the asymptomatic early stage of the disease, resulting in 70 - 75% of cases that are diagnosed at advanced stages[74]. In addition, genomic predispositions recognizing up to 15% of all EOC[74] include hereditary breast ovarian cancer syndrome (HBOC) and lynch syndromes[75] as well as Peutz-Jegher and rarer disorders, such as Gorlin syndrome[74]. These predispositions increase the likelihood of women developing ovarian cancer

by 30-40%[76,77]. As the disease progresses to an advanced stage, patients often present with symptoms such as bloating, difficulty eating and severe pain in the pelvic and abdominal area with or without the presence of fluid build-up (ascites)[76]. However, these symptoms are also commonly mistaken for other benign health issues, adding to the difficulty in diagnosing this disease.

The ovaries are the female reproductive organs that conduct three important functions: to secrete hormones, to protect the large supply of oocytes (egg cells) and to induce maturation of oocytes for possible fertilization. Epidemiology research has shown that ovarian cancer may be associated with the frequency of accumulated ovulation[78-81]. During ovulation, the ovum or egg is released from the ovary into the fallopian tube, breaching the ovarian surface and is associated with a number of inflammatory factors to initiate repair of the ovarian surface. This repair initiation entails apoptosis of cells as well as proteolysis and vascular remodelling by the replication of cells in an inflammatory environment, which can increase sporadic mutations that fuel the oncogenic process and cumulative risk of inefficient DNA repair[82]. Studies suggest that the origin of this disease is the fallopian tube, where cancer cells migrate to the ovarian surface epithelium to form ovarian carcinomas, although it has not been discounted that the origin, in some cases, is the surface epithelium of the ovary, and in this context cancer cells may migrate to the fallopian tube[83]. The most significant risk factors for ovarian cancer are age, the number of lifetime ovulations, family history, benign gynecological conditions (including endometriosis, polycystic ovary syndrome and pelvic inflammatory disease) and presence of hereditary genetic mutations[74,84,85].

1.1.3.1 Characterization of Ovarian Cancer Subtypes

The most common type of ovarian cancer, constituting 90% of all cases, is EOC[86] with a median age at diagnosis of 63 years. The remaining 10% of ovarian cancer cases develop from germ cells or granulosa theca cells pertaining to the stromal portion of the ovary[76]. Within the EOC group, there are five different subtypes including high-grade serous (HGS)[85-87], low-grade serous (LGS)[85,88], mucinous[85,89], endometrioid[85,90] and clear cell carcinomas[85,91]. Each subtype is distinct[92] and can be differentiated by specific histopathological features as well as the presence of specific biomarkers[93,94] (Table 1, Figure 5).

Among the various subtypes of EOC, HGS is the most common, constituting approximately 70% of all EOC diagnosed cases[74,85,95].

Table 1. Histopathology of different subtypes of epithelial ovarian cancer.

Subtype	Cellular Features	Cytological features	Biomarker	% of diagnosis
High-grade serous carcinoma	Solid masses of cells showing papillary, glandular or cribrifom architecture resembling the surface epithelium	High-grade nuclear atypia with large hyperchromatic and pleomorphic nuclei	TP-53 mutated and WT-1 positive	70-80%
Low-grade serous carcinoma	Solid masses of cells with slit-like fenestrations, often showing papillary, glandular or cribrifom architecture resembling the surface epithelium	High-grade nuclear atypia with large hyperchromatic and pleomorphic nuclei	TP-53 WT and WT-1 positive	2%
Mucinous carcinoma	Cystic spaces lined by gastrointestinal-type mucinous epithelium with stratification and filiform papillae with minimal stromal support	Slightly large nuclei, presence of atypia and stromal invasion and increased mitosis	WT-1 negative, HNF1B positive and ARID1A negative	4%
Endometrioid carcinoma	Glandular with confluent or cribriform pattern that resembles uterine carcinoma, foci of squamous differentiation	Numerous isolated cells, strips or crowded glands, palissading and elongated columnar shaped nuclei	WT-1 negative, PR positive and HNF1B negative	10%
Clear cell carcinoma	Tubulocystic, papillary and solid pattern with hobnai-type cells.	Contains glycogen with large clear cytoplasm	WT-1 negative, PR negative and ARIDIA positive	10-13%

WT: wild-type, WT-1: Wilm's tumor protein, ARID1A: AT-Rich Interaction Domain 1A, PR: progesterone receptor. Information of obtained from the following references [85,87-91].

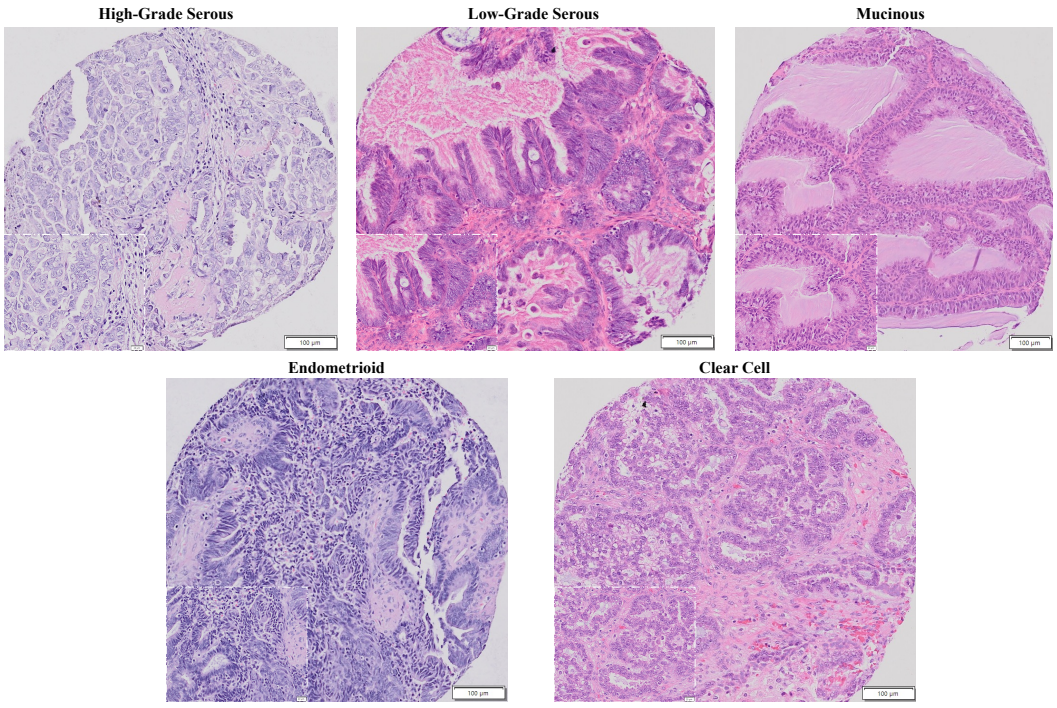

Figure 5. – Histopathology of ovarian cancer. Hematoxylin and Eosin staining of tumor tissue from micro array punches of patient tumors showing distinguished features of the different subtypes of ovarian cancer. Images were taken with permission from the optimization tissue micro-array cohort belonging to the Gynecological Biobank of the CRCHUM.

1.1.3.2 Treatment of Ovarian Cancer

For all subtypes, the standard of care treatments consists of a debulking surgery, which removes the affected pelvic organs, followed by a six-cycle combinatorial platinum and taxane-based chemotherapy regimen[76], which can be done in an adjuvant or neoadjuvant setting. The commonly used platinum-based chemotherapy to treat ovarian cancer patients is carboplatin, usually combined with the taxane, paclitaxel. The ICON-3 clinical trial study compared single carboplatin treatment versus combination carboplatin-paclitaxel treatment and showed that the overall survival of patients receiving the combination treatment was increased by several months with low toxicity levels[96]. However, 70% of EOC patients[74] will have a recurrence after first-line treatment in a median time of 12 to 18 months, resulting in a 5-year overall survival of 45%[76]. Recent clinical studies have suggested that approximately 25% of HGS EOC patients have a deficiency in DNA repair pathway including gene mutation, methylation or deletion of breast cancer genes 1 or 2 (BRCA1/2), rendering them more susceptible to PARPi treatment. Although Olaparib and Niraparib

are both FDA approved drugs for ovarian cancer patients, they have been approved only for maintenance therapy for patients with complete or partial response to first-line platinum-based therapies regardless of BRCA status as well as strongly recommended for patients harbouring a mutation in a DNA repair gene[97,98]. The goal of using this agent as a maintenance therapy is to continue accumulating single-strand DNA breaks resulting in excessive double-strand DNA breaks produced that would overwhelm HR pathway leading to cellular death[99]. Altogether, a better understanding of the biology of ovarian cancer is needed to develop new interventions and new targeted approaches to address the limited number of therapeutic agents that are currently available to treat EOC.

1.1.3.3 Evaluation of Clinical Response

The Gynecological Cancer Intergroup (GCIG) has defined measures for identifying the therapeutic response and disease progression of EOC patients with a cut-off at 3-6 months after the end of the sixth chemotherapy cycle[74]. It relies on the Response Evaluation Criteria in Solid Tumors (RECIST) criteria and the level of the serum marker cancer antigen 125 (CA-125)[100]. The RECIST criteria standardizes response assessments of patients by using imaging modalities such as abdominal-pelvic scans to evaluate tumor burden and metastatic lesion appearance[101]. Therapeutic response is defined as the reduction of tumor size and CA-125 levels (normal range between 0 – 35 U/mL) during and after treatment (see details in Table 2)[100]. Ovarian cancer response is characterized in three categories; platinum-sensitive are patients with a first recurrence or platinum-free interval of more than 6 months, platinum-resistant are patients with a first recurrence at the 3-6 month interval and platinum-refractory are patients with a first recurrence at or prior to the 3 month period[74]. By following these criteria, clinicians can assess disease progression and determine further courses of action for each patient.

Table 2. Clinical response evaluation in ovarian cancers.

Therapeutic Response	Evaluation of lesions by abdomino-pelvic scan	CA-125 (U/mL)
Complete Response (CR)	Disappearance of all target lesions	CA-125 falls to reference range 28 days after end of treatment
Partial Response (PR)	At least 30% decrease in sum of longest diameter of all targeted lesions	50% reduction between pre-treatment CA-125 but never reaches reference range at 28 days after end of treatment
Progressive Disease (PD)	At least 20% increase in longest diameter of targeted lesion using as reference the size of lesion at treatment start point or by appearance of one or more new lesions	Less than 50% reduction between pre-treatment CA-125 at 28 days after end of treatment
Stable Disease (SD)	Neither sufficient shrinkage to qualify for PR nor sufficient increase to qualify for PD	No changes in CA-125

Details were obtained from the following refences [100,101].

1.1.4 Prostate Cancer

PC is the most frequently diagnosed cancer of men, affecting approximately 21,300 men yearly, which accounts for 20.3% of all new cases in Canada. Approximately 1 out of 8 men develop PC in their lifetime. PC is often diagnosed at an early localized stage due to effective screening measures[102], which are generally recommended for men over 50 years of age. Screening consists of a rectal exam and measurement of serum levels of prostate-specific antigen (PSA). PC can be a slow-growing indolent disease and progression often occurs several years after initial diagnosis. Approximately 20% of patients will eventually die of PC resulting in an estimated 4,100 deaths in Canada per year, making it the third leading cause of cancer-related deaths in men[102]. As such, the development of targeted therapies is especially necessary for patients with aggressive PC.

The prostate is an exocrine gland of the male reproductive system that is composed of two distinct cell types: luminal and basal epithelial cells. In general, luminal cells contain a large number of androgen receptors (AR) that are activated upon binding to androgens, which are produced in the testicles in response to endocrine hormones (for details, see Figure 6A, B). The main androgen that binds to AR is testosterone; however, it has a low affinity for AR and is primarily converted to dihydrotestosterone (DHT) by the cytochrome P450 (CYP)-17A1 enzyme, located within the luminal cells. DHT has a strong affinity for AR, enabling their interaction in the cytoplasmic region of luminal cells. This complex translocates to the nucleus to bind to androgen response elements on DNA, further stimulating the translation of proliferative, survival

and secretory proteins such as PSA (Figure 6C). Thus, these luminal cells show a high dependency on androgens to activate AR for maintenance of cellular homeostasis and survival[103]. Consequently, PC is thought to originate in the luminal secretory epithelial cells and androgens are considered as potent mediators to cancer growth and progression[104]. Various studies have shown that the deregulation of genes involved in prostate development and maturation as well as the activation of various oncogenes and abrogation of tumor suppressors are at the core of PC development and progression. Aberrant activation of prostate-specific proteins such as NKX3.1, FOXA1 and AR increase the risk of disease development[104] and are extremely important for all stages of prostate differentiation. In addition, the oncogene *Myc* and the gene fusions of TMPRSS2:ETS have been shown to be elevated throughout PC progression as well as a loss of PTEN and RB expression may promote the castrate-resistant PC (CRPC) form[104]. Other risk factors that lead to PC development include age and family history[103,104].

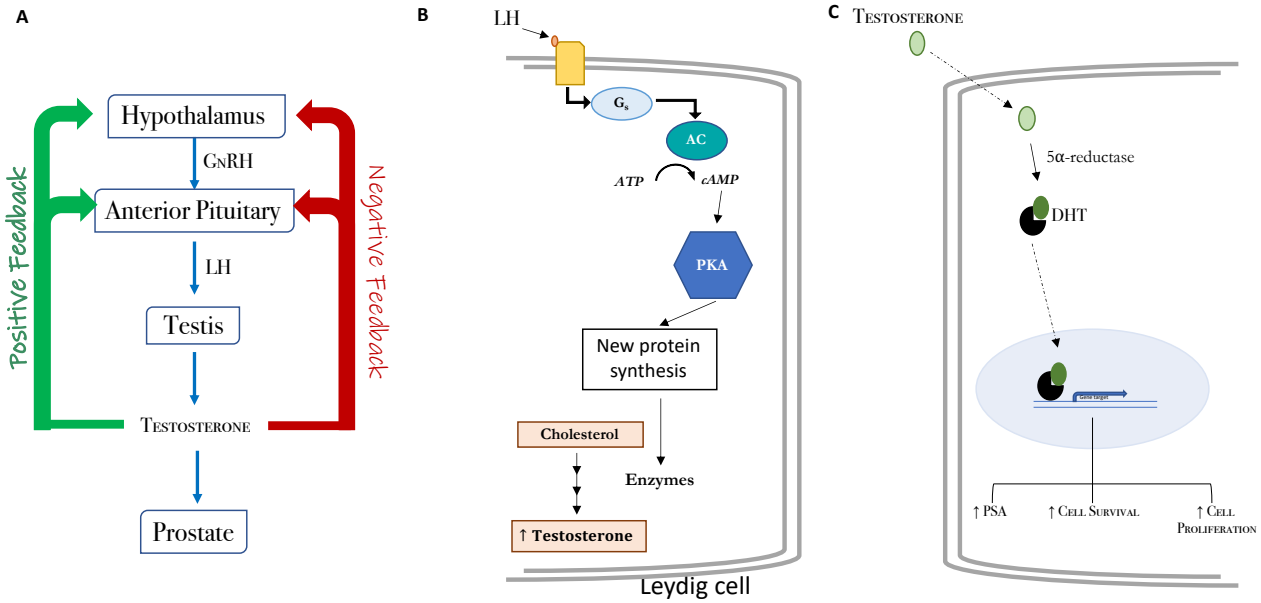

Figure 6. – Endocrine system in the production of testosterone for stimulation of prostate development. A. Endocrine system showing the hormone stimulation process from the CNS, hypothalamus to the anterior pituitary gland and then to the testis B. Testosterone is produced in the testis in response to luteinizing hormone (LH). C. Testosterone enters the luminal cells in the prostate activating androgen receptors to stimulate transcription of genes involved in cell proliferation, survival, and production of prostate specific antigen (PSA).

1.1.4.1 Prostate Cancer Progression and Treatment

The grading system of PC includes the aggressivity of the tumor and is based on the World Health Organization (WHO) classification that takes into account gland formation and differentiation of basal and luminal cells (Table 3). Grading classification gives insight into potential clinical outcomes and risk of progression and helps determine the specific treatment course for the patient[102,105,106].

Table 3. Grading of prostate cancer

WHO Grading	Gleason Score	Description of glands and cells
Group 1	≤ 6	Small, well-formed, and uniform glands
Group 2	3 + 4 = 7	Well-formed glands with large portion of stroma between glands
Group 3	4 + 3 = 7	Poorly formed, fused or cribriform glands with distinctly infiltrative margins
Group 4	8	Poorly formed/fused/cribriform glands with irregular masses of neoplastic glands
Group 5	9 or 10	Lacks gland formation (with or without necrosis) with occasional gland formation

Details are found in the following references [105,106]

Patients are often diagnosed at an early, localized PC stage, and approximately 90% of patients at this stage are cured. However, patients in the 3-5 group grading classification have a higher risk of progression and are usually among the 30-50% of patients who progress. The treatment course for PC patients depends on individual tumor growth patterns (Figure 7). Patients with a higher risk of progression undergo surgical radical prostatectomy, which removes the entire prostate, or radiotherapy. However, the large proportion of intermediate or high-risk patients will progress and eventually receive androgen deprivation therapy (ADT). These are synthetic hormone analogs of the endocrine system that will suppress the production and release of testosterone in the blood circulation, further reducing the fueling agent of prostate cancer cells. However, over time the majority of patients undergoing ADT will eventually develop CRPC, by inducing overexpression of AR, synthesizing de novo androgens or developing mutations and variants of AR to promote an androgen-independent phenotype, thereby enabling AR activation even without androgens. At this stage, patients with non-metastatic PC are treated with an new generation AR targeted therapy such as apalutamide, enzalutamide, and darolutamide. For patients with metastatic lesions, various taxane-based chemotherapies such as docetaxel and cabazitaxel as well as new generation hormonal

therapies such as enzalutamide and abiraterone are given. Enzalutamide inhibits AR activation and prevents its nuclear translocation and interaction with DNA, preventing the transcription of proliferative proteins and indirectly initiating cellular apoptosis. These therapies are used to treat patients at late stages of the disease, in a palliative care setting and have been shown an increase in patient overall survival in several clinical trials[107].

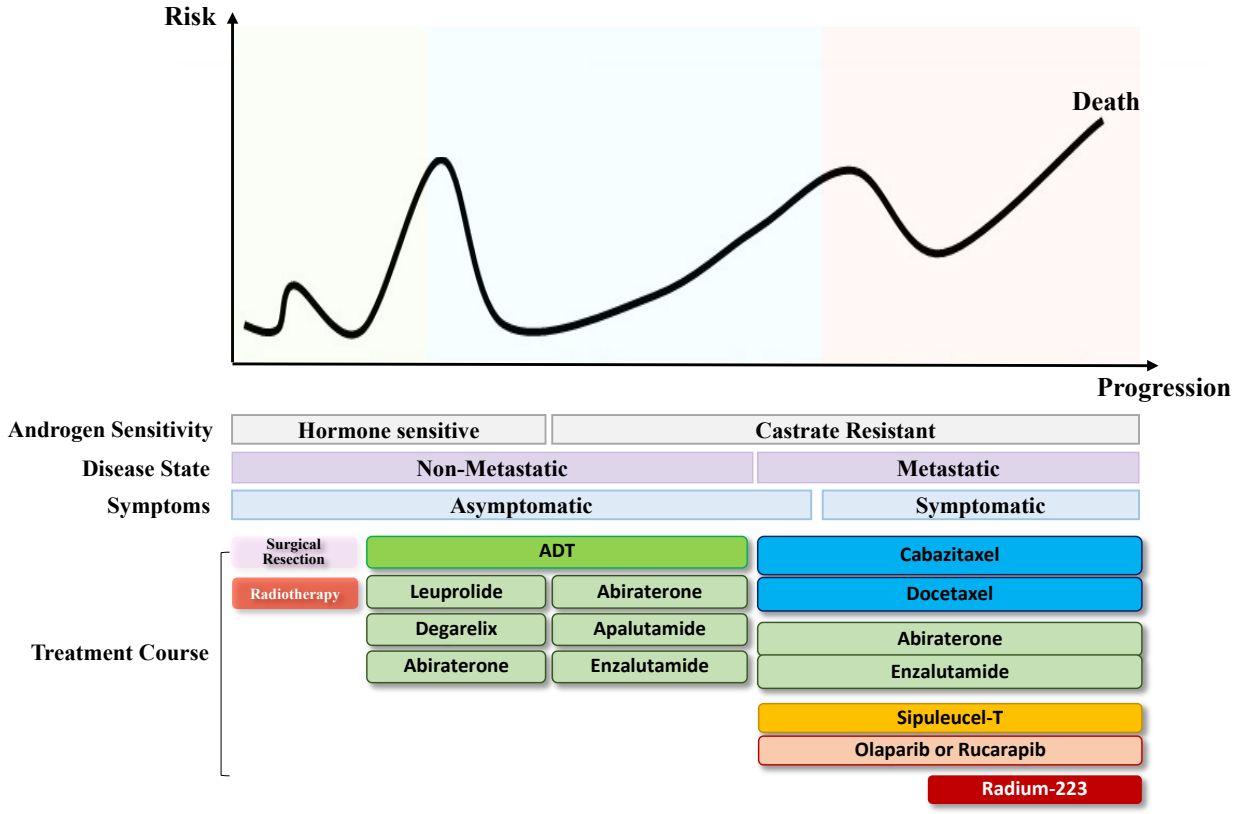

Figure 7. – Progression of intermediate or high-risk prostate cancer. Graph showing an example of the progression of a patient diagnosed with a Gleason score between 7 and 10 associated with the androgen sensitivity, disease state, symptoms, and treatment course available.

1.1.4.2 Novel Potential Treatments for Castrate-Resistant Form of PC

Current therapies for metastatic CRPC are insufficient in maintaining a durable response. The Cancer Genome Atlas have shown that 19% of primary PC tumors harboured alterations in DNA-repair genes[108]. In addition, epigenomic studies have shown an increased mutational burden in CRPC patients with metastatic regression. It was established that 23-30% of metastatic CRPC patients had a genomic aberration

in DNA-repair genes including BRCA2, ATM, MSH2, FANCA, and RAD51B/C, amongst others[108,109]. This led to clinical trials in PC that tested the efficacy and usefulness of the PARPi, Olaparib. One study showed an increase in patient overall survival when treated with Olaparib alone and several ongoing clinical trials have shown the benefits of other PARPi in monotherapy as well as in combination with abiraterone and enzalutamide[110,111]. Currently, several phase 3 clinical trials are underway to determine PARPi efficacy and its potential as a treatment option in PC.

1.1.4.3 Evaluation of Clinical Response and Progression

PC progression is evaluated based on Prostate Cancer Working Group (PCWG) clinical practice guidelines, which takes into consideration the level of serum PSA and the use of imaging modalities such as bone scans, computed tomography (CT), and occasionally magnetic resonance imaging (MRI)[105,106]. PSA levels provide insight into disease progression. Normal serum levels are often between 0-4 ng/mL as PSA is mostly retained in the prostate. However, in the presence of cancer, the basal membrane becomes disrupted and allows the protein to leak into the bloodstream, increasing PSA serum levels. Imaging tool such as MRI, bone and CT scans are more commonly used when the tumor progresses and develops into more aggressive or metastatic forms of the disease[102].

1.2 Cancer Research Models and Novel Technologies

1.2.1 2D and 3D Models for Cancer Research

Cancer research has based fundamental and preclinical findings on classical two-dimensional (2D) and three-dimensional (3D) cell models, which include 2D monolayer cell cultures [112,113], 3D spheroids [114,115], cell line xenografts[116,117], PDX[118,119] and organoids[120,121] (Figure 8). They have been used to evaluate key phenotypic and genotypic characteristics of cancer cells as well as evaluate newly developed therapeutics. However, each model is associated with disadvantages that may limit their use in predicting patient-specific responses to treatment (Table 4).

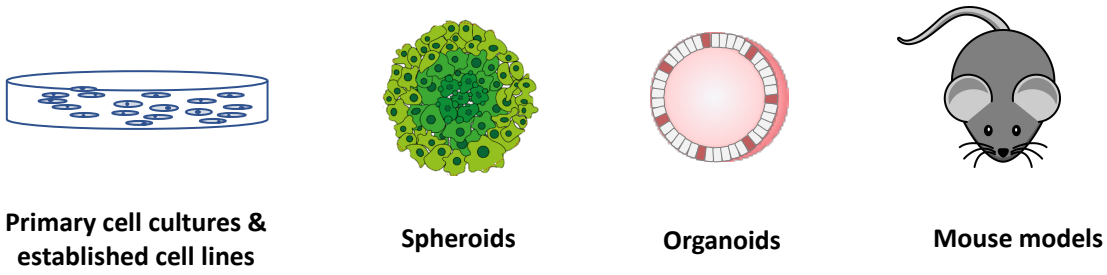

Figure 8. – Model systems for cancer research. All model types are derived from patient tumors. *In vitro* primary cell cultures and established cell lines are cultured on artificial plastic plates. *In vitro* spheroids are characterized by aggregates of cells forming three distinct cell layers. *Ex vivo* organoids are made of several different cell types and highly rich media to recreate the disease state. *In vivo* mouse model recreate the complexity of tumors.

Table 4. Comparison of current cancer models for cancer research.

	2D established cell lines[112,113]	**3D spheroids**[114,115]	**3D cell line xenograft** [116,117]	**Patient-derived xenograft (PDX)** [118,119]	**Organoids**[120,121]
Generation efficiency	30%	60-80%	60-80%	10-70%	70-100%
Tumor tissue source	Surgically resected specimens	Surgically resected specimens	Surgically resected specimens	Surgically resected specimens	Surgically resected specimens
Retention of heterogeneity	No	No	No	Yes	Yes
Generation time	3-12 months	2-14 days	2-5 months	6-10 months	4-12 weeks
Effective for drug discovery screening	Yes	Yes	Yes	Yes	Yes
Immune component	No	No	No	No	Yes
Cost	Low	Low-medium	High	High	Medium
Prediction of clinical response	No	No	No	Yes	Yes

Details can be found in references indicated within the table.

Monolayered cell line cultures, spheroids and cell line xenograft models have proved to be irreplaceable for translational and fundamental research. They are easy to handle, have a limitless growth potential and are homogeneous in culture due to successive passaging and clonal selection to achieve an immortalization stage, thereby representing an ideal model for high-throughput experiments. Over the past century, cell line cultures have been the backbone of targeted drug discoveries as well as the generation of gene expression signatures for patient stratification. In addition, spheroids and cell line xenografts are

routinely used for preclinical pharmacodynamic and pharmacokinetic analyses of novel drugs. For 2D cultures, their lack of heterogeneity representing different cancer clones[122] hampers their ability to accurately predict patient response. Furthermore, the loss of various components of the TME, including immune, stromal and endothelial cell components critical for cancer progression is a major limitation of 2D models to correctly model the effect of therapeutic agents[123,124]. In addition, *in vitro* 2D tumor cell lines grown in an artificial environment may be open to potential irreversible genetic changes, altering their genotypic and phenotypic characteristics[125,126]. In contrast, 3D spheroid models are composed of self-aggregating monolayer cell cultures in which the size of the spheroid may vary. As an advantage, this model represents the spatial tumor heterogeneity incorporating proliferative, quiescent, and necrotic cell layers, allowing for the study of hypoxia-induced mechanisms and chemosensitivity[114,127,128]. However, these 3D models also lack necessary TME components. For 3D cell line xenograft models, the stromal infiltration from the mouse-host also impairs the accurate evaluation of treatment response.

Additional 3D models have been developed over the past decade to circumvent limitations associated with cell line-based models, with emphasis on preserving tumor heterogeneity and some of the original TME. In particular, *in vivo* PDX models involve the implantation of fresh patient tissue in immune-deficient mice. Thus, in addition to retaining intratumor heterogeneity, PDX models maintain histopathology features, gene expression profiles, copy number variants and metastatic behaviour of the original cancer[129,130]. They have shown to be beneficial for putative resistance analysis and biomarker discovery; however, their low throughput potential, high cost and long generation time means that they are not feasible to determine the chemosensitivity of a patient before initiation of the first treatment (Table 4). To palliate some of these weaknesses organoids represent another model system where solid tumors are dissociated and allowed to re-associate in 3D structures. These models have been used to demonstrate the causative potential of various genomic alterations that initiate or promote tumorigenesis, allowing for a better understanding of tumor biology[120]. Organoids have also been shown to be a good predictor of patient response[131,132]. However, cancer organoids remain challenging as a platform for personalized medicine as they can take between 4-12 weeks to produce[121] and the success take rate in culture is highly

variable[121,133,134]. Moreover, all these models remain incapable of predicting patient response to treatment in a clinically relevant timeframe with sufficient accuracy and are not practical for routine application. Therefore, an ideal model would not only preserve the genetic and phenotypic heterogeneity and microenvironment of tumors but would also be suitable for empirical drug testing in a personalized medicine manner within a feasible timeframe.

1.2.2 Development of Organotypic Tissue Slice Cultures for Prediction of Drug Response

The development of functional assays to better stratify patient response to novel therapeutics regimens remains an important clinical challenge. This requires a viable model system that closely resembles *in vivo* characteristics of the tumor and its complex microenvironment. Organotypic tissue slice cultures have been shown to address the many challenges associated with cell based 2D and 3D model systems.

1.2.2.1 Overview of Organotypic Tissue Slice Cultures

Tissue slice models were first introduced in 1951 by Black et al[135] who sought to understand the effect of drugs on the dehydrogenase activity of the tissues in the context of epithelial carcinomas. However, this model was not ideal since these organotypic slice cultures could not be maintained in culture for more than 48 hours[135,136]. Since this first description discovery, refinements in the approach have allowed organotypic slice cultures to be produced without damaging the structure of the tissue and reducing stress-induced apoptosis. Consequently, organotypic tissue slice cultures have been utilised extensively over the past decade[137-140]. This model system is derived from surgically resected tumors through mechanical precision-cut techniques such as manual slicing, tissue slice choppers and vibratome, and can be performed in just a few hours. Interestingly, it has been reported to predict patient response in a clinically relevant manner[141-144]. The relative size reduction of these tumors allows for a more adequate diffusion of oxygen and nutrients to the center of the tissue during culture. These macro-sized tumor slices can be further cultured in a variety of culture platforms. A main advantage to this model is its ability to maintain the original structure, architecture, and cell-matrix interactions of the original tumor specimen[145]. As such,

tissue slice cultures show promise as a predictive model system for determining patient response to drugs in a time frame suitable for clinical decision-making.

1.2.2.2 *Ex Vivo* Tissue Characteristics

Improvements to the tissue slice model have focused on the tissue and culture conditions to promote and replicate cell content found within the natural TME. Further studies have shown that various tissue slicing techniques do not interfere with cellular morphology and tissue function, thereby maintaining tumor viability[145]. To further ensure viability and reduce tissue deterioration, tumor samples must be processed within hours of surgical resection and placed immediately in favourable culture conditions. Overall, *ex vivo* tissues are easy to handle, fast to produce and can be treated in a time-efficient manner that is ideal for personalized medicine.

Traditional culture conditions of organotypic tissue slices involve submersion in media in plastic 48 or 96-well plates, which may induce loss of tissue integrity. To circumvent this drawback and to improve the diffusion of oxygen and nutrients, additional culture platforms have been developed. This includes the incorporation of membrane inserts that promote either complete submersion of the tissue in media or an air-liquid interface that exposes the top tissue slice layer to the air while the bottom layer is supplemented with nutrients[140]. These culture platforms have been combined with rotational movements using orbital shakers. In addition, the type of culture media used is highly dependent on the tissue origin and may require specific nutrients and growth factors to promote or maintain tumor proliferation. Standard media is often combined with antibiotics and either patient serum or fetal boivine serum (FBS)[145,146] to create a favourable environment for cell growth and are essential for maintaining their TME. However, even with these measures in place, hypoxia induction pathways often occur after 7 days of culture[138], thus reducing the potential utility of the macro-sized organotypic tissue slice model systems.

The lack of oxygen supply to the center of the tissue induces hypoxic cores, which leads to cell death and shortens the longevity of the tissue slices. It has been postulated that this was due to the size and diameter of the organotypic tissue slice culture. Thomlinson and Gray's group studied mass transport

limitations on organotypic tissue slice cultures and described a critical diameter (between 250 and 500 μm) range for the tumor slice that should not be exceeded to allow proper nourishment. These results were based on the diffusive properties of metabolites and the general intake of nutrients by the tissue[136] and were later validated by our group in 2016 using mathematical algorithms and numerical simulation techniques[6]. In addition to size restrictions, medium replenishment is another factor that greatly influences the longevity of organotypic tissue slice cultures. The tissue volume controls glucose consumption: the larger the tissue, the faster glucose will be consumed and the more often medium should be refreshed[147]. For macro-sized tissue culture, continuous perfusion of medium is preferable. However, this increases labour time and reduces the number of tissue slices that can be handled at once, limiting the throughput screening capabilities.

1.2.2.3 Recent Developments in Tissue Slice Culture Platforms

Multiple laboratories and companies have created tissue slice culture platforms for personalized medicine approaches to quantitate patient drug response. Two organotypic tissue slice platforms in particular, Mitra Biotech's CANScript™ and PREDECT™, have been promoted to support oncology drug development and provide a read-out system to predict the clinical outcome of patients.

Mitra Biotech CANScript mission is to provide sufficient data on both the responsiveness of tumor types and effective drug combinations, while interrogating mechanisms of resistance. In their 2015 publication, Mitra Biotech revealed a complex supplementation of their culture medium consisting of high levels of insulin, L-glutamine and various growth hormones including epidermal growth factors, hepatocyte growth factors, vascular endothelial growth factors and macrophage colony-stimulating factor, all of which were used to support the TME within their model system[144]. In addition, tissue slices from fresh tumor specimen were cultured in 48-well flat bottom plastic plates that were coated with extracellular matrix proteins[144]. These extra components complicated their procedure, which became more time consuming and introduced phenotypic and genotypic alterations. In addition, the specifications of tissue size were not mentioned, a factor that greatly impacts tissue longevity. Also, their culture platform requires the use of plastic well plates, which can induce loss of tissue integrity and was not addressed by the authors. The lack

of these essential details to recreate their findings demonstrate important limitations in the platform for widespread clinical use.

PREDECT is a collaborative platform funded by the Innovative Medicines Initiatives (IMI), which is a partnership between 21 public-private laboratories of the European Union. The goal of the IMI is to develop advanced and transferable *in vitro* models for breast, prostate and lung cancers. They have a series of 2D and 3D models produced from fresh tumor specimens, including primary cell cultures, organoids, PDX and tumor slice explants, and altogether represent a consortium of various model systems to reconstruct tumor complexities for genomic and proteomic profiles. The IMI platform is focused on preclinical target validation to predict drug efficacy in patient cohorts. Their tumor slice explant model, similar to the Mitra Biotech CANScript, relies on fresh tumor slices produced with a vibratome and culturing in titanium gridded 6-well plastic plate containing culture medium supplemented with high levels of glucose and L-glutamine[148]. The main approach of the IMI model is based on a case-by-case basis. While both CANScript and the IMI models have demonstrated promise with their platforms, both have not yet shown the reliability and reproducibility for routine, standardized use for personalized medicine.

1.2.3 Microfluidic Technology

New advances in biomaterials, microfluidics and tissue engineering have allowed for specialized *ex vivo* culture systems that maintain tumor cells in a controlled environment replicating *in vivo* characteristics. In particular microfluidic devices rely on techniques that facilitates the trapping of individual micrometre- to millimetre-scaled tissue samples under unique culturing conditions, permitting the analysis of biological pathways including therapy-induced cell fates, resistance mechanisms and protein activation induced by specific stimuli[147].

The use of engineered microfluidic devices has gained much interest over the past decade. They have been shown to promote the longevity of *ex vivo* tumors as well as decrease handling time and increase the number of experiments performed[6]. The devices parameters can also be modified to specific research aims, creating a flexible and valuable platform for research[147]. The complexity in the culture system design

is dependent on the need for a perfusion-based device, which requires pumps and highly intricate machinery to streamline the operation and allow a continuous supply of nutrients to the tissue slice cultures. In contrast, non-perfused devices have a simpler system, allowing for culture of smaller tissue volumes[147] making it more amenable for high-throughput analysis.

1.2.3.1 Fabrication of Microfluidic Devices

Microfluidic devices are available in a variety of shapes and sizes, and dependent upon chip specifications tailored to project goals. The type of material used for the fabrication of these devices can be plastic, glass or polymer-based. Polymer is highly recommended as it has pore-like features that permits air passage, which is not permitted with plastic or glass surfaces. Poly di-methyl siloxane (PDMS) is a polymer-based material that is extensively used in the microfluidic field. In addition to its low production costs, PDMS has pore-like features that allow for a continuous supply of oxygen to the tissue specimen and is transparent, which allows for direct observation and analysis of entrapped samples using various imaging modalities[6,147]. Consequently, PDMS in the microfluidic field is frequently used for the design of *ex vivo* culture models.

1.2.3.2 Advantages of Incorporating Microfluidic Technology to Predict Drug Response

Microfluidic technologies in cancer diagnostics have allowed the miniaturization of *ex vivo* culture models and procedures. The reduction in sample size and reagent consumption is especially beneficial when tissue samples are scarce and reagents, such as chemotherapeutics and small molecules, are expensive. Microfluidic devices are designed to incorporate channels and wells, promoting easy changes of the medium and providing homing matrices for the micro-scaled tissue specimen, respectively[147]. In addition, the high surface-to-volume ratio of microfluidic channels allows for heat transfer, enabling quick temperature changes and accurate temperature control. The channels are often long and narrow to enforces a laminar flow for precise spatiotemporal control of fluids. When comparing micro-scale to macro-scale microfluidic devices, the diffusion of solutions in and out of the wells is much faster in micro-scaled devices, increasing the efficiency of chemical reactions and reducing the overall time spent per analysis[147]. Another advantage

of using microfluidic technologies is the ease in manipulation and trapping of tissue specimens within wells without direct physical contact while reducing potential environmental contamination. The detailed fabrication of microfluidic devices broadens their capacity for a constant supply of nutrients while removing waste and controlling access to oxygen[147]. Therefore, microfluidic technology for cancer therapeutic strategies presents an ideal platform to create point-of-care applications while understanding the fundamental aspects of drugs and predicting patient responsiveness.

1.2.4 Micro-Dissected Tissues, a Novel *Ex Vivo* Model System for Personalized Medicine

Microfluidic technology has emerged in the field of cancer therapeutics as a viable option for micro-scale tumor tissue model to increase longevity as well as permit a broader applicability. By combining microfluidic technologies with micro-dissection procedures to circumvent the limitations of macro-sized tissue slice cultures, our group has developed a micro-sized tumor-on-a-chip model system to address issues of tissue longevity and low applicability of current tumor-derived model systems. In previous studies, we have characterized our novel 3D *ex-vivo* tumor-derived micro-dissected tissue (MDT) model[6] to demonstrate its potential applicability to predicting therapeutic response. The clinical challenge that our model may addresses is the need to accurately identify the most suitable treatment regimen for each cancer patient.

1.2.4.1 Device Fabrication to Fit to Our *Ex Vivo* Model System

The device fabrication used for our *ex vivo* model is specifically designed to culture and individually entrap MDTs in a non-perfused setting. This platform relies on the plasma bonding of two layers. The top layer contains the inlet and outlet inputs for the addition and removal of solutions. The bottom layer consists of two fluidic levels (Figure 9A, B) where the top level contains the channels for fluid circulation over the MDTs and the bottom level contains the gravitational traps securing the MDTs and providing a homing matrix that mimic the human physiological environment, allowing for similar confined space with presence of necessary supply of nutrients providing proper culturing and interaction with drugs (Figure 9C). The length of the channel can be modified to increase the total number of traps[6]. The distance between each trap

is critical as it determines the amount of nutrients that each MDT has access to[147]. The main transport mechanism is diffusion driven[6] such that through manual medium changes, the nutrient-rich medium enters the chambers, carrying nutrients to the samples while cellular waste exits out of the wells. This mechanism is key for maintaining viable tumors with high stability. Through theoretical replenishment simulations, the rate of nutrient deprivation within a microfluidic device can be calculated according to physical properties of the device, nutrient uptake until glucose consumption reaches the Michaelis-Menten kinetic constant and knowledge of tissue volume. These simulations have shown that MDTs having a diameter of 300 – 500 µm require a manual medium replenishment every 48 – 72 hours[6,147] to contain a viable level of nutrients in the media.

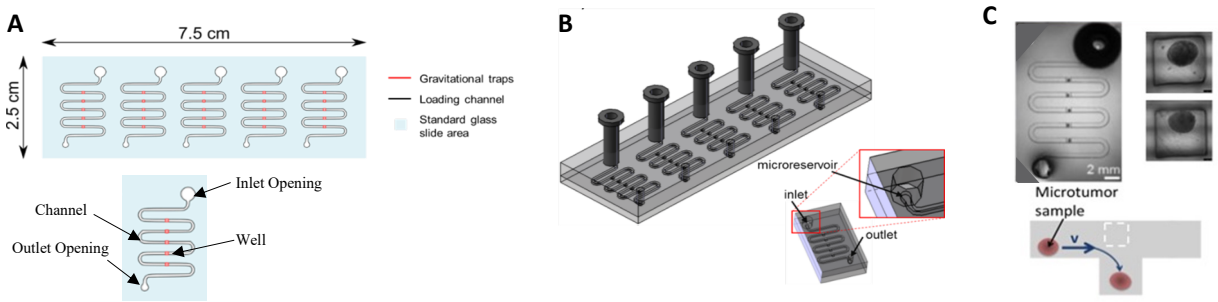

Figure 9. – Microfluidic device. Schematic representation of the 25-well microfluidic device for MDTs. A. showing dimensions and various sections B. overview of design and C. sedimentation process and view of MDTs in their well. Scale bars = 2 mm. Images were taken and modified with permission from "Micro-dissected tumor tissues on chip: an ex vivo method for drug testing and personalized therapy" by Astolfi et al., 2016, Lab on Chip, 16: 312, 25.

1.2.4.2 Micro-Dissection Procedure of Patient Tissues

Our model relies on the micro-dissection of surgically resected patient tumors into sub-microliter sized tissue samples, described as MDTs[6]. The freshly resected tumor was dissected into tissue slices of 350 µm thickness using a McIlwain tissue chopper. Tissue slices were then micro-dissected using a 500 µm biopsy punch to obtain spherically dense tumors of approximately 480 µm in diameter. On average, a 10 mm tumor section produced hundreds of MDTs, which were then trapped individually within microfluidic devices using a laminar force executed by pipetting medium in and out of the outlet region for precise spatiotemporal control of the MDTs[6] (Figure 10).

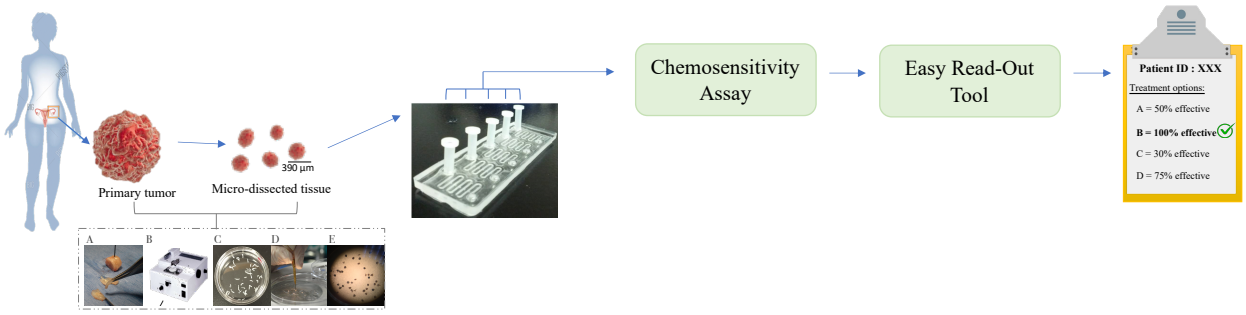

Figure 10. – Schematic overview of the *ex vivo* mode system using MDTs. Tumor resected from consented patients is microdissected using a scalpel, McIllwain tissue chopper and a 500 µm biopsy punch to produce MDTs. The MDTs are loaded into 32-well microfluidic devices for further chemosensitivity assay. An easy read-out system is then used to analyze the response of MDTs to drugs to identify the most effective treatment plan for each patient. Images were modified with permission from "Micro-dissected tumor tissues on chip: an ex vivo method for drug testing and personalized therapy" by Astolfi et al., 2016, Lab on Chip, 16: 312, 25.

The use of microfluidic technologies promotes the maintenance of individually entrapped tumors (Figure 9) that contain their own TME matrix, where the microfluidic chamber mimics the natural human environment, allowing sustained tumor growth. The medium within the microfluidic devices provides supplementation specific to the tumor specimen. In our model system, ovarian cancer specimens were cultured using commercially available OSE medium and PC specimens were cultured with standard RPMI medium, both supplemented with FBS and antibiotics. In comparison to other groups, our medium does not contain additional growth factors or supplements that could potentially alter the epigenetics or phenotype of the tumor specimen.

1.2.5 Analysis Techniques to Measure Treatment Response in Our *Ex Vivo* Model

Astolfi et al[6] demonstrated that MDTs derived from cell line xenograft OC and PC tumors as well as patient specimens had a long-term viability for up to 8 days of culture. In addition, this study showed the possibility of studying the survival of MDTs in presence of drugs. These results were obtained using two imaging modalities, confocal microscopy and flow cytometry. The transparency of PDMS material allows for various direct imaging modalities such as confocal microscopy. In addition, the easy assembly and disassembly of the microfluidic device allows for sample harvest for subsequent flow cytometry techniques.

These two commonly used techniques can assess viability and cellular composition of MDTs in the presence or absence of various therapeutic agents, but also have limitations.

1.2.5.1 Confocal Microscopy

Confocal microscopy is a laser scanning that recognizes fluorescent reagents to produce a 3D image of the specimen. The benefit of using confocal microscopy is the ability to analyze cellular fate in real time by incubating the MDTs with metabolic antibodies detecting live and dead cells to observe the direct effect of drugs. However, the diameter depth of the MDTs is larger than the imaging depth limit (around 100 μm) of the confocal microscopy[149], creating a "black" undefined region in the center of the MDTs that results in an underestimation of the overall cell mortality. Thus, this technique alone is insufficient for a thorough measurement of MDT viability.

1.2.5.2 Flow Cytometry

To complement confocal microscopy, flow cytometry was incorporated for analysis of MDTs cellular content and cancer cell viability. Flow cytometry is often used to detect and measure physical characteristics of cell populations in suspension. The protocol requires the complete digestion of the tumor sample and incubation with fluorescent reagents in order to analyze protein-specific characteristics of single cells[150]. However, dissociation of tissue through enzymatic digestion and mechanical can induce cellular stress, impacting the overall survival of cells. In addition, the dissociation of a tumor into a suspension counteracts the preservation of tissue architecture and morphology, destroying sample integrity and preventing further analysis with the tissue.

1.3 Thesis Hypothesis and Objectives

1.3.1 Challenges

Solid tumors are treated with an initial surgical resection procedure followed by chemotherapeutic-based treatment regimens. Fundamental and translational studies have shown that tumors of the same cancer subtype have molecular and genetic variabilities, which contributes to patient-specific responses and have

revealed differences in drug efficacy as well as identified novel therapeutic targets. This has changed the therapeutic approach from a one-size-fits-all to a more personalized medicine approach. In turn, clinicians are faced with a clinical challenge of deciphering the nuances in different potential therapeutic regimens with no knowledge of patient's susceptibility or response to these novel therapies. Thus, their ability to accurately identify the most suitable treatment plan for patients in a personalized manner is severely hampered.

1.3.2 Hypotheses

The hypothesis of this thesis is that the tumor-derived *ex vivo* MDT model coupled with appropriate analysis tools serve as a surrogate to predict response to treatment.

1.3.3 Research Objectives

There are three main objectives of this thesis:

1. To develop a read-out system that relies on histopathology tools to assess tissue architecture, cellular morphology and biomarker analysis as well as to evaluate drug response. To do so, we aimed to develop a new histological tool that preserves the tissue architecture and cellular morphology of patient tumors. The Micro-Dissected Tissue Micro-Array (MDTMA) was evaluated as to its utility as a read-out system for drug response.
2. To compare the chemosensitivity profile of MDTs derived from cell line xenograft tumors to *in vivo* models. We used five cell line xenograft tumors to produce MDTs to identify the appropriate treatment regimen for the drug of interest. We then compared the chemosensitivity to the same drug between the *in vivo* and *ex vivo* model systems. The correlative ranking of chemosensitivity for five cell lines between their *in vivo* xenograft tumor response versus their *ex vivo* tumor response was evaluated to infer the model's capability to represent the patient response.
3. To demonstrate that MDTs preserve and maintain gene expression profiles and TME to demonstrate their ability to reflect *in vivo* tumor characteristics. For this, we produced MDTs from patient primary tumor samples and performed expression profiling as well as immunofluorescence assays to examine

the epigenetic profile and various cell populations present in the TME, respectively. We also performed matched treatment comparison analysis to determine the predictive potential of MDTs using patient samples.

2 RESULTS

2.1 Chapter 1: Paraffin-Embedding Lithography And Micro-Dissected Tissue Micro-Arrays: Tools For Biological And Pharmacological Analysis Of *Ex Vivo* Solid Tumor

2.1.1 Article 1: Résumé en francais

Titre en français: Lithographie par enrobage de paraffine et micro-étalage de tissus disséqués: Outils d'analyse biologique et pharmacologique des tumeurs solides *ex vivo*

Il existe un besoin urgent et un fort intérêt clinique et pharmaceutique pour le développement d'essais permettant de tester directement des agents thérapeutiques sur des tissus primaires. Les technologies actuelles ne parviennent pas à fournir la longévité des échantillons, le débit et l'intégration avec les tests standard éprouvés en clinique. Nous présentons ici une plateforme micro-histologique microfluidique qui permet la culture *ex vivo* d'un large éventail de tissus micro-disséqués (MDT) de cancers de la prostate et de l'ovaire, suivie d'une fixation et d'une paraffination directement sur la puce, un processus que nous appelons lithographie de paraffine. Le résultat est un micro-étalagesmicro-réseaux de tissus micro-disséqués (MDTMA) de haute densité compatible avec l'histopathologie clinique standard qui peut être utilisé pour analyser *ex vivo* la réponse tumorale et la résistance aux agents thérapeutiques. La morphologie cellulaire et l'architecture tissulaire sont préservées dans les MDT tout au long de la période de culture de 15 jours. Nous démontrons également comment cette méthodologie peut être utilisée pour étudier les voies moléculaires impliquées dans le cancer en réalisant une caractérisation approfondie des mécanismes biologiques et pharmacologiques tels que la translocation nucléaire de p65 via des stimuli TNF, et pour prédire le résultat du traitement en clinique via la réponse des MDT aux thérapies à base de taxane.

2.1.2 Article 1: Original version published in the journal Lab on a Chip

Lab on a Chip. 2019 Jan; 19(3): 693-705. DOI: 10.1039/cBlc00982a.

Paraffin-embedding lithography and micro-dissected tissue micro-arrays: tools for biological and pharmacological analysis of *ex vivo* solid tumors

Simeone K[1,2]*, Guay-Lord R[1,3]*, Lateef AM[1,2], Péant B[1,2], Kendall-Dupont J[1,2], Orimoto AM[1,2], Carmona E[1,2], Provencher D[1,2], Saad F[1,2], Gervais T[1,3†], Mes-Masson A-M[1,2†].

1 Centre de recherche du Centre hospitalier de l'Université de Montréal (CRCHUM)/ Institut du cancer de Montréal,Montreal, Canada, 2 Department of Medicine, Université de Montréal, Montreal, Canada, 3 Polytechnique de Montreal, Université de Montréal, Montreal, Canada.

*These authors contributed equally to the work

Corresponding authors: Anne-Marie Mes-Masson, Department of Medicine, Université de Montréal, CRCHUM-Institut du cancer de Montréal, 900 rue St-Denis, Montreal, Quebec, Canada, H2X 0A9 Tel: (514) 890-8000 ext. 25496 Fax: (514) 412-7591, Email: anne-marie.mes-masson@umontreal.ca & Thomas Gervais, Department of engineering physics, Polytechnique de Montréal, Institut du cancer de Montréal, 2500 Chemin de Polytechnique, Montreal, Quebec, Canada H3T 1J4 Tel: (514) 340-4711 ext. 3752 Fax: (514) 340-3218, Email: thomas.gervais@polymtl.ca.

Keywords: *ex vivo*, micro-dissected tissue, histology, technique, cell-line xenograft, tumors

2.1.2.1 Abstract

There is an urgent need and strong clinical and pharmaceutical interest in developing assays that allow for the direct testing of therapeutic agents on primary tissues. Current technologies fail to provide the required sample longevity, throughput, and integration with standard clinically proven assays to make the approach viable. Here we report a microfluidic micro-histological platform that enables *ex vivo* culture of a large array of prostate and ovarian cancer micro-dissected tissue (MDT) followed by direct on-chip fixation and paraffination, a process we term paraffin-embedding lithography (PEL). The result is a high-density MDT-Micro Array (MDTMA) compatible with standard clinical histopathology that can be used to analyse *ex vivo* tumor response or resistance to therapeutic agents. Cellular morphology and tissue architecture are preserved in MDTs throughout the 15-day culture period. We also demonstrate how this methodology can be used to study molecular pathways involved in cancer by performing in-depth characterization of biological and pharmacological mechanisms such as p65 nuclear translocation via TNF stimuli, and to predict treatment outcome in the clinic via MDT response to taxane-based therapies.

2.1.2.2 Introduction

The inability to adequately predict response to therapeutic agents in the clinic is a major challenge in clinical oncology. This often leads to significant delays in optimal therapeutic decisions and contribute to reduce overall survival rates for many solid tumors[1-3]. This finding supports the broadly shared concern in cancer research that currently used *in vitro,* and *in vivo* models are generally inaccurate recreations of the TME found in primary tumor[4]. For example, cell line-based models systematically represent a selected sub-population[5] of cancer cells, which grow in artificial environments, and do not recapitulate the complexity of variable cell-cell interactions and heterogeneity seen in patient tissues. By contrast, murine xenograft models recapitulate many of these interactions[6]. However, *in vivo* assays are costly and take several months to produce. As such, they cannot enable the prediction of patient-specific response to therapeutic agents in a suitable clinical time frame. There is thus a longstanding need for assays that allow for the direct testing of approved or newly synthesized pharmacological agents on primary tissues[7,8]. Organotypic tissue models

represent a promising path to achieve this goal as they preserve the original architecture and cell-stromal interactions of the primary tissue and can be generated just a few hours after the initial tumor harvest. In particular, chemotherapy sensitivity and resistance assays (CSRAs) on organotypic tissue models could help characterize specific tissue response to various therapies[9,10]. Additionally, these methods can help track treatment effects on a patient's sample over time and identify resistance mechanisms, which, in turn, would inform us on additional molecules to target therapeutically. Black et al were the first to report CSRA on organotypic models of surgically-extracted epithelial carcinoma[11], however their approach failed due to severe anoxia as they were constrained to using large tissue specimen (> 400 μm in depth)[12]. The advent of microfluidics and live microdissection technologies, a few decades later, marked a new era for organotypic models[13-18]. Microfluidic culture platforms offer spatiotemporal control over the biological sample and its microenvironment, while preserving the tissue architecture and viability in the appropriate culture conditions. Furthermore, microfluidics allows high-throughput manipulations through automation and multiplexing as well as the potential for seamless integration with standard instrumentation and assays (e.g.: imaging modalities, immunological assays, etc.). Organotypic approaches using microfluidics have been used extensively to study biological and pharmacological mechanisms in various tissue explants, including liver[19,20], brain[17,18,21], lung[22,23], breast[15,24] and gut[15,25]. However, these methods still rely on fresh tissue slices (~300-400 μm thickness) and on continuous perfusion and complex culture platforms to prevent hypoxia[12] and consequently generally remain low throughput.

To measure treatment effect, CSRAs generally rely on imaging and antibody-based assays[26-28] and assess the viability of various cells of interest. However, most approaches lack the ability to thoroughly evaluate the therapeutic effect at a molecular level, while preserving tissue morphology. Because the assessment of cancer tissue morphology by histopathology (HP) is the current gold standard for diagnosis and treatment selection, many research groups have reported using HP techniques as read-outs to their organotypic CSRAs[15,17,18,20,21,24,29-31]. However, HP assays require that individually cultured samples be removed from the culture platform to be processed, requiring extensive manual labour and resulting in low

throughput, increasing the risk of tissue damage while contributing to high reagent consumption and biomarker variability.

To circumvent the limitations in tissue size and hypoxia of these approaches, we have recently developed an *ex vivo* patient-derived model[28] that relies on the micro-dissection of solid tumor tissue into hundreds of sub-millimeter-sized tissue cores (~380 µm in diameter). These micro-dissected tissues (MDTs) are trapped and cultured in multiplexed microfluidic devices that serve as a homing matrix where they can be exposed to various therapeutic agents and followed by an easy analysis of cancer cell fate. The miniaturization of the tumor specimen circumvents mass transport limitations[28] and anoxia induction[12], which were measured by Grimes et al. to occur in spherical tissue samples with diameters larger than d = 460 ± 40 µm[32]. These measurements and others[33] agree well with previously published theoretical calculations made from simple 1D diffusion-reaction models (d = 450 µm) and from full 3D simulations[28,34] for well-based assays in PDMS chips. Additionally, the large number of MDT samples obtained from a single biopsy or post-surgical specimen allows for the analysis of multiple treatments in a time-efficient manner while also taking into account the heterogeneous nature of the tumor.

To enable the study of both the molecular mechanisms and the microenvironment factors that influence a tumor's ability to resist or respond to various treatments, we herein introduce a microfluidic micro-histological platform that complements confocal microscopy and FACS analyses. We describe high-density array HP analyses enabled by a "Paraffin embedding lithography" (PEL) technique (Figure 1) that adapts and optimizes standard formalin-fixed paraffin-embedding (FFPE) protocols so that all steps can be performed directly on chip. The high-density microfluidic chip integrates a large number of tissue samples that can be analysed at once within the MDT-Micro Array (MDTMA) block. Using this approach, evaluation of tissue architecture as well as cellular viability and proliferation assessment are carried out using standard HP techniques on up to 32 MDTs from a single chip simultaneously. We demonstrate that the resulting MDTMA provides a high-density array of aligned tissue samples similar to tissue micro-arrays (TMAs)[35-37]. This type of CSRA supports the observation of cancer cell behaviour as well as the study of simultaneous *ex vivo*-induced response to various biological and pharmacological agents on the same HP slide, within a

clinically relevant time frame. The proposed approach is simple, robust, and opens a whole new framework for using conventional histopathology techniques to assess treatment responses using minimal amounts of tissue.

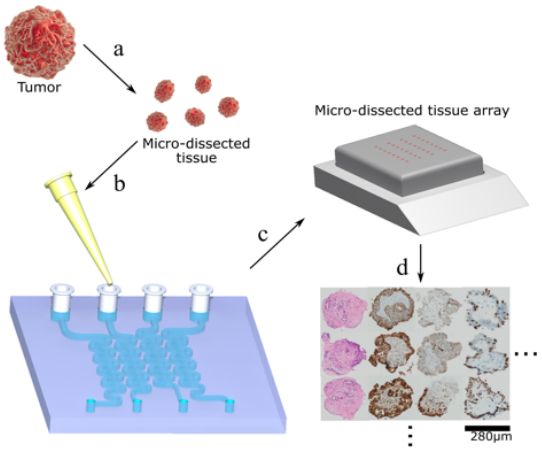

Figure 1: General workflow for the development of a patient-derived *ex vivo* model and micro-dissected tissue micro-array tool. a, Micro-dissection of surgically resected tumor or biopsy specimen into sub-microliter sized samples as micro-dissected tissues (MDTs). **b,** Loading, culturing and treating of MDTs in the microfluidic device. **c,** Paraffin-embedding protocol to form MDT-Micro Arrays (MDTMAs). **d,** Microtome slicing and IHC analyses to evaluate morphology, viability and proliferation of multiple MDTs.

2.1.2.3 Methods

Ovarian and prostate cancer cell lines for xenograft production

Different human carcinoma cell lines derived from metastatic prostate cancer tumors (LNCaP and DU145, ATCC, Manassas, USA) and ovarian cancer ascites (OV2295[38], OV1946[39]) were used to produce mouse xenografts. Cells were grown as monolayers (2D culture) in either RPMI (PC cells) or OSE (EOC cells) media supplemented with 10% FBS, 55 mg/L gentamicin and 0.6 mg/L amphotericin B. After harvesting, cell suspensions were mixed with Matrigel (1,000,000 cells) (BD Biosciences, Franklin Lakes, USA) before subcutaneous injection into the flank of immunodeficient NOD.Cg-*Rag1*^{tm1Mom} *Il2rg*^{tm1Wjl}/SzJ male or female mice (Charles River Development, Burlington, USA). After a growth period varying from 21 to 70 days, depending on the cell line injected, the solid tumors were

harvested once they reached a volume between 800 and 1,500 mm^3. All protocols involving animals were reviewed and approved by the Comité institutionnel de protection des animaux (CIPA) at the CRCHUM.

Design of microfluidic device and fabrication

The microfluidic device is composed of two poly-dimethyl siloxane (PDMS) layers obtained by a replica-moulding process on poly(methyl methacrylate) moulds micro-machined using a CNC mill (Roland MDX-40A, Irvine, California, USA). To form both layers, PDMS and curing agent (Sylgard® 184 silicone elastomer kit, Dow Corning, Midland, USA) were mixed at a ratio of 10:1, degassed and cured for 1 hour at 80°C. The bottom layer contains four fluidic channels of 0.9 x 1.1 mm rectangular cross-sections, each featuring an inlet and outlet of 3.2 mm and 1.5 mm, respectively. The bottom layer consists in a 4 x 8 array of 0.7 mm square cross-section wells that serve as traps for the MDT (see Figure 2a). The top and bottom layers are plasma-bonded and aligned under the microscope to form four enclosed channels, each capable of holding up to eight MDTs.

Finite element simulation methodology

Finite element methods using commercially available COMSOL Multiphysics (COMSOL Inc, Burlington, Maine, USA) were used to simulate the different convection and diffusion processes that take place in the device during medium changes and treatments using a P200 micropipette. The geometry of the model (dimensions shown in Supplementary Table 1) was drawn using the built-in COMSOL drawing tools. Navier-Stokes equation for incompressible flow were used to model the convection, and convection-diffusion equations were used to model the diffusive transport of diluted species in the culture medium. Both these equations are sequentially solved using the built-in time-dependent solver. We simulated a certain volume of fluid at a fixed concentration entering the inlets at a speed determined by the hydraulic resistance of the channels and by the difference of height between the liquid in the inlets and the outlets. We then simulated the passive diffusion process that occurs in the device after rinsing and monitored the concentration of the new fluid in the bottom of the last well of the device. We repeated this process of

sequential convection-diffusion until the medium was completely refreshed in all the wells of the device. By adjusting the volume of liquid used to rinse at each cycle and the diffusion times for each step, we optimized the rinsing process to minimize the required volume of reagent and the time needed to fully refresh the culture conditions in the device.

Monte-Carlo simulations on whole-tissue images

We developed a Monte-Carlo image analysis tool that simulates the microdissection sampling process to study the effects of the sheer number of MDTs sampled on the precision and accuracy of the method. Starting with whole-tissue images of IHC stained primary xenografts, we generated field-of-views (FOVs) of fixed size (250x250 μm) at random locations in the primary xenograft and generated an IHC score for each of these FOVs. By varying the sheer number of FOVs, we followed the effects of the number of MDTs sampled on the standard error of the mean in the resulting distribution of IHC scores and compare it with the average IHC score of the whole tissue. As expected, when sampling a normal distribution, the standard error of the mean varies inversely proportional to the square root of the number of samples ($\frac{1}{\sqrt{x}}$). Using this simulation on various PC and EOC cell line xenografts, we observed a general trend amongst the different xenografts where we see very little gain in precision when sampling more then 15 to 20 MDTs (Supplementary Figure 3). These findings corroborate our experimental results, which suggest that we should sample 15 MDTs or more to be representative of the primary xenograft.

MDT production from cell line xenograft tumors

The method for the production of micro-dissected tumor samples from tumor-extracted tissue samples was an adapted version of the one previously published by our group[19]. Briefly, a scalpel was used to cut the biopsied sample into thin tissue fragments (1.5 x 5 mm) which were kept in a balanced saline solution (HBSS, 311-516-CL, Wisent Inc., Saint-Bruno-de-Montarville, Canada) supplemented with 10% FBS, 55 mg/L gentamicin and 0.6 mg/L amphotericin B. The tissue fragments were further cut into sphere-

like MDTs using a 400 µm diameter tissue punch (Zivic Instruments, Pittsburgh, USA) and kept in HBSS supplemented with the antibiotics without serum until the loading procedure.

Loading, trapping and culture of the MDTs in the microfluidic device

Similar to our previous work[28], for each individual channel, eight MDTs were collected using a P20 micropipette and introduced in the HBSS-filled inlets where they sediment to the bottom of the channel. Flow was induced in the microfluidic channels by aspirating fluid from the outlet of the device using the same micropipette. Carried by the flow, the MDTs travel in the channel and the flow is suspended for approximately 1-2 seconds when an MDT above the desired well is allowed to sediment to the bottom of the trap. The same procedure is repeated to fully load the four fluidic channels of the device, resulting in a total number of 32 MDTs per device. Once the 32 MDTs were loaded, the liquid volume was replaced with a tissue-specific culture medium. The four independent channels allow the MDTs to be exposed to three different therapeutic agents or a combination of therapeutic agents while keeping one non-treated channel as a control.

Treatment of MDTs within the microfluidic device

The MDTs of PC origin were treated with docetaxel (8078A002, Mckensson Canada Corporation, Canada) at 1X, 10X of the monolayer IC_{50} (1 nM) for 12 hours then replaced with culture medium and analysed after a recovery period of 12 hours. The MDTs were also treated with recombinant human tumor-necrosis factor alpha (TNF- α; 300-01A, PeproTech, New Jersey, USA) at a concentration of 10 ng/mL for either 0, 30, 60 or 120 minutes.

Micro-dissected tissue micro-array procedure

The adapted paraffin-embedding on-chip procedure consisted of fixing the MDTs with formalin (F-6050, Capitol Scientific, Austin, Texas) involving two rinses of 5 minutes each followed by a 30-minute incubation. The MDT connective tissue was then coloured using phloxine-B (P4030, Sigma-Aldrich, Oakville, Ontario) for 20 minutes and dehydrated by a stepwise application of an ethanol gradient consisting of 50, 70, 80, 90, 95 and 100% ethanol (20 minutes each). Three incubations of 5 minutes each with Xylene

Substitute (9990505, Thermo FisherScientific, Massachuusetts, United States) were used to remove all the ethanol. The two PDMS layers were separated and the bottom layer was placed in a metal cassette immerged in liquid Paraplast X-TRA® paraffin (P3808, Sigma-Aldrich) at 56°C for 90 minutes then solidified at 4°C for 40 minutes. The remaining PDMS layer was removed and the newly exposed surface of MDTs were covered with a layer of liquid paraffin. The block was re-melted at 58°C for 90 minutes and re-solidified first at room temperature overnight and then at 4°C for 25 minutes to produce an MDTMA block. The paraffin blocks were sliced in 4 µm-thick slices using a microtome and placed on microscope slides for further analysis yielding approximately 30 slides per MDTMA block.

Immunohistochemistry/immunofluorescence staining

The 4 µm sections were stained with various antibodies to assess cell population composition and viability. For hypoxia, a tissue from a metastatic clear cell renal carcinoma (CCRC) patient sample was used as a positive control for the carbonic anhydrase 9 (CA9) staining as this CCRC patient presented with a VHL gene inactivation[40] driving the activation of the hypoxia pathway via HIF, resulting in the overexpression of CA9[41-43]. Subsequent slides were stained using the BenchMark XT automated stainer (Ventana Medical System Inc Tuscan, AZ). Antigen retrieval was carried out with Cell Conditioning 1 (VMSI; #950-123) for 30 minutes (caspase-3), 60 minutes (CK8/18, anti-mitochondria, Ki67, p65) or 90 minutes (CA9). Rabbit anti-CA9 (1:2000) antibody (ab15086, Abcam, Cambridge, United Kingdom), rabbit anti-CK8/18 (1:2) antibody (IR09461-2, Agilent, California, USA), mouse anti-mitochondria (1:5000) antibody (ab92824, Abcam), rabbit anti-Ki67 (1:500) antibody (RM9106, ThermoScientific), rabbit anti-cleaved caspase-3 (1:500) antibody (9661, Cell Signaling Technology, Massachusetts, USA) and mouse anti-p65 (1:200) antibody (sc8008, Santa-Cruz Biotechnology, California, USA) were automatically dispensed. The slides were incubated at 37°C for 60 minutes and developed by the Ultra-View DAB detection kit (VMSI#760-091). All sections were scanned with a 20x 0.75NA objective with a resolution of 0.3225 µm (bx61vs, Olympus, Toronto, Ontario).

Quantification of immunohistochemistry and immunofluorescence staining

Stained MDTs (15 to 20) were quantified using VisiomorphDP software (VisioPharm, Denmark).[44] For IHC analyses, quantification was performed in two different ways, depending on the cellular localisation of the protein of interest. Cytoplasmic staining (CK8-18, anti-mitochondria) was quantified by thresholding the deconvoluted DAB image and evaluating the ratio between the stained area and the total area of the tissue core. Nuclear staining (Ki67) was quantified by dividing the number of positively stained nuclei by the total number of nuclei present in the tissue core. The IF quantification of cleaved caspase-3 was performed by first extrapolating the tissue core surface area through the DAPI channel. The mean intensity of fluorescence, corresponding to our protein of interest, within the tissue core was then calculated. The average quantified expression of all MDTs within the same condition was then calculated (n=number of MDTs analysed for a same xenograft). Statistical analysis of the IHC and IF results were performed using one-way ANOVA analyses. The visual quantification of IF staining of p65 was performed by identifying the localisation of the protein expression either in the nucleus or cytoplasm. The total number of positive MDTs within each group was calculated and contingency statistical analyses were performed using GraphPad.

Off-chip analysis of MDTs by FACS

Fluorescence-activated cell sorting (FACS) was used as an end-point validation assay to measure the survival of individual cells constituting the MDTs after their incubation in the microfluidic platform. The MDTs were removed from the microfluidic device by separating the two PDMS layers, without affecting the position of the MDTs, and further pipetting them out of their wells. To obtain a single cell suspension, 15 MDTs were removed and digested for 15 minutes at room temperature with 4 mg/mL crude collagenase (C9407, Sigma) and 1 mg/mL collagenase type 1A (C9891, Sigma) in PBS. Once the MDTs were completely dissociated, FBS was added and the single cell suspension was then passed through a 35 µm cell strainer (352235, Corning Inc., Corning, USA). Prior to analysis by FACS, a set of MDTs was used as negative and positive controls to set the photomultiplier tool (PMT) levels and thresholds in the annexin

V, DRAQ7 and Alexa-488 fluorescent secondary antibody channels. The MDTs being evaluated were first stained with apoptotic fluorescent Annexin V (4:100 dilution) (PE Annexin V Apoptosis Detection Kit I 640908, BD Biosciences) and DRAQ7 (1:100 dilution) (ab109202, Abcam). For the Mito staining, which is intracellular, a fixation and permeabilization (88-8824-00, ThermoFisher Scientific) procedure was performed prior to primary (human Mito) and secondary antibody (Alexa-488) labeling. The data from each acquisition was analyzed using FlowJo (FlowJo LLC, Ashland, USA) by gating the cell population in the FSC/SSC graph, removing doublets, identifying the human epithelial cells and associating them to one of three populations according to its fluorescent labeling: early apoptotic cells (annexin V-stained only), late apoptotic or dead cells (double stained with annexin V and DRAQ7), and live cells (non-stained). Experiments were done in batches and used the same xenograft as starting material. However, each batch of experiment was performed using internal triplicates of 15 MDTs from the same xenograft (n=45 MDTs). The FACS results were analysed for statistical relevance using one-way ANOVA analyses.

Immunocyctochemistry analysis of cell line cultures

Cells were seeded onto coverslips in 24-well plates at a concentration of 20 000 cells per well. 24 hours after seeding, the cells were treated with TNF-α at a concentration of 10 ng/mL for 0 or 10 minutes. The culture medium was removed, and cells were rinsed with PB. The cells were further fixed with formalin and permeabilized with 0.1% Triton X-100 (Sigma-Aldrich Inc). After blocking (1% BSA and 0.1% tween in PBS), the coverslips were incubated with anti-p65 (1:200) primary antibody overnight at 4˚C in a humidified box. They were further incubated with Cy-5 (1:250) secondary antibody for 1 hour at room temperature away from the light. Coverslips were mounted onto slides using Prolong® Gold anti-fade reagent with DAPI (Life Technologies Inc, Burlington, Ontario). Images were obtained using a Zeiss microscope (Zeiss observer ZI, Carl Zeiss, Jena, Germany).

Western Blot analysis

Cells were seeded in 60 mm plates with a total cell count of 400,000 cells and treated 24 hours after

seeding with TNF-α for 0, 10, 30, 60 and 120 minutes or with staurosporine (4 μM) for 4 hours as positive control. Fifteen micrograms of total protein extracts were separated on 10% SDS-polyacrylamide gels and transferred onto nitrocellulose membrane. The membranes were blocked with 5% skim milk in PBS-Tween for 1 hour and probed with primary antibodies (cleaved caspase-3 diluted 1:200 and Actin diluted at 1:1000) overnight at 4˚C. The HRP-conjugated secondary antibody was added, and the proteins were detected by chemoluminescence using a BioRad apparatus. The protein expression level was quantified using Image Lab.

2.1.2.4 Results

High-density Microfluidic device design and fabrication

The micro-dissected tissue micro-array device was designed to optimize the viability of cultured tissue in non-perfused conditions, eliminating the need for micro-pumps and complex fluidic connections, which can be cumbersome in an eventual clinical application. We have previously determined, through numerical simulations of mass transfer within 3D cell cultures, that to ensure optimal viability over 24 hours in non-perfused microfluidic channels, each sample should have access to a volume of media of approximately 100 times its volume[34]. Taking this into account, we developed a microfluidic device allowing us to trap and analyse up to 32 samples in a high-density array within an area small enough to fit in a histology cassette used for subsequent paraffin embedding (Figure 2a). The dimensions of each of the 32 microfluidic wells were optimized to allow simple sedimentation trapping of 380 μm samples with minimal displacement during the medium changes (as described in Ref.[34]). In the 32-plex devices, the inlets and outlets of each channel were spaced so as to minimize the chance of cross-contamination between adjacent channels. The design allows for a simple loading process of MDTs within the microfluidic device, and in a typical micro-dissection procedure we could reliably load more than 20 of the 32-well devices. Because each device is subdivided into four channels, it is possible to expose tumors to 80 different conditions in one experiment.

In non-perfused mode, nutrient and metabolite transport within the MDTs (Figure 2b) is diffusion limited. The culture medium must therefore be refreshed periodically every 2-3 days to ensure limited development of hypoxic cores within the MDTs throughout the culture period. Indeed, we have performed IHC using the hypoxia marker CA9, which is a downstream target of the Hypoxia-inducible factor 1-alpha (HIF1A) known to be up-regulated in hypoxic conditions[41-43]. Our results show low or no staining in our MDTs cultured for up to 15 days in our microfluidics devices (supplementary Figure 1). As expected, some areas of positive staining can be observed in the primary xenograft tissue, and a strong staining can be observed in the positive control tissue (i.e. a clear cell renal carcinoma metastasis to the pancreas; see Methods). Furthermore, finite element simulations were carried out using COMSOL Multiphysics® to define an optimal rinsing process to fully refresh the culture medium in all device wells for a given chip geometry (see Materials and Methods). Using a micropipette to rinse with 70 µL of reagent every 5 minutes, we determined that a total of four repeats was sufficient to refresh the culture conditions (>95%), independent of the reagent (culture medium and chemotherapy) used (Figure 2b). These simulations show that fluid refreshment in the device, due to flow recirculation during medium replacement (Re ~100), is limited by diffusive reagent transport from the channel to the wells, i.e with a characteristic time scaling with the second power of the total diffusion length ($\sim (h + w)^2$, where h and w are the channel height and the well depth). As such, the height of the microfluidic channel in the final design was fixed to a relatively low value (0.9 mm) to allow rapid fluid exchange and thus expedite sample processing. While higher sample density in the paraffin block could be achieved by increasing channel height, this would significantly increase the time required for each fluid exchange, potentially limiting the applicability of the technique in a clinical context.

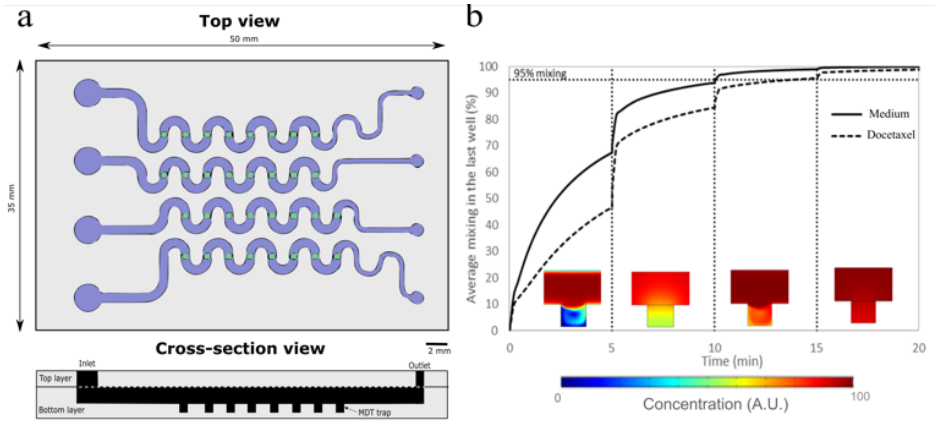

Figure 2: Design and operation of microfluidic device. a, Schematic representation of the microfluidic device. **b,** Finite element simulations of the average mixing in the last well of a channel during the rinsing process for different reagents. Subset images show carboplatin concentration distribution (arbitrary units) in the well at 1, 6, 11 and 16 minutes.

Paraffin-embedding lithography

Formalin-fixed paraffin-embedding (FFPE) is widely used in pathology to diagnose patient tumor specimens as it allows both tissue morphology-based diagnosis and molecular-level characterization of the samples. However, the technique has been designed to study large tissue fragments and is challenging to apply to sub-milimeter sized tissue samples. Tissues of this size are challenging to align, hard to visualize and slow to manipulate individually. The method defined here circumvents these challenges by confining samples within a specifically designed microfluidic chip that yields precise FFPE of MDTs assembled in a high-density MDTMA (see details in Materials and Methods) that maintains the spatiotemporal structure of the tissue specimen to better understand the effect of pharmacological agents on cancer cells. The presented methodology eliminates the need to individually manipulate the samples by fixing and dehydrating them directly in the device prior to casting them all at once in a paraffin block. We added a phloxine-B connective tissue staining step to facilitate sample visualization as their size and low contrast renders them otherwise indistinguishable from the paraffin block (Figure 3a). A xylene substitute was added, slightly swelling the PDMS layers and facilitating their separation (Figure 3b). In a second phase, MDTs within the trapping layer of the channel were cast in a stainless-steel mould containing liquid paraffin (Figure 3c). The paraffin

block was then solidified and the remaining PDMS layer peeled off, resulting in a notched surface with the MDTs embedded in each protrusion (Figure 3d). A second layer of liquid paraffin was added to smooth out the surface, with the side effect of inducing a slight out-of-plane drift of the MDTs within the block (Figure 3e). To overcome this, the MDTMA block was completely re-melted on a levelled hot plate located in an oven at 58˚C (Figure 3f) to let the MDTs sediment and align in a single plane against the bottom of the casting mould (Figure 3g). This step is crucial and ensures that each microtome slice contains every MDT in the array with the trade-off of a slight lateral misalignment that is inconsequential for further analyses (Figure 3h). The specific conditions for the procedure have been optimized for proper preservation of the cellular morphology and tissue architecture of the MDTs (Figure 3i). For formalin fixation, the fixation time as a function of tissue dimension is known to be on the order of 1 mm per hour[45]; thus, a tissue of ~380 µm in thickness would need to be fixed for approximately 30 minutes. Therefore, PEL reduces the required fixation period by 98% (from 24-48 hours in conventional histopathology). Overall, the MDTMA approach preserves the spatial organization of the samples, greatly reduces the time and labour required to fix a large number of samples and limits the chance of sample damage and mishandling as they are shielded within the chip during fixation. Finally, compared to FFPE standard protocols, our procedure reduces reagent consumption per device and procedure time (dehydration to paraffin embedding) by 60%.

A single block incorporating MDTs produced an average amount of 30 ± 1.01 4-µm thick slices (n = 60 blocks). After fixation and Hematoxylin and Eosin (H&E) staining, average MDT diameter was 279 µm (supplementary Figure 2), ~73% of their original size (characterized previously at ~380 µm). The shrinkage is similar to that reported for FFPE whole tissue samples[46,47].

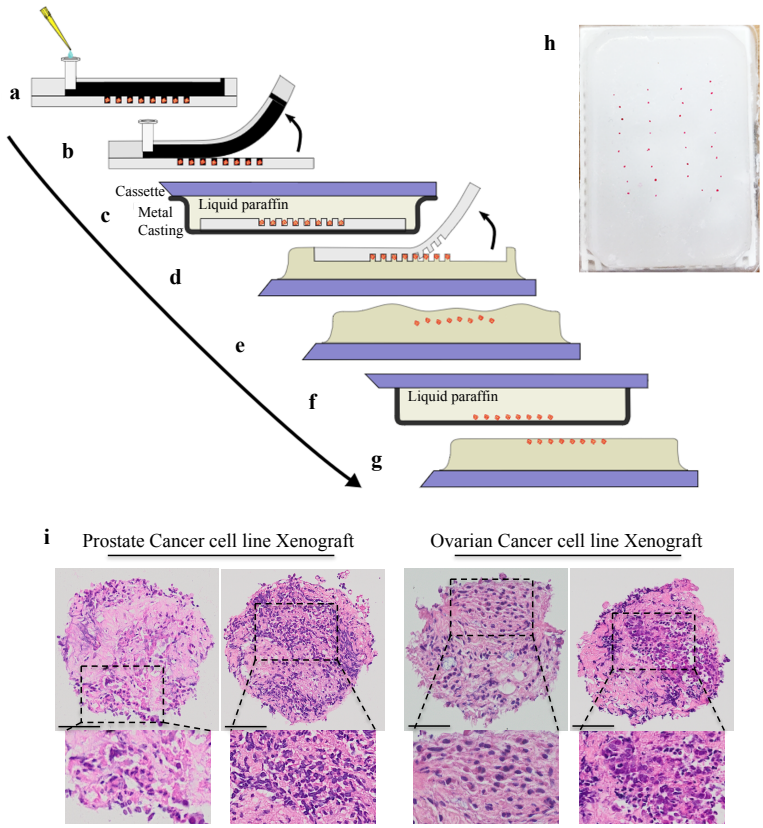

Figure 3: Paraffin-embedding lithography protocol to produce micro-dissected tissue micro-array. a, Formalin fixation and dehydration of the MDTs in the microfluidic device. **b,** Peeling apart of the two PDMS layers. **c,** Replica moulding of the channel layer by immersion in liquid paraffin followed by solidification. **d,** Removal of the remaining PDMS layer from the solid paraffin block. **e,** Conserving the exposed MDTs with liquid paraffin and solidification. **f,** Re-melting of the block to align the MDTs on the same plane. **g,** Completed MDTMA block ready to be sliced. **h,** MDTMA block (24 x 37 x 5 mm) containing 4 channels with 8 MDTs within each channel. **i,** H&E of various MDTs derived from prostate cancer and ovarian cancer cell line xenografts showing preservation of cellular morphology and tissue architecture. Scale bar = 70 µm.

MDTs are representative of the heterogeneous components found in primary xenografts

Tumors heterogeneity plays a crucial role in cancer progression[7,8,48]. To demonstrate that heterogeneous components found within tumors are represented in MDTs, human prostate cancer (PC) and epithelial ovarian cancer (EOC) derived cell line xenografts were produced in immuno-compromised NOD-RAG-Gamma mice. The harvested tumors were split into two equally mirrored sections: one section was formalin-fixed to produce a standard FFPE tumor specimen and the other section was used to produce MDTs. Using histological and protein expression analysis, we compared MDTs and FFPE whole-tumor

xenograft specimen fixed on the day of the harvest (day 0). As expected, MDTs produced from PC and EOC cell line xenografts mirrored the heterogeneous compartments of the corresponding primary xenograft tissue (Figure 4a, d), showing varying levels of epithelial cells (CK8/18 and human Mito) (Figure 4b, c, e, f). The human Mito antibody defines the human cells to clearly distinguish between human epithelial and infiltrating mouse-stromal cells. To demonstrate the similarity between MDTs and the FFPE specimen, we analysed 15 randomly selected MDTs and 15 randomly selected regions of the primary xenograft, corresponding to the same surface area as the MDTs (250 µm x 250 µm). We found no significant difference in distribution of fraction of area stained with the CK8/18 or Mito marker (Figure 4g, h). These results demonstrating that our procedure mirrors the heterogeneous architecture of the tumor tissues within a set of MDTs derived from this tissue. These findings were further validated with a custom Monte-Carlo simulation based on stained whole-tissue primary xenografts to determine the number of MDTs that had to be sampled to recapitulate whole-tissue antibody analysis. In order to minimize sampling error, our simulations suggest that using 15 MDTs (or 2 rows of 8 MDTs) we can derive the IHC staining score with a 95% confidence interval of 10% or less (see Material and Methods; supplementary Figure 3). Taken together, these results suggest that a random analysis of 15 MDTs is sufficient to represent the primary xenograft specimen in its entirety and does not impose a significantly greater sampling bias than the original tumor section.

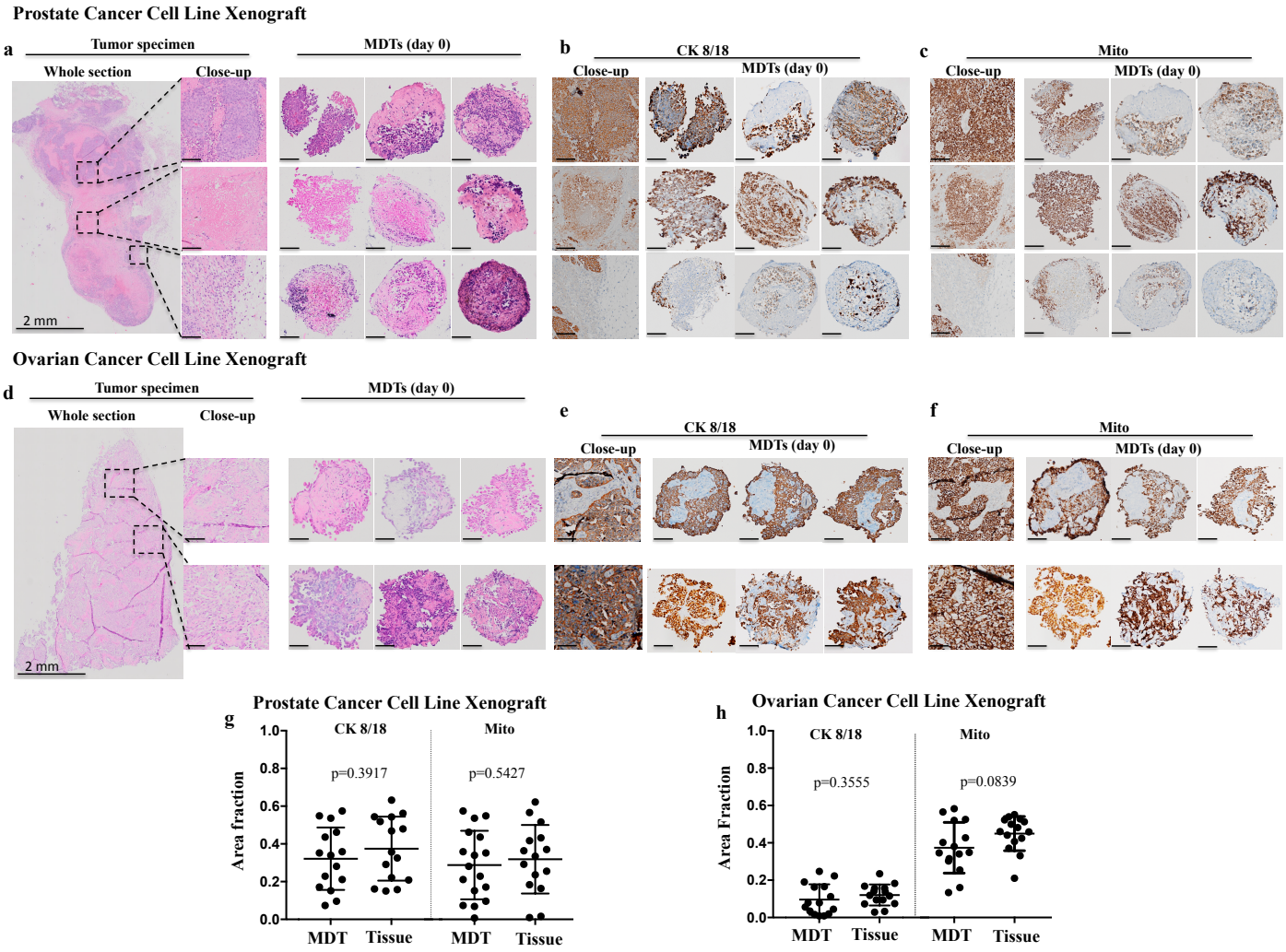

Figure 4: Representation of heterogeneous compartmentalization of PC and EOC primary xenograft. a, PC cell line (LNCaP) xenograft **d**, EOC cell line (OV2295) xenograft as a cross section of the entire primary xenograft tissue, magnified tissue areas and corresponding MDTs stained with H&E. **a,d,** Corresponding magnified primary xenograft tissue from the same specimen as **b,e**, and MDTs stained with epithelial cell marker (CK 8/18) and **c,f,** human Mito distinguishing between human epithelial cells and infiltrating mouse-stromal cells (negative staining). **g,h,** IHC scoring of 15 primary xenograft magnified regions (250 x 250 µm field of view) and 15 MDTs chosen randomly. All experiments were done using the same xenograft as starting material. Scale bar = 50 µm. Error bar = ± SEM.

Morphology, viability and proliferation activity are preserved in MDTs for up to 15 days

To ensure that the MDTMA microfluidic device could maintain epithelial cell and tissue viability within the MDTs, we examined the MDTs over a 15-day culture period. MDTs produced from both PC and EOC (Figure 5) xenografts were analysed after 0, 5, 10 and 15 days in culture. MDTMA analyses using H&E staining suggest that general tissue architecture was preserved, including epithelial structures and their spatial relation with stromal components. Similar to other research groups[15,17,24,31], Ki-67 and cleaved caspase-3 antibodies had been selected for cell proliferation and viability specific analysis. The results show that the micro-dissection procedure induces a mechanical stress on the cancer cells located within the MDTs, hindering the viability of MDTs at day 0. However, a recovery period of 3 to 5 days is sufficient to increase their overall viability, as seen by an increasing proliferative capacity while maintaining a low and stable apoptotic fraction over the 15-day culture period (Figure 5a, b, d, e). To confirm the results obtained through IHC, we carried our FACS analyses on dispersed off-chip MDTs to assess the viability of the human epithelial cell (Mito) cells within the MDTs. As in the IHC analyses, FACS results showed a similar epithelial component within the MDTs over the 15-day culture period. Furthermore, the cancer cells within the MDTs showed no significant decrease in viability over time (93% ± 1.5; Figure 5c, f). Taken together, these results suggest that the MDTMA culture platform adequately supports cancer cell viability and proliferation over a 15-day period.

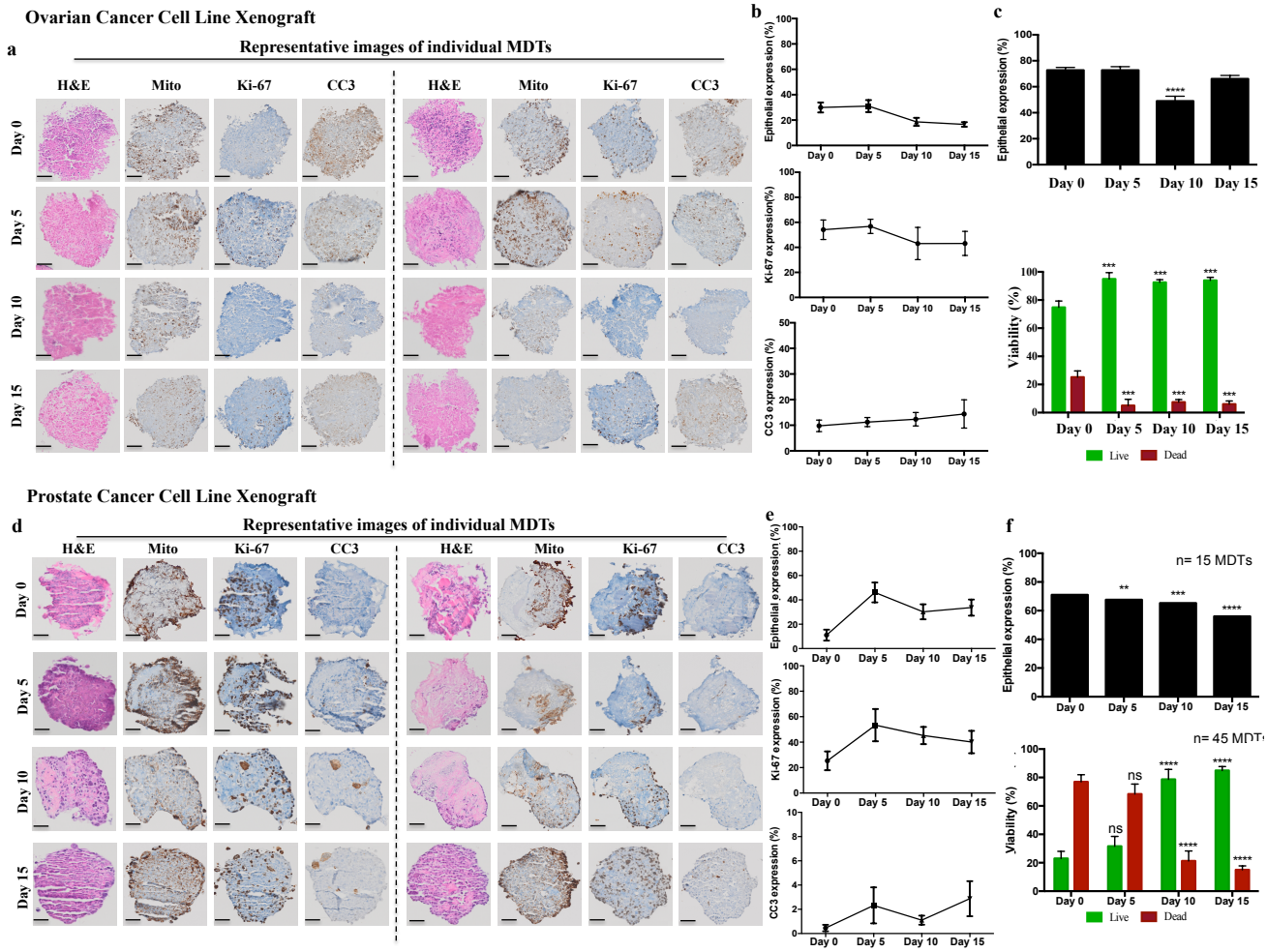

Figure 5: Maintenance of MDT viability over 15-day culture period using EOC and PC cell line xenograft model. a,d, Representative images of individual EOC (OV1946) and PC (DU145) derived MDTs at different time-points (day 0, 5, 10, 15) stained with H&E, or following IHC for human epithelial cells (human Mito), cell proliferative (Ki-67) and cell apoptosis (cleaved caspase-3; CC3). **b,e,** IHC scoring of MDTs showing stable epithelial cell expression and sustained proliferation over the 15-day period (n=15 MDTs per time point). **c,f,** FACS analysis of MDTs at Day 0, 5, 10, 15 stained with Mito, Annexin V (detection of early apoptosis) and DRAQ7 (detection of dead cells) for epithelial cell expression and tissue viability assessment (n=45 MDTs). All experiments were done using the same xenograft as starting material. Scale bar = 50 µm. Error bar = ± SEM. ***p<0.0001, ****p<0.00001 with respect to viability at day 0.

MDTMAs can track *ex vivo* biological and pharmacological responses

After characterizing the composition and viability of arrayed MDTs, we sought to demonstrate the ability of MDTMAs to follow various biological responses. TNF is a pro-inflammatory cytokine commonly secreted by tumor-recruited immune cells, which can induce a variety of cell fates. TNF is known to stimulate the nuclear translocation of p65 subunit of the nuclear factor κB (NF-κB)[49,50] thereby inducing transcription of NF-κB-target genes. Long exposures to TNF can also induce cell stress, leading to cellular apoptosis via caspase-3 activation[51]. We therefore assessed the response of MDTs originating from PC and EOC (Figure 6) cell line xenografts exposed to TNF at a concentration of 10 ng/mL for 0, 30, 60 or 120 minutes. As expected, IF staining of the p65 NF-κB subunit was restricted to the cytoplasm in the untreated MDTs; however, MDTs treated with TNF for 30 minutes showed a significant increase in nuclear p65 (Figure 6a, b, c); similar responses were also observed in 2D cell cultures (Figure 6d). Following TNF exposures of 60 or 120 minutes, we observed increased cleaved caspase-3 staining (supplementary Figure 4a, b, c) as previously reported for 2D cultures[51]. These results suggest that MDTMAs can be used to investigate the response of tumor samples to cytokines.

Next, we used MDTMAs to assess the response of our *ex vivo* 3D PC cell line xenograft models to the chemotherapeutic docetaxel. Three days after they were established, MDTs were treated for 12 hours and analyzed after a 12-hour recovery period. As anticipated, IF (Figure 7a) and IHC (supplementary Figure 5) staining of cleaved caspase-3 showed a significant increase in apoptotic cells (Figure 7b, supplementary Figure 5) after treatment, and the proportion of apoptotic cells was docetaxel-dose-dependent. These results were further confirmed by flow cytometry analyses (Figure 7c) and show that MDTMAs can enable the systematic characterization of the response of tumor specimens to small molecule pharmacological agents. Combined with the ability to track the response of *ex vivo* cancer samples to biological agents, such as TNF, this demonstrates that MDTMAs represent a path toward miniaturized and efficient CSRAs.

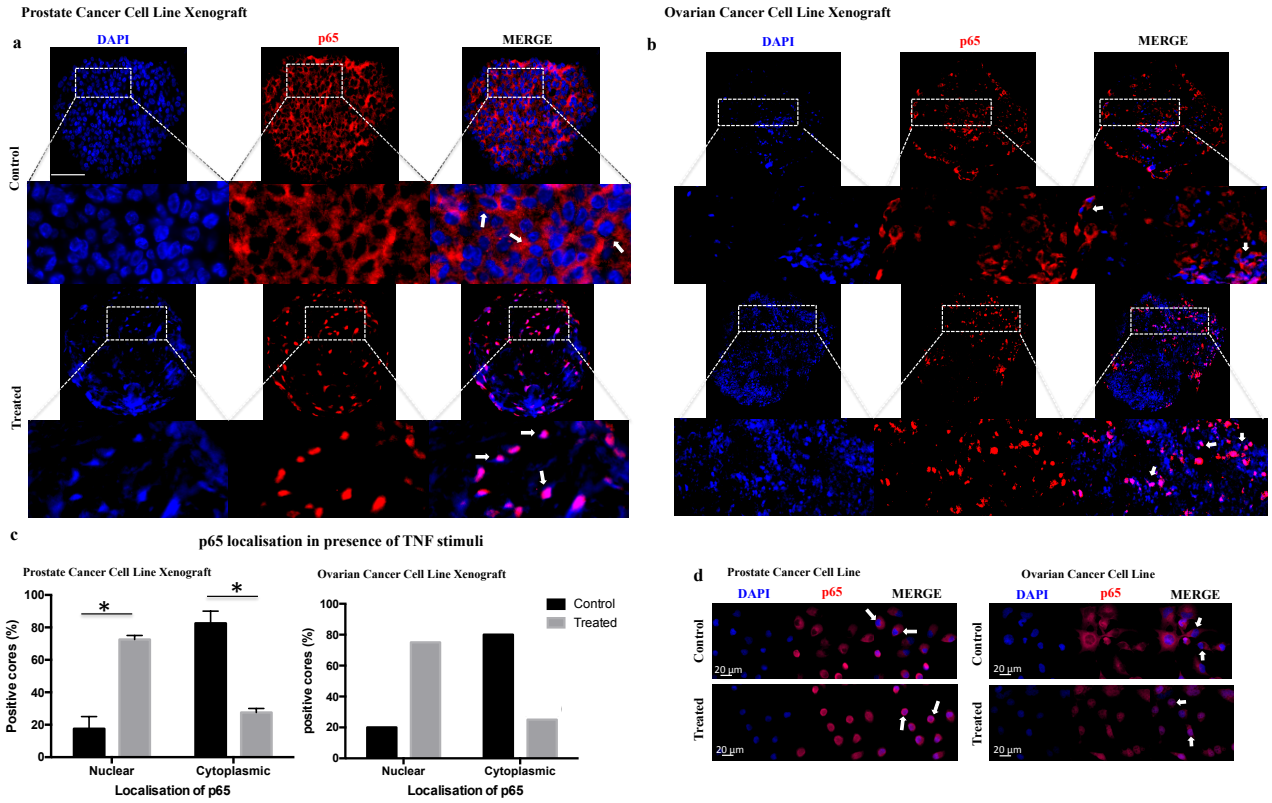

Figure 6: PC and EOC cell line MDTs exposed to TNF- α showing p65 nuclear translocation. MDTs produced from PC (DU145) and EOC (OV1946) cell line xenograft tumors were treated with either RPMI media or TNF-α at a concentration of 10 ng/mL for 30 minutes. **a,b,** The MDTs were fixed using the PEL technique and stained with p65 antibody using IF (DAPI in blue and p65 in red) **c,** Visual analysis of p65 localisation was identified on an average of 100 cells per MDT in both conditions. Identified MDT cores were scored as positive when p65 staining was located in the nucleus. All MDT associated experiments were done using two separate xenografts as starting material, resulting in a total of 23 analysed MDTs. *p<0.05. **d,** Immunocytochemistry (DAPI, p65) of PC cell line treated with either RPMI or TNF-α at a concentration of 10 ng/mL for 10 min. N=2 for DU145 and N=1 for OV1946. Scale bar = 70 µm. Error bar = ± SEM.

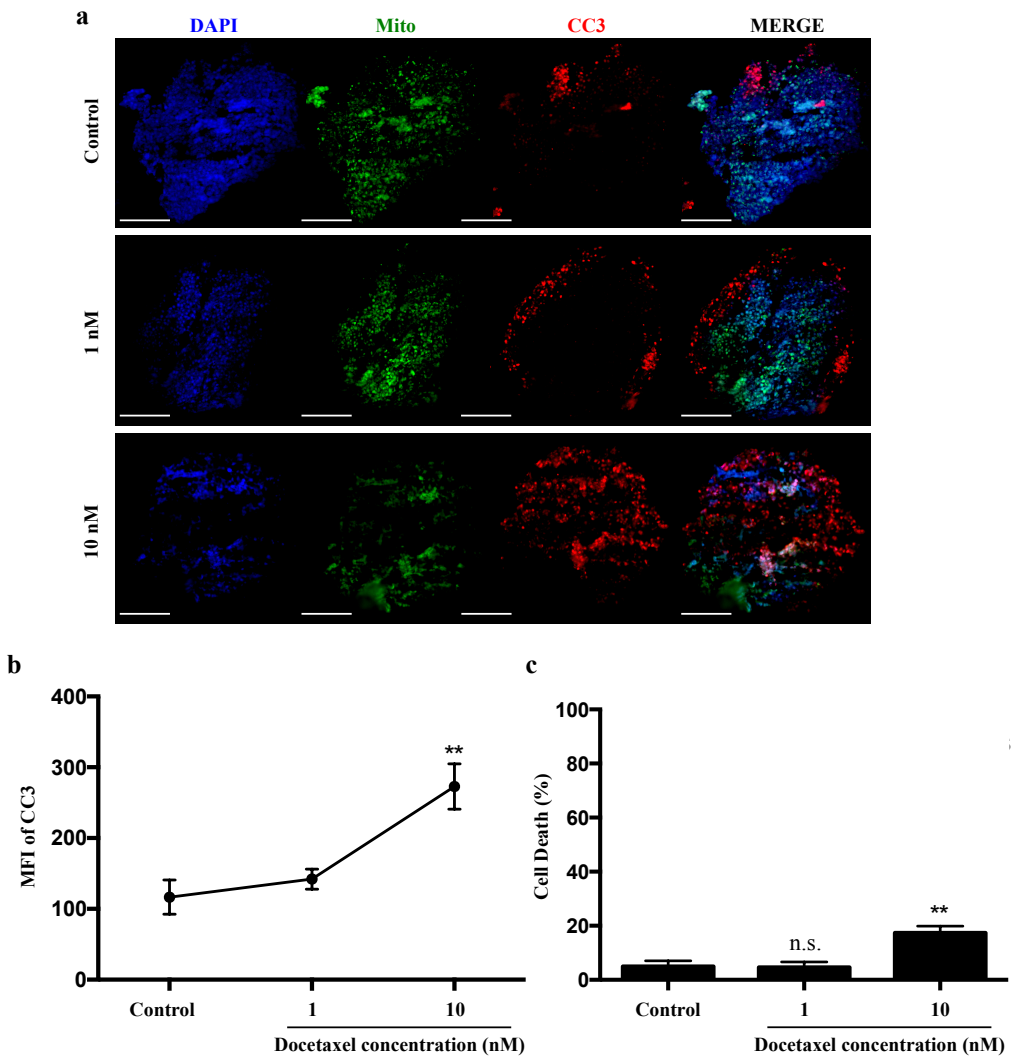

Figure 7: Dose-Response analysis of PC (LNCaP) cell line xenograft MDTs. MDTs treated with two concentrations (1, 10 nM) of docetaxel (IC_{50} for monolayer cultures is 1 nM) for 12 hours at day 3. MDTs were fixed and analyzed after 12 hours of recovery period. **a,** IF staining of MDTs (DAPI in blue, Mito in green and cleaved caspase-3 in red). **b,** IF analysis of overall expression of cleaved caspase-3 (n=15 MDTs/condition). **c,** FACs analysis n=45 MDTs (Annexin V and DRAQ7). All experiments were done using the same xenograft as starting material. Error bar = ± SEM. *p<0.05, **p<0.001.

2.1.2.5 Discussion

A critical bottleneck in the improvement of cancer care is the dearth of methods to accurately determine the chemosensitivity profile of a patient and thus facilitate clinical decision-making. To address this, we developed a platform for CSRAs in *ex vivo* solid tumor-derived models that could support the identification of response or resistance to specific therapeutic agents in a timeframe suitable for clinical decision-making. We used human cancer cell line xenograft models to validate the potential of MDTMAs to characterize cellular behaviour and pathway activations at a molecular level. Based on standard principles of *ex vivo* cultures[12,28,52], our model is efficient in evaluating treatment response in patient tumor samples using robust and widely adopted IHC and IF as endpoint measurements. These assays are compatible with both clinical and pharmaceutical current practices and allow the monitoring of multiple biological pathways. Furthermore, because they preserve the viability of the tissue for at least 15 days, MDTMAs may allow the study of longer-term effects of multiple treatment cycles on the same tissue specimen. In turn, this may yet enable the *ex vivo* study of delayed cell fate choices caused by both cytotoxic and cytostatic agents such as apoptosis, quiescence and senescence[53] as well as acquired resistance to treatment, which are likely to be missed using shorter culture periods.

Compared to other organotypic slice models, where fragile consecutive tissue slices are laboriously manipulated and independently exposed to various treatments, the current MDTMA configuration allows multiple treatment conditions to be evaluated on the same slide. This should greatly reduce the assay variability known to arise from experiment-to-experiment in IHC staining[15,17,31]. Moreover, because the MDTs are randomly selected from different regions of the tumor, MDTMAs can provide a more representative assessment of treatment response than would organotypic slices, where each region of the tumor may be exposed to different therapeutic agents[16,18]. Casting all the samples in paraffin with simple steps reduces the potential tissue damage caused by off-chip manipulation of the tissue sample. In addition, our methodology can readily be integrated with other promising technologies using pre-clinical organotypic models to predict patient-specific sensitivity to treatment. This has the potential to improve the throughput potential of these models[31].

The power of MDTMAs could be further extended by integrating other promising innovations in pre-clinical studies using organotypic models such as careful modeling of tumor ecosystems[31], and improving their throughput. Although our study focused on PC and EOC xenograft tumors, MDTMAs should be amenable to study any type of solid tumor including tumors that incorporate an immune component and thus encompass the effect of the TME. Furthermore, through appropriate sampling, the tumor-derived MDTs can mirror the intra-tumor heterogeneity found in many solid tumors, making MDTMAs a powerful approach to study heterogeneity-related phenomena such as resistance or immune-based responses to treatment. In addition, the improved assay throughput of MDTMAs should enable simultaneous characterization of multiple biological pathways engaged in the response of tumor samples to biological or pharmaceutical agents, leading to mechanistic insight into these responses. With improved throughput, our method could also help reduce the cost and time needed to identify and test leading compounds in a drug discovery setting. Finally, PEL is general technique that can be applied beyond the organotypic modeling of solid tumors. Indeed, it can be applied to spheroids, organoids[54], to study both normal physiology and the response to pathogens; to embryo culture[55] and to small multicellular organisms such as C. elegans or Planaria[56].

2.1.2.6 Acknowledgements

We acknowledge Kim Leclerc Désaulniers for technical assistance. We thank Liliane Meunier, Véronique Barrès and Gabriella Fragoso of the Molecular Pathology core facility of the CRCHUM for performing the IHC and IF staining and slide scanning. We thank Drs. Hang Lu (Georgia Institute of Technology) and Suzanne Gaudet (Harvard University) for useful discussions. K.S. and R.G-L. received bursaries from the Canderel fund of the Institut du Cancer de Montréal. K.S. received a scholarship and B.P. expertise in the field is made possible by the TransMedTech Institute and its main funding partner, the Canada First Research Excellence Fund. The research was supported with grants from the Canadian Cancer Society Research Institute, the Cancer Research Society partnered with Ovarian Cancer Canada, the Prostate Cancer Canada, the Canadian Urological Oncology Group, and the National Science and Engineering

Research Council of Canada. Tumor banking was in part supported by the Banque de tissus et de données of the Réseau de recherche sur le cancer of the Fonds de recherche du Québec Santé (FRQS) affiliated with the Canadian Tumor Repository Network (CTRNet). We thank the Fonds de Recherche du Québec for supporting this work. A.-M.M.-M., D.P. and F.R. are researchers of CRCHUM which receives support from the FRQS.

2.1.2.7 Conflict of interest

K.S., R.G-L, B.P,A-M.M-M, and T.G. declare a conflict of interest under the form of a patent.

2.1.2.8 Author contributions

Conceptualization: K.S., R.G-L, B.P., E.C., T.G., A-M.M.M. designed the research. Methodology: K.S., R.G-L, A.M.L, B.P., E.C., A.M.O, J.K-D., conducted the micro-dissection procedure. K.S., L.A.M, B.P., E.C., designed and optimized the MDTMA procedure. R.G-L, T.G., designed and fabricated the microfluidic device. R. G-L. carried out the mathematical modeling. K.S., carried out the biological assays. Analysis: R.G-L., K.S., conducted the quantifications and statistical analysis. Resources: D.P., F.S. provided clinical support. Writing – original draft: K.S., R.G-L., B.P., E.C., T.G. wrote the manuscript. Writing – review and editing: B.P., E.C., D.P., F.S., T.G., A-M.M-M. supervised the project and revised the paper.

2.1.2.9 References

1. R. L. Siegel, K. D. Miller and A. Jemal, *CA: a cancer journal for clinicians*, 2017, **67**, 7-30.
2. C. C. S. A. Committee, *Journal*, 2017.
3. C. R. UK, *Journal*, 2017.
4. M. R. Junttila and F. J. de Sauvage, *Nature*, 2013, **501**, 346-354.
5. J. P. Gillet, A. M. Calcagno, S. Varma, M. Marino, L. J. Green, M. I. Vora, C. Patel, J. N. Orina, T. A. Eliseeva, V. Singal, R. Padmanabhan, B. Davidson, R. Ganapathi, A. K. Sood, B. R. Rueda, S. V. Ambudkar and M. M. Gottesman, *Proceedings of the National Academy of Sciences of the United States of America*, 2011, **108**, 18708-18713.
6. M. M. Morgan, B. P. Johnson, M. K. Livingston, L. A. Schuler, E. T. Alarid, K. E. Sung and D. J. Beebe, *Pharmacol Ther*, 2016, **165**, 79-92.
7. M. Verma, *J Pers Med*, 2012, **2**, 1-14.
8. R. Bartlett, W. Everett, S. Lim, N. G, M. Loizidou, G. Jell, A. Tan and A. M. Seifalian, *Transl Oncol*, 2014, **7**, 657-664.

9. J. A. Hickman, R. Graeser, R. de Hoogt, S. Vidic, C. Brito, M. Gutekunst, H. van der Kuip and I. P. Consortium, *Biotechnol J*, 2014, **9**, 1115-1128.
10. D. J. Samson, J. Seidenfeld, K. Ziegler and N. Aronson, *J Clin Oncol*, 2004, **22**, 3618-3630.
11. M. M. Black, I. S. Kleiner and F. D. Speer, *Proc Soc Exp Biol Med*, 1951, **77**, 611-615.
12. R. H. Thomlinson and L. H. Gray, *Br J Cancer*, 1955, **9**, 539-549.
13. C. Humpel, *Neuroscience*, 2015, **305**, 86-98.
14. N. Sachs and H. Clevers, *Curr Opin Genet Dev*, 2014, **24**, 68-73.
15. V. Vaira, G. Fedele, S. Pyne, E. Fasoli, G. Zadra, D. Bailey, E. Snyder, A. Faversani, G. Coggi, R. Flavin, S. Bosari and M. Loda, *Proceedings of the National Academy of Sciences of the United States of America*, 2010, **107**, 8352-8356.
16. S. M. Hattersley, D. C. Sylvester, C. E. Dyer, N. D. Stafford, S. J. Haswell and J. Greenman, *Ann Biomed Eng*, 2012, **40**, 1277-1288.
17. F. Merz, F. Gaunitz, F. Dehghani, C. Renner, J. Meixensberger, A. Gutenberg, A. Giese, K. Schopow, C. Hellwig, M. Schafer, M. Bauer, H. Stocker, G. Taucher-Scholz, M. Durante and I. Bechmann, *Neuro Oncol*, 2013, **15**, 670-681.
18. T. C. Chang, A. M. Mikheev, W. Huynh, R. J. Monnat, R. C. Rostomily and A. Folch, *Lab Chip*, 2014, **14**, 4540-4551.
19. S. M. Hattersley, J. Greenman and S. J. Haswell, *Biomed Microdevices*, 2011, **13**, 1005-1014.
20. C. Guyot, C. Combe, H. Clouzeau-Girard, V. Moronvalle-Halley and A. Desmouliere, *Virchows Arch*, 2007, **450**, 503-512.
21. Y. Huang, J. C. Williams and S. M. Johnson, *Lab Chip*, 2012, **12**, 2103-2117.
22. M. Umachandran and C. Ioannides, *Toxicology*, 2006, **224**, 14-21.
23. D. S. Pushparajah, M. Umachandran, T. Nazir, K. E. Plant, N. Plant, D. F. Lewis and C. Ioannides, *Toxicol In Vitro*, 2008, **22**, 128-145.
24. H. van der Kuip, T. E. Murdter, M. Sonnenberg, M. McClellan, S. Gutzeit, A. Gerteis, W. Simon, P. Fritz and W. E. Aulitzky, *BMC Cancer*, 2006, **6**, 86.
25. S. R. Abner, P. C. Guenthner, J. Guarner, K. A. Hancock, J. E. Cummins, Jr., A. Fink, G. T. Gilmore, C. Staley, A. Ward, O. Ali, S. Binderow, S. Cohen, L. A. Grohskopf, L. Paxton, C. E. Hart and C. S. Dezzutti, *J Infect Dis*, 2005, **192**, 1545-1556.
26. F. M. Robertson, M. A. Ogasawara, Z. Ye, K. Chu, R. Pickei, B. G. Debeb, W. A. Woodward, W. N. Hittelman, M. Cristofanilli and S. H. Barsky, *J Biomol Screen*, 2010, **15**, 820-829.
27. S. Stempin, A. Engel, N. Winkler, T. Buhrke and A. Lampen, *Cancer Cell Int*, 2015, **15**, 110.
28. M. Astolfi, B. Peant, M. A. Lateef, N. Rousset, J. Kendall-Dupont, E. Carmona, F. Monet, F. Saad, D. Provencher, A. M. Mes-Masson and T. Gervais, *Lab Chip*, 2016, **16**, 312-325.
29. K. Rambani, J. Vukasinovic, A. Glezer and S. M. Potter, *J Neurosci Methods*, 2009, **180**, 243-254.
30. Y. Berdichevsky, H. Sabolek, J. B. Levine, K. J. Staley and M. L. Yarmush, *J Neurosci Methods*, 2009, **178**, 59-64.
31. B. Majumder, U. Baraneedharan, S. Thiyagarajan, P. Radhakrishnan, H. Narasimhan, M. Dhandapani, N. Brijwani, D. D. Pinto, A. Prasath, B. U. Shanthappa, A. Thayakumar, R. Surendran, G. K. Babu, A. M. Shenoy, M. A. Kuriakose, G. Bergthold, P. Horowitz, M. Loda, R. Beroukhim, S. Agarwal, S. Sengupta, M. Sundaram and P. K. Majumder, *Nat Commun*, 2015, **6**, 6169.
32. D. R. Grimes, C. Kelly, K. Bloch and M. Partridge, *J R Soc Interface*, 2014, **11**, 20131124.
33. D. Shweiki, M. Neeman, A. Itin and E. Keshet, *Proceedings of the National Academy of Sciences of the United States of America*, 1995, **92**, 768-772.
34. N. Rousset, F. Monet and T. Gervais, *Sci Rep*, 2017, **7**, 245.
35. V. Ouellet, T. H. Ling, K. Normandin, J. Madore, C. Lussier, V. Barres, D. Bachvarov, C. Rancourt, P. N. Tonin, D. M. Provencher and A. M. Mes-Masson, *BMC Cancer*, 2008, **8**, 346.
36. P. O. Gannon, L. Lessard, L. M. Stevens, V. Forest, L. R. Begin, S. Minner, P. Tennstedt, T. Schlomm, A. M. Mes-Masson and F. Saad, *Eur J Cancer*, 2013, **49**, 2441-2448.
37. M. Kobel, K. Rahimi, P. F. Rambau, C. Naugler, C. Le Page, L. Meunier, M. de Ladurantaye, S. Lee, S. Leung, E. L. Goode, S. J. Ramus, J. W. Carlson, X. Li, C. A. Ewanowich, L. E. Kelemen,

B. Vanderhyden, D. Provencher, D. Huntsman, C. H. Lee, C. B. Gilks and A. M. Mes Masson, *Int J Gynecol Pathol*, 2016, **35**, 430-441.
38. I. J. Letourneau, M. C. Quinn, L. L. Wang, L. Portelance, K. Y. Caceres, L. Cyr, N. Delvoye, L. Meunier, M. de Ladurantaye, Z. Shen, S. L. Arcand, P. N. Tonin, D. M. Provencher and A. M. Mes-Masson, *BMC Cancer*, 2012, **12**, 379.
39. V. Ouellet, M. Zietarska, L. Portelance, J. Lafontaine, J. Madore, M. L. Puiffe, S. L. Arcand, Z. Shen, J. Hebert, P. N. Tonin, D. M. Provencher and A. M. Mes-Masson, *BMC Cancer*, 2008, **8**, 152.
40. J. Tostain, G. Li, A. Gentil-Perret and M. Gigante, *Eur J Cancer*, 2010, **46**, 3141-3148.
41. S. Ivanov, S. Y. Liao, A. Ivanova, A. Danilkovitch-Miagkova, N. Tarasova, G. Weirich, M. J. Merrill, M. A. Proescholdt, E. H. Oldfield, J. Lee, J. Zavada, A. Waheed, W. Sly, M. I. Lerman and E. J. Stanbridge, *Am J Pathol*, 2001, **158**, 905-919.
42. S. E. Rademakers, P. N. Span, J. H. Kaanders, F. C. Sweep, A. J. van der Kogel and J. Bussink, *Mol Oncol*, 2008, **2**, 41-53.
43. L. Tomes, E. Emberley, Y. Niu, S. Troup, J. Pastorek, K. Strange, A. Harris and P. H. Watson, *Breast Cancer Res Treat*, 2003, **81**, 61-69.
44. I. Labouba, C. Le Page, L. Communal, T. Kristessen, X. You, B. Peant, V. Barres, P. O. Gannon, A. M. Mes-Masson and F. Saad, *PloS one*, 2015, **10**, e0131024.
45. W. T. Dempster, *Am J Anat*, 1960, **107**, 59-72.
46. C. H. Chen, M. Y. Hsu, R. S. Jiang, S. H. Wu, F. J. Chen and S. A. Liu, *J Chin Med Assoc*, 2012, **75**, 109-113.
47. M. J. Kerns, M. A. Darst, T. G. Olsen, M. Fenster, P. Hall and S. Grevey, *J Cutan Pathol*, 2008, **35**, 1093-1096.
48. P. L. Bedard, A. R. Hansen, M. J. Ratain and L. L. Siu, *Nature*, 2013, **501**, 355-364.
49. B. Peant, J. S. Diallo, L. Lessard, N. Delvoye, C. Le Page, F. Saad and A. M. Mes-Masson, *Mol Cancer Res*, 2007, **5**, 87-94.
50. M. Karin and Y. Ben-Neriah, *Annu Rev Immunol*, 2000, **18**, 621-663.
51. F. Marques-Fernandez, L. Planells-Ferrer, R. Gozzelino, K. M. Galenkamp, S. Reix, N. Llecha-Cano, J. Lopez-Soriano, V. J. Yuste, R. S. Moubarak and J. X. Comella, *Cell Death Dis*, 2013, **4**, e493.
52. I. C. McLean, L. A. Schwerdtfeger, S. A. Tobet and C. S. Henry, *Lab on chip*, 2018, DOI: 10.1039/C8LC00241J.
53. F. Rodier, J. P. Coppe, C. K. Patil, W. A. Hoeijmakers, D. P. Munoz, S. R. Raza, A. Freund, E. Campeau, A. R. Davalos and J. Campisi, *Nat Cell Biol*, 2009, **11**, 973-979.
54. A. Schepers, C. Li, A. Chhabra, B. T. Seney and S. Bhatia, *Lab Chip*, 2016, **16**, 2644-2653.
55. K. Chung, Y. Kim, J. S. Kanodia, E. Gong, S. Y. Shvartsman and H. Lu, *Nat Methods*, 2011, **8**, 171-176.
56. B. C. Kraemer, B. Zhang, J. B. Leverenz, J. H. Thomas, J. Q. Trojanowski and G. D. Schellenberg, *Proceedings of the National Academy of Sciences of the United States of America*, 2003, **100**, 9980-9985.

2.1.2.10 Supplemental Tables and Figures

Supplementary Table 1: Description of the parameters defined for COMSOL simulations to characterize the rinsing process in the device.

Parameter	Value	Reference
Geometry		
Channel Height	0.9 mm	-
Channel Width	1.1 mm	-
Well Height	800 μm	-
Well Width	800 μm	-
Channel length	51 cm	-
Distance between wells	4 mm	-
Diffusion parameter		
Diffusion of ethanol in water	1.24×10^{-5} cm^2/sec	(Hills 2011)
Diffusion of glucose in water	9.6×10^{-6} cm^2/sec	(Suhaimi 2015)
Diffusion of paclitaxel in water	4.2×10^{-6} cm^2/sec	(Cremasco 2012)
Physical parameter		
Water density at 37°C	993.3 kg/m^3	(Kestin 1978)
Water viscosity at 37°C	0.692 mPa s	(Kestin 1978)

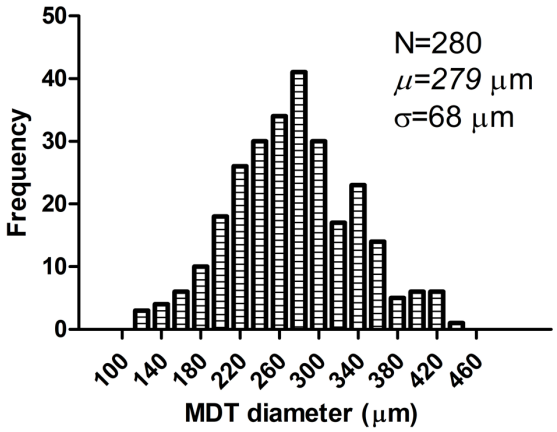

Supplementary Figure 1: Histogram of average diameter of fixed MDTs. The diameter distribution of 280 MDTs; average: μ = 297 μm, standard deviation: σ = 68 μm

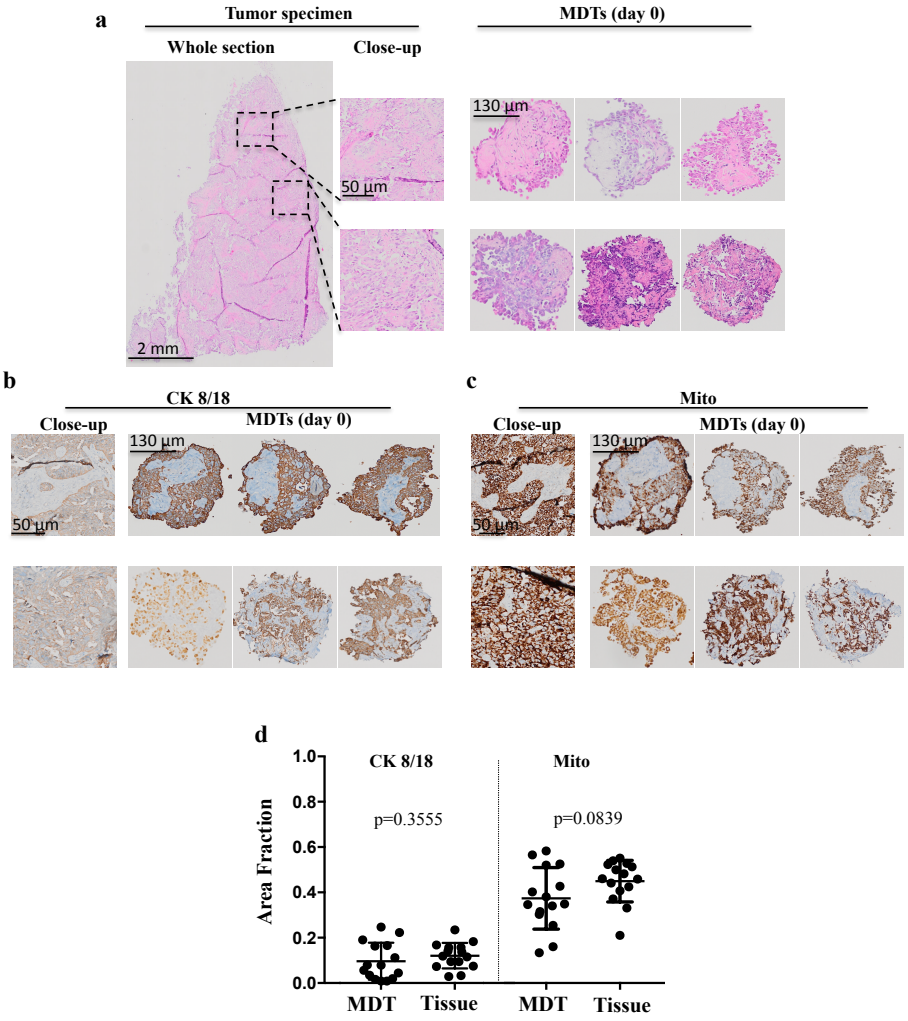

Supplementary Figure 2: Representation of heterogeneous compartmentalization of an EOC primary tumor. **a,** EOC cell line xenograft represented as primary tumor whole tissue, magnified tissue section, and MDTs stained with H&E. **b,** Corresponding magnified primary tumor tissue section and MDTs stained with the epithelial cell marker (CK 8/18) or **c,** human Mito distinguishing between human epithelial cells and infiltrating mouse-stromal cells (negative staining). **d,** IHC scoring of 15 magnified primary tumor regions (250 x 250 µm field of view) and 15 MDTs chosen at random. All experiments were done using the same xenograft as starting material, error bar = ± SEM. $p > 0.05$.

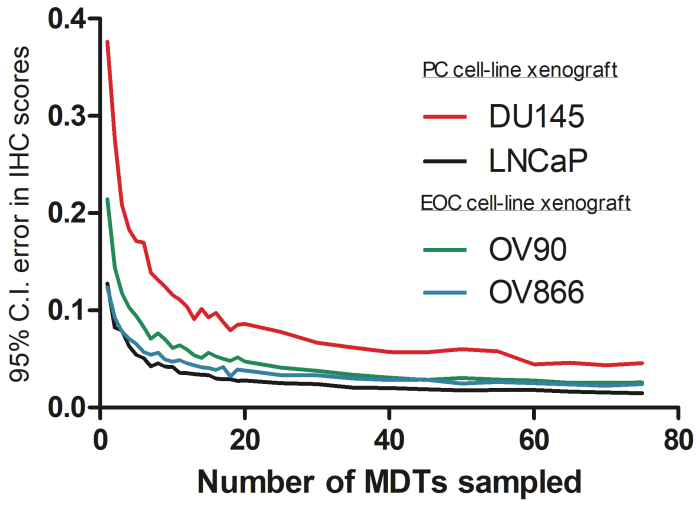

Supplementary Figure 3: **Monte-Carlo simulation of the sampling process.** 95% Confidence interval for the distribution of IHC scores when sampling different number of MDTs.

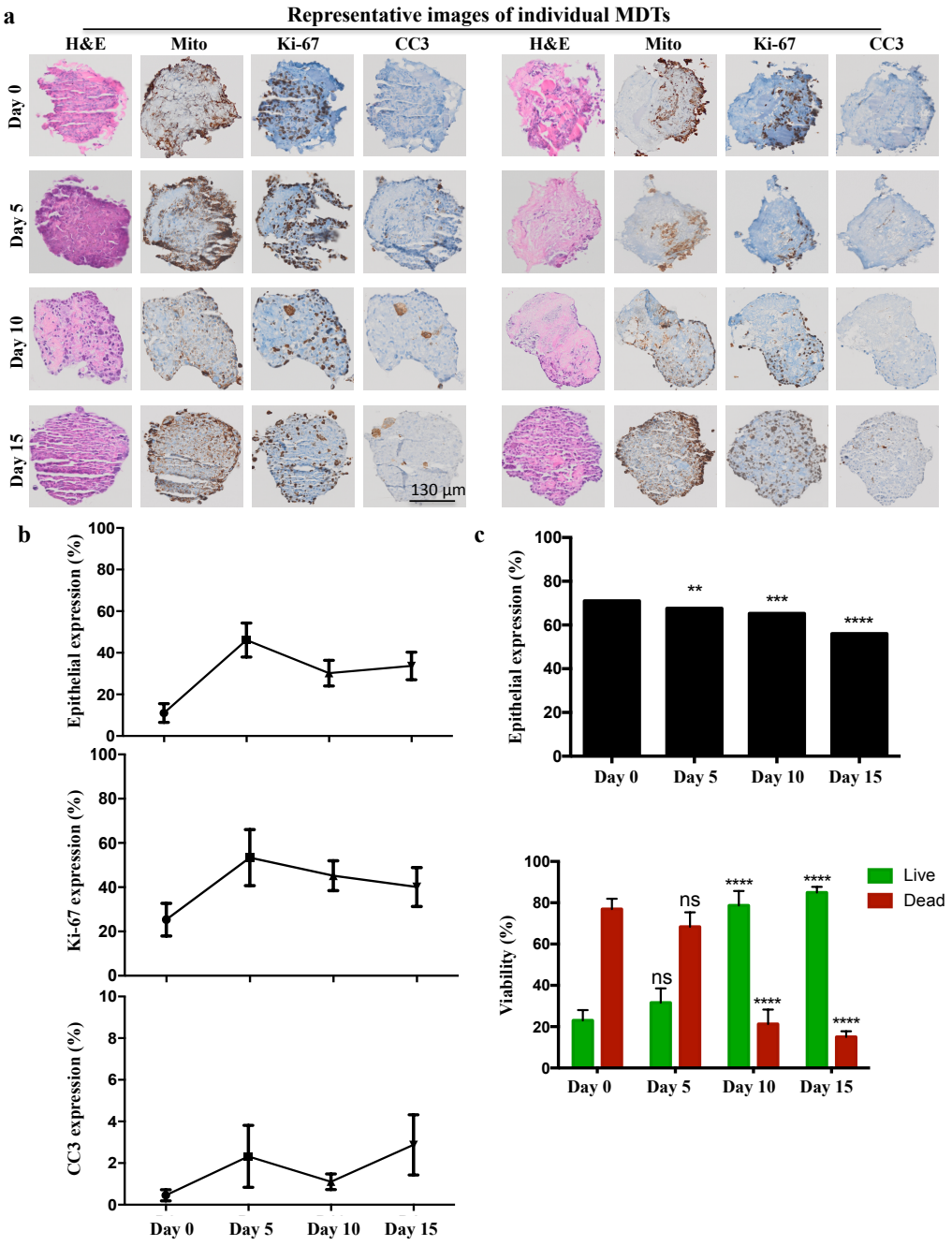

Supplementary Figure 4: Maintenance of the MDT viability over a 15-day culture period using a PC cell line xenograft model. a, Representative images of individual PC derived MDTs at different time-points (day 0, 5, 10, 15) stained with H&E, Mito, cell proliferative (Ki-67) and cell apoptosis (cleaved caspase-3; CC3) biomarkers. **b,** IHC scoring of MDTs showing stable epithelial expression and sustained proliferation over the 15-day period (n=15/time-point). **c,** FACs analysis of MDTs at Day 0, 5, 10,15 stained with Mito, Annexin V (detection of early apoptosis) and DRAQ7 (detection of dead cells) for epithelial cell expression and tissue viability assessment (n=45 MDTs). All experiments were done using the same xenograft as starting material. Error bar = ± SEM. *p<0.05, ***p<0.0001.

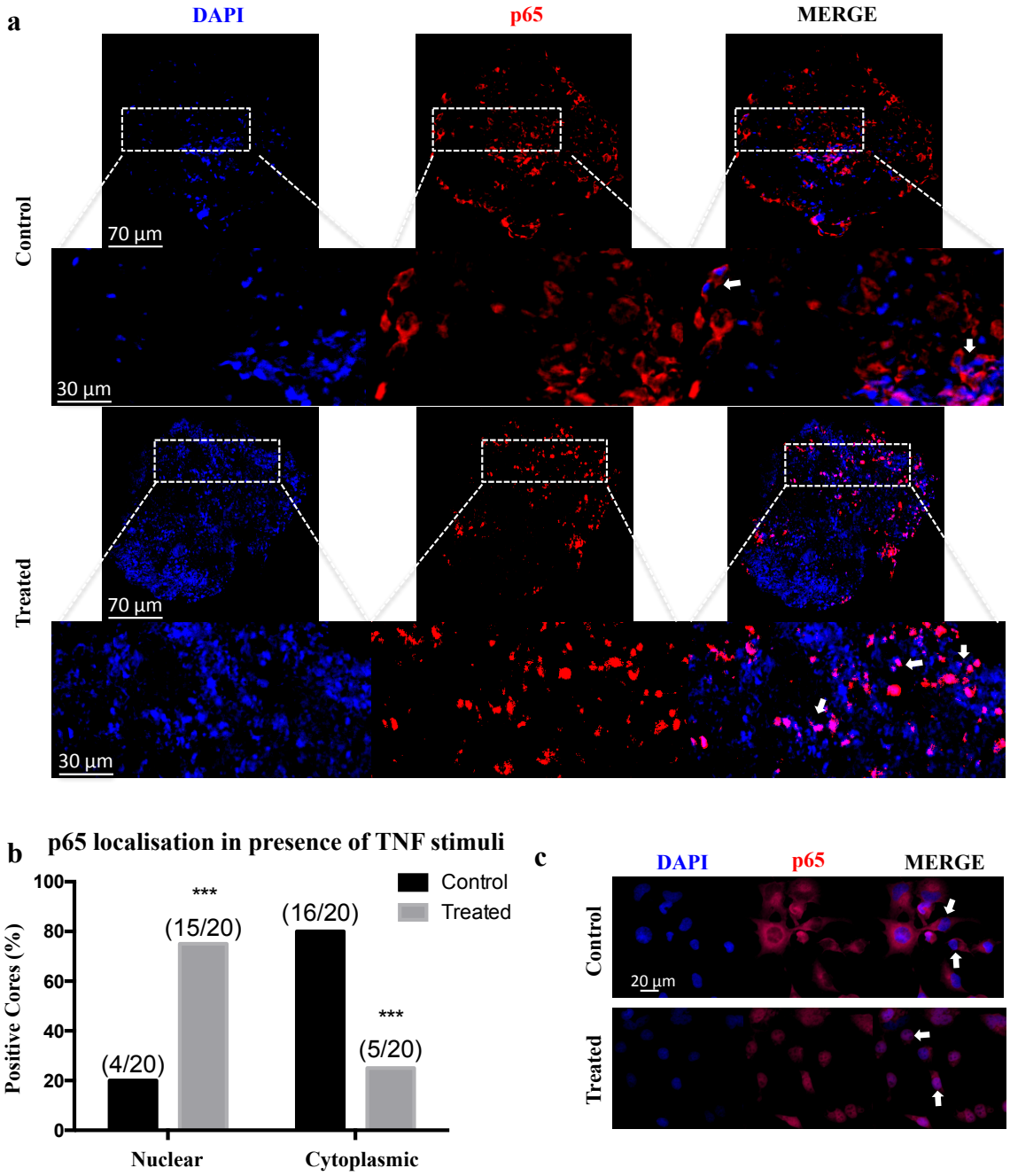

Supplementary Figure 5: EOC cell line MDTs treated with TNF-α showing p65 nuclear translocation. MDTs produced from EOC cell line xenograft tumors (n=20 MDTs/condition) were treated with either OSE media or TNF-α at a concentration of 10 ng/mL for 30 minutes. **a,** The MDTs were fixed using the PEL technique and stained with p65 antibody using IF (DAPI in blue and p65 in red). Arrows indicate cells within MDT cores as positive when p65 staining was located in nucleus. **b,** Quantification of IF p65 localisation in controls and following TNF stimulation. All experiments were done using the same xenograft as starting material. *p<0.05. **c,** Immunocytochemistry (DAPI, p65) of EOC cell line treated with either OSE or TNF-α at a concentration of 10 ng/mL for 10 min. N=2.

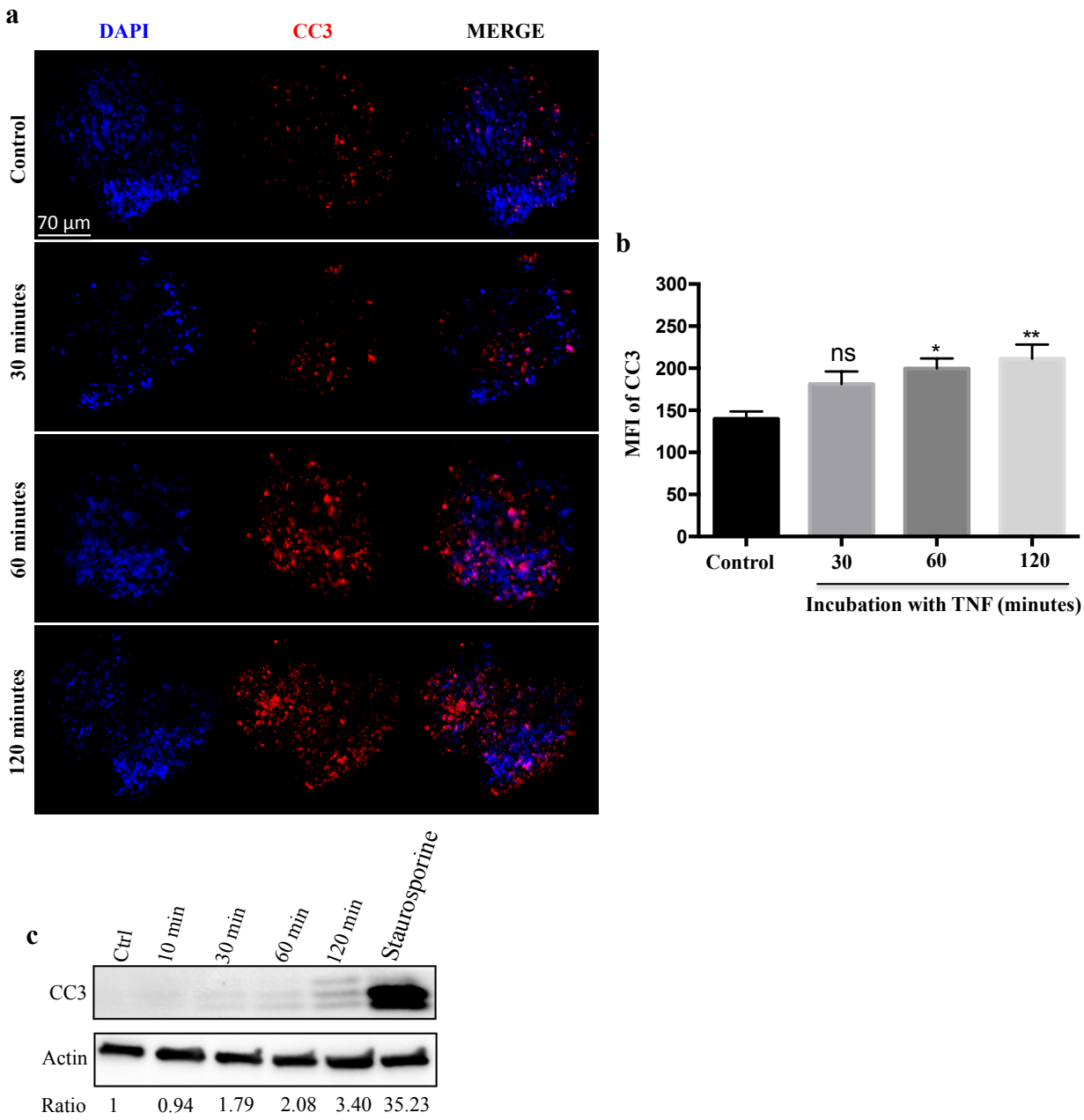

Supplementary Figure 6: Caspase-3 activation induced by over induction of TNF-α stimulator. MDTs produced from EOC cell line xenograft tumor treated with either OSE media or TNF-α at a concentration of 10 ng/mL for 0, 30, 60 and 120 minutes. **a,** MDTs were fixed and stained with cleaved caspase-3 antibody using IF (Dapi in blue and CC3 in red) (n=20 MDTs/condition). **b,** IF analysis of overall caspase-3 activation. All experiments were done using the same xenograft as starting material. *p<0.05, **p<0.001. **c,** Western blot of EOC cell line treated with TNF-α at a concentration of 10 ng/mL for 0, 10, 30, 60, 120 minutes. Staurosporine was added as a positive control. N=2.

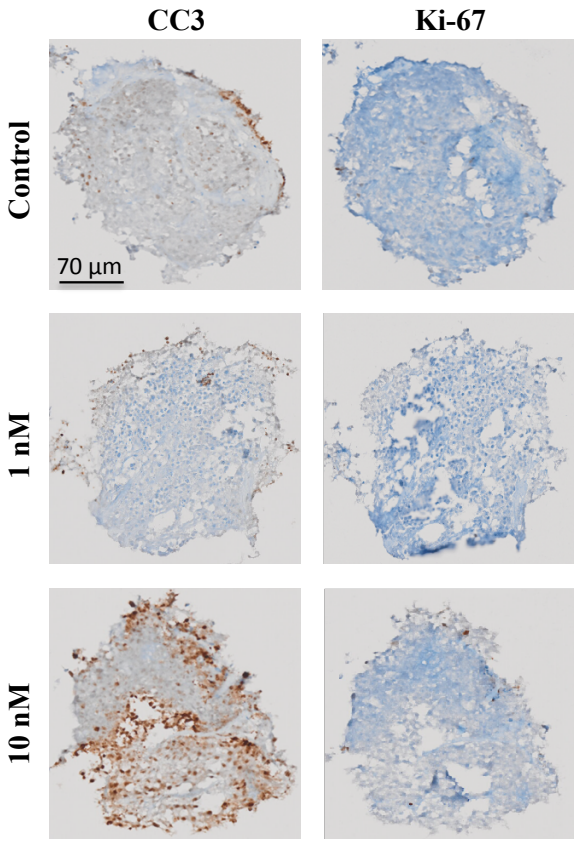

Supplementary Figure 7: IHC of dose-response analysis in PC cell line xenograft MDTs. MDTs were treated with two concentrations (1, 10 nM) of docetaxel (IC_{50} = 1 nM) for 12 hours at day 3. MDTs were fixed and analyzed after 12 hours of recovery period. IHC staining of cleaved caspase-3 (CC3) and Ki-67 to monitor apoptosis and cell proliferation respectively. All experiments were done using the same xenograft as starting material.

2.2 Chapter 2: Carboplatin Response in Preclinical Models for Epithelial Ovarian Cancer: Comparison of 2D Monolayers, 3D Spheroids, *Ex Vivo* Tumors And *In Vivo* Models

2.2.1 Article 2: Résumé en français

Titre en français: Réponse au carboplatine dans des modèles précliniques de cancer de l'ovaire : comparaison de culture en monocouches 2D, de sphéroïdes, de tumeurs *ex vivo* et de modèles *in vivo*.

Le cancer épithélial de l'ovaire (COE) est le cancer gynécologique le plus meurtrier. L'un des principaux défis à relever pour mettre au point des thérapies efficaces est d'améliorer les modèles précliniques utilisés dans la filière de découverte des médicaments, dans laquelle les taux d'abandon de molécules et les coûts des médicaments atteignent des niveaux critiques. Des travaux antérieurs ont mis en évidence les divergences de réponse thérapeutique entre les modèles *in vitro* et *in vivo* actuels. Pour y remédier, nous avons mené une étude comparative afin de différencier la réponse à la chimiothérapie au carboplatine dans quatre systèmes de modèles cellulaires différents des monocouches en 2D, des sphéroïdes en 3D, des tumeurs *ex vivo* en 3D et des modèles de xénogreffe de souris. Nous avons utilisé six lignées cellulaires CEO caractérisées précédemment et présentant une chimiosensibilité variable, et nous avons effectué des tests de viabilité pour chaque modèle. Les résultats *in vivo* du modèle de souris étaient en corrélation avec la réponse 2D dans 3/6 lignées cellulaires, tandis qu'ils étaient en corrélation avec les sphéroïdes 3D et le modèle *ex vivo* dans 4/6 et 5/5 lignées cellulaires, respectivement. Nos résultats soulignent la variabilité de la réponse thérapeutique d'un modèle à l'autre et démontrent que la réponse au carboplatine dans les lignées cellulaires CEO cultivées dans un modèle 3D *ex vivo* présente la meilleure corrélation avec la réponse *in vivo*. Ces résultats mettent en évidence un modèle préclinique plus réalisable, plus fiable et plus rentable, avec un meilleur potentiel d'application pour le criblage de médicaments et les études de prédiction dans le CEO.

2.2.2 Article 2: Original version published in Scientific Reports

Scientific Reports. 2021 Aug; DOI: 10.1038/s41598-021-97434-w

Carboplatin response in preclinical models for ovarian cancer: comparison of 2D monolayers, spheroids, *ex vivo* tumors and *in vivo* models

Melica Nourmoussavi Brodeur[1]*, Kayla Simeone[1]*, Kim Leclerc-Deslauniers[1], Hubert Fleury[1], Euridice Carmona[1], Diane M. Provencher[1,2], Anne-Marie Mes-Masson[1,3]

[1] Centre de recherche du Centre hospitalier de l'Université de Montréal (CRCHUM) and Institut du cancer de Montréal (ICM), Montreal, Quebec, Canada

[2] Division of Gynecologic Oncology, Université de Montréal, Montreal, Quebec, Canada

[3] Department of Medicine, Université de Montréal, Montreal, Quebec, Canada

*Theses authors contributed equally

Corresponding author: Anne-Marie Mes-Masson, CRCHUM, 900 Saint-Denis, Montreal, Quebec, Canada, H2X0A9 Phone: 514-890-8000 ext. 25496. Fax: 514-412-7703. Email: anne-marie.mes-masson@umontreal.ca

Keywords: ovarian cancer preclinical models, mouse xenografts, spheroids, *ex vivo* models, carboplatin

2.2.2.1 Abstract

Epithelial ovarian cancer (EOC) is the most lethal gynecological cancer. Among the key challenges in developing effective therapeutics is the poor translation of preclinical models used in the drug discovery pipeline, which leaves drug attrition rates and costs at an unacceptably high level. Previous work has highlighted the discrepancies in therapeutic response between current *in vitro* and *in vivo* models. To address this, we conducted a comparison study to differentiate the carboplatin chemotherapy response across four different model systems including 2D monolayers, 3D spheroids, 3D *ex vivo* tumors and mouse xenograft models. We used six previously characterized EOC cell lines of varying chemosensitivity and performed viability assays for each model. *In vivo* results from the mouse model correlated with 2D response in 3/6 cell lines while they correlated with 3D spheroids and the *ex vivo* model in 4/6 and 5/5 cell lines, respectively. Our results emphasize the variability in therapeutic response across models and demonstrate that the carboplatin response in EOC cell lines cultured in a 3D *ex vivo* model correlates best with the *in vivo* response. These results highlight a more feasible, reliable, and cost-effective preclinical model with the highest translational potential for drug screening and prediction studies in EOC.

2.2.2.2 Introduction

Epithelial ovarian carcinoma (EOC) is the most lethal gynecological cancer. In 2019, 22,530 women were diagnosed with EOC in the United States and 13,980 died of the disease[1]. Most women are diagnosed at late metastatic stages III-IV, for which only 30.2% will survive 5 years after diagnosis[2]. Although these patients initially respond to first-line treatment (combination of cytoreductive surgery and platinum-based chemotherapy), most patients will eventually recur and develop resistance[3]. Despite the appeal for personalized medicine, no biomarkers have been clinically accepted to accurately predict first-line therapeutic response. To date, carboplatin chemosensitivity remains the main predictor of EOC clinical prognosis[4].

Significant research efforts have been invested in the discovery of new cancer treatments, with limited focus on the actual experimental models used to test new agents[5]. The current drug discovery

pipeline is dependent on 2D cell culture model systems that are devoid of the inherent complexity of their original tumors, which are better captured by *in vivo* models. In particular, 2D cultures put into question the proper representation of tumor heterogeneity due to cell selective pressures and remain devoid of immune cells and a tumor microenvironment (TME) including the extracellular matrix (ECM), tumor cell-stromal cell interactions, and additional important components[6]. While 2D cell models remain as the primary method of *in vitro* preclinical testing, attrition rates of anti-cancer drugs continue to be high and EOC survival remains low. To address this, more reliable and practical preclinical models are needed to study drug response and putative biomarkers.

An ideal preclinical model for drug response has optimal physiologic relevance and downstream analysis compatibility, can be translated in a clinically relevant timeframe, and is affordable[7]. To bridge the gap between the shortcomings of 2D models and animal experimentation, there has been a shift to further develop 3D cell culture systems. Overall, 3D spheroids better mimic the structural cell-cell interactions and the chemical nutrient and oxygen gradients[5,8-10] featured in different cell layers: proliferative, quiescent, and necrotic[5,9-11]. In the setting of EOC, this model is particularly relevant given the physiologic development of ascites (abdominal fluid accumulation) that contain clusters of cells (spheroids)[12]. Additionally, tumor-derived *ex vivo* models may better mimic the tumor heterogeneity by preserving original TME characteristics, allowing the study of interactions with cancer-associated cells.

Our group recently showed that response to chemotherapy varies significantly from one *in vitro* model to another (2D and 3D) for the same cell line and that this variation did not follow the same trend across cell lines[13]. This calls into question the precision of EOC preclinical models, and it is currently unclear whether these *in vitro* models or an *ex vivo* model reliably reflects the *in vivo* gold standard response. To better understand the carboplatin response, we investigated two different *in vitro* systems (2D monolayers, 3D spheroids) and one *ex vivo* system (3D micro-dissected tumors[14]) and compared them to the *in vivo* therapeutic response (xenograft mouse model) (Fig. 1). Using a panel of six EOC cell lines, we show that previously characterized carboplatin response from 2D cultures differs significantly from the *in vivo* response of the xenograft mouse model. Furthermore, we find that our *ex vivo* 3D model correlates

reliably with the *in vivo* results. These findings highlight the variability in therapeutic response across model systems and the advantages of a cost-effective 3D *ex vivo* model for preclinical drug development and testing in EOC.

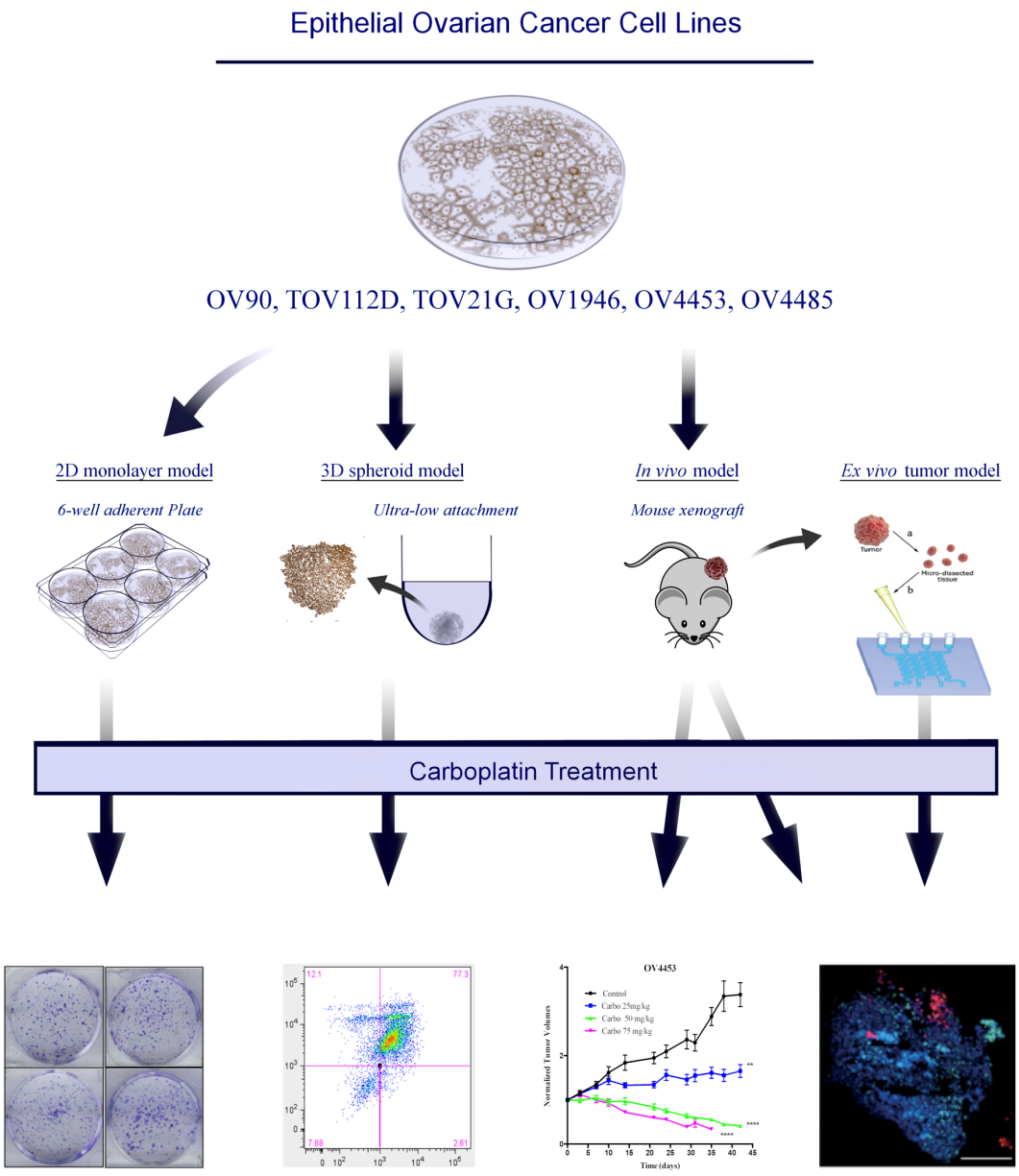

Figure 1. Schematic illustration of study design. Carboplatin chemotherapy response of six EOC cell lines was compared under different model systems: 2D monolayers, 3D spheroids, *ex vivo* MDTs of tumors, and *in vivo* xenograft mouse model. Using ultra-low attachment plates, 3D spheroids were treated and analyzed by flow cytometry. Cell lines were injected in immunodeficient mice for xenograft formation and analyzed for tumor volume curves and immunofluorescence. Control xenografts from five cell lines were used for *ex vivo* tumor generation and placed in microfluidics devices for treatment and analysis by immunofluorescence.

2.2.2.3 Methods

Cell lines

Six EOC cell lines were selected for their different carboplatin sensitivities (Supplementary Table S1) and their ability to form tumors in immunodeficient mice: OV90 (Cellosaurus ID: CVCL_3768), OV4485 (Cellosaurus ID: CVCL_9T21), OV4453 (Cellosaurus ID: CVCL_9T20), TOV21G (Cellosaurus ID: CVCL_3613), TOV112D (Cellosaurus ID: CVCL_3612) and OV1946 (Cellosaurus ID: CVCL_4375)[13, 15-19]. Cell lines originated from patient tumors (TOV) or ascites (OV). OV4485 and OV4453 are *BRCA1* and *BRCA2* mutated cell lines, respectively[16]. Cells were cultured in complete OSE medium (316-030-CL, Wisent Inc, Saint-Bruno, QC, Canada) supplemented with 10% fetal bovine serum (FBS, 088-150, Wisent), 2.5 ug/mL of amphotericin B (450-105-QL, Wisent) and 50 µg/mL of gentamicin (450-135, Wisent). Cells were cultured under conditions previously determined[15-17]. OV90, TOV21G, TOV112D and OV1946 cells were maintained at 21% O_2 and 5% CO_2 at 37°C. OV4485 and OV4453 were kept at 7% O_2 and 5% CO_2 at 37°C. Experiments were carried out with cells between passage 70 to 80 (at ~90% confluence). Mycoplasma testing and short tandem repeat (STR) analysis were performed for all cell lines.

Xenograft mouse model

All animal procedures were performed in accordance with the guidelines for the Care and Use of Laboratory Animals of the CRCHUM as well as the recommendations in the ARRIVE guidelines. This study was approved by the Comité institutionnel de protection des animaux (Animal Ethics Committee, protocol number C18028AMMs). NOD.Cg-Rag1^{tm1Mom}Il2rg^{tm1Wjl}/SzJ immunodeficient female mice (007799, The Jackson Laboratory-JAX, Bar-harbor, Maine, USA)[20,21] were used to establish xenograft tumors with cell lines. A 200 µL suspension of 1 x 10^6 cells in 100 µL cold Dulbecco's PBS (311-425-CL, Wisent) with 100 µL of Matrigel® Matrix (CACB356237, Corning Inc., NY, USA) was injected subcutaneously in the flank of each mouse for the TOV112D, TOV21G and OV90 cells, while 5 x 10^6 cells were injected for the OV1946, OV4453 and OV4485 cells. Eight mice were used for the control (vehicle)

group and for each of the three carboplatin treatment groups per cell line (see section Carboplatin treatment). Treatment was initiated once tumor size was 200 mm^3 as drug effects can vary if below this value[22]. Mice were between the ages of 11-24 weeks at the start of treatment and given dietary supplementation, DietGel® Recovery and DietGel® Boost (Clear H_2O, Portland, USA), twice weekly. Tumors were measured with calipers 2-3 times weekly. To alleviate the known negative side effects of carboplatin treatment, anti-nausea medications (1 mg/kg of maropitant and 0.8 mg/kg of ondansetron) were given one hour before the chemotherapy dose and at 24- and 48-hours following treatment. Mice were sacrificed at the end of treatment period or if ethical limits were attained through an intraperitoneal injection of euthanyl (pentobarbital sodium) at a dose of 400 mg/kg (concentration of 240 mg/ml). Tumors were collected, measured and were formalin-fixed and paraffin-embedded (FFPE). FFPE tumor blocks were cut into 4 µm sections for histological hematoxylin & eosin (H&E) staining.

3D spheroid formation

Rapid, compact and uniform homogenous formation of EOC spheroids was achieved by using 96-well concave-bottom, ultra-low attachment (ULA) microplates (4515/4520, Corning)[8,11,13,16,23]. For all cell lines, 2,000-2,500 cells in 100 µL of complete OSE medium were seeded in each well. Plates were centrifuged at 1,000 rpm for 5 minutes at room temperature. Spheroids were allowed to form over 48 hours in their respective incubation conditions (see Cell lines), generating spheroids of approximately 500 µm in diameter. Spheroids were treated with three carboplatin concentrations (based on optimized IC_{50} dose ranges; see Carboplatin treatment). For each cell line, 20 spheroids were seeded for each carboplatin concentration as well as control groups. Two replicates per condition, containing 10 spheroids for each replicate, were analyzed for each cell line by flow cytometry. In parallel, 10 untreated spheroids were transferred into microfluidic devices at 48 and 96 hours for fixation.

Micro-dissected tissue (MDT) production from cell line xenograft tumors

The micro-dissection procedure was adapted from previously published work[14,24]. Briefly, tumors were sliced into 1 cm thick sections by a scalpel and placed on the McIlwain™ tissue chopper to obtain 350 μm thick slices. Tumor slices were placed in Hank's balanced salt solution (HBSS, 311-516-CL, Wisent) supplemented with 10% FBS, 2.5 μg/mL of amphotericin B (Wisent) and 50 μg/mL of gentamicin (Wisent). A biopsy punch of 500 μm (PUN0500, Zivic Instruments, Pittsburgh, USA) pierced tumor slices to produce sphere-like MDTs, which were placed in HBSS supplemented with antibiotics without serum until the loading procedure. The loading, trapping, and culturing of MDTs were performed as described in our previous work[14].

Fixation of MDTs and spheroids within microfluidic devices

MDTs were fixed with 10% formalin (F6050, Produits Chimiques A.C.P. Chemicals Inc, Saint-Leonard, Qc, Canada) after carboplatin treatment and recovery periods, including respective controls. Untreated spheroids were similarly fixed after 48 and 96 hours of formation. All specimens were further processed through the previously published paraffin-embedding lithography procedure to create micro-dissected tissue microarray (MDTMA) blocks[14], which were cut into 4 μm sections for histological H&E staining. Specimen sizes shrink after this processing technique as previously reported[14].

Carboplatin treatment

Xenograft mouse model

Based on pilot toxicity studies, carboplatin (Hospira Healthcare Corporation, Saint-Laurent, QC) treatment in the xenograft models was given once weekly by intraperitoneal (IP) injections at either 25, 50, and 75 mg/kg for up to six cycles. The carboplatin vehicle, 0.9% NaCl solution, was used for controls.

3D spheroid model

Optimization studies with spheroids determined the carboplatin treatment range. Thereafter, spheroids were treated by adding 100 µL of three different concentrations of carboplatin (within 0 to 3000 µM final in-well concentration), whereas the control received 100 µL of complete OSE medium. Spheroids were treated for 24 hours followed by a 24-hour recovery period, based on literature suggesting that 24 hours of drug exposure is required to penetrate the spheroid[25-27]. A 24-hour recovery was chosen based on published *in vitro* studies demonstrating the effect of chemotherapy only after its removal[27,28] and to mimic the physiologic metabolism of the drug. The optimal concentration range was determined for each cell line for minimal growth inhibition and for an effect well below the 50% threshold.

3D ex vivo tumor model

MDTs obtained from untreated xenograft tumors of our cell lines were treated with 6-7 different carboplatin concentrations based on the IC_{50} values from monolayers and 3D spheroids. Two carboplatin regimens were tested for MDTs: a 10-hour treatment induction followed by a 14-hour recovery, and a 16-hour induction followed by a 24-hour recovery.

Clonogenic survival assay

The IC_{50} values for carboplatin for OV4453, OV4485, TOV112D and OV90 were previously determined by clonogenic survival assay[13,16,19]. Carboplatin sensitivity for the OV1946 and TOV21G cell lines was determined in this study using the same clonogenic assay[16]. Briefly, cells were seeded in a 6-well plate at a volume of 1mL/well and at a density that allowed the formation of individual colonies (1,000 or 1,500 cells/well for TOV21G or OV1946, respectively). Cells were allowed to adhere for 16 hours in 5% CO_2 at 37°C. Then an additional 1mL of medium containing carboplatin (final concentrations 0–100 µM) was added in each well and cells were incubated for 24 hours. After this period, medium was completely removed and replaced with fresh OSE complete medium. When colonies became visible at 2X magnification, plates were fixed with cold methanol and stained with a solution of 0.5% blue methylene

(Sigma–Aldrich Inc., St. Louis, MO) in 50% methanol. Colonies were counted under a stereomicroscope and reported as percent of control. IC_{50} values were determined using Graph Pad Prism 6 (GraphPad Software Inc., San Diego, CA). Each individual experiment was performed in duplicate and repeated three times.

Flow cytometry analysis of 3D spheroids

After treatment and recovery, 10 spheroids (one replicate) were pooled per condition and dissociated with trypsin-EDTA (0.05%) for 30-45 seconds to obtain single-cell suspensions. Two replicates were done per experiment. Single cells were labelled using the LIVE-DEAD^{TM} Fixable Aqua Dead Cell Stain Kit (Thermofisher, Massachusetts, USA) stain at 1:100 dilution. After an incubation of 15 minutes at room temperature, stained cells were analyzed by flow cytometer, LSR-Fortessa (BD Biosciences, Mississauga, ON), using 405 nm excitation, and fluorescence emission was monitored at 525 nm. Data were analyzed using FlowJo (FlowJo LLC, Ashland, USA), identifying dead cells (stained) and live cells (non-stained). Normalized live and dead cell rates were plotted using GraphPad Prism 6 (GraphPad Software Inc.) to generate dose-response inhibition curves with respective IC_{50} values. Each experimental analysis was performed in duplicate and repeated three times.

Immunofluorescence (IF) and immunohistochemistry (IHC)

FFPE xenograft blocks were cut into 4 µm sections and placed on Fisherbrand superfrost plus microscope slides (Fisherbrand, Ottawa, Ontario). MDTMA blocks (MDT and spheroids) were sliced into 4 µm thick slices and placed on Matsunami TOMO® hydrophilic adhesion slides (VWR, Mont-Royal, QC, Canada). Treatment response in xenograft and MDT experiments was assessed by IF, and viability in untreated spheroids was assessed by IHC. Anti-Ki-67 antibody (cell proliferation) and DAPI (nuclei detection) were used for xenografts and MDTs. Anti-human mitochondria and anti-cytokeratin 8/18 (human epithelial cancer cells) antibodies were additionally used for MDTs. Lastly, antibodies for IHC in spheroid experiments included anti-Ki-67 and anti-cleaved caspase-3 (CC3, apoptosis).

IF/IHC slides were stained using the BenchMark XT automated stainer [Ventana Medical System Inc. (VMSI), Tucson, AZ]. TOMO slides were incubated at 60˚C for 20 minutes before staining. For IF staining, antigen retrieval was carried out with Cell Conditioning 1 solution (VMSI) for 60 minutes. Mouse anti-Ki-67 (1:500) antibody (9449, Cell Signaling Technology, Massachusetts, USA), mouse anti-CK8 (1:200) antibody (MA514428, Lab Vision, Sweden), mouse anti-CK18 (1:200) antibody (6259, SantaCruz, California, USA), and mouse anti-human mitochondria (1:2500) antibody (ab92824, Abcam, Cambridge, UK) were automatically dispensed. Slides were incubated at 37°C for 60 minutes. Secondary antibodies (dilution 1:250) including Alexa 488 (A11001, Life Technologies, CA, USA) and TRITC (A11030, Life Technologies) were added at room temperature. For IHC staining, antigen retrieval was carried out automatically with Cell Conditioning 1 solution for 30 minutes (CC3) and 60 minutes (Ki-67). Rabbit anti-CC3 (1:200) antibody (9661, Cell Signalling Technology) and mouse ant-Ki-67 (1:500) were automatically dispensed followed by horseradish peroxidase secondary antibody. Counterstaining was achieved with hematoxylin and bluing reagent (VMSI). All sections were scanned with an Olympus BX61 microscope using 20 x 0.75 NA objective with a resolution of 0.3225 μm (Bx61vs, Olympus, Toronto, Ontario).

IF Quantification

Stained tumor sections were quantified using VisiomorphDP software version 2020.08 (VisioPharm, Denmark, http://visiopharm.com).

Xenograft experiments

IF filters for DAPI and anti-Ki-67 were DAPI and TRITC, respectively. IF quantification of Ki-67 was calculated as a ratio of the total area of Ki-67 positive cells over the detected tissue core area.

MDT experiments

IF filters used for DAPI, epithelial cancer cells, and anti-Ki-67 were DAPI, Alexa-488 and TRITC, respectively. Treatment response was quantified as follows: 1) detection of core surface area through DAPI, 2) detection and calculation of total epithelial area within the core through Alexa-488, 3) identification of

nuclei of each epithelial cell and calculating total nuclei area through DAPI, and 4) identification of Ki-67 positive nuclei and calculating total positive area for each stain through TRITC.

Statistical analyses

Values are expressed as the means ± standard error of the mean (SEM) from at least three independent experiments in the case of 3D spheroids. We used eight tumors per condition per cell line for the xenograft model and 15 MDTs per condition per cell line. Comparison between multiple groups (different carboplatin concentrations) was determined by one-way ANOVA comparison test. The IC_{50} of 3D models was calculated by transforming all concentrations into logarithms, normalizing the response, and performing nonlinear regression analysis (dose-response inhibition equation – variable slope). *P* values <0.05 were considered significant. All statistical analyses were done using GraphPad Prism version 6 (GraphPad Software Inc., http://graphpad.com).

2.2.2.4 Results

Carboplatin sensitivity of 2D EOC cell cultures differs from the *in vivo* response

The selected EOC cell lines have been extensively characterized[13,15-19] and represent the diverse range of EOC subtypes (dedifferentiated = TOV112D; clear cell = TOV21G; and high-grade serous = OV90, OV1946, OV4453, OV4485) and response to carboplatin treatment (Supplementary Table S1). Based on clonogenic assays, these EOC cell lines have been classified according to pre-determined cut-offs: carboplatin sensitive cell lines in 2D cultures have IC_{50} values below 1 μM (TOV21G and OV4453) and resistant cell lines have IC_{50} values above 10 μM (TOV112D and OV90). Cell lines with IC_{50} values in between are categorized as intermediate (OV1946 and OV4485). This same 2D carboplatin sensitivity criteria have been used previously by others[29].

Xenografts were generated from EOC cell lines and treated following the protocol depicted in Fig. 2A. Tumor volumes were recorded throughout carboplatin treatment (Fig. 2B). Chemosensitivity of each cell line was based on inhibition of *in vivo* tumor growth. OV1946 and OV4453 were categorized as

sensitive, demonstrating tumor volumes that were significantly lower than the controls at time of sacrifice for all three carboplatin doses (highly responsive). OV90 and OV4485 showed intermediate responses with a significant decrease in tumor volumes at the two highest doses but no response to the lower dose (partially responsive). TOV21G and TOV112D were resistant as they showed no statistical difference at even the highest dose (unresponsive). IF with Ki-67 was quantified from collected xenografts after carboplatin treatment (Fig. 2C) and showed that the response was dose- and cell-line dependent. Results were largely concordant with the tumor volume measurements, confirming chemosensitivity classification. However, treatment response in the xenograft model varied significantly from the 2D culture ranking (Supplementary Table S1); a positive correlation of 2D sensitivity with the *in vivo* response was found in 3/6 EOC cell lines (Table 1).

Table 1. Summary of carboplatin sensitivity of EOC cell lines across model systems

Cell lines	**2D monolayers**	**3D spheroids**	**3D MDTs**	**Xenograft**	***In vivo* correlation**
OV4453	Sensitive	Resistant	Sensitive	Sensitive	**2D + 3D MDTs**
TOV21G	Sensitive	Resistant	Resistant	Resistant	**3D spheroids/MDTs**
OV1946	Intermediate	Sensitive	Sensitive	Sensitive	**3D spheroids/MDTs**
OV4485	Intermediate	Resistant	Intermediate	Intermediate	**2D + 3D MDTs**
TOV112D	Resistant	Resistant	Resistant	Resistant	**2D + 3D spheroids/MDTs**
OV90	Resistant	Intermediate	Not performed	Intermediate	**3D spheroids**

MDTs = micro-dissected tissues

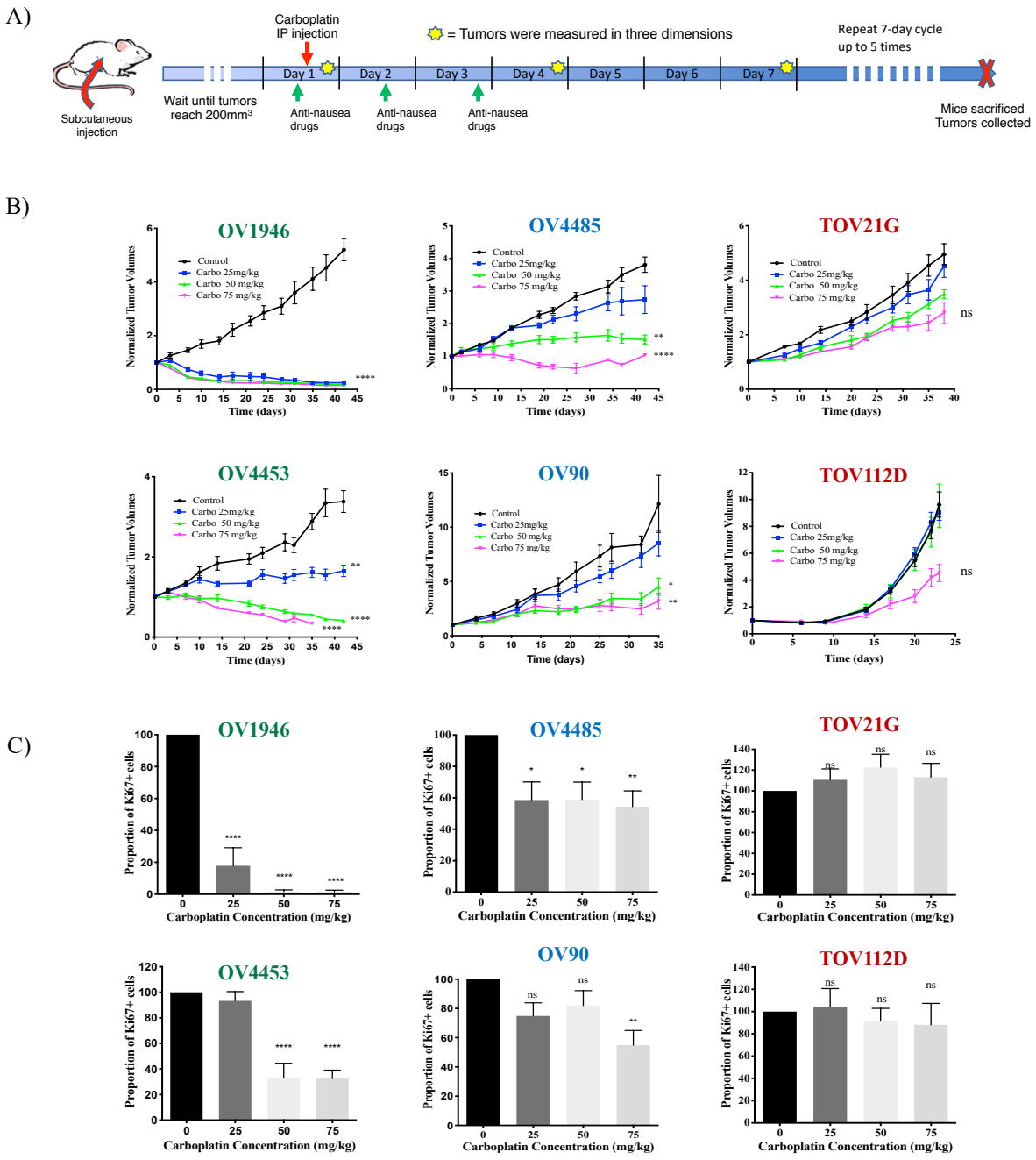

Figure 2. *In vivo* response of EOC xenografts to carboplatin treatment. (A) Timeline for weekly *in vivo* chemotherapy cycle in our xenograft mouse model. Carboplatin was delivered intraperitoneally (IP). (B) Volume measurements of xenograft tumors (N=8 per condition) throughout carboplatin treatment. (C) IF quantification of Ki-67 stain (normalized to control). Sensitive cell lines are indicated in green fonts, intermediate in blue and resistant in red. Data are the mean± SEM. ns = non-significant. *$p < 0.05$, **$p < 0.01$, ***$p < 0.001$, ****$p < 0.0001$.

Carboplatin response of 3D EOC spheroids improves the correlation with the *in vivo* response compared to 2D cultures

All six EOC cell lines formed 3D spheroids in ULA plates. OV90 and OV1946 formed compact spheroids (Fig. 3A), whereas TOV112D, TOV21G, OV4485 and OV4453 formed dense aggregates (Fig. 3B). To demonstrate that cells in the spheroids remained proliferative throughout the experiment, we performed IHC staining to evaluate the level of apoptotic (CC3) and proliferative cells (Ki-67) in spheroids at 48 hours (time of spheroid formation) and at 96 hours (end of experiment) in the untreated controls (Supplementary Fig. S1). Cells in the spheroids stained strongly for Ki-67 at both time-points with low expression of CC3, demonstrating that they remained proliferative throughout the treatment course.

Flow cytometry was used to evaluate the proportion of viable cells in spheroids after carboplatin treatment (Fig. 3C). IC_{50} values were generated using dose-response inhibition analyses (Fig. 3D). In all cell lines, the 3D spheroid IC_{50} values were significantly higher than that seen in 2D models (Supplementary Table S1). However, the fold change in carboplatin sensitivity between 3D and 2D models varied significantly, depending on the cell line (Supplementary Table S2). The change from 2D to 3D models increased the IC_{50} value by 280-fold for TOV21G, but only 7-fold for OV90, highlighting cell line-dependent changes. Cut-off for resistance to carboplatin treatment was based on response to the physiologic conversion of carboplatin bioavailability (269.4 μM, rounded to 250 μM) in patients (carboplatin dosing of an AUC of 5 corresponding to an average concentration of 300 mg/m^2, body surface area 1.6 m^2, blood volume 4.8 L)[30]. Therefore, cell lines with IC_{50} values higher than 250 μM were considered resistant. On the other hand, response to doses below 100 μM were considered sensitive based on previous reports of carboplatin treatment of 3D ovarian cancer models[31,32]. Response between the two cut-offs were considered intermediate. Using these criteria, OV1946 was categorized as sensitive, OV90 as intermediate, and TOV21G, TOV112D, OV4453 and OV4485 as resistant. These results show a positive correlation with the *in vivo* response for 4/6 EOC cell lines (Table 1).

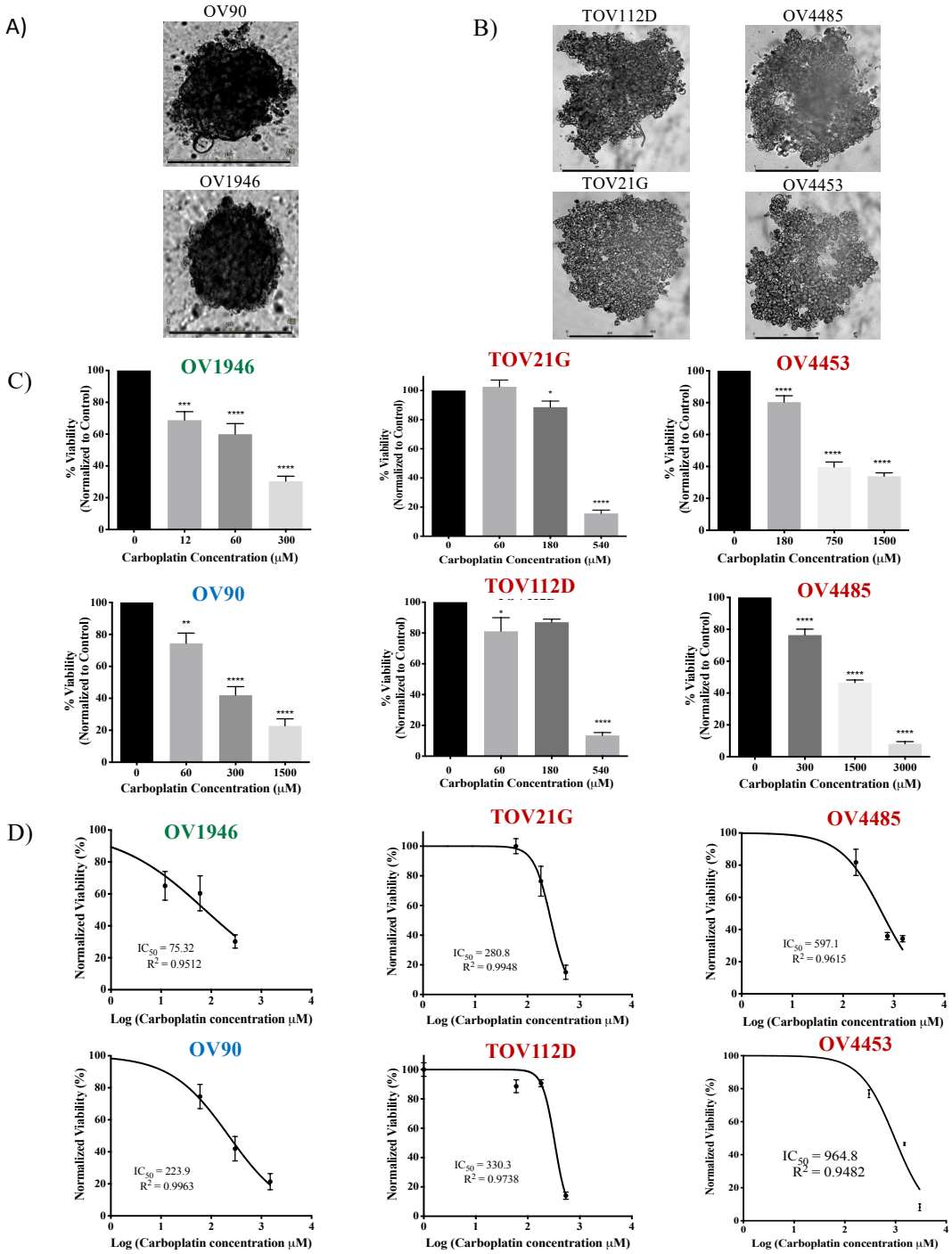

Figure 3. Carboplatin response of EOC 3D spheroids. Representative pictures of EOC cell lines forming at 48 hours (**A)** compact spheroids or (**B)** dense aggregates. (**C)** Normalized viability of spheroids after a 24-hour carboplatin treatment with a 24-hour recovery. (**D)** Dose-inhibition response curves with their corresponding IC_{50}. Sensitive cell lines are indicated in green fonts, intermediate in blue and resistant in red. Data are the mean ± SEM of three independent experiments, two replicates per condition. Scale bar on images (A, B) = 400 µm, $*p < 0.05$, $**p < 0.01$, $***p < 0.001$, $****p < 0.0001$.

The 3D *ex vivo* tumor model demonstrates a reliable correlation with the *in vivo* carboplatin response

Previous studies have shown that MDTs can assess the response to chemotherapeutic drugs in cell line xenograft models[14,24]. Here, we sought to compare the carboplatin sensitivity profiles of cell line xenograft tumor-derived MDTs (Supplementary Fig. S2A) to our ovarian cancer model systems including 3D spheroids and *in vivo* xenografts using IF analysis (Fig. 4A). The OV90 cell line was excluded for *ex vivo* analysis due to an insufficient level of cancer cells present in the xenograft tumor precluding the generation of statistically significant results. We first tested two different treatment regimens of carboplatin in our MDTs using OV1946, OV4453 and TOV21G cell lines. This included a 10-hour treatment induction followed by a 14-hour recovery period (10-14) (Supplementary Figure S2B-D), and a 16-hour treatment induction followed by a 24-hour recovery period (16-24) (Fig. 4B-C, Supplementary Fig. S2B). Both treatment regimens gave similar cell fate responses (proliferation, apoptosis) as well as similar IC_{50} (Supplementary Fig. S2C and S2D, and Fig. 4C). Based on these results, we used the 16-24 treatment regimen to perform the remaining experiments. To compare the chemosensitivity of cell line-based MDTs to 3D spheroids and the *in vivo* model, we quantified the proliferation capacity of cells after carboplatin treatments (Fig. 4B) and determined IC_{50} values (Fig. 4C). According to our criteria for 3D spheroids, OV1946 and OV4453 were categorized as sensitive (IC_{50} < 100 μM), TOV21G and TOV112D were resistant (IC_{50} > 250 μM), and OV4485 was intermediate. These findings were in complete agreement with the *in vivo* chemosensitivity results (5/5 EOC cell lines) and provided the best correlation compared to the other two *in vitro* models (Table 1).

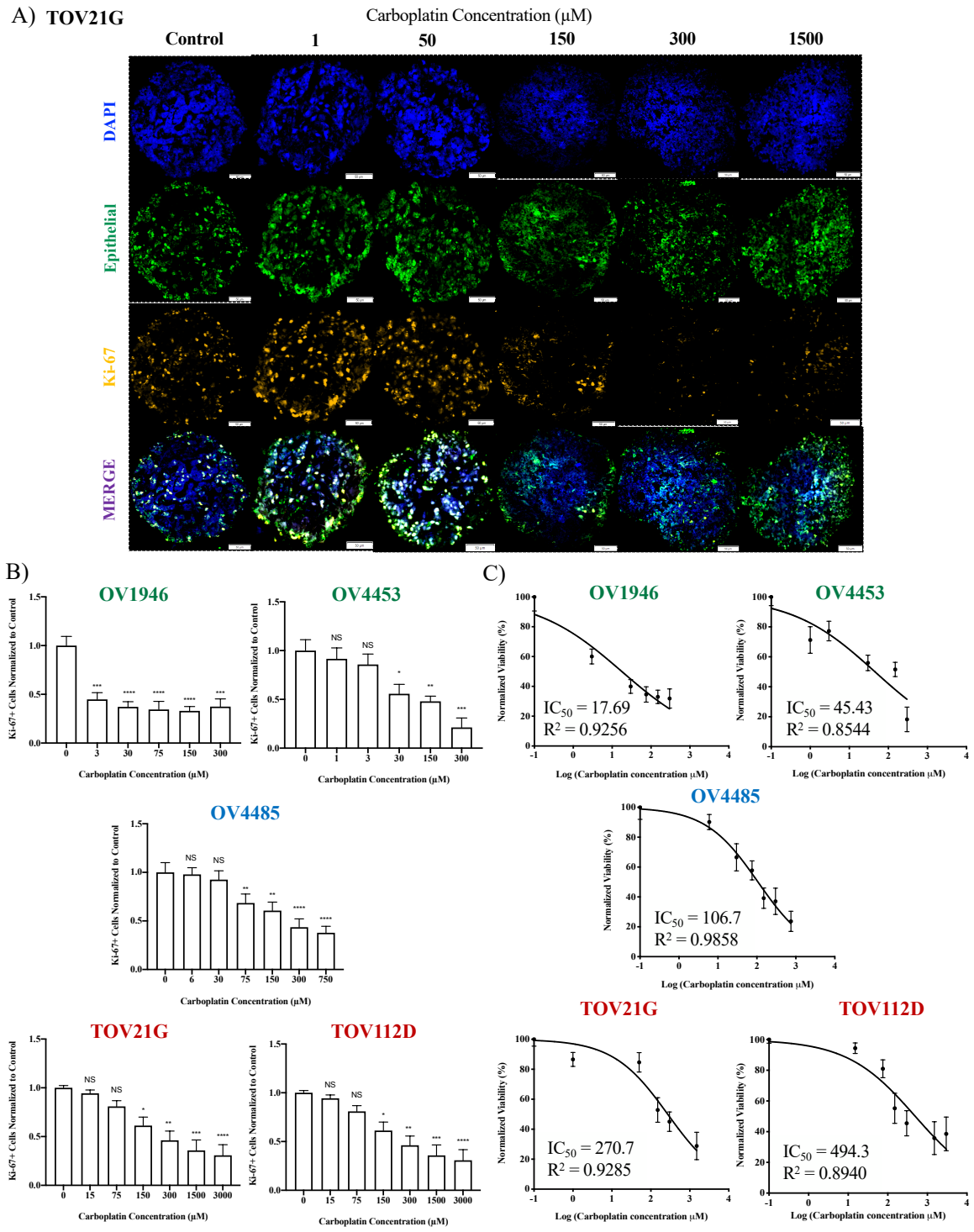

Figure 4. Response of EOC 3D *ex vivo* tumor model to carboplatin. MDTs derived from several cell line xenograft tumors (OV1946, OV4453, OV4485, TOV21G and TOV112D) were treated with carboplatin at various concentrations (µM) for a 16-hour induction followed by a 24-hour recovery treatment regimen. (**A)** Representative IF staining for DAPI, mitochondria and cytokeratin 8/18 (human epithelial cancer cells) and Ki-67 of treated TOV21G MDTs. (**B)** Proliferation index, bar graphs are Ki-67 staining normalized to control for each cell line. (**C)** Dose-inhibition curves

showing IC_{50} of each cell line. Sensitive cell lines are indicated in green fonts, intermediate in blue and resistant in red. Data are the mean ± SEM. A total of 15 MDTs (technical replicates) were analyzed per condition for each cell line from one xenograft. Scale bar = 50 μm, Magnification = 20x. N.S. = non-significant. *$p < 0.05$, **$p < 0.01$, ***$p < 0.001$, ****$p < 0.0001$.

2.2.2.5 Discussion

This study highlights the importance of preclinical model selection for drug sensitivity analysis and understanding the variation that exists between experimental models. As most early-phase clinical trial designs rely heavily on preclinical data, it is important to consider these variations when performing drug screening or therapeutic response prediction studies, especially in the era of personalized medicine.

The mainstay of preclinical studies remains cell line-based and the *in vivo* response from animal models is often used as the gold standard in preclinical testing of novel therapies/combinations. To our knowledge, only one study[33] using bladder carcinoma cells reported that the 3D spheroids model reflected better the chemoresponse found in their mouse xenograft model, and higher drug resistance was seen with the 3D model compared to 2D cultures. In our study, we compared four translational model systems, including 2D monolayers, 3D spheroids, *ex vivo* MDTs and *in vivo* xenografts. Our data suggest better concordance in carboplatin sensitivity between our 3D *ex vivo* model (MDTs) and *in vivo* responses. Interestingly, we observed some notable differences between 2D culture and *in vivo* carboplatin responses. In the case of TOV21G, both its clear cell histology and microsatellite instability[17,34,35] supports the *in vivo* response of a platinum-resistant cell line. However, 2D culture experiments have consistently shown this cell line as carboplatin sensitive (Supplementary Table S1[29,36,37]). For OV90 and OV1946, an increased sensitivity to carboplatin is seen in mice. This may be due to their histological high-grade serous subtype of which the majority of patients respond to first-line platinum treatment[3]. Indeed, none of our high-grade serous cell lines showed *in vivo* resistance to carboplatin, but showed sensitivity in the 2D or 3D spheroid models.

Given that each model has unique features, their relative response to cytotoxic therapy may vary. Immortalized EOC monolayer cultures offer little cell-cell interaction and consist uniquely of a sub-clonal population of epithelial cancer cells. While spheroids also consist of epithelial cancer cells, they offer a 3D

structure with inherent cell layers, cell-cell interactions and chemical/nutrient gradients[25,38]. Increasing in model complexity is our *ex vivo* tumor model of MDTs that not only offers a 3D structure, but also includes mouse-infiltrating stromal cells which may impact the tumor response to a therapeutic agent. *In vivo* models further increase model complexity by incorporating important elements such as drug metabolism, influence of endogenous hormones and mammalian physiology[39]. In general, our study suggests that the relative carboplatin response of our 3D models was in line with *in vivo* results. However, two cell lines, OV4453 and OV4485, did not have concordant results as 3D spheroids and demonstrated higher carboplatin resistance in our spheroid model. We suspect that this may be related to their low oxygen culture conditions (7%), which was specific for only these two cell lines. *Hirst et al.*[40] showed that an increase in hypoxia-regulated genes and markers of stemness were present in the core of 3D spheroids but not in monolayered cells and that this induced chemoresistance and phenotypic changes. In addition, these cell lines formed spheroid aggregates that were not compact and had larger spheroid diameters, which has been shown to influence drug resistance[38,41].

Importantly, our 3D *ex vivo* model provided a complete concordant correlation with *in vivo* responses. *Ex vivo* models are attractive for fundamental and translational research as they can predict patient response to drugs in a clinically relevant timeframe. Important advantages of this model include minimal waste of tissue and culture/drug reagents[24], control of fluids and constant supply of nutrients[42], long-term viability[14,43-44] and the maintenance of MDTs and their TME[14,24] without need of growth supplements[45,46]. This model further allows testing multiple cycles of cytotoxic therapies as well as studying the effects of cytostatic drugs that require longer incubation periods. This underscores the need to incorporate these models into the drug development pipeline to better evaluate the potential efficacy of new drugs or combinations prior to entering in expensive clinical trial settings.

Although this study has some limitations, such as use of a single drug, choice of flow cytometry for 3D spheroid analyses and limited utility of *ex vivo* tumors with low epithelial count, the reproducible comparison between model systems while using the same cell lines clearly shows the relevance of using various preclinical models to better characterize response to novel therapies. We are aware that cell lines

are often devoid of many elements of the natural TME such as stromal and immune cells, which have been shown to influence response, and may not fully represent the primary tumor heterogeneity. However, the use of cell lines currently remains common practice in most preclinical models. Furthermore, a mouse model may not entirely reflect the human drug response. Hence, *ex vivo* models derived directly from patient samples would eliminate this bias in the drug development pipeline. Alternatively, similar analyses in comparing these preclinical models could be applied to other drugs in ovarian cancer treatment, such as paclitaxel, poly (ADP-ribose) polymerase (PARP) inhibitors and other drugs currently in preclinical studies such as HIF, WEE1 and TGFß inhibitors. Unfortunately, 3D analysis methods have traditionally relied on 2D culture methods or confocal microscopy analyses, which have their limitations. Thus, it would be interesting to include novel techniques such as light sheet microscopy and tissue clearing as well as IF staining of MDTMAs to allow optimal analysis of tissue without disturbing its natural environment.

Platinum resistance remains an important obstacle in EOC with dismal survival and limited options at advanced stages of disease progression. With the overall high attrition rate of oncologic treatments, more cost-effective predictive cancer models that accurately reflect patient response are needed. With this study, we clearly demonstrate a heterogeneity in therapeutic responses of EOC cell lines when cultured in different systems, which underscores the need to consider multiple factors when selecting a preclinical model for drug discovery and screening studies. This may avoid rejecting potentially effective drugs while eliminating ineffective drugs at the preclinical stage. This could also help reduce the rate of failed clinical trials in which patients experience drug toxicities with minimal efficacy, particularly for rare cancers[23], which are more difficult to accrue for clinical trials. In the era of personalized medicine, future applications would be to optimize treatment selection based on the individual tumor and patient characteristics rather than a ‘one treatment fits all’ approach. Thus, validation and feasibility studies of newer and more complex models are needed to enhance the current standards.

2.2.2.6 Acknowledgements

We thank the technical staff of the research platforms at the Centre de recherche du CHUM (CRCHUM): Liliane Meunier and Véronique Barrès (Molecular Pathology), Aurélie Cléret-Buhot and Isabelle Clément (Cellular Imaging), Jennifer Kendall-Dupont (Microfluidics), Paméla Thibeault (Flow Cytometry), Jacqueline Chung (manuscript editing). We acknowledge Thomas Montminy Brodeur for graphics. We also thank the CRCHUM animal facility for helping with the *in vivo* experiments. Cell lines used in this study were provided by the CRCHUM ovarian tumor bank, which is supported by Ovarian Cancer Canada (OCC) and by the *Banque de tissus et de données of the Réseau de recherche sur le cancer of the Fonds de recherche du Québec - Santé* (FRQS) affiliated with the Canadian Tumor Repository Network (CTRNet). We gratefully acknowledge M.N.B. salary support for this work provided by the following funding agencies/institutions: Canadian Institute of Health Research, Fonds de recherche du Québec – Santé, Centre de recherche du Centre hospitalier de l'Université de Montréal, Institut du cancer de Montréal, and Université de Montréal. K.S. was funded by the TransMedTech Institute and its main funding partner, the Canada First Excellence Fund, as well as by a studentship from the Canderel Fund of the Institut du cancer de Montréal (ICM). H.F. received the ICM Michèle St-Pierre Bursary and the ICM Canderel studentship.

2.2.2.7 Competing financial interest

The authors declare no competing interests.

2.2.2.8 Grant support

This work was supported by the Canadian Institute for Health Research (CIHR MOP142724 to A.M.M.M and D.M.P.) and the ICM (Fonds Défi Spyder and Anne-Marie Chagnon to D.M.P.). A-M.M-M. and D.M.P. are researchers of the CRCHUM/ICM, which receives support from the FRQS.

2.2.2.9 Author contributions

M.N.B., K.S. and E.C. wrote the main manuscript text. M.N.B. prepared Figs 1, 2B-C, 3, and S1 as well as Table 1, S1 and S2. H.F. prepared Fig 2A. K.S. prepared Figs 4 and S2. All authors reviewed the manuscript. Conception/design: M.N.B., E.C., A-M.M-M. Data acquisition: M.N.B., K.S., K.L-D, H.F. Data analysis: M.N.B., K.S., K.L-D., H.F., E.C.. Data interpretation: M.N.B., K.S., E.C., A-M.M-M. Supervision: E.C. and A-M.M-M. Funding acquisition: D.M.P. and A-M.M-M.

2.2.2.10 References

1 Siegel, R. L., Miller, K. D. & Jemal, A. Cancer statistics, 2019. CA Cancer J Clin 69, 7-34, doi:10.3322/caac.21551 (2019).

2 Howlader, N. et al. SEER Cancer Statistics Review, 1975-2017, National Cancer Institute. Bethesda, MD, <https://seer.cancer.gov/csr/1975_2017/> (2020).

3 Lheureux, S., Gourley, C., Vergote, I. & Oza, A. M. Epithelial ovarian cancer. Lancet 393, 1240-1253, doi:10.1016/S0140-6736(18)32552-2 (2019).

4 Wilson, M. K. et al. Fifth Ovarian Cancer Consensus Conference of the Gynecologic Cancer InterGroup: recurrent disease. Ann Oncol 28, 727-732, doi:10.1093/annonc/mdw663 (2017).

5 Lovitt, C. J., Shelper, T. B. & Avery, V. M. Cancer drug discovery: recent innovative approaches to tumor modeling. Expert Opin Drug Discov 11, 885-894, doi:10.1080/17460441.2016.1214562 (2016).

6 Aihara, A., Abe, N., Saruhashi, K., Kanaki, T. & Nishino, T. Novel 3-D cell culture system for in vitro evaluation of anticancer drugs under anchorage-independent conditions. Cancer Sci 107, 1858-1866, doi:10.1111/cas.13095 (2016).

7 Bregenzer, M. E. et al. Physiologic Patient Derived 3D Spheroids for Anti-neoplastic Drug Screening to Target Cancer Stem Cells. J Vis Exp, doi:10.3791/59696 (2019).

8 Hamilton, G. & Rath, B. Applicability of tumor spheroids for. Expert Opin Drug Metab Toxicol 15, 15-23, doi:10.1080/17425255.2019.1554055 (2019).

9 Gencoglu, M. F. et al. Comparative Study of Multicellular Tumor Spheroid Formation Methods and Implications for Drug Screening. ACS Biomater Sci Eng 4, 410-420, doi:10.1021/acsbiomaterials.7b00069 (2018).

10 Weiswald, L. B., Bellet, D. & Dangles-Marie, V. Spherical cancer models in tumor biology. Neoplasia 17, 1-15, doi:10.1016/j.neo.2014.12.004 (2015).

11 Sarisozen, C., Abouzeid, A. H. & Torchilin, V. P. The effect of co-delivery of paclitaxel and curcumin by transferrin-targeted PEG-PE-based mixed micelles on resistant ovarian cancer in 3-D spheroids and in vivo tumors. Eur J Pharm Biopharm 88, 539-550, doi:10.1016/j.ejpb.2014.07.001 (2014).

12 Al Habyan, S., Kalos, C., Szymborski, J. & McCaffrey, L. Multicellular detachment generates metastatic spheroids during intra-abdominal dissemination in epithelial ovarian cancer. Oncogene 37, 5127-5135, doi:10.1038/s41388-018-0317-x (2018).

13 Patra, B. et al. Carboplatin sensitivity in epithelial ovarian cancer cell lines: The impact of model systems. PLoS One 15, e0244549, doi:10.1371/journal.pone.0244549 (2020).

14 Simeone, K. et al. Paraffin-embedding lithography and micro-dissected tissue micro-arrays: tools for biological and pharmacological analysis of ex vivo solid tumors. Lab Chip 19, 693-705, doi:10.1039/c8lc00982a (2019).

15 Ouellet, V. et al. Characterization of three new serous epithelial ovarian cancer cell lines. BMC Cancer 8, 152, doi:10.1186/1471-2407-8-152 (2008).

16 Fleury, H. et al. Novel high-grade serous epithelial ovarian cancer cell lines that reflect the molecular diversity of both the sporadic and hereditary disease. Genes Cancer 6, 378-398 (2015).
17 Provencher, D. M. et al. Characterization of four novel epithelial ovarian cancer cell lines. In Vitro Cell Dev Biol Anim 36, 357-361, doi:10.1290/1071-2690(2000)0362.0.CO;2 (2000).
18 Karnezis, A. N. et al. Re-assigning the histologic identities of COV434 and TOV-112D ovarian cancer cell lines. Gynecol Oncol 160, 568-578, doi:10.1016/j.ygyno.2020.12.004 (2021).
19 Létourneau, I. J. et al. Derivation and characterization of matched cell lines from primary and recurrent serous ovarian cancer. BMC Cancer 12, 379, doi:10.1186/1471-2407-12-379 (2012).
20 Pearson, T. et al. Non-obese diabetic-recombination activating gene-1 (NOD-Rag1 null) interleukin (IL)-2 receptor common gamma chain (IL2r gamma null) null mice: a radioresistant model for human lymphohaematopoietic engraftment. Clin Exp Immunol 154, 270-284, doi:10.1111/j.1365-2249.2008.03753.x (2008).
21 Mombaerts, P. et al. RAG-1-deficient mice have no mature B and T lymphocytes. Cell 68, 869-877, doi:10.1016/0092-8674(92)90030-g (1992).
22 Gould, S. E., Junttila, M. R. & de Sauvage, F. J. Translational value of mouse models in oncology drug development. Nat Med 21, 431-439, doi:10.1038/nm.3853 (2015).
23 Colella, G. et al. Sarcoma Spheroids and Organoids-Promising Tools in the Era of Personalized Medicine. Int J Mol Sci 19, doi:10.3390/ijms19020615 (2018).
24 Astolfi, M. et al. Micro-dissected tumor tissues on chip: an ex vivo method for drug testing and personalized therapy. Lab Chip 16, 312-325, doi:10.1039/c5lc01108f (2016).
25 Shan, F., Close, D. A., Camarco, D. P. & Johnston, P. A. High-Content Screening Comparison of Cancer Drug Accumulation and Distribution in Two-Dimensional and Three-Dimensional Culture Models of Head and Neck Cancer. Assay Drug Dev Technol 16, 27-50, doi:10.1089/adt.2017.812 (2018).
26 Sokolova, E. et al. Penetration Efficiency of Antitumor Agents in Ovarian Cancer Spheroids: The Case of Recombinant Targeted Toxin DARPin-LoPE and the Chemotherapy Drug, Doxorubicin. Pharmaceutics 11, doi:10.3390/pharmaceutics11050219 (2019).
27 St-Georges-Robillard, A. et al. Long-term fluorescence hyperspectral imaging of on-chip treated co-culture tumour spheroids to follow clonal evolution. Integr Biol (Camb) 11, 130-141, doi:10.1093/intbio/zyz012 (2019).
28 Mulholland, T. et al. Drug screening of biopsy-derived spheroids using a self-generated microfluidic concentration gradient. Sci Rep 8, 14672, doi:10.1038/s41598-018-33055-0 (2018).
29 Ishiguro, K. et al. Cataloging antineoplastic agents according to their effectiveness against platinum-resistant and platinum-sensitive ovarian carcinoma cell lines. J Transl Sci 2, 117-124, doi:10.15761/JTS.1000127 (2016).
30 Ekhart, C. et al. Flat dosing of carboplatin is justified in adult patients with normal renal function. Clin Cancer Res 12, 6502-6508, doi:10.1158/1078-0432.CCR-05-1076 (2006).
31 Ricciardelli, C. et al. Novel ex vivo ovarian cancer tissue explant assay for prediction of chemosensitivity and response to novel therapeutics. Cancer Lett 421, 51-58, doi:10.1016/j.canlet.2018.02.006 (2018).
32 Das, T. et al. Empirical chemosensitivity testing in a spheroid model of ovarian cancer using a microfluidics-based multiplex platform. Biomicrofluidics 7, 11805, doi:10.1063/1.4774309 (2013).
33 Erlichman, C. & Vidgen, D. Cytotoxicity of adriamycin in MGH-U1 cells grown as monolayer cultures, spheroids, and xenografts in immune-deprived mice. Cancer Res 44, 5369-5375 (1984).
34 Talhouk, A. et al. Confirmation of ProMisE: A simple, genomics-based clinical classifier for endometrial cancer. Cancer 123, 802-813, doi:10.1002/cncr.30496 (2017).
35 Okamoto, A. et al. Gynecologic Cancer InterGroup (GCIG) consensus review for clear cell carcinoma of the ovary. Int J Gynecol Cancer 24, S20-25, doi:10.1097/IGC.0000000000000289 (2014).
36 Beaufort, C. M. et al. Ovarian cancer cell line panel (OCCP): clinical importance of in vitro morphological subtypes. PLoS One 9, e103988, doi:10.1371/journal.pone.0103988 (2014).

37 Bélanger, F. et al. Replication Protein A Availability during DNA Replication Stress Is a Major Determinant of Cisplatin Resistance in Ovarian Cancer Cells. Cancer Res 78, 5561-5573, doi:10.1158/0008-5472.CAN-18-0618 (2018).
38 Gong, X. et al. Generation of Multicellular Tumor Spheroids with Microwell-Based Agarose Scaffolds for Drug Testing. PLoS One 10, e0130348, doi:10.1371/journal.pone.0130348 (2015).
39 Fisher, M. F. & Rao, S. S. Three-dimensional culture models to study drug resistance in breast cancer. Biotechnol Bioeng 117, 2262-2278, doi:10.1002/bit.27356 (2020).
40 Hirst, J. et al. Licofelone Enhances the Efficacy of Paclitaxel in Ovarian Cancer by Reversing Drug Resistance and Tumor Stem-like Properties. Cancer Res 78, 4370-4385, doi:10.1158/0008-5472.CAN-17-3993 (2018).
41 Lee, J. M. et al. A three-dimensional microenvironment alters protein expression and chemosensitivity of epithelial ovarian cancer cells in vitro. Lab Invest 93, 528-542, doi:10.1038/labinvest.2013.41 (2013).
42 Rousset, N., Monet, F. & Gervais, T. Simulation-assisted design of microfluidic sample traps for optimal trapping and culture of non-adherent single cells, tissues, and spheroids. Sci Rep 7, 245, doi:10.1038/s41598-017-00229-1 (2017).
43 Davies, E. J. et al. Capturing complex tumour biology in vitro: histological and molecular characterisation of precision cut slices. Sci Rep 5, 17187, doi:10.1038/srep17187 (2015).
44 Powley, I. R. et al. Patient-derived explants (PDEs) as a powerful preclinical platform for anti-cancer drug and biomarker discovery. Br J Cancer 122, 735-744, doi:10.1038/s41416-019-0672-6 (2020).
45 Majumder, B. et al. Predicting clinical response to anticancer drugs using an ex vivo platform that captures tumour heterogeneity. Nat Commun 6, 6169, doi:10.1038/ncomms7169 (2015).
46 Nagaraj, A. S. et al. Establishment and Analysis of Tumor Slice Explants As a Prerequisite for Diagnostic Testing. J Vis Exp, doi:10.3791/58569 (2018).

2.2.2.11 Supplemental Tables and Figures

Table S1. Characteristics and 2D culture carboplatin response of EOC cell lines

Cell line	EOC histology subtype	Origin of cell line	IC_{50} (µM) (clonogenic assay)	Chemosensitivity	References	Cellosaurus number[a]
OV4453	High-grade serous	ascites	0.23±0.074	Sensitive	16	CVCL_9T20
TOV21G	Clear cell	tumor	1.0±0.23[b]	Sensitive	17	CVCL_3613
OV1946	High-grade serous	ascites	3.4±0.18[b]	Intermediate	15	CVCL_4375
OV4485	High-grade serous	ascites	6.1±0.27	Intermediate	16	CVCL_9T21
TOV112D	Dedifferentiated	tumor	13.9	Resistant	17, 18, 19	CVCL_3612
OV90	High-grade serous	ascites	31.8±5.4	Resistant	13, 17	CVCL_3768

[a] Cellosaurus is an online knowledge resource on cell lines (https://web.expasy.org/cellosaurus/)
[b] Values obtained are from this present study

Table S2. Fold change in carboplatin IC_{50} values between 2D and 3D models

Cell Line	3D IC_{50}/2D IC_{50} (Spheroids)	3D IC_{50}/2D IC_{50} (MDTs)
OV4453	659.1/0.23 = 2865.7	45.43/0.23 = 197.5
TOV21G	280.8/1= 280.8	270.7/1 = 270.7
OV1946	75.32/3.4 = 22.1	17.69/3.4 = 5.2
OV4485	597.1/6.1 = 97.9	106.7/6.1 = 17.5
TOV112D	330.3/13.4 = 24.7	494.3/13.4 = 36.9
OV90	223.9/31.8 = 7.0	-

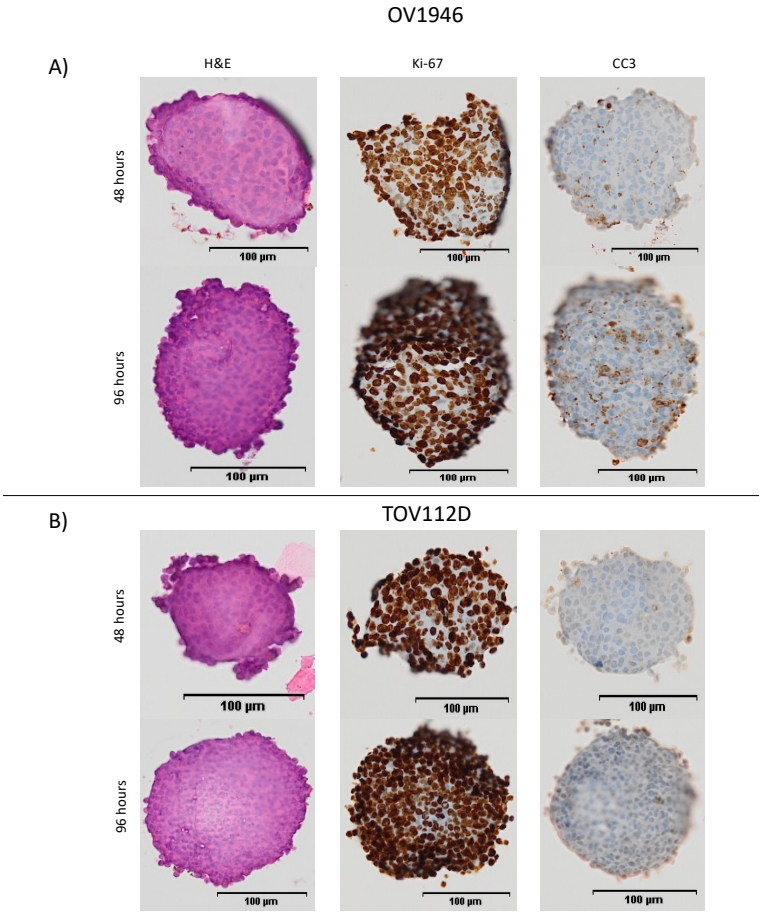

Figure S1. 3D spheroids remain proliferative throughout 96-hour experiment period. Representative photographs of **A)** sensitive EOC cell line OV1946 and **B)** resistant EOC cell line TOV112D at spheroid formation (48 hours) and at the end of the experiment (96 hours). Representative staining for H&E (left), Ki-67 (middle) and cleaved caspase-3, CC3, (right). Scale bar = 100 µm.

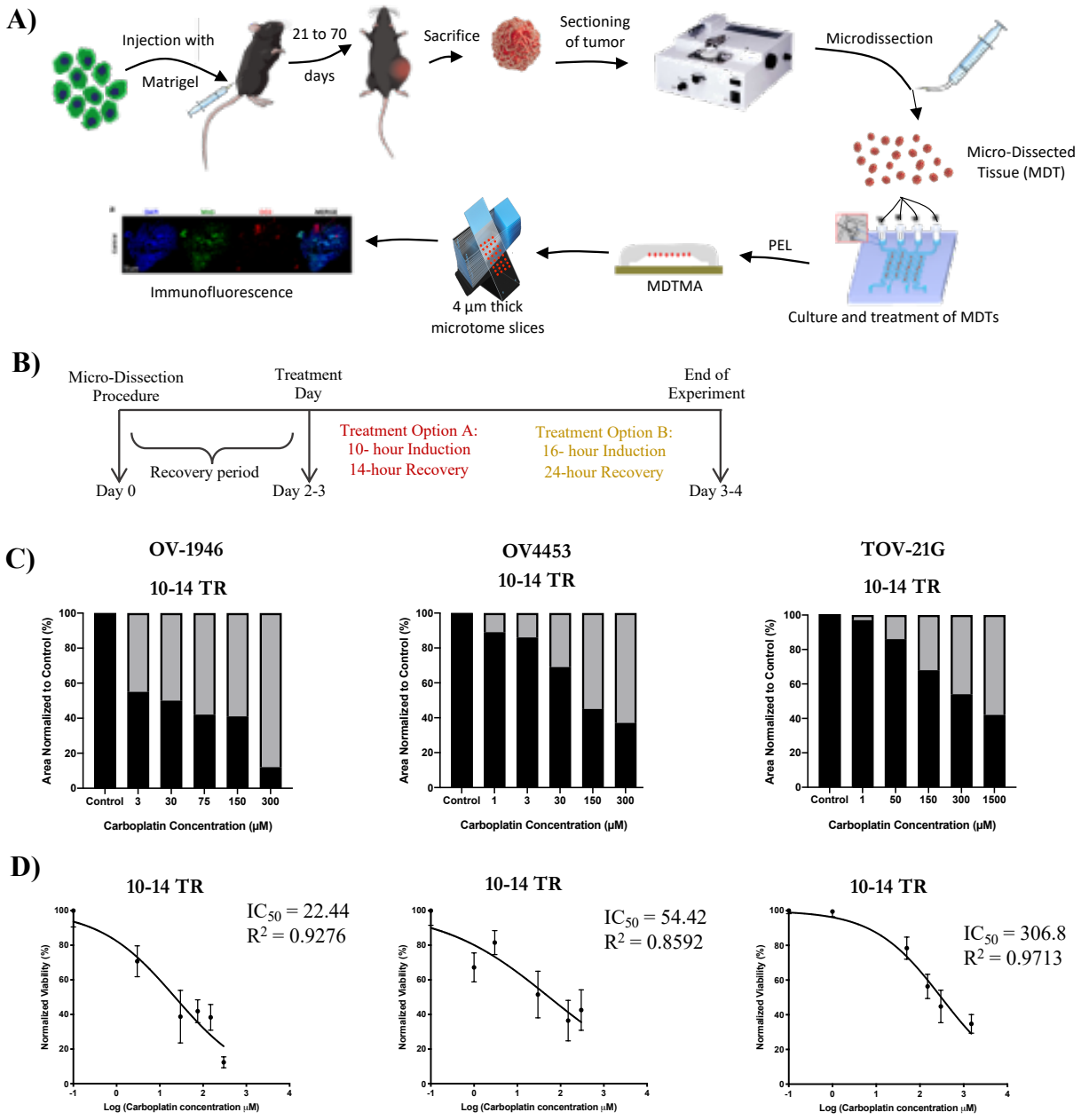

Figure S2. Identification of treatment regimen for *ex vivo* tumor model. A. Schematic representation of MDTs generated from a tumor surgically removed from a cell line xenograft model. **B.** Timeline used for carboplatin treatment of MDTs with two different therapeutic regimens: 10-hour incubation followed by 14-hour recovery (10-14 TR) or 16-hour incubation followed by 24-hour recovery (16-24 TR). **C.** Cell fate represented in graphs showing percentage of proliferative, quiescent and apoptotic cells within MDTs with or without carboplatin at various concentrations for each treatment regimen for three cell lines (OV1946, OV4453 and TOV21G). **D.** Dose-inhibition curves for 10-14 TR to determine IC_{50}. Data are the mean $\pm$ SEM. A total of 15 MDTs were analyzed per condition for each cell line from one xenograft.

2.3 Chapter 3: *Ex Vivo* Model Preserved Natural Tumor Microenvironment To Accurately Predict Clinical Response To Chemotherapy

2.3.1 Article 3: Résumé en français

Titre en français: Un modèle *ex vivo* préserve le microenvironnement tumoral naturel pour prédire la réponse clinique des patients à la chimiothérapie.

La sélection des options thérapeutiques les plus appropriées et efficaces pour chaque patient est cruciale pour la personnalisation des soins contre le cancer. Les modèles *ex vivo* dérivés de tumeurs permettent de tester directement des agents thérapeutiques sur un échantillon de patient. Nous avons évalué si notre modèle de tissus micro-disséqués (MDTs) *ex vivo* préserve et maintien son microenvironnement tumoral (TME) naturel afin de mieux expliquer la corrélation entre les MDTs et la réponse clinique du patient. À partir d'une cohorte de 25 patientes atteintes d'un cancer de l'ovaire, nous avons généré des MDTs pour les mettre en culture pour 15 jours. Nous avons comparé le transcriptome et l'architecture histologique entre les MDTs et leurs tumeurs appariées. Les MDTs ont également été exposés à une combinaison de chimiothérapie, comparable à la clinique. Nos résultats ont montré que la composition génétique des MDTs était maintenue pendant la période de culture de 15 jours et qu'elle était représentative de la tumeur primaire. En outre, le TME naturel, incluant les cellules immunitaires, stromales et épithéliales, est maintenu dans les MDTs à un niveau de répartition cellulaire proportionnel à la tumeur primaire. La réponse induite par la chimiothérapie dans les MDTs a montré une corrélation positive de 92,8 % avec la réponse clinique du patient. Nous présentons un modèle *ex vivo* robuste qui fournit un modèle préclinique pertinent pouvant servir de plateforme pour prédire la réponse du patient dans un délai cliniquement adapté.

2.3.2 Article 3: In preparation

Ex Vivo Micro-Dissected Tissue Model Preserved Natural Tumor Microenvironment to Accurately Predict Clinical Response to Chemotherapy

Kayla Simeone [1], Jennifer Kendall-Dupont [1], Euridice Carmona [1], Benjamin Péant [1], Thomas Gervais [1,2], Fred Saad [1,3], Diane Provencher [1,4], Anne-Marie Mes-Masson [1,5].

[1] Centre de recherche du Centre hospitalier de l'Université de Montréal (CRCHUM) and Institut du cancer de Montréal (ICM), Montreal, Quebec, Canada,

[2] Polytéchnique de Montréal, Université de Montréal, Montreal, Quebec, Canada,

[3] Department of Surgery, Université de Montréal, Montreal, Quebec, Canada,

[4] Division of Gynecologic Oncology, Université de Montréal, Montreal, Quebec, Canada,

[5] Department of Medicine, Université de Montréal, Montreal, Quebec, Canada

Corresponding author: Anne-Marie Mes-Masson, CRCHUM, 900 Saint-Denis, Montreal, Quebec, Canada, H2X0A9 Phone: 514-890-8000 ext. 25496. Fax: 514-412-7703. Email: anne-marie.mes-masson@umontreal.ca

Keywords: micro-dissected tissue, ovarian cancer, chemotherapy, clinical response, prediction, tumor microenvironment

2.3.2.1 Abstract

Selecting the most appropriate and effective treatment options for each patient is crucial to personalized cancer care. *Ex vivo* tumor-derived models enables direct testing of therapeutic agents on a patient specimen to accurately predict a patient's response to various drugs. Here, we evaluated our previously described *ex vivo* micro-dissected tissue (MDT) model system for preservation and maintenance of the natural tumor microenvironment (TME) including endothelial, immune, epithelial and stromal lineages, in culture to better explain the correlation between MDT and patient drug responses. Using a cohort of 27 patients with ovarian cancer, we generated MDTs from primary tumors and cultured them over a 15-day period. We compared transcriptomic and histological analyses between MDTs and their matched tumors to investigate the genetic similarities, as well as the cell lineage composition found in the TME. MDTs were also exposed to a chemotherapy combination, with parameters comparable to clinical treatments, to verify their predictive potential. Our results showed that the genetic composition of MDTs was maintained over the 15-day culture period and that was representative of the primary tumor. In addition, the cell lineages that compose the natural TME including immune, stromal and epithelial cells were maintained in MDTs over the culture period and proportional to the primary tumor. The chemotherapy induced response in MDTs showed a 88.2% positive correlation with the patient's clinical response. We present a robust *ex vivo* model derived from primary tumors that provides a robust preclinical model that can serve as a platform to predict patient response in a clinically suitable timeframe.

2.3.2.2 Introduction

Ovarian Cancer (OC) is the most lethal gynaecological cancer, and 5th leading cause of malignancy-related deaths in North American women[1]. The most common form is epithelial ovarian cancer (EOC)[2,3], which is further classified into subtypes with specific morphology, etiology, pathogenesis, molecular biology, prognosis and somatic mutational profiles[4-12]. Around 75% of patients present with a high-grade serous carcinoma (HGSC), and less common subtypes include mucinous, low-grade serous, clear-cell and endometrioid carcinomas[9,13]. Despite being different diseases, the multiple subtypes of EOC are treated with

the same standard front-line therapy: primary debulking surgery followed by a combination of platinum- and taxane-based chemotherapy for 6 cycles[3,12,14-16]. In general, despite 70-80% of patients initially responding to first-line regimens, the 5-year survival rate of OC is 45%[9,13]. The remaining 20-30% of patients usually either relapse 3-6 months after the last treatment cycle or fail to respond at all to first-line treatment[2,3,12]. This puts into perspective the clinical need to quickly identify this minority of patients pre-emptively plan for more effective therapeutic regimens.

The standard of care for cancer treatment is still largely based on local (surgical resection or radiology) and systemic (chemotherapy, hormone therapy, immunotherapy, etc.) control for a vast majority of solid tumors including OC[17-20]. However, individual response rates can differ when exposed to same therapeutic agent[21,22], emphasizing the genetic and molecular variabilities of an individual tumor and the lack of preclinical models that translate to the patient response. Current preclinical models rely on cell-line based systems, including 2D monolayer cell cultures[23], 3D spheroids[24] and *in vivo* models[25], to evaluate drug response, and pharmacodynamics and pharmacokinetics of newly developed therapeutics[26]. These models are limited in their capacity to mimic tumor complexity, mainly due to their lack of cell population heterogeneity[27,28]. Although, novel models, such as *in vivo* patient-derived xenograft (PDX)[29,30] and *ex vivo* organoids[31-33] mimic tumor heterogeneity, their lengthy production times limit their use for predicting drug response in a clinically relevant timeframe. This factor adds to the clinical challenges of identifying the best treatment option for patients. Recent studies have also shown the importance of the tumor microenvironment (TME) and the interaction between various cell lineages in tumor drug resistance[34,35]. Thus, there remains a clinical need in developing ex vivo tumor-derived models that reflect the genetic and phenotypic complexities of patient tumors, and that maintain an intact natural tumor microenvironment (TME) for accurate drug testing within an acceptable timeframe.

Over the past decade, *ex vivo* tissue explant models have gained interest and have shown their ability to predict drug response in non-small cell lung cancer[36], head and neck squamous cell carcinoma[36], colorectal cancer[36], renal carcinoma[37] and advanced prostate[38] and bladder cancers[39], presenting them as a reliable preclinical model for drug efficacy evaluation. However, tissue slice cultures have reduced

longevity and a higher risk of hypoxia-induced necrosis due to its size. To address this, our group has developed an *ex vivo* micro-sized tumor-derived model system, using micro-dissected tissues (MDTs) from primary tumor specimens cultured within specifically designed microfluidic devices[40,41]. The use of microfluidic technologies promotes the maintenance of individually entrapped tumors that contain their own TME matrix such that the microfluidic chamber mimics the enclosed human environment, allowing tumors to continue their malignancy course. In addition, the reduced tumor size and small volumes of reagents (less than 20 μL/MDT) permits use of scarce tissues and prevents the waste of expensive reagents and drugs. Using cell-line xenograft tumors, we have previously shown that our MDT model system accurately reproduces the primary tumor cell lineage composition and can mimic treatment response in a timeframe of less than a week[41].

It has been established that the TME plays a key role in cancer growth, metastasis, and drug resistance, and has gained greater attention in the design of 3D models for more accurate disease simulation and drug screening (Balkwill). Here, we present the first preclinical correlative study using MDTs to preserve the TME in OC patient samples and demonstrate their ability to predict patient-specific responses in a timeframe suitable for clinical decision-making. This study used a cohort of 27 EOC patients to show that the genetic integrity and cell lineage composition of the natural TME within MDTs was maintained over a 15-day culture period (Figure 1). Using standardized protein detection procedure, we evaluated the correlation of treatment response to the standard front-line carboplatin/paclitaxel combination therapy for OC. We obtained a 88.2% positive response correlation between the *ex vivo* analyses and patient-matched clinical responses. Our results suggest that MDTs provide a sophisticated preclinical model to recapitulate the primary tumor response and may serve as a platform to test new therapeutics, as well as a clinical guidance tool to predict patient response to various drugs.

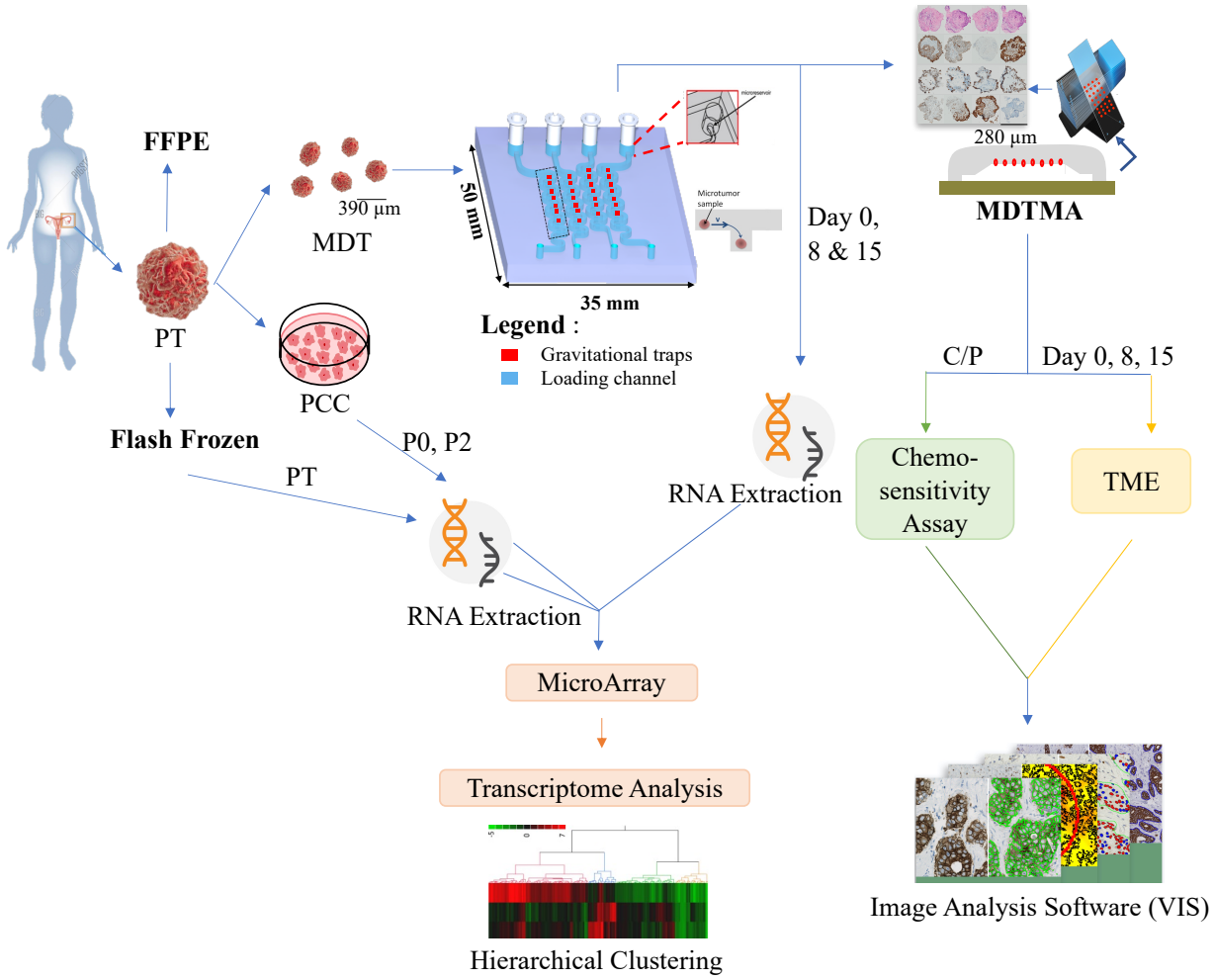

Figure 1: Schematic overview of our model system experiment concept. Resected tumor was separated into four sections; two sections were used to produce primary cell cultures and MDTs, a third section was flash frozen, and the last section was formalin-fixed and paraffin embedded. Primary cell cultures were grown in Petris dishes until 80% confluency was attained before splitting. MDTs were cultured and treated in microfluidic devices made up of polydimethylsiloxane (PDMS). At experimental endpoints, RNA was extracted from all sample types for microarray gene expression profiling to perform transcriptome analyses. In parallel, MDTs cultured for the same time-points, as well as treated MDTs, were formalin-fixed for IF analysis of TME and chemosensitivity.

2.3.2.3 Methods

Patient cohort

OC tumor specimens were collected from 25 patients undergoing debulking surgery at the Centre hospitalier de l'Université de Montréal (CHUM) and Division of Gynecologic Oncology following

informed consent. The staging of each patient was determined at the time of surgery by an on-site gynaecologic oncologist following the FIGO classification criteria[42]. Tumor grading and histological characteristics were identified by a gynecologic-oncology pathologist of the CHUM following FIGO recommendations. The study was approved by the relevant institutional ethics committee, the Comité d'éthique de la recherche du CHUM (2015-5622 CE 14.175-CA).

MDT production, loading in microfluidic devices and medium changes

Primary OC tumor specimens from patients were separated into three sections. One section underwent a micro-dissection procedure that was adapted from previously published work[40]. Another section was used for formalin-fixation and paraffin-embedded procedures and the last section was flash frozen for RNA extraction (Figure 1).

For the microdissection procedure, the tumor specimen was sliced into 1 cm thick sections using a scalpel and then placed on the McIlwain™ tissue chopper (Stoelting, Wood Dale, Illinois, USA). The tumor sections were chopped at a thickness of 350 µm to produce tissue slices and placed in Hank's balanced salt solution (HBSS, 311-516-CL, Wisent Inc., Saint-Bruno-de-Montarville, Canada) supplemented with 10% fetal bovine serum (FBS, 088-150, Wisent), 2.5 µg/mL of amphotericin B (450-105-QL, Wisent) and 50 µg/mL of gentamicin sulfate (450-135, Wisent). Using a 500 µm biopsy punch (PUN0500, Zivic Instruments, Pittsburgh, USA), the tumor slices were punctured to produce disk-like MDTs and placed in serum-free HBSS supplemented with antibiotics until they were ready for loading in their microfluidic devices. The loading, trapping and culturing of MDTs was then performed as described in our previous work[40]. MDTs were cultured in OSE complete medium (316-030-CL, Wisent Inc, Saint-Bruno, QC, Canada) containing 10% FBS, 2.5 µg/mL of amphotericin B and 50 µg/mL of gentamicin sulfate.

Generating primary cell cultures

Five to six of the 350 µm thick tissue slices were placed in a 60 mm Petri dish (430166, VWR, Quebec, Canada) with OSE complete medium and incubated in 5% CO2 at 37°C. The following day, the

medium was changed to remove all shedding debris from the tumor specimen and replaced with fresh OSE complete medium. Two to three Petri dishes were used for each patient. As epithelial cells reached 80% confluency or when fibroblasts started to outgrow tumor cells, cells were split and one third was reserved for RNA extraction. This procedure continued as long as tumor cells continued to grow[43].

Combination chemotherapy treatment

MDTs derived from OC patient samples were treated with a regimen of 300 μM carboplatin (Hospira Healthcare Corporation) and 80 nM paclitaxel (Hospira Healthcare Corporation). The treatment regimen used for these patient samples consisted of a 10-hour treatment period followed by a 14-hour recovery period, which was previously optimized in a dose-response analysis using mouse xenograft MDTs. MDTs were formalin-fixed at the end of the recovery period.

MDT fixation and paraffin-embedding

MDTs were fixed with 10% formalin (F0650, Produits Chimiques A.C.P. Chemicals Inc, Saint-Leonard, Qc, Canada) and further processed through the previously published paraffin-embedding lithography procedure to create micro-dissected tissue micro-array (MDTMA) blocks[41]. These blocks were cut into 4 μm sections using a microtome and placed on Matsunami TOMO® hydrophilic adhesion slides (10478-172, VWR) for histological analyses and protein-specific visualization.

RNA extraction and gene expression analysis

A section of the flash frozen primary tumor specimen was sliced and placed in a tube with 500 μL of RLT lysis buffer (74004, Qiagen, Hilden, Germany) for mechanical disruption using the TissueRuptor II (9002755, Qiagen) for 10-30 seconds.

MDTs were harvested in 1.5 mL Eppendorf microtubes (72-690, Sigma, Darmstadt, Germany) at appropriate time points, and culture medium was rinsed out using 10X phosphate buffered saline (PBS, 811-012-LL, Wisent) diluted to 1X with RNase, DNase and proteinase-free water (10977-015, Thermofisher,

Waltham, MA). Samples were placed on dry ice and MDTs were crushed into small debris using a plastic piston, and 200 µL RLT lysis buffer was then added for several minutes.

When primary cell cultures reached confluency, a third of the cells were harvested into a 1.5 mL microtube. The medium was rinsed out with 1X RNase-free PBS solution and then replaced with RLT lysis buffer for several minutes.

The RNeasy Micro Kit (74004, Qiagen) was used to perform the RNA extraction of the primary tumors, MDTs and primary cell cultures. RNA was quantified and analyzed for suitable quality and purity by the NanoDrop (Denovix) and Bioanalyzer (Agilent), respectively. The RNA extracted for five HGSOC patients were sent to Genome Quebec for an Affymetrix Clariom S HT pico gene expression analysis.

The Transcriptome Analysis Console™ (TAC) software version 4.0.2 (ThermoFisher Scientific) was used for normalization of expression data, control probe verification and comparison studies of differentially expressed genes. The TM4 Multi-Experiment Viewer (MeV) software version 4.8.1 was used to perform principal component analyses (PCA) and unsupervised hierarchical clustering. KEGG pathway analysis was also performed to identify differentially expressed pathways.

Immunofluorescence & histological staining

The 4 µm sliced sections of each block for each patient underwent hematoxylin and eosin (H&E) staining and immunofluorescence (IF) staining to assess the presence of various cell lineages and the treatment response of patient specimens. Prior to IF staining, TOMO slides were first incubated in a 60˚C oven for 20 minutes.

For all IF staining, antigen retrieval was carried out automatically with the Cell Conditioning 1 solution (VMSI; #950-123) for 60 minutes with primary antibodies (Supplementary table 1). Primary antibodies were automatically dispensed, and the slides were incubated at 37°C for 60 minutes. For the anti-FAP, no detergent agent was used during the dehydration procedure. Secondary antibodies (supplementary Table 1) were added at room temperature.

All sections were scanned with a 20 x 0.75 NA objective with a resolution of 0.3225 µm (BX61VS, Olympus, Toronto, Ontario).

Statistical analysis

Values are expressed as the mean ± standard error of the mean (SEM) derived from a single experiment using a minimum of 15 MDTs per condition. Comparisons between multiple groups (time points or TME) were evaluated by one-way ANOVA comparison tests. Comparisons for *ex vivo* treatment response were evaluated by Student's t-tests. P values <0.05 were considered significant. All statistical analyses were performed using GraphPad Prism 9.0 software (GraphPad Software Inc., San Diego, CA). Receiver operating characteristics (ROC) curves were plotted in SPSS 26 software (IBM, Armonk, NY) to determine cut-off ratios for *ex vivo* treatment response analysis.

2.3.2.4 Results

Characteristics of the patient cohort

The patient cohort included 27 women diagnosed with EOC at varying stages (I to IV) and subtypes (Table 1). The cohort reflected the frequency of EOC subtypes reported in the literature[12,19], 80% HGSC, 12% endometrioid, 4% carcinosarcoma and 4% Brenner tumor, a much rarer subtype. Patient cohorts were selected randomly based on tissue volume, characteristics, and feasibility. Thus, several patient tumor specimens were used for more than one experimental procedure. Due to the low production rate of primary cell cultures, only five HGSC patient samples produced adequate primary cell cultures that were sustained for a minimum of two consecutive passages. These five patient samples were first used to perform microarray gene expression profiling and transcriptome analyses. In addition, 10 patient were used to investigate the TME and 17 patient samples were used to investigate the MDTs ability to predict treatment response (Table 1). All patients within this response prediction group underwent cytoreductive surgery with

little to no residual disease. All patients had no prior cancer history, were chemo-naïve and were treated with a combination of carboplatin and paclitaxel as first-line treatment (Supplementary Figure 2).

Table 1: Patient Cohort Characteristics

	Biobank ID	Laterality	Subtype	Staging	Experiments performed
1	**7873**	RPI	HGS	IIIC	Microarray
2	**8093**	L	HGS	IIIC	Microarray
3	**8244**	R	Carcinosarcoma	IIIC	TME
4	**8288**	R	HGS	IV	TME
5	**8393**	L	HGS	IIIC	Microarray & TME
6	**8588**	P	HGS	IIIC	Microarray & TME
7	**8970**	L	HGS	IIA	Microarray
8	**9061**	R	Endometrioid	IV	Response Prediction
9	**9443**	O/OM	HGS	IIIC	Response Prediction
10	**9447**	R	HGS	IIIC	Response Prediction
11	**9454**	R	HGS	IIIA	TME & Response Prediction
12	**9532**	R	Endometrioid	IIA	Response Prediction
13	**9562**	L	HGS	IIIC	Response Prediction
14	**9704**	R	HGS	IC-II	TME & Response Prediction
15	**9808**	L	HGS	IIB	Response Prediction
16	**10329**	R	HGS	IIIA	Response Prediction
17	**10381**	L	HGS	IC-I	Response Prediction
18	**10412**	L	HGS	IC-I	TME
19	**10499**	L	HGS	IIB	TME & Response Prediction
20	**10505**	R	HGS	IIIC	TME & Response Prediction
21	**10520**	L	HGS	IIB	Response Prediction
22	**10547**	R	HGS	IIA	Response Prediction
23	**10549**	L	Brenner	IC-I	TME
24	**10550**	L	Endometrioid	II	TME
25	**10557**	R	HGS	IIA	Response Prediction
26	**10627**	R	LGS	IIIC-I	Response Prediction
27	**10645**	R	Endometrioid	IVB	Response Prediction

HGS: high-grade serous; L: left ovary; LGS: low-grade serous; O/OM: omentum; TME; P: peritoneum; R: right ovary; RPI: right pelvic implant; tumor microenvironment

MDTs are genetically stable and similar to their matched primary tumor

A 3D *ex vivo* organotypic model should maintain stable genetic composition over its culture period to accurately represent the primary tumor. To investigate the maintenance of genetic stability in our *ex vivo* model system, we used five HGSC patient samples (Table 1) to compare transcriptomic data of patient-

matched primary tumors (PT), MDTs at various culture time-points (day 0, day 8 and day 15) and primary cell cultures (PCC) at two distinct passages (passage 0, passage 2). As PCC have shown a close resemblance to patient-specific responses and have the potential to be used for personalized tumor therapy assays[44,45], we compared the transcriptomic profiles of these cultures to our *ex vivo* model system and to the PT of origin. The gene expression analysis of each patient-matched models showed similar results for all five HGSOC patients. Principal component analysis (PCA) showed that the MDTs clustered close together to matched PTs, whereas PCCs clustered separately (Figure 2A). To confirm this relationship, we performed an unsupervised hierarchical clustering (UHC) analysis. This analysis groups together samples within branches, where each branch indicates samples that are biologically similar to one another at a transcriptome level. The results showed that the gene expression profile of MDTs matched their PTs, whereas the PCCs branched away (Figure 2B, Supplementary Figure 1A), suggesting a loss of cellular heterogeneity over their culture period. In addition, the PCA and UHC analyses confirmed that MDTs at day 0 were highly similar to their respective PT, whereas MDTs cultured for 8 and 15 days were closely associated.

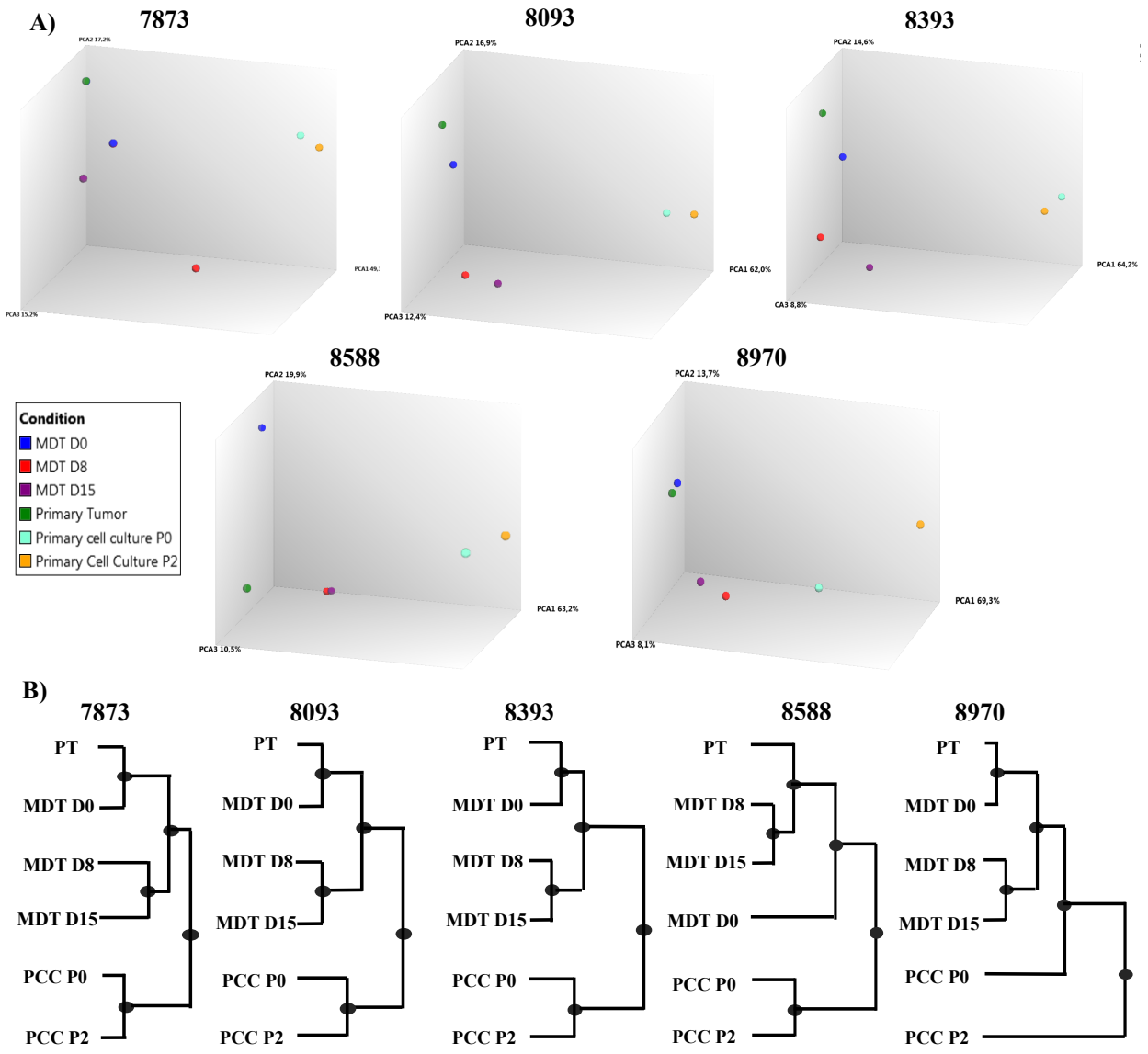

Figure 2: The genomic integrity of MDTs is maintained over a 15-day culture period. A) Principal Component Analysis (PCA) and B) simplified hierarchical clustering tree of patient samples. A total of 15 MDTs (technical replicates) were analyzed per condition for each patient and, one section of the primary tumor was used for each patient. PT: primary tumor, D0: day of microdissection, D8: day 8, D15: day 15, P0: passage 0, P2: passage 2.

Next, we performed a comparison study to better identify the genes that were differentially expressed between each model type and their matched PTs. We confirmed that the PCCs had a higher number of differentially expressed genes set compared to MDTs (Figure 3A, Supplementary Figure 1B). These results were consistent for all five patients, highlighting the magnitude of differences between each model type and their matched PT. A pathway analysis also showed more deregulated pathways between

PCCs and the PTs than between MDTs and PTs (Figure 3). We further observed that MDTs at day 0 had upregulated pathways in cellular metabolism including galactose, sucrose and starch metabolism and carbohydrate digestion and absorption but also an increase in necroptosis compared to PTs, confirming that the microdissection procedure does impact the cells nutritional value and increase stress factors (Figure 3B). Notably, these pathways related to stress-induced cell fate were then shown to be downregulated in MDTs after 8 and 15 day of culture whereas pathways involved in cell homeostasis, energy metabolism, and cellular survival were upregulated including Ras, Chemokine, PI3K-AKT signalling (Figure 3C), This suggests that MDTs retain a stable cellular state. However, PCCs have a large list of differentially expressed genes and pathways compared to the PTs including upregulation in metabolism, necroptosis and cell interaction pathways and downregulation in cell lineage, cell survival and inflammatory pathways (Figure 3D). Altogether, these results suggest that gene expression profile is more profoundly altered in PCCs than in MDTs, when compared with PTs.

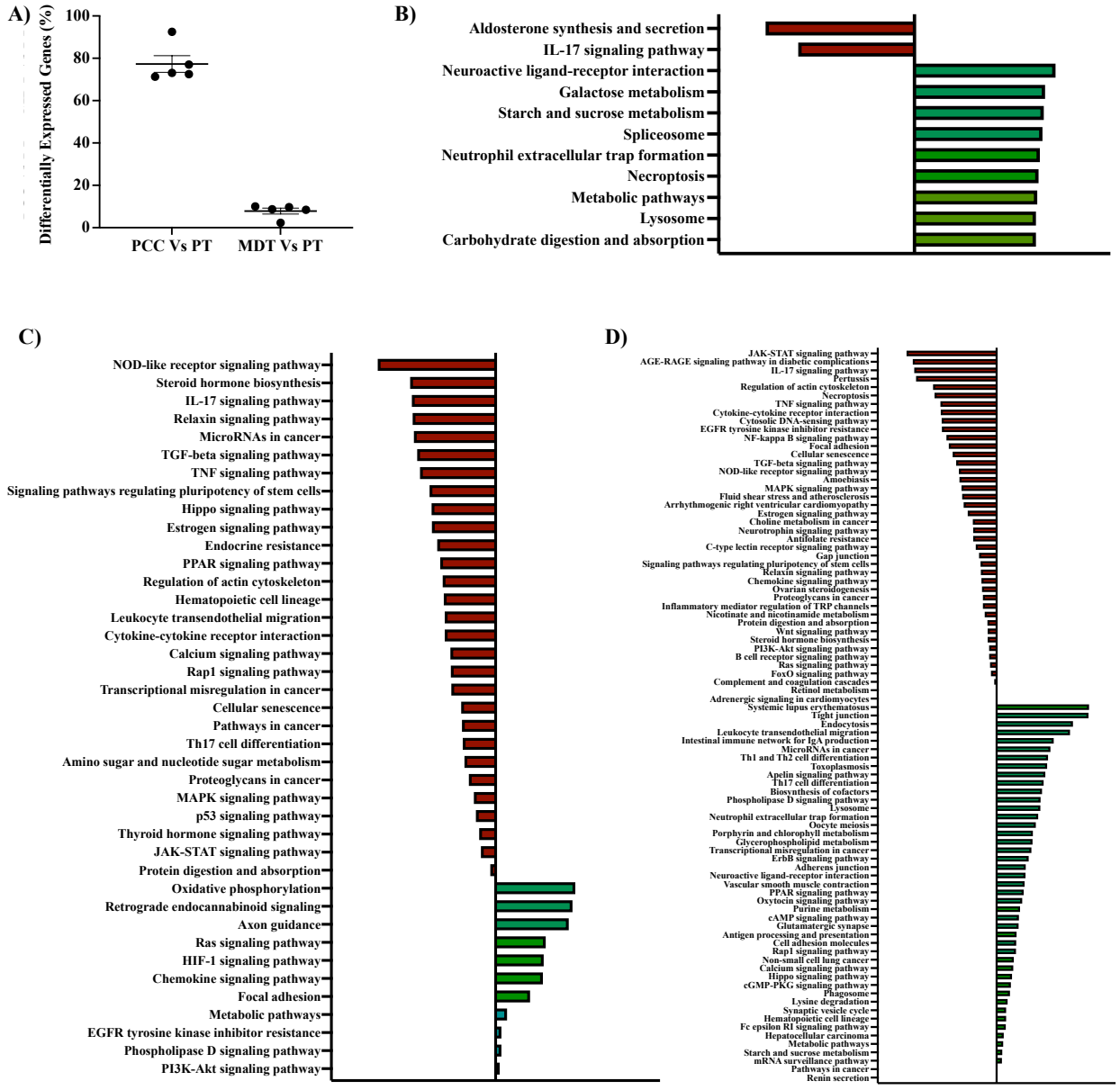

Figure 3: A smaller number of genes and pathways were differentially expressed in MDTs compared to PCCs. A) Scatter line plot of the percentage of differentially expressed genes (between PCCs and PTs and between MDTs and PTs. Upregulated and downregulated pathway analyses between B) MDTs at D0 C) MDTs at D8 and D15 of culture and D) PCCs compared to PTs. Fold-change cut-off is ± 2 for all gene set. The bars represent the net sum of upregulated and downregulated genes per pathway.

The TME is maintained in MDTs over a 15-day culture period

The TME plays a critical role in the patient-specific response to chemotherapy[35]. Therefore, the sustained presence of the TME in a predictive model system is important to obtain an accurate therapeutic read-out. To evaluate the presence of various cell lineages found in the TME, we performed IF analyses on formalin-fixed MDTs to identify endothelial cells/hematopoietic cells (anti-CD34), leucocytes (anti-CD45), monocytes (anti-CD68) and cancer-associated fibroblasts (identified by fibroblast activation protein alpha [anti-FAP]) (Figure 4A-E). We show that the vasculature component, consisting of endothelial/hematopoietic cells, is significantly reduced within the MDTs compared to the PTs in all 10 patients. Globally, we have expected a reduction in endothelial/hematopoietic cells since the microdissection procedure breaks up the circulatory system present within the PTs. However, the number of endothelial/hematopoietic cells present at day 0 was maintained over the complete culture period, however in 3 out of the 10 patients an increase of endothelial/hematopoietic cells was seen (Fig 4B, Supplementary Figure 2A). This would signify that the cells present within the MDTs are adequately nourished to maintain a viable state. In addition, our results suggest that the immune cell components, represented by monocytes and leucocytes, were present within the MDTs and at a level comparable to the PTs with non-significant changes over time (Figure 4C-D, Supplementary Figure 2B). Moreover, we observed a consistent number of cancer-associated fibroblasts within MDTs that was equivalent to their matched PTs (Figure 4E, Supplementary Figure 2C). Even with a smaller surface area, the cell lineage surface to core ratios were highly similar between MDTs and matched PT. We also observed similarities in the proportion of epithelial cancer cells (Figure 4F) between MDTs and matched PTs. Lastly, we previously determined that 15 MDTs[41] would suffice to obtain statistically significant results. Overall, all patients provided an adequate number of MDTs (≥15 MDTs) with epithelial cancer cells that remained consistent over the total culture period (Figure 4G). Taken together, these results reflect the stability of various cell lineages present within MDTs, demonstrating a sophisticated 3D model system that preserves the natural TME.

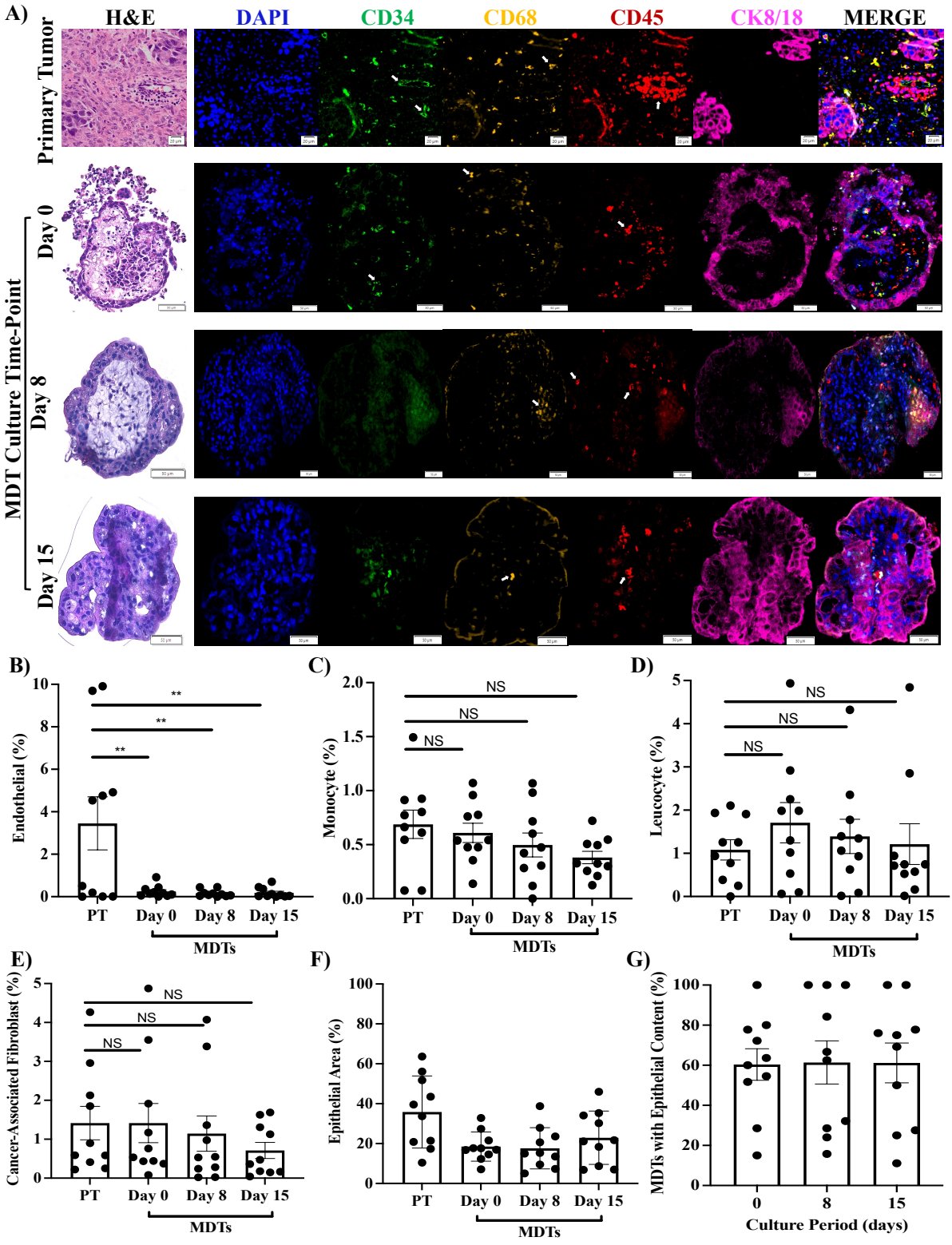

Figure 4: MDTs maintain their natural tumor microenvironment over a 15-day culture period. A) Representative images of the PT and MDTs of patient 10549 stained with TME antibodies: CD34 for endothelial cells, CD68 for monocytes, CD45 for leucocytes and cytokeratins 8 and 18 (CK8/18) for epithelial cells. Scatter box plots

of the average expression of the marker for all 10 patients in the cohort for B) endothelial cells, C) monocytes, D) leucocytes E) cancer-associated fibroblast, F) epithelial content and G) percentage of MDTs with epithelial content per experimental condition. Data are represented as the mean ± SEM. A minimum of 15 MDTs (technical replicates) were analyzed per condition for each patient and each dot represents the average of each patient. Scale bars = 50 μm, magnification = 20x. Statistical significance $p<0.05$ (Student's t-test). NS: non significant.

MDTs are highly viable over a 15-day culture period

A key feature in establishing an adequate *ex vivo* response prediction model is the ability to maintain the viability of cancer cells over a certain culture period. We have previously shown that MDTs derived from cell-line xenograft tumors could maintain a stable viability over a 15-day culture period[41]. We evaluated the proportion of apoptotic and proliferative epithelial cells by cleaved caspase-3 (CC3) and Ki-67 IF staining, respectively, in MDTs immediately after the microdissection as well as after 4, 8 and 15 days of culture (Figure 5). Our results showed that the MDTs maintained high levels of epithelial cell viability over time (Figure 5) and suggested that the level of sustained viability was highly dependent on the cellular composition and tissue used. Of note, MDTs at day 0 showed higher levels of apoptosis, which may be due to potential stress factors induced by the microdissection procedure.

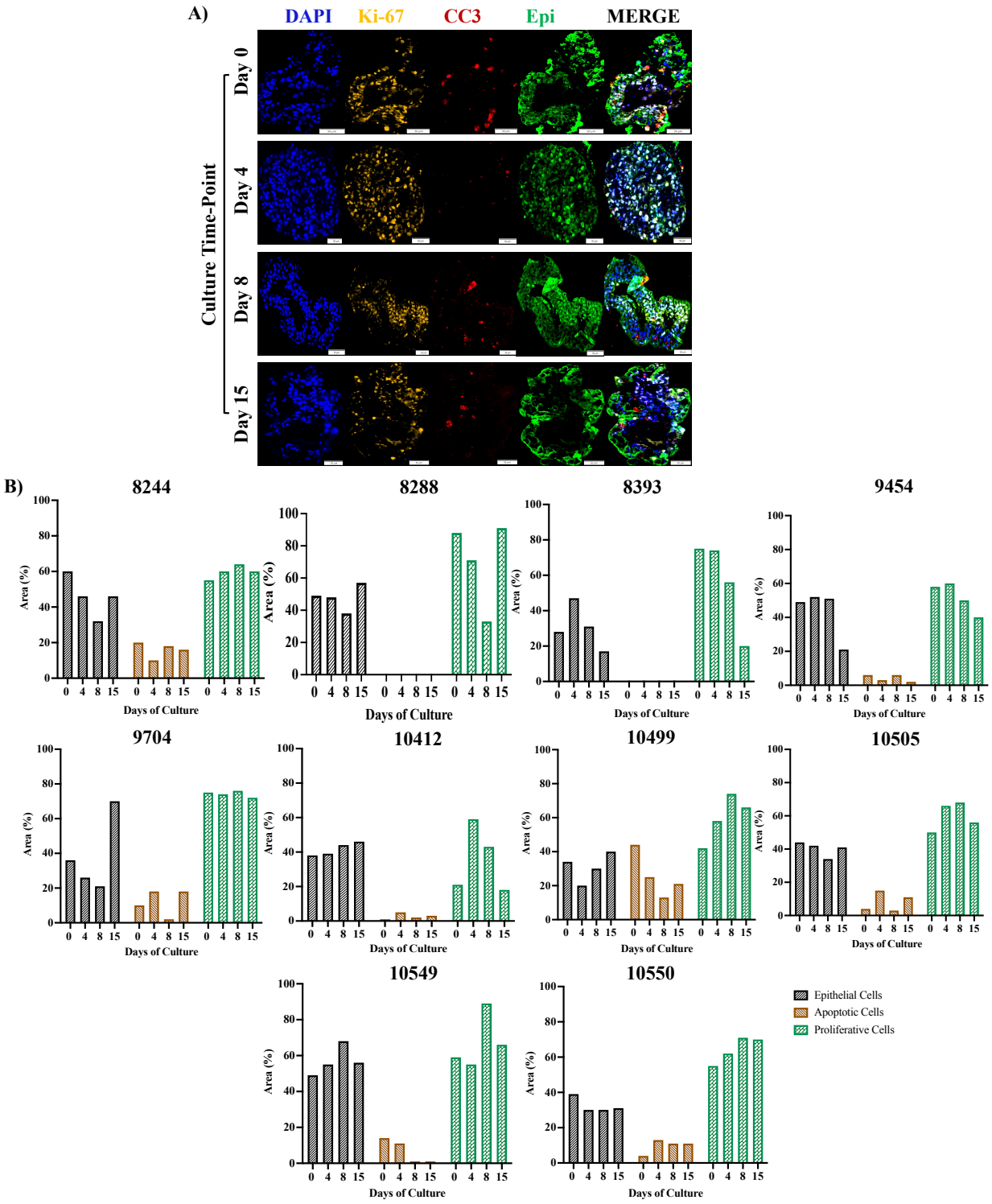

Figure 5: High viability was sustained in epithelial content within MDTs over a 15-day culture period. A) Representative images of the PT and MDTs of patient 9454, stained for apoptotic (CC3) and proliferative (Ki-67) markers, as well as CK8/18 for epithelial cells. B) Histograms of epithelial content, and apoptotic and proliferative

ratios for each patient. A minimum of 15 MDTs (technical replicates) were analyzed per condition. Scale bar = 50 μm, magnification = 20x.

MDTs show potential to predict patient clinical response to combination chemotherapy

A major obstacle in the clinic is the inability to identify with sufficient accuracy the most effective therapeutic regimen for each individual patient with sufficient accuracy. To validate the utility of our *ex vivo* model system for this purpose, we compared the treatment response of MDTs to the patient-matched clinical response of the same therapeutic combination, carboplatin/paclitaxel (C/P). All OC patients underwent cytoreductive surgery followed by the standard first-line chemotherapy treatment (Supplementary Table 2). The *ex vivo* C/P concentration was based on the approximate physiological blood concentrations calculated in patients, at 300 μM and 80 nM respectively (using a carboplatin dosage of 300 mg/m2 and a paclitaxel dosage of 175 mg/m2, an average body surface area of 1.7 m2 and an average blood volume of 4.5 L). The clinical response of patients in the cohort was determined based on the Gynecological Cancer Intergroup (GCIG) definitions of fluctuations in CA-125 levels during and after six chemotherapy treatment cycles[46]. Abdominal-pelvic scans were also taken into consideration at 3 to 6 months after the last treatment cycle to detect the presence of metastatic lesions (Supplementary Table 2). Patient clinical responses were classified into three categories: sensitive (CA-125 in normal range with no presence of metastatic lesion 6 months after the last chemotherapy cycle), platinum-resistant (CA-125 increase with the presence of metastatic lesions between 3-6 months after the last chemotherapy cycle) and refractory (continuous high CA-125 levels with the presence of metastatic lesions at 3 months after the last chemotherapy cycle). To identify treatment response in MDTs, IF assays were conducted to compare the proportion of apoptotic (CC3) and proliferative (Ki-67) epithelial cells between untreated and treated MDTs. We plotted our predicted *ex vivo* analysis versus the matched patient clinical response based on patient sensitivity to chemotherapy within the SPSS program to produce ROC curves (Figure 6A) to pinpoint the most stringent ratios for classification of patient response in an *ex vivo* setting. Our results showed that the cut-off values were 1.785 for CC3 ratios and 0.705 for Ki-67 ratios (Figure 6A). Therefore, a ROC classification of 1 was given for values of CC3 ratio lower than 1.785 and for values of Ki-67 ratio higher

than 0.705 (Table 2). This divided patient-derived MDT chemo-sensitivity into two groups: responders (sensitive) with a ROC status of 0, and non-responders (platinum-resistant and refractory) with a ROC response status of 1-2 (Table 2). An example of a responder and non-responder classification is shown in Figure 6B-D: MDTs derived from patient 10505 showed significantly higher apoptotic (3.83) and lower proliferation (0.27) ratios than non-treated controls (responder), whereas MDTs from patient 9454 showed no significant changes in proliferation (0.75) or apoptotic (1.53) ratios (non-responder) (Figure 6C-D). Importantly, a similar epithelial cell content was observed between untreated and treated MDTs (Figure 6B). These classifications corresponded to the clinical outcomes of these patients indicated by clinical CA-125 levels (Figure 6E, Table 2). Our response prediction panel is composed of 17 patients in which complete clinical follow-up. The comparison results showed a positive correlation of 88.2% (Figure 6F, green cases) between the MDT treatment response (Table 2) and clinical response (Supplementary Table 2) in our cohort. These results suggest that MDTs have strong potential in predicting the patient sensitivity to treatment.

Table 2: *Ex Vivo* response and classification

Biobank ID	Treatment	Ex Vivo Response	Apoptotic Ratio	Apoptotic Classification†	Proliferative Ratio	Proliferative Classification‡	Response Status*
9061		NR	1.03	1	0.94	1	2
9443		NR	1.18	1	1.13	1	2
9447		NR	0.61	1	0.45	0	1
9454		NR	1.53	1	0.75	1	2
9532		R	4.20	0	0.32	0	0
9562		R	2.08	0	0.62	0	0
9704		R	2.54	0	0.54	0	0
9808		R	3.65	0	0.46	0	0
10329	C/P	R	2.04	0	0.31	0	0
10381		R	2.60	0	0.62	0	0
10499		R	2.11	0	0.57	0	0
10505		R	3.83	0	0.27	0	0
10520		R	6.03	0	0.28	0	0
10547		R	3.04	0	0.42	0	0
10557		NR	0.85	1	1.06	1	2
10627		R	5.71	0	0.34	0	0
10645		R	2.08	0	0.45	0	0

C/P: Carboplatin/Paclitaxel; NR: non-responder (response status of 1 or 2), R: responder (response status of 0), †: Apoptotic ROC of 1 if CC3 ratio < 1.785, ‡: Proliferative ROC of 1 if Ki-67 ratio > 0.705, *: Response status was calculated as the sum of both ROC values. Dashed lines indicate that the values apply to all lines.

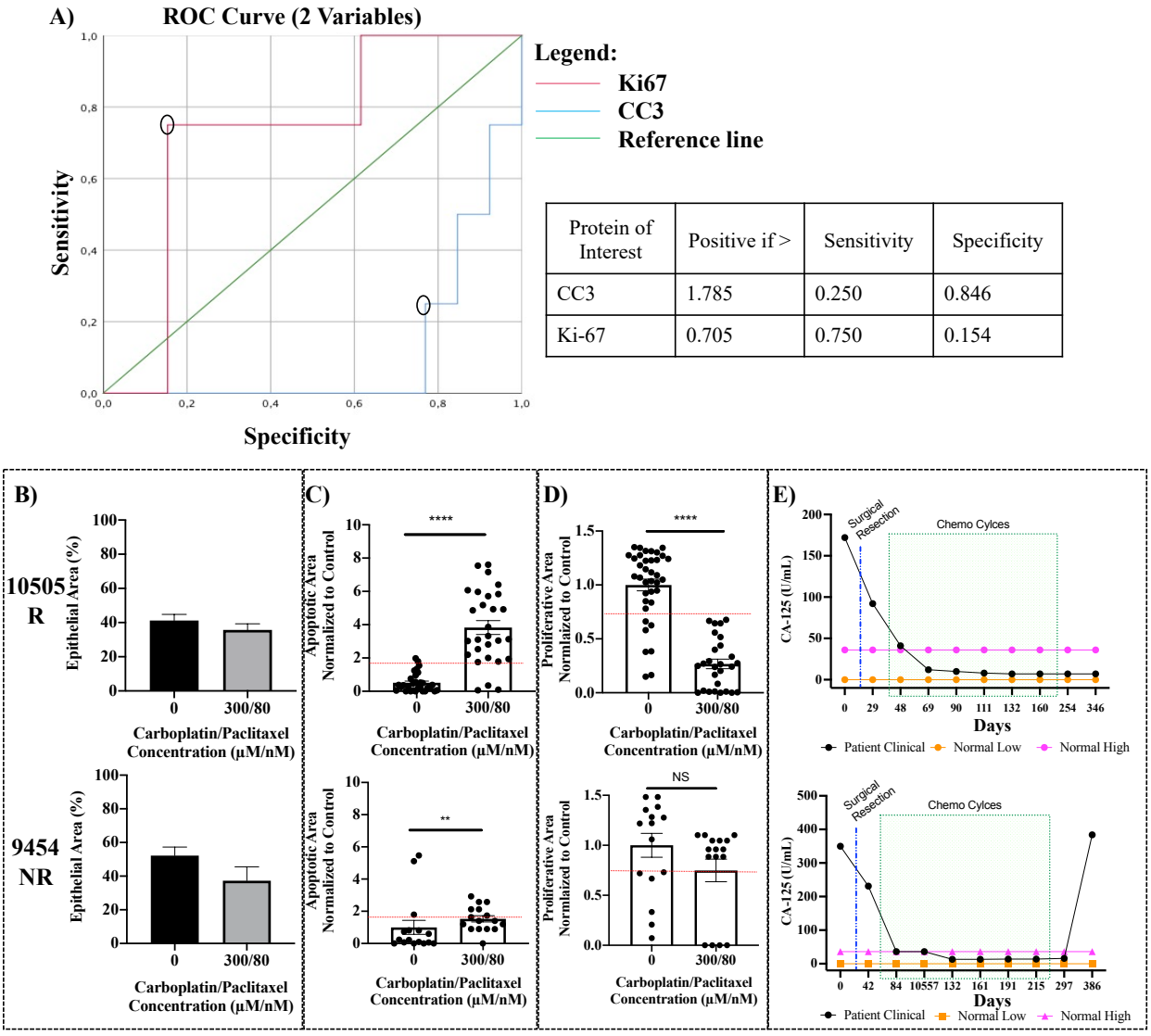

Protein of Interest	Positive if >	Sensitivity	Specificity
CC3	1.785	0.250	0.846
Ki-67	0.705	0.750	0.154

F)

Response	Patients																
	9061	9443	9447	9454	9532	9562	9704	9808	10329	10381	10499	10505	10520	10547	10557	10627	10645
Ex Vivo	2	2	1	2	0	0	0	0	0	0	0	0	0	0	2	0	0
Clinical	R	S	PR	R	S	S	S	S	S	S	S	S	S	S	S	S	S
Correlation																	

Figure 6: MDTs accurately predict patient clinical response to combination chemotherapy. A) ROC curve used to classify *ex vivo* response using two variables. B) Bar graph showing percentage of epithelial cell content between untreated and treated MDTs. Scatter box plots of the normalized area of expression of C) apoptosis marker CC3 and D) proliferation marker Ki67 for two patient samples representative of each response group. E) Clinical CA-125 levels of both patients over time. F) Table showing the correlation between *ex vivo* and clinical response (green signifies a positive correlation, red signifies a negative correlation and yellow signifies lack of clinical follow-up to confirm prediction). A minimum of 15 MDTs (technical replicates) were analyzed per condition.

2.3.2.5 Discussion

The complexity of primary tumors reflects the different response rates of individuals to the same drug regimens. Fundamental studies suggest that tumors are composed of a sub-population of cancer cells that contain different genotypic alterations and phenotypic characteristics that allow them to control their microenvironment to benefit their growth[17,18,47]. The TME has been shown to markedly impact the response rate of patients, hence the high importance of incorporating its presence in preclinical models to better reflect patient-specific responses to drugs[35]. Here, we show that our *ex vivo* tumor-derived model system better maintained the primary tumor's genetic composition than PCCs. However, we observed some discrepancies in MDTs between the day of microdissection procedure and days 8 and 15 of culture. KEGG analyses showed that pathways involved in stress-induced cell fate were downregulated when compared to the PTs. We hypothesize that when MDTs were given the time to recover from the microdissection, they were able to overcome certain stress factors. In addition, we show that the various TME cell lineages were maintained from the PTs over the course of a 15-day culture period, and that the epithelial cancer cell count in our MDTs maintained a highly viable state, representing accurate controls for drug response assays. This would provide the opportunity to study the effect of cytostatic drugs, which take longer to attain a statistically significant drug response.

The use of treatment response markers is pivotal in accurately predicting the patient's drug response. The C/P combination is the standard first-line treatment course for all OC patients. Carboplatin[48] is an alkylating agent that disrupts DNA function and paclitaxel[49] is a microtubule-stabilizing drug that causes cell cycle arrest in the mitosis phase. Both drugs induce cell death by activating the intrinsic apoptotic pathway in cells, which was monitored by CC3 and Ki-67 markers to classify responsiveness to chemotherapy in our EOC cohort. Caspase-3 is an executive protein that is activated by cleavage in the late stages of cellular apoptosis induced by various stimuli including chemotherapeutics. Ki-67 is a marker involved in all phases of proliferation and is considered an important biomarker in pathology. Thus, the level of Ki-67 positive cells within a primary tumor is frequently analyzed to assess aggressivity of cancer cells and is correlated to disease staging[50-52]. Thus, in our EOC patient cohort, cleaved caspase-3 (CC3) and

Ki-67 markers were used to classify response to chemotherapy (assess cells activating the apoptosis pathway versus cells strong enough to resist treatment). This proof of principle study showed that MDTs reliably predicted the clinical response of 15/17 EOC patients. However, further validation of the sensitivity of the model's predictive potential is required on a larger patient cohort.

PDX[53-55] and organoid[56,57] models of EOC have shown promise, predicting anti-cancer drug response with clinical data in matched patients. These tumor-derived model systems are important preclinical models for the screening and development of novel therapies to closely resemble clinical response. Genetically, these models show a close relationship to the matched primary tumor. However, PDXs often rely on the use of immunodeficient mouse models without retention of the natural TME of the patient and are subject to the infiltration of mouse cells over the course of sequential passaging. For organoid models, production is based on the complete dissociation of the tumor specimen into single cell suspensions to re-establish the tumor using Matrigel and nutrient-rich medium, while removing components of the TME or sub-clonal population of cancer cells. Furthermore, the use of these models as a clinical guidance tool is impractical as they have lengthy generation times and low succession efficiency.

Amongst other *ex vivo* models, tissue slices and recently published 3D patient-derived spheroids have shown similar positive correlations to the clinical response. Tissue slices are often 300-500 μm thick slices of varying lengths and often rely on plastic 96-well dishes for culture, which reduces the oxygen supply to the tissue core and increases hypoxia-induced necrosis, reducing the potential use of this model system[36-39]. 3D patient-derived spheroids have recently been developed[56] as an analytical tool to predict patient response in EOC patient samples. While the authors showed a 90% success rate in producing spheroids from whole tissue and biopsy specimens, the dissociation procedure resulted in low cell viability. In addition, response was evaluated by the presence of a panel of cytokeratins, which are not indicative of drug-induced responses. In contrast to tissue slices and 3D patient-derived spheroids, MDTs are cultured in specifically designed microfluidic devices fabricated from polydimethylsiloxane (PDMS) that is gas permeable, allowing a constant supply of oxygen. The size of channel to media volume ratio allows MDTs to have access to sufficient nutrients for up to 72 hours[40]. We show that the natural TME is maintained, and

that the survival of various cell lineages is sustained for a 15-day culture period using the MDTMA histological tool. Furthermore, the micro-size of our model system also broadens the use of limited tumor specimens, especially biopsies, which determine the diagnosis for many cancers.

Due to its high viability over a prolonged culture period, our model system allows for more testing of different drugs that require more time for anticancer activity, including chemotherapeutics, small molecules and monoclonal antibodies. More specifically, poly (ADP-ribose) polymerase inhibitors (PARPi) have been approved as a maintenance treatment in EOC patients that carry BRCA mutations and have a complete or partial response to chemotherapy[58]. Preclinical studies have shown that PARPis takes up to 6 days to induce an apoptosis cascade[59,60], which is feasible using our model. Accordingly, we can further test PARPis alone or in combination with chemotherapies in biopsied specimen to evaluate their effect in a neo-adjuvant or adjuvant setting. Furthermore, our MDTMA read-out tool can easily be adapted to analyze specific antibodies associated with drugs of interest. For example, PARPis induce DNA damage that can be detected by increased γ-H2AX foci within Ki-67-positive cancer cells. Our model provides opportunities to adapt for different cancer types and treatment alternatives to better predict patient assessment in a clinically relevant timeframe.

Beyond facilitating a personalized approach in cancer care, our model system is an integral tool for fundamental research studying cancer cells and their TME components for the discovery of novel targeted therapeutic strategies. In addition, drug discovery pipelines are long and costly with success rates of only 11.8% for novel drugs entering the market[61], due in part to a lack of adequate preclinical models. Thus, the incorporation of our *ex vivo* tumor-derived MDTs as a more representative preclinical model can serve to evaluate the efficacy of novel therapeutics prior to conducting costly clinical phase trials.

Our results show that MDTs can serve as a platform model to evaluate the efficacy of drugs on patient samples, which would improve patient-personalized treatment plans and increase patient overall survival, while eliminating ineffective agents with lots of undesirable secondary effects. Moreover, our model can give preclinical insight for potential clinical phase studies, to ameliorate the percentage of effective drugs entering the marketplace.

2.3.2.6 Acknowledgements

We thank the technical staff of the research platforms at the Centre de recherche du CHUM (CRCHUM): Liliane Meunier and Véronique Barrès (Molecular Pathology), Jennifer Kendall-Dupont (Microfluidics) and Jacqueline Chung (manuscript editing). We acknowledge Alex Sauriol for revising and providing KEGG analysis protocol. We also thank the CRCHUM ovarian tumor bank, which is supported by Ovarian Cancer Canada (OCC) and by the *Banque de tissus et de données of the Réseau de recherche sur le cancer of the Fonds de recherche du Québec - Santé* (FRQS) affiliated with the Canadian Tumor Repository Network (CTRNet). We gratefully acknowledge K.S salary support for this work provided by the following funding agencies/institutions: FRQS, Centre de recherche du Centre hospitalier de l'Université de Montréal and Canderel Fund of the Institut du cancer de Montréal.

2.3.2.7 Competing financial interest

K.S., B.P, A-M.M-M, and T.G. declare a conflict of interest under the form of a patent. T.G. declares a conflict of interest as the co-founder, Chief Technological Officer, and minority shareholder of MISO Chip Inc., a company operating in the field of *ex vivo* tissue culture.

2.3.2.8 Grant support

This work was supported by grants from the Cancer Research Society partnered with Ovarian Cancer Canada (#20103 to AMMM, DP and TG), the Canadian Cancer Society Research Institute (#702952 to AMMM, DP and TG), the National Science and Engineering Research Council of Canada (#RGPIN-06409 to TG), and the ICM (Fonds Défi Spyder and Anne-Marie Chagnon to DP). This research was conducted as part of the TransMedTech Institute's activities and supported, in part, by funding from the Canada First Research Excellence Fund. This research was carried out in part using the CRCHUM Microfluidics Core Facility supported by the TransMedTech Institute and its main financial partner, the Canada First Research Excellence Fund. Ovarian tumor banking was supported by Ovarian Cancer Canada (OCC) and by the Banque de tissus et de données of the Réseau de recherche sur le cancer of the FRQS affiliated with the Canadian Tumor Repository Network (CTRNet). AMMM, DP and FS are researchers of

the CRCHUM/ICM, which receive support from the FRQS. KS was supported by the TransMedTech Institute and FRQS as well as by a studentship from the Canderel Fund of the ICM. The funders had no role in study design, data collection and analysis, decision to publish, or preparation of the manuscript.

2.3.2.9 Author contributions

K.S., B.P. and E.C. wrote the main manuscript text and prepared the figures and tables. All authors reviewed the manuscript. Conception/design: K.S., B.P., E.C., A-M.M-M. Data acquisition: K.S., J.K-D. Data analysis: K.S. Data interpretation: K.S., B.P., E.C., D.P., A-M.M-M. Supervision: B.P., E.C., F.S. and A-M.M-M. Funding acquisition: F.S., T.G., D.P. and A-M.M-M.

2.3.2.10 References

1. Siegel RL, Miller KD, Fuchs HE, et al: Cancer Statistics, 2021. CA Cancer J Clin 71:7-33, 2021
2. Torre LA, Trabert B, DeSantis CE, et al: Ovarian cancer statistics, 2018. CA Cancer J Clin 68:284-296, 2018
3. Lheureux S, Gourley C, Vergote I, et al: Epithelial ovarian cancer. Lancet 393:1240-1253, 2019
4. Cancer Genome Atlas Research N: Integrated genomic analyses of ovarian carcinoma. Nature 474:609-15, 2011
5. Cybulska P, Paula ADC, Tseng J, et al: Molecular profiling and molecular classification of endometrioid ovarian carcinomas. Gynecol Oncol 154:516-523, 2019
6. Murakami R, Matsumura N, Brown JB, et al: Exome Sequencing Landscape Analysis in Ovarian Clear Cell Carcinoma Shed Light on Key Chromosomal Regions and Mutation Gene Networks. Am J Pathol 187:2246-2258, 2017
7. Teer JK, Yoder S, Gjyshi A, et al: Mutational heterogeneity in non-serous ovarian cancers. Sci Rep 7:9728, 2017
8. Previs RA, Sood AK, Mills GB, et al: The rise of genomic profiling in ovarian cancer. Expert Rev Mol Diagn 16:1337-1351, 2016
9. Meinhold-Heerlein I, Fotopoulou C, Harter P, et al: The new WHO classification of ovarian, fallopian tube, and primary peritoneal cancer and its clinical implications. Arch Gynecol Obstet 293:695-700, 2016
10. Ryland GL, Hunter SM, Doyle MA, et al: Mutational landscape of mucinous ovarian carcinoma and its neoplastic precursors. Genome Med 7:87, 2015
11. Bashashati A, Ha G, Tone A, et al: Distinct evolutionary trajectories of primary high-grade serous ovarian cancers revealed through spatial mutational profiling. J Pathol 231:21-34, 2013
12. Lheureux S, Braunstein M, Oza AM: Epithelial ovarian cancer: Evolution of management in the era of precision medicine. CA Cancer J Clin 69:280-304, 2019
13. Kossai M, Leary A, Scoazec JY, et al: Ovarian Cancer: A Heterogeneous Disease. Pathobiology 85:41-49, 2018
14. Marth C, Reimer D, Zeimet AG: Front-line therapy of advanced epithelial ovarian cancer: standard treatment. Ann Oncol 28:viii36-viii39, 2017
15. Lazarevic T, Rilak A, Bugarcic ZD: Platinum, palladium, gold and ruthenium complexes as anticancer agents: Current clinical uses, cytotoxicity studies and future perspectives. Eur J Med Chem 142:8-31, 2017

16. Weaver BA: How Taxol/paclitaxel kills cancer cells. Mol Biol Cell 25:2677-81, 2014
17. Cooper GM: A Molecular Approach, in Associates S (ed): The Cell (ed 2nd). MA, Sunderland, 2000
18. Simmons DPSMJ: Principles of Genetics (ed 6th), John Wiley & Sons, Inc., pp 581-600
19. Committee CCSA: Ovarian Cancer Statistics 2019. Toronto, ON, Canadian Cancer Society, 2019
20. International Collaborative Ovarian Neoplasm G: Paclitaxel plus carboplatin versus standard chemotherapy with either single-agent carboplatin or cyclophosphamide, doxorubicin, and cisplatin in women with ovarian cancer: the ICON3 randomised trial. Lancet 360:505-15, 2002
21. Vasan N, Baselga J, Hyman DM: A view on drug resistance in cancer. Nature 575:299-309, 2019
22. Arul M, Roslani AC, Cheah SH: Heterogeneity in cancer cells: variation in drug response in different primary and secondary colorectal cancer cell lines in vitro. In Vitro Cell Dev Biol Anim 53:435-447, 2017
23. Sauriol A, Simeone K, Portelance L, et al: Modeling the Diversity of Epithelial Ovarian Cancer through Ten Novel Well Characterized Cell Lines Covering Multiple Subtypes of the Disease. Cancers (Basel) 12, 2020
24. Heredia-Soto V, Redondo A, Berjon A, et al: High-throughput 3-dimensional culture of epithelial ovarian cancer cells as preclinical model of disease. Oncotarget 9:21893-21903, 2018
25. Magnotti E, Marasco WA: The latest animal models of ovarian cancer for novel drug discovery. Expert Opin Drug Discov 13:249-257, 2018
26. Zakarya R, Howell VM, Colvin EK: Modelling Epithelial Ovarian Cancer in Mice: Classical and Emerging Approaches. Int J Mol Sci 21, 2020
27. Morgan MM, Johnson BP, Livingston MK, et al: Personalized in vitro cancer models to predict therapeutic response: Challenges and a framework for improvement. Pharmacol Ther 165:79-92, 2016
28. Bounaix Morand du Puch C, Nouaille M, Giraud S, et al: Chemotherapy outcome predictive effectiveness by the Oncogramme: pilot trial on stage-IV colorectal cancer. J Transl Med 14:10, 2016
29. Izumchenko E, Paz K, Ciznadija D, et al: Patient-derived xenografts effectively capture responses to oncology therapy in a heterogeneous cohort of patients with solid tumors. Ann Oncol 28:2595-2605, 2017
30. Scott CL, Becker MA, Haluska P, et al: Patient-derived xenograft models to improve targeted therapy in epithelial ovarian cancer treatment. Front Oncol 3:295, 2013
31. Fan H, Demirci U, Chen P: Emerging organoid models: leaping forward in cancer research. J Hematol Oncol 12:142, 2019
32. Nero C, Vizzielli G, Lorusso D, et al: Patient-derived organoids and high grade serous ovarian cancer: from disease modeling to personalized medicine. J Exp Clin Cancer Res 40:116, 2021
33. Nanki Y, Chiyoda T, Hirasawa A, et al: Patient-derived ovarian cancer organoids capture the genomic profiles of primary tumours applicable for drug sensitivity and resistance testing. Sci Rep 10:12581, 2020
34. Junttila MR, de Sauvage FJ: Influence of tumour micro-environment heterogeneity on therapeutic response. Nature 501:346-54, 2013
35. Balkwill FR, Capasso M, Hagemann T: The tumor microenvironment at a glance. J Cell Sci 125:5591-6, 2012
36. Majumder B, Baraneedharan U, Thiyagarajan S, et al: Predicting clinical response to anticancer drugs using an ex vivo platform that captures tumour heterogeneity. Nat Commun 6:6169, 2015
37. Roelants C, Pillet C, Franquet Q, et al: Ex-Vivo Treatment of Tumor Tissue Slices as a Predictive Preclinical Method to Evaluate Targeted Therapies for Patients with Renal Carcinoma. Cancers (Basel) 12, 2020
38. Zhang W, van Weerden WM, de Ridder CMA, et al: Ex vivo treatment of prostate tumor tissue recapitulates in vivo therapy response. Prostate 79:390-402, 2019
39. van de Merbel AF, van der Horst G, van der Mark MH, et al: An ex vivo Tissue Culture Model for the Assessment of Individualized Drug Responses in Prostate and Bladder Cancer. Front Oncol 8:400, 2018
40. Astolfi M, Peant B, Lateef MA, et al: Micro-dissected tumor tissues on chip: an ex vivo method for drug testing and personalized therapy. Lab Chip 16:312-25, 2016

41. Simeone K, Guay-Lord R, Lateef MA, et al: Paraffin-embedding lithography and micro-dissected tissue micro-arrays: tools for biological and pharmacological analysis of ex vivo solid tumors. Lab Chip 19:693-705, 2019
42. Prat J, Oncology FCoG: Staging classification for cancer of the ovary, fallopian tube, and peritoneum. Int J Gynaecol Obstet 124:1-5, 2014
43. Theriault BL, Portelance L, Mes-Masson AM, et al: Establishment of primary cultures from ovarian tumor tissue and ascites fluid. Methods Mol Biol 1049:323-36, 2013
44. Miserocchi G, Mercatali L, Liverani C, et al: Management and potentialities of primary cancer cultures in preclinical and translational studies. J Transl Med 15:229, 2017
45. Kodack DP, Farago AF, Dastur A, et al: Primary Patient-Derived Cancer Cells and Their Potential for Personalized Cancer Patient Care. Cell Rep 21:3298-3309, 2017
46. Brown J, Friedlander M, Backes FJ, et al: Gynecologic Cancer Intergroup (GCIG) consensus review for ovarian germ cell tumors. Int J Gynecol Cancer 24:S48-54, 2014
47. Hanahan D, Weinberg RA: Hallmarks of cancer: the next generation. Cell 144:646-74, 2011
48. Dilruba S, Kalayda GV: Platinum-based drugs: past, present and future. Cancer Chemother Pharmacol 77:1103-24, 2016
49. Florian S, Mitchison TJ: Anti-Microtubule Drugs. Methods Mol Biol 1413:403-21, 2016
50. Soliman NA, Yussif SM: Ki-67 as a prognostic marker according to breast cancer molecular subtype. Cancer Biol Med 13:496-504, 2016
51. Foltyn W, Zajecki W, Marek B, et al: The value of the Ki-67 proliferation marker as a prognostic factor in gastroenteropancreatic neuroendocrine tumours. Endokrynol Pol 63:362-6, 2012
52. Rodel F, Zhou S, Gyorffy B, et al: The Prognostic Relevance of the Proliferation Markers Ki-67 and Plk1 in Early-Stage Ovarian Cancer Patients With Serous, Low-Grade Carcinoma Based on mRNA and Protein Expression. Front Oncol 10:558932, 2020
53. Aguilar-Mahecha A, Joseph S, Cavallone L, et al: Precision Medicine Tools to Guide Therapy and Monitor Response to Treatment in a HER-2+ Gastric Cancer Patient: Case Report. Front Oncol 9:698, 2019
54. Topp MD, Hartley L, Cook M, et al: Molecular correlates of platinum response in human high-grade serous ovarian cancer patient-derived xenografts. Mol Oncol 8:656-68, 2014
55. Ricci F, Bizzaro F, Cesca M, et al: Patient-derived ovarian tumor xenografts recapitulate human clinicopathology and genetic alterations. Cancer Res 74:6980-90, 2014
56. Shuford S, Wilhelm C, Rayner M, et al: Prospective Validation of an Ex Vivo, Patient-Derived 3D Spheroid Model for Response Predictions in Newly Diagnosed Ovarian Cancer. Sci Rep 9:11153, 2019
57. Maenhoudt N, Defraye C, Boretto M, et al: Developing Organoids from Ovarian Cancer as Experimental and Preclinical Models. Stem Cell Reports 14:717-729, 2020
58. Montemorano L, Lightfoot MD, Bixel K: Role of Olaparib as Maintenance Treatment for Ovarian Cancer: The Evidence to Date. Onco Targets Ther 12:11497-11506, 2019
59. Fleury H, Carmona E, Morin VG, et al: Cumulative defects in DNA repair pathways drive the PARP inhibitor response in high-grade serous epithelial ovarian cancer cell lines. Oncotarget 8:40152-40168, 2017
60. Fleury H, Malaquin N, Tu V, et al: Exploiting interconnected synthetic lethal interactions between PARP inhibition and cancer cell reversible senescence. Nat Commun 10:2556, 2019
61. Scannell JW, Bosley J: When Quality Beats Quantity: Decision Theory, Drug Discovery, and the Reproducibility Crisis. PLoS One 11:e0147215, 2016.

2.3.2.11 Supplemental tables and figures

Supplemental Table 1: Primary and secondary antibodies used for immunofluorescence analysis

Primary Antibody	Dilution	Primary Antibody Reference	Secondary Antibody	Secondar Antibody Reference
Mouse Anti-CD34	1:2	1563230, Agilent, Saint-Laurent, Quebec, Canada	Mouse Alexa-488	A11029, Thermofisher
Mouse anti-CD45	1:50	M0701, Agilent	Mouse Cy5	A21236, Thermofisher
Mouse anti-CD68	1:50	M0876, Agilent	Mouse Alexa-546	A11035, Thermofisher
Rabbit anti-CK8/18	1:2	IR094, Agilent	Rabbit Alexa-750	A21039, Thermofisher
Mouse anti-FAP	1:200	MAB3715, Cedarlane, Cork, Ireland	Mouse Alexa-546	A11035, Thermofisher
Mouse anti-Ki67	1:500	9449, Cell Signaling Technology, Danvers, MA	Mouse Alexa-546	A11035, Thermofisher
Rabbit anti-CC3	1:200	9661, Cell Signalling Technology	Rabbit Cy5	A10523, Thermofisher
Mouse anti-CK8	1:200	MA514428, Thermofisher	Mouse Alexa-488	A11029, Thermofisher
Mouse anti-CK18	1:200	6259, SantaCruz, Dallas, Texas	Mouse Alexa-488	A11029, Thermofisher

Supplementary Table 2: Clinical data of patients in response prediction experiment

Biobank ID	Cyto-Reductive Surgery, Residual Disease†	Type of First-Line Treatment	CA-125					Abdominal-Pelvic Scan Post-C/P Response	Other pertinent information
			Pre-Surgery	Pre-C/P	End of C/P	3 mox post-C/P	6 mos post-C/P		
9061	Complete		918	110	29	62	-	**Refractory**	**Pacli/Bevacizumab 2 months post C/P**
9443	Optimal		320	234	78	41	77	**Sensitive**	**Slow progressive tumor**
9447	Sub-Optimal		5821	2653	134	473	4801	**Platinum-Resistant**	**Carboplatin/ Caelyx 4 months post C/P**
9454	Complete		350	231	14	48	384	**Refractory**	
9532	Complete		214	12	10	8	8	**Sensitive**	
9562	Sub-optimal		1549	1095	9	7	6	**Sensitive**	
9704	Complete		302	10	8	8	8	**Sensitive**	
9808	Complete	Carboplatin/ Paclitaxel	660	37	13	13	13	**Sensitive**	
10329	Complete		302					**Sensitive**	
10381	Complete		81	14	14	12	12	**Sensitive**	
10412	Complete		13		6.6	6.6			
10499	Complete		1157	1297	17	17	17	**Sensitive**	
10505	Complete		172	41	7	7	19	**Sensitive**	
10520	Complete		1136	60	3	3	3	**Sensitive**	
10547	Complete		1850	-	7	7	7	**Sensitive**	
10549	Complete		795	656					
10557	Complete		38	38	5	5			**Hormone therapy 3 months post C/P**

C/P: carboplatin/paclitaxel; †Residual Disease: optimal if ≤1 cm, sub-optimal if ≥1.0 cm, complete if no lesions; Dashed lines indicate that the values apply to all lines. Yellow denotes lack of clinical follow-up for the indicated timepoints.

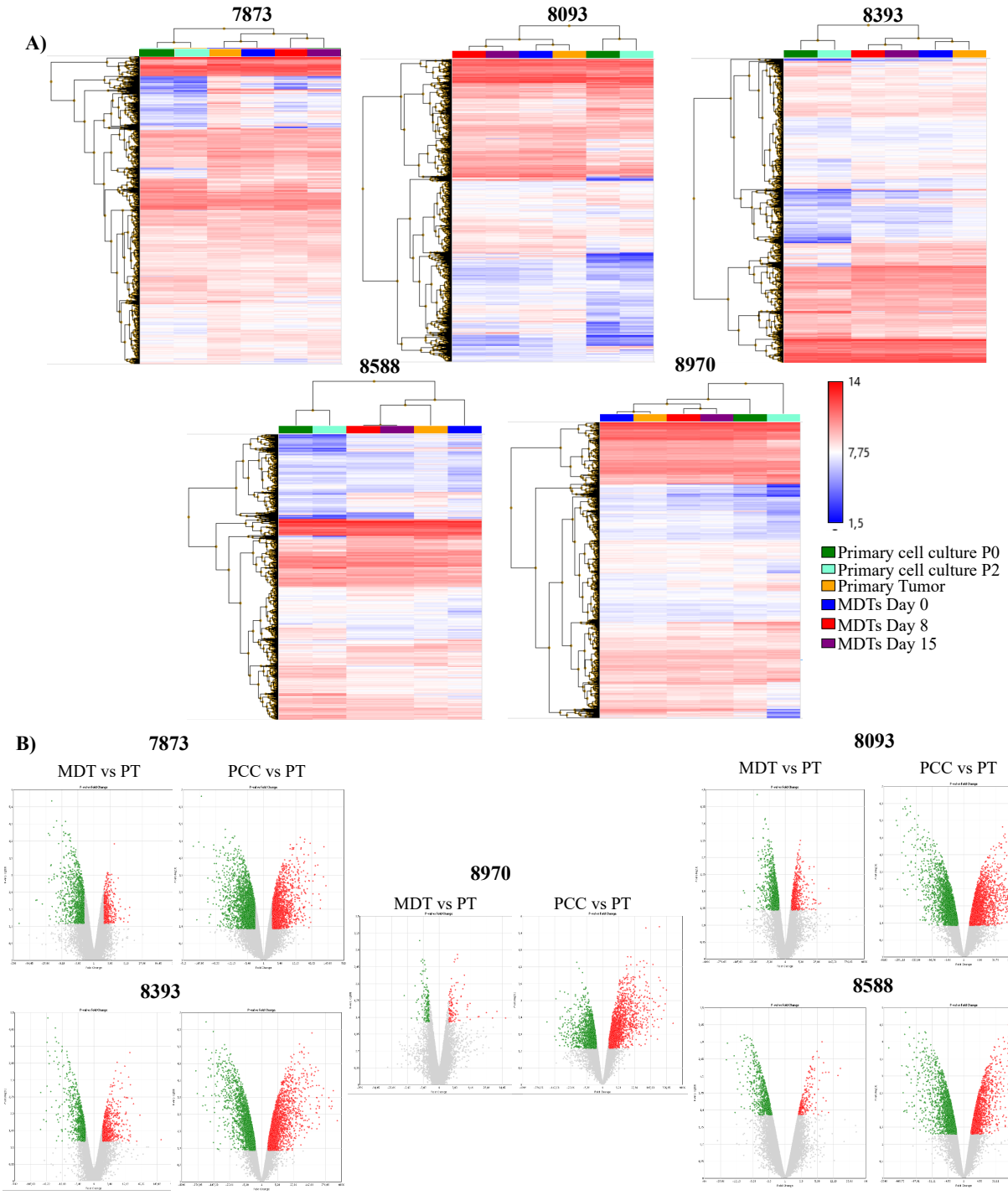

Supplemental Figure 1: Microarray analysis of patient samples. A) Hierarchical clustering analysis of over 20,000 genes performed with MeV. B) Volcano plots showing the number of differentially expressed genes between each model type and PTs for all five patients. A total of 15 MDTs (technical replicates) were analyzed per condition. P0: passage 0, P2: passage 2.

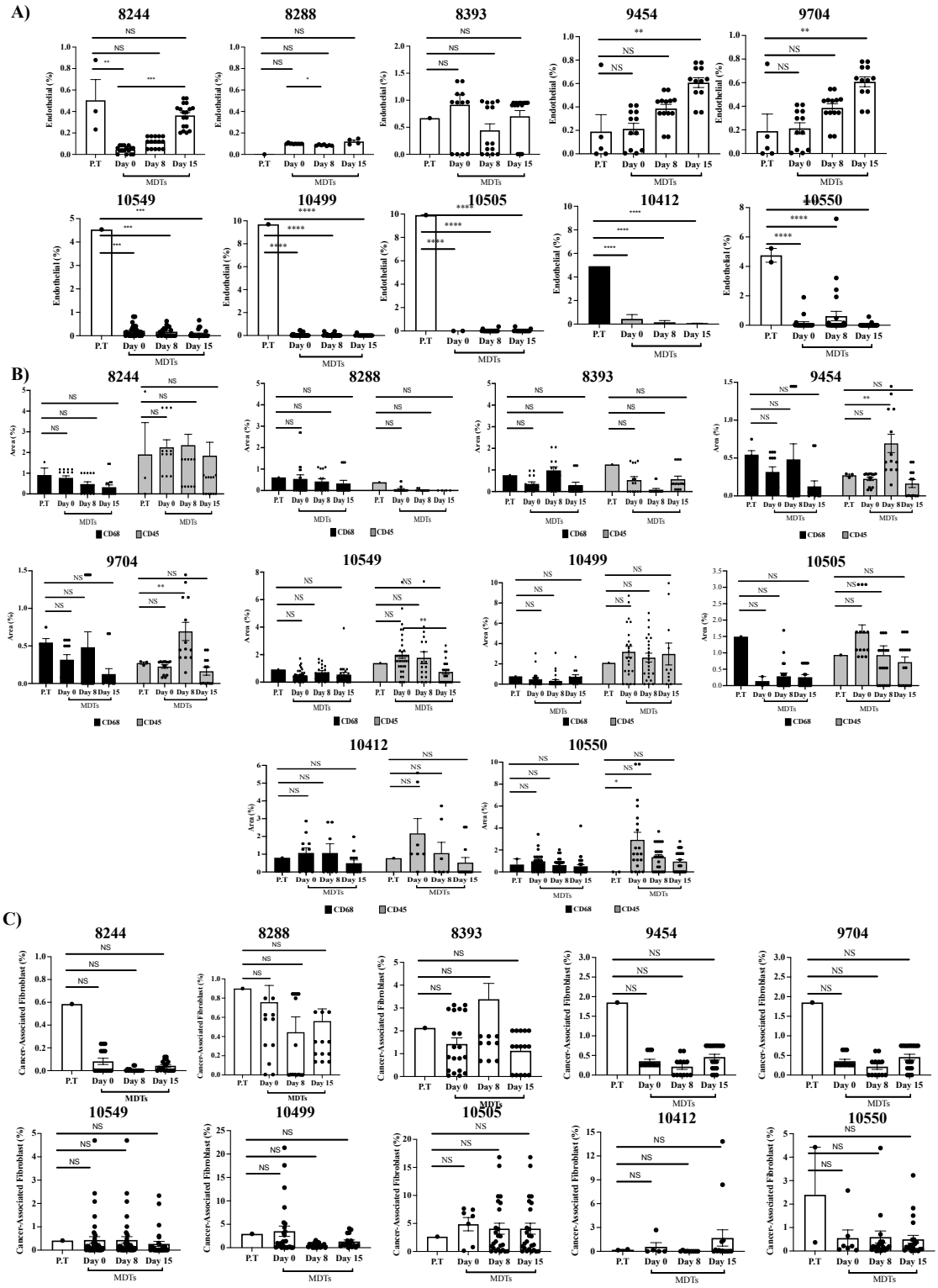

Supplemental Figure 2: Tumor microenvironment cell lineage present for each patient over a 15-day culture period. Scatter box plots of the average expression of the marker for A) endothelial cells, B) monocytes, leucocytes and C) cancer-associated fibroblasts for each patient. Data are represented as the mean ± SEM. A minimum of 15

MDTs (technical replicates) were analyzed per condition for each patient. Statistical significance $p<0.05$ (Student t-test). NS: non significant.

3 DISCUSSION

This thesis describes the characterization and validation of the *ex vivo* tumor-derived model system. The first chapter of this thesis confirmed the feasibility of casting MDTs in paraffin with simple steps, reducing the potential tissue damage caused by off-chip manipulations. Preliminary characterization of MDTs produced from cell line xenograft tumors suggested that MDTs, derived from cell line xenograft tumors, mirrored the intra-tumor heterogeneity found in solid tumors and maintained high viability for 15 days of culture that was comparable between the MDTMA technique and flow cytometry. In addition, the utility of MDTs can be expanded to simultaneous characterizations of multiple biological pathways in the response to stimuli to examen mechanistic effects. The second chapter of this thesis highlighted the importance of MDTs as a preclinical model. Our comparison of cancer models validated that by establishing a proper treatment regimen for a drug of interest, the *ex vivo* models reliably mirrored the chemosensitivity profile of *in vivo* models. This demonstrated that the complexity of *ex vivo* tumor-derived model systems was similar to gold standard *in vivo* pre-clinical models that test for drug efficacy. Finally, the third chapter of this thesis characterized the TME within MDTs derived from patient tumor samples and was the first clinical comparison study to evaluate their predictive potential and utility as a clinical guidance tool. The results from this study revealed that the gene expression profiles between MDTs and matched primary tumors were highly correlated compared to primary cell cultures. In addition, the TME, which plays a pivotal role in patient-specific response to drugs, is well preserved within MDTs over the course of the 15-day highly viable culture period. Also, preliminary data performed on a small cohort of EOC patients showed that prediction of response was highly sensitive and allowed therapeutic responses to be evaluated prior to treatment. Ultimately, our work suggests that this model system can be used for a variety of solid tumors, benefiting not only OC and PC cancers but other types of cancers that are faced with similar clinical challenges.

MDTs have several advantages as a preclinical model to screen drug efficacy on patient tumors as well as a clinical guidance tool to personalize treatment plans. The main advantage of MDTs when comparing

to other *ex vivo* tissue slice cultures are their size and culture platform that utilizes microfluidic technology. This combination strategy reduces sample size needed and reagent consumption[6] benefiting the use of scarce tissue and lower volume of expensive therapeutic agents. The specific design of the microfluidic device allows for precise spatiotemporal control of fluids and ability to maintain a constant supply of oxygen[147] as well as size to media volume ratio to sustain enough nutrients for several days in a non-perfused setting. In addition, the culture platform allows for micro-sized tumors to preserve their natural TME better mimicking human malignancy[6,151]. In comparison with other *ex vivo* models[144,148], MDTs are cultured in media without supplemental growth factors that can alter cellular responses and the cell epigenome. The average viability of *ex vivo* tissue slice cultures remain limited to 8 days[140,146] whereas MDTs can sustain a confirmed viability of 15[151] days widening the range of therapeutic and biological studies analyzable including various cycles of chemotherapy or the effectiveness of cytostatic drugs. This suggests that patient samples can be analyzed, depending on the course of treatment given, in a 1 to 3-week time frame, representing an ideal drug prediction model.

3.1 Importance of results

The work shown throughout this thesis contains important additions to the literature. The robustness and simple design of our *ex vivo* model system rationalizes its potential impact in a translational research, clinical and pharmaceutical setting. The throughput casting of MDTs in paraffin was developed to be reliable and easily adaptable to PDMS-based microfluidic culture platforms. This histological read-out methodology was adapted from the commonly used FFPE procedure that is the gold standard technique in clinical pathology. Similarly, our procedure reflects the ability to produce a substantial amount of analyzable slices[151], which is proportional to the tissue volume, allowing for the analysis of a large spectrum of antibodies to be done in a consecutive manner. In comparison to other *ex vivo* tissue slice studies, FFPE remains the standard technique used. Kang et al group[152] created a micro-pillar array for hydrogel-supported 3D spheroids in order to cast spheroids in OCT and paraffine for imaging further resembling our MDT and MDTMA methodology. This technique relies on the production of spheroids within a hydrogel and

incorporation into an OCT or paraffin block without disrupting the spherical nature of the model and while maintaining the original alignment of the spheroids within the hydrogel. In contrast, their technique is restricted to 3D spheroids model and have a low throughput potential due to its 9-spheroid capacity[152]. In addition, we showed that our model can follow biological pathways involved in tumor progression including NF-kB pathway and drug response by following the activation of an apoptosis effector, caspase-3[151]. These experiments were chosen to provide the proof of concept to support the use of this platform to study tumor biology, to validate fundamental research on tumor biology and drug efficacy on fresh tissue samples. Compared to the literature, very few papers have shown similar findings using their *ex vivo* models.

To compliment methodological and proof of concept findings, we've validated the preclinical relevance of our *ex vivo* model system. The use of preclinical models in drug discovery is crucial to the development of effective therapeutic options. The model comparison study (Chapter 2.2) showed that the carboplatin-sensitivity profile of MDTs better reflects gold standard *in vivo* models whereas 2D monolayers and 3D spheroid models provide some discrepant results. In the literature, very few papers have compared sensitivity profiles of standardly used drugs between typically used preclinical models. In 1984, Erlichman and Vidgen[153] were amongst the few to compare the cytotoxicity of adriamycin in colon cancer models showing that 3D spheroid models better reflect *in vivo* response compared to monolayer cell cultures. Thus, this work brings high impact and relevance to the literature as it incorporates a more modern spheroid formation methodology and sophisticated tumor-derived model system. The strength of our work relies on the comparison of independent carboplatin sensitivity ranking across models using same cell lines, normalizing the variability between model systems. In addition, the analysis was performed on 6 cell lines of different histological subtypes of ovarian cancer, broadening the feasibility and reproducibility of the results. This study further highlights the importance of properly selecting preclinical models for drug sensitivity assays as well as better understanding the heterogenous variations that exists between the different model systems.

From a clinical perspective, fresh tumor-based model systems continue to show relevance in representing the heterogeneity found in solid tumors compared to cell line-based models. The extensive characterization

of our *ex vivo* tumor-derived MDT model supports its ability to reflect patient-specific drug responses. These findings demonstrate that MDTs can maintain similar gene expression profile, throughout their 15-day culture period, as in the primary tumors. In addition, the natural TME is also maintained reflecting an abundance of nutrients in culture media to sustain high viability and preservation of cell lineages in the tumor model as well as a high predictive potential. In comparison to the literature, there exists a large spectrum of patient-derived model systems that have impacted scientific research including tissue slices[142,144,146], PDX[130,154,155], organoids[120,133,156] and novel patient-derived spheroids[131]. Our model system adds to this impact by providing a micro-dissected version of tumor-derived model system to compliment some of the limitations seen in these models. Extensive studies have been made on PDX and organoid models showing major limitations in its usefulness as clinical guidance tool. There is a lack of TME components found in PDX[130,154,155] and organoid[120,133,156] models as well as a low production rate and highly time-consuming. In addition, no paper, thus far, has characterized the TME seen in tissue slice and tumor-spheroid models, only similar genetic composition as matched primary tumors[131,142,144,146]. There is an importance in characterizing the TME in patient-derived models to show the potential to explore different therapeutic avenues and increase its utility as a preclinical and clinical model in a research, clinic, and pharmaceutical setting. In addition, the pilot study performed on MDTs showing its relevance in predicting patient-specific responses to chemotherapy was done on a small cohort of patients, bringing a limitation in the study compared to tissue slice culture models[142,144,146]. This needs to be further validated on a larger cohort. Based on Peduzzi et al., a cohort of a minimum of 100 patients should be used to have the same predictive value as other studies in the literature[157]. This patient number cohort is based on the cancer progression rate and the number of variables under investigation (treatment, biomarkers, comparison strategy). Furthermore, *ex vivo* models have created a scientific research platform to aid in scientific and clinical research to better dictate patient response to drugs. The long-term advantage of this model will reduce the use of ineffective therapies on cancer patients and minimalize the burden of failed clinical trials of drugs with high toxicity.

3.2 Methodological challenges encountered

There exists a variety of analysis modalities in cancer research that have been shown to accurately evaluate the treatment response and drug monitoring. Our *ex vivo* model's culture platform is fabricated using a transparent polymer, PDMS, to facilitate the use of imaging modalities including confocal microscopy. The simplicity of the culture platform design allows easy disassembly to gain access to the MDTs allowing for flow cytometry analysis to be performed. However, each of these techniques have limitations. Confocal microscopy has an imaging depth limitation, which creates an undefined region at the core of the MDTs resulting in poor visualization of response. On the other hand, flow cytometry requires a complete dissociation of the MDTs to obtain single-cell suspension, which impacts overall survival of cells and results in destruction of tissue architecture and morphology.

To circumvent the disadvantages related to confocal microscopy and flow cytometry, we developed an assay that would preserve the tissue architecture and morphology while identifying treatment response using well-known biomarkers. Histological staining in combination with predictive biomarkers for diagnostic purposes, further facilitates clinical decision-making. The predictive potential of patient outcome using these biomarkers relies on computed statistical analysis in which clinicians may over-estimate the likelihood of response. To prevent this, we developed a Micro-Dissected Tissue Micro-Array (MDTMA), merging the standard paraffin embedding protocol with microfluidic technologies to empirically test the patients' response to therapeutic agents through the use of proliferative and viability biomarkers. MDTMAs represent an innovative tool that takes advantage of the throughput nature of microfluidics and Tissue Micro-Arrays (TMAs) to handle, probe and analyze large quantities of patient samples with simple manipulations and clinically available techniques. The advantage of this technique is highlighted by their pathology-based nature and semi-automatable applications, which the clinic is highly familiar with compared to confocal microscopy and flow cytometry.

The development and optimization of this histological tool to assess tissue architecture and cellular morphology of MDTs was very challenging due to precise multi-step procedures. The ultimate goal to transfer the MDTs from their original culture platform into a paraffin block, without manipulating the

specimens, was based on standard FFPE protocols. This procedure is initiated with an important formalin fixation step to inhibit cellular processes, preventing tissue degradation and preserving tissue architecture[158,159]. The effective exposure time was identified based on theoretical and experimental understanding of the fixative to avoid an over fixation of tissue, which can lead to epitope masking and decreased immunoreactivity[160,161]. A dehydration process is further assessed to maintain and preserve cellular morphology. This process remains the most crucial such that water retention within the tissue impacts the morphological features of the cells and tissue composition. The visualisation of MDTs is performed during the dehydration process such that the cytoplasm and connective tissue regions of the MDTs were stained with a red biological stain, phloxine B, which does not interfere with histological techniques including IHC, IF or H&E staining. A clearing agent such as xylene is then used prior to paraffin-embedding to help displace the ethanol within the tissue and allow for better infiltration of paraffin wax[162]. The infiltration of paraffin within the tissue can take between 20 minutes to several hours depending on tissue size, however the incubation time does not affect the overall result[160] (Appendix 2). With this technique, all MDTs from the chip could be integrated into a block while maintaining their natural microfluidic alignment, further allowing the analysis of up to 4 different treatment conditions with just one MDTMA slice. Every step of the procedure was thoroughly optimized to obtain samples with accurate architecture, morphology and proper epitope presentation (Appendix 3, Figure 1).

The ability to retain MDTs on microscope slides is extremely important to obtain high-density analyses. As previously mentioned, the number of MDTs, at experimental endpoint, is a limiting factor in attaining statistically significant results. Thus, sliced MDTMA blocks were placed on superfrost™ microscope slides and histological techniques were done to look at various cellular components and cell fates. The results suggested that H&E staining techniques did not highly influence the retention of MDTs on the microscope slide, however, some MDTs moved and so were not in their original placement. In addition, IHC and IF staining using a BenchMark XT automated stainer on same slides showed over 80% loss of MDTs. Several staining experiments were performed on MDTs derived from various cell line xenograft tumors showing same level of loss (Appendix 3, Figure 2A). In addition to MDT loss, the MDTs

remaining on the microscope slide were folded or blurry justifying a low retention (Appendix 3, Figure 2B). To resolve this problem, we extensively investigated different microscope slides and focused on the Matsunami TOMO® hydrophilic adhesion slides, which have a strong positive charge increasing adhesive properties for high tissue and cell retention. In addition, the hydrophilic surface is highly durable to thermal treatment. Experiments were conducted comparing MDT retention between the two types of microscope slides. The results suggest that the TOMO slides have a higher retention rate than the superfrost™ slides, the staining was adequate for analysis and tissue folding did not occur (Appendix 3, Figure 2C). This critical optimization greatly improved the ability to maintain and preserve MDTs for histological staining.

Primary tumors contain high heterogeneity, playing a pivotal role in treatment specific responses. This feature has been highly discussed throughout various chapters of this thesis. One of the studies performed characterized the number of MDTs that were required to attain statistical significance, done in collaboration with Polytechnique de Montréal. This study was based on cell line xenograft tumors that were highly homogenous. Mathematical simulation, based on the Monte Carol method (a computerized algorithm that relies on repeated random sampling), a minimum of 15 MDTs were needed to attain statistical significance and that the standard deviation was not drastically altered when compared to 20 MDTs. This theoretical calculation was applied by randomly identifying 15 regions of the primary tumor that were identical in size as the MDTs and comparing their protein expression of epithelial markers to 15 MDTs. The results showed that the average expression between the 15 randomly chosen regions of the primary tumor and 15 MDTs were extremely similar with ± 3.5% difference[151]. Since patient primary tumors are heterogeneous, the number of MDTs required for statistical significance would be highly dependent on the tumor cell content within primary tumors. On average, we estimate that a minimum of 15 MDTs is sufficient. In addition, depending on tissue characteristics, there can be some loss of MDTs through media change and histological techniques performed, reducing the total number of MDTs at the end. With the uncertainty of the percentage of cancer cells within a tumor specimen due to high heterogeneity and precise knowledge of technique, a larger number of analyzed MDTs is recommended to attain relevant statistical significance with small error bars.

3.3 Clinical challenges and limitations

Our *ex vivo* 3D organotypic model was optimized to address the multiple critical clinical challenges described throughout this thesis. The main goal was to develop a tumor-based model system that could predict treatment response in patients who were diagnosed with solid tumors. Early studies[6,147] have shown the merits of the micro-dissection procedure performed on whole tumors and biopsies, in preserving specific tissue characteristics and the stabilization of micro-scaled tumors within microfluidic devices. However, there are several clinical challenges and limitations that have created hurdles in the development of MDTs as a preclinical model.

There are three principal tissue characteristics identified, which restrain the production of workable MDTs. First, friable tissue required fast and efficient microdissection as these tissue slices and MDTs are more likely to break apart and expand in a saline solution. Second, gelatinous tissues are often quite sticky and elastic and do not slice and punch well. Among the MDTs that are produced from gelatinous tissues, they are either too large or too small to perform any experiments. Third, tissue with a high fat content is not usable in our model as they produced MDTs that float in solution and will not stabilize within the chambers of the microfluidic device. This will result in complete loss of MDTs during medium changes and treatment induction. Therefore, tumor specimens that are gelatinous or of soft tissue with cloud-like features and high in adipose tissue are not compatible with our system. These types of tissues are not amenable to slicing and chopping, which can result in tissue fragments of inadequate diameter. Moreover, tissue punches with these types of specimens form empty pockets that generate small inferior MDTs for loading or MDTs that float and cannot be trapped in the devices. Therefore, our model system is tissue- and cancer subtype-dependent.

In addition to the tissue characteristic challenges, the tumor cell content is highly important for any biomarker-based analysis, thus the cancer site that is under investigation will affect the usability of the MDTs produced. This is a hurdle that should be thoroughly characterized prior to initiating extensive treatment response analyses. In general, our results show that low levels of cancer cells present within the tumor specimen will provide inadequate representation level of cancer cells within the MDTs produced. This will further reduce the significance of the results. For example, PC is diagnosed at an early stage due

to adequate screening measures. For this cancer, there is a clinical need to differentiate between low and high-risk PC patients to provide a better treatment plan for those with indolent versus aggressive PC disease. As a result, there is a lack of cancer cells present in and around all glands of the prostate, which may be a limiting factor for our 3D *ex vivo* tumor-derived model. To overcome this limitation, a larger number of MDTs, per experimental condition is needed to evaluate drug response, further reducing the throughput potential of this model system. Unpublished proof of concept data showed that by using 3-4 biopsy specimens, only 25% of MDTs analyzed had sufficient material to study viability and drug response using both flow cytometry and histological techniques. In addition, we performed treatment response analyses on very few PC patient samples, reflecting a high variation in culture viability in untreated specimen as well as an accurate representation of treatment response according to level of risk of the patient (Appendix 3, Figure 3). The little data obtained on PC samples suggests that in this model system it may be more valuable, from a clinical perspective, to test drug efficacy on advanced stages of PC specimen such as cancer cell rich transurethral resections of the prostate (TURP) to better guide treatment in advanced disease.

As previously described, each tumor will retain various challenges that can either be simple or difficult to overcome. Solid tumors including melanoma, renal, hepatic, pancreatic, cervical and uterine cancers amongst others, may easily overcome some minor hurdles such as identifying the most suitable media due to their natural high tumor content, however other cancers may have a larger list of hurdles as seen in PC, such as breast, bladder, esophageal cancers among others. In the context of breast cancer would be challenging due to its high fat content, that tends to float in solution. To explore the avenues and potentially resolve this hurdle, there are several collaborative measures that can be ideal. It has been shown that spectroscopic techniques including raman spectroscopy[163] would potentially help differentiate between fat and tissue content as well as normal versus malignant cells. Raman spectroscopy relies on light scattering techniques where molecules vibrate at different wavelengths according to chemical structure, phase and polymorphy chances as well as crystallinity and molecular interactions. By these means, fat cells can be discriminated from cancer cells and normal cells to help identify usable tissue specimen for MDT production. The improvement of technology can impact the ability to overcome certain difficulties.

Our model system contains various other limitations involving its ability to recreate certain characteristics of the human component. The TME results stipulated that the vasculature system located in the patient tumor specimen is affected by the microdissection procedure due to slicing of the circulatory component. Consequently, studies that examine the effect of drugs on the angiogenesis mechanism in cancer cells, such as Bevacizumab, would be difficult to study. In addition, the model itself is not a representation of how cancer subsists in the human body. The microfluidic device acts as a homing matrix for the tumor specimen and provides the appropriate amount of nutrients and oxygen to the MDTs for growth and nourishment. However, since the host components including a working liver and gut microbiome, studies that aim at understanding the role of drug metabolism by the liver or the gut microbiome implication in drug response create hurdles that are quite hard to overcome but not impossible. There already exists various microfluidic designs to study the vasculature system[164,165], however, to study microbial bacteria implication on drug efficacy remains a challenge. In addition, there exists numerous culture organ-on-a-chip platforms[166,167], to study the effect of drug metabolism and metastatic burden as well as to evaluate how tumor cells communicate with normal tissue via exosome excretion. These platforms broaden the ability to overcome some hurdles. For example, by combining the culture platform designed for MDTs with the organ-on-a-chip design it would be possible to study how drugs are metabolized by the liver and how much active moiety reaches the tumor of interest. By forming collaborations and exploring other avenues of microfluidic technology the development of culture platforms can readily help better understand cancer biology and drug efficacy further exploiting clinical avenues that are challenging.

3.4 Reflecting clinical assessment

Response to drugs can vary between different cell types and tumors, such that each drug will implement a new challenge. Therefore, an adequate characterization and optimization of the drug of interest must be evaluated on an individual basis for the specific cancer type. The greatest difficulty in *ex vivo* modelling is defining the treatment regimens and concentrations that allow for clinical interpretation. Parameters in understanding drug activity and administration including equivalent drug concentration,

bioavailability, drug half-life and treatment course, need to be addressed in order to ensure that drug pharmacokinetics is comparable to what patient receive.

One of the widely used standard treatments in cancer care consist of chemotherapeutics. These are often administered intravenously for several cycles to ensure efficacy. In OC care, a combination therapy is often used, such that the dose recommendations differ per drug. Ideally, model systems should be able to replicate the effect of the drug when administered at a dosing equivalent to the clinic. There exist various strategies to calculate equivalent clinical drug concentration for *ex vivo* model. One of the most widely used is based on the drug concentration, drug molecular weight, body surface area and blood volume for an average individual diagnosed with the disease in question. These various components must be taken into consideration prior to investigating the effect of a drug.

The MDTMA microfluidic chip design was developed for histological analysis procedures, which is based on the use of antibodies to evaluate drug response and efficacy. There are several drug-induced cell fates such as cellular apoptosis[168], senescence[169], hypoxia and autophagy[170,171] among others. For each cell fate, there are specific proteins that are activated or inhibited in the presence of a drug and can be assessed using histological techniques (Table 5). However, to clearly confirm the induction of cell fates including senescence and autophagy, other analysis techniques that are standardly used can be adapted for *ex vivo* MDTs. These include ELISA, Western blots and PCR techniques. As mentioned in Table 5, cells that develop senescence phenotypes will produce a senescence-associated secretory phenotype (SASP) that can be collected in the media and analyzed through ELISA techniques. In addition, there are several proteins and genes that are highly expressed in a senescent, necrotic and autophagic cell that have been optimized for Western blot and PCR analysis, respectively[26,170,172]. We have optimized a technique to dissociate cells to extract RNA, DNA and protein in order to perform these analyses, increasing the robustness of this *ex vivo* model in a fundamental and translational research setting. To date however we have not integrated these techniques in our treatment response analysis dataset. Depending on the cell fate under study, various techniques may be needed to fully understand the effect of the drug of interest. In addition, a better

understanding of the pathways involved in these cell fates induced by the drug of interest is crucial to properly designing the experimental procedures needed to fully validate the effective response of the drug.

Table 5. Classic therapy-induced cell fate decision pathways

Cell fate	Proteins/genes to analyze	Analysis Technique
Apoptosis	Cleaved Caspase-3, cleaved PARP-1	IF, IHC, Western blot
Senescence	SASP p21, p16	Elisa Western blot
Hypoxia	HIF-1, CA-XI	IF, IHC, Western blot
Autophagy	P62, LC3-1/LC3-2 Downregulation Bad & Bim YAP	Western blot PCR IF, IHC, Western blot

In this thesis, we focused on histological analysis to analyze chemotherapy-induced cell fate responses. To do so, we based our understanding of the cell fates induced by chemotherapy extensively characterized by *in vitro* studies[56,169,173]. These studies provide insight in the various factors to consider evaluating the effect of chemotherapeutic drugs on cancer cells and the mechanism involved in these various cell fates. For one, various studies conducted in our laboratory showed that drug sensitivity invariably change when moving from a 2D *in vitro* model to 3D spheroids and *in vivo* models, increasing the effective drug concentration in order to obtain an observable response[174,175]. Also, the timing involved in inducing and characterizing proteins involved in cell fate pathways should be thoroughly investigated. We based our work on chemotherapy-based drugs such as carboplatin to optimize treatment conditions. We also conducted a study comparing the response to carboplatin in different cancer models to identify a treatment regimen that would effectively assess drug response. We based our chemotherapy-induced cell fate response on cell death through the activation of the apoptosis pathway, which the literature concludes can take anywhere between 24 to 48 hours[168,176]. To identify the time frame of drug induction for an effective response, a dose-response study comparing various treatment regimens, restricting the drug induction to a 24-hour period. These results showed that a minimum induction period of 10-hours was sufficient to initiate apoptosis. However, we recognized that a sufficient amount of time is needed to be able to identify the cells that have entered an apoptotic state. While our results concluded that a 10-hour induction followed by a 14-hour

recovery period was ideal, this treatment regimen was impractical based on daily work. We then compared this initial regimen to a 16-hour induction followed by a 24-hour recovery period, remaining within the 24 to 48-hour apoptotic window. The results suggested that both treatment regimens were adequate and produced similar dose-inhibition curves, with the latter presenting a more feasible and practical regimen in terms of a normal daily workflow. To better characterize the response to chemotherapy-based treatments, antibody detection of various markers involved in the cell cycle and apoptosis, such as Ki-67 and caspase-3, respectively, were then chosen. Therefore, these allowed an adequate evaluation of the drug effect on the cancer cells.

Chemotherapy induced responses were assessed to facilitate the comparison between *ex vivo* and clinical responses for predictive value. However, we also explored another drug that had a different induction path, the PARPi Olaparib. Since Olaparib is approved as a maintenance treatment in OC and breast cancer and its use is currently under investigation in PC, we decided to perform a small optimization study. We characterized Olaparib in PC cell line xenograft tumors for future use to include in the drug panel of interest. For information, PARPi inhibits the PARP enzymes that are involved in repairing single-strand DNA damages[177]. Based on cell death induced by synthetic lethality, the function of this drug is dependent on tumors harbouring a deficiency in proteins involved in the repair of double-stranded DNA damages that are provoked by the inability to repair single-stranded DNA damaged induced by PARPi. To define the response of this drug in a 3D *ex vivo* model system, starting concentrations and regimens were based upon 2D *in vitro* results conducted in our laboratory[60] and then optimized for the same cell line xenograft tumors cultured in our *ex vivo* model. Fleury et al.[61] showed that maintenance therapy of PARPi induced various cell fates including apoptosis and senescence. In general, the apoptotic phenomenon was indicative of response after 4 days of treatment induction[60,61]. However, after 6 days of PARPi stimulation, the remaining cells showed pronounced signs of cellular senescence including cell enlargement and the presence of SASP. Olaparib induces an accumulation of DNA damage that can be detected by the presence of g-H2AX, which accumulates as the concentration of the drug increases. This marker can also be combined with proteins involved in the S-G2 phase of the cell cycle, such as geminin antibody, so to restrict the analysis to dividing

cells with g-H2AX staining only in dividing cells. As previously mentioned, Olaparib can induce various cell fate responses depending on the timeframe induced. Thus, we decided to characterize the apoptosis response, in which occurs within 4 days of consistent treatment with Olaparib in 2D settings. We conducted an experiment on MDTs derived from PC cell line xenograft tumors using increasing concentrations of Olaparib for either 4, 6, or 8 days of treatment. We saw that the apoptosis marker (CC3) expression followed a dose-response curve at all timepoints, however as the time of treatment increased their expression increased exponentially. To confirm that this result was due to Olaparib induction, Y-H2AX foci expression was also examined and resulted in similar dose and time-dependent reliance on exposure to Olaparib. Senescence phenotypes, however, were not observed during this experiment but would have allowed to better compare which cell induced fates were initiated at the different timepoints. These results suggested that an induction period between 4 to 6 days would suffice to obtain significant cell apoptosis response in concordance with drug concentrations (Appendix 3, Figure 4). This type of experiment can also be performed to identify cell fate responses at the clinically equivalent concentration of Olaparib in patients to better identify what happens at the physiological bioavailibity dose in patients.

3.5 Developing MDTs for personalized medicine

This *ex vivo* model and the complementary MDTMA histological tool provide significant benefits in a pre-clinical and clinical setting. After patients undergo a biopsy or surgical resection of the tumor region, a pathologist-confirmed diagnosis is given 4-6 weeks after the surgical procedure. Considering our model system's ability to maintain specimen viability for at least 15 days, the drug efficacy response can be obtained within a 2–3-week span, enabling clinicians to quickly identify the most effective treatment course for an individual patient. In addition, the histological read-out system of MDTMA is simple to use and very adaptable, such that the established protocol can be used for various types of tissue and tumor characteristics. Furthermore, depending on the mode of action of the drug, a large set of antibodies are available and can easily be optimized to evaluate the effect of the drug. Moreover, micro-sized tumors permit the use of biopsy specimens and minimizes the amount of tissue sample needed to perform the necessary experiments. This

is also compliant with current clinical standards that aim to reduce tumor size for better visualization and control of tumor burden by treating patients in a neo-adjuvant setting. Lastly, the model provides tissue longevity of 15 days expanding its use to evaluate different types of drugs with longer inductions times, including cytostatic drugs such as PARPi and immunotherapies.

There remains some work to be conducted to confirm the predictive value of this model system and validate its usefulness in a clinical setting. These include the ability to clearly discriminate the various level of response seen in patients, the incorporation of a normogram based classifiers to compile patient-specific responses facilitating clinical interpretation and the reproducibility of response by other laboratories. In the case of OC, we see that patients are categorized as having a complete, partial or no response to chemotherapy. Based on the data accumulated to date, the MDTMA technique analyzing two-specific antibodies still presents challenges to properly discriminate between the three responses. Encouragingly, the classification between responders and non-responders allowed us to successfully classify patients accordingly. To better characterize the response, other cell proliferation markers can be used such as proliferating cell nuclear antigen (PCNA) or minichromosomal maintenance (MCM), or flow cytometry techniques can be used as a complement to identify cells in various stages of the cell cycle through propidium iodine (PI) dye. However, the integration of more techniques may reduce the easy use of the model design. Once the predictive value of the model is validated in a larger patient cohort, it may be possible to compile the results to create an artificial intelligence algorithm that would facilitate the classification of response based on patient sensitivity, in a clinical setting, improving the usefulness of this model. In addition, by incorporating a fresh tissue freezing protocol, the samples can be frozen to allow biomarker specific and genetic alterations assays to be completed to better stratify and personalize the drug panel for individual patients. Once the analyses on the primary tumor are obtained, tumors can be defrosted and tested with strategically identified targeted therapies to better stratify patient sensitivity to drugs. By combining biomarker and genetic alterations analysis to the MDT drug response platform, the personalization of drug response can be more stringent and help increase patient overall survival. The idea to combine microfluidic technology with MDT drug response techniques opened new avenues to be

scientifically explored. For this, the CRCHUM has opened a platform that designs various microfluidic chips for their use in different projects as well as develops biological and histological approaches to use MDTs in a fundamental or therapeutic setting. With this, other laboratories will be able to test their drugs on MDTs to show their efficacy on patient samples and the reliability of MDTs as a therapeutic prediction model.

The ability to transpose this MDT platform in the clinic is going to be extremely challenging, as there are several obstacles that will have to be overcome. As previously mentioned, there are specific and meticulous techniques that must be mastered prior to working with MDTs and MDTMA, such that hours of training should be anticipated to perfect and understand how to work these techniques. There are several questions that should be kept in mind when deciding where this platform should take place including: does the facility contain the proper spacing for all the sterile and nonsterile equipment needed to perform the needed techniques; are the personal properly trained and how can everyone take advantage of this facility. The build-up of a platform and transposing from a research to clinical setting can be rather hard to do since there would be several unforeseen hurdles[178]. Due to expert knowledge, this platform would be best if it relied on a centralized testing setting, where all samples would be directed to one destination for manipulation, testing, and analysis. With the optimization of freezing techniques, frozen samples can be sent to the facility simplifying the uptake of samples and distribution from one center to another. Should the technique be adopted by other facilities, meticulous training needs to be provided and appropriate quality control measures would have to be implemented.

4 CONCLUSION AND PERSPECTIVES

4.1 Conclusion

In conclusion, this thesis describes the characterization and validation of an *ex vivo* tumor-derived model system that uses MDTs, microfluidics and a novel histological tool, the MDTMA. We showed that MDTs were a valid preclinical model that retained the intra-tumor heterogeneity and characteristics of primary tumors and could replicated the chemosensitivity profile observed on *in vivo* models when compared to *in vitro* and 3D spheroids. The integration of microfluidics elevates our MDT model to allow for tissue longevity, maintenance of TME with few epigenetic and phenotypic alterations. The development of a histological tool that accompanied this model is compatible with principal histopathology procedures and involved several optimizations of FFPE procedures to ensure a reliable, reproducible read-out of antibody-based analyses to determine drug activity, response and efficacy. Comparison with other cancer models shows that our model has more potential due to its size and microfluidic culture platform to serve as an ideal model for personalized therapy.

4.2 Perspectives

Our patient cohort study in chapter 3 highlighted a need for concise validation of the clinical significance of the model. Accordingly, to gain predictive value, power calculations suggest that a minimum of 100 patients would be necessary for significance power, and to support the inclusion of this model in treatment decision-making. Nonetheless, our cohort of 14 patients, with complete follow-up, was able to determine a stringent cut off to classify response. This in turn could be used to stratify the validation patient cohort. In addition, the usefulness of the platform would be greatly increased by studying more tumor types and a wider variety of therapeutics. The validation of this model as a clinical guidance tool would open up the possibility of testing various drugs simultaneously as well as various combination of drugs.

As previously mentioned, there are several optimization procedures that must be taken into account prior to conducting a drug response study on patient specimen. In parallel to validating the model's ability

to predict patient response, the optimization of treatment regimen of currently used targeted therapies as well as drugs in clinical phase trials should be performed. These include small molecules such as PARPi, hormone therapy and immunotherapy. An optimization of the PARPi Olaparib has been initiated using PC cell line xenograft tumors. However, validation of these results requires a comparison with the same experiments performed on EOC cell line xenograft tumors (Appendix 3).

MDTs also provide a tool to better understand how hormone therapy agents act and through what mechanism they induce cellular death. For example, proof of principal studies on PC patient samples treated with androgen deprivation therapy (bicalutamide) for 24 hours followed by a 48-hour recovery period showed a cell death response using flow cytometry. However, more studies are required to evaluate the state of cells using MDTMA and to optimize the treatment regimen. For immunotherapies, it would be possible to perform some studies to better understand how the immune component located within the tumor is affected by immunotherapies. However, various optimization strategies will have to be conducted to study the effect of immunotherapies on MDTs. To increase the percentage of immune cells or even understand how immunotherapies direct immune cells from the vascular system to the tumor, various other microfluidic chip design strategies would have to be adapted to integrate a host vascular and immune system presence with microfluidic devices. In addition, various tumor-on-a-chip devices are available to study immunotherapies[179-181] such that our simple microfluidic device can be modified to attain important characteristics that would allow a better understanding of immunotherapies. In addition, oncolytic viruses that help guide the immune cells to attack cancer cells can also be analyzed as immunotherapies. Several collaborations have already been established to understand the effect of oncolytic viruses on tumor specimens. Promising preliminary 2D studies on the previously mentioned therapies could be assessed with our *ex vivo* model system as a preclinical model to bring forward the efficacy of drugs on patient samples and further improve clinical phase trials, accelerating the clinical integration of novel therapies.

This thesis has shown that the MDT model suggests a more comprehensive way of predicting patient progression than the standard clinical CA-125 and would provide an invaluable tool for fundamental research in resistance mechanisms to drugs. For example, MDTs derived from patient samples can be treated

with single or combinatorial agents and undergo treatment response analysis using MDTMAs as well as gene expression profiling. Our 25-patient cohort analysis allowed the *ex vivo* response to be performed in parallel to establishing a prediction signature that reflects the response to each treatment. From these results, a correlation between resistance mechanisms and the patient response can be further investigated through protein expression analysis. This study can improve the understanding of patient specific resistance development that can be further explored using gene expression databases and cell line-based models.

Bibliography

Uncategorized References

1. Siegel RL, Miller KD, Fuchs HE, et al: Cancer Statistics, 2021. CA Cancer J Clin 71:7-33, 2021
2. Cooper GM: A Molecular Approach, in Associates S (ed): The Cell (ed 2nd). MA, Sunderland, 2000
3. Simmons DPSMJ: Principles of Genetics (ed 6th), John Wiley & Sons, Inc., pp 581-600
4. Shields M: Fundamentals, Applications and Strategies Pharmacognosy, Academic press, 2017, pp 295-313
5. Vasan N, Baselga J, Hyman DM: A view on drug resistance in cancer. Nature 575:299-309, 2019
6. Astolfi M, Peant B, Lateef MA, et al: Micro-dissected tumor tissues on chip: an ex vivo method for drug testing and personalized therapy. Lab Chip 16:312-25, 2016
7. Hanahan D, Weinberg RA: The hallmarks of cancer. Cell 100(1):57-70, 2000
8. Hanahan D, Weinberg RA: Hallmarks of cancer: the next generation. Cell 144:646-74, 2011
9. Davies MA, Samuels Y: Analysis of the genome to personalize therapy for melanoma. Oncogene 29:5545-55, 2010
10. Jiang BH, Liu LZ: PI3K/PTEN signaling in angiogenesis and tumorigenesis. Adv Cancer Res 102:19-65, 2009
11. Yuan TL, Cantley LC: PI3K pathway alterations in cancer: variations on a theme. Oncogene 27:5497-510, 2008
12. Sozou PD, Kirkwood TB: A stochastic model of cell replicative senescence based on telomere shortening, oxidative stress, and somatic mutations in nuclear and mitochondrial DNA. J Theor Biol 213:573-86, 2001
13. Hayflick L: Mortality and immortality at the cellular level. A review. Biochemistry (Mosc) 62:1180-90, 1997
14. Heaphy CM, Subhawong AP, Hong SM, et al: Prevalence of the alternative lengthening of telomeres telomere maintenance mechanism in human cancer subtypes. Am J Pathol 179:1608-15, 2011
15. Okamoto K, Seimiya H: Revisiting Telomere Shortening in Cancer. Cells 8, 2019
16. Grossman HB, Liebert M, Antelo M, et al: p53 and RB expression predict progression in T1 bladder cancer. Clin Cancer Res 4:829-34, 1998
17. Seluanov A, Hine C, Azpurua J, et al: Hypersensitivity to contact inhibition provides a clue to cancer resistance of naked mole-rat. Proc Natl Acad Sci U S A 106:19352-7, 2009
18. Pavel M, Renna M, Park SJ, et al: Contact inhibition controls cell survival and proliferation via YAP/TAZ-autophagy axis. Nat Commun 9:2961, 2018
19. Szaszi K, Amoozadeh Y: New insights into functions, regulation, and pathological roles of tight junctions in kidney tubular epithelium. Int Rev Cell Mol Biol 308:205-71, 2014
20. Vaux DL, Cory S, Adams JM: Bcl-2 gene promotes haemopoietic cell survival and cooperates with c-myc to immortalize pre-B cells. Nature 335:440-2, 1988
21. Asmarinah A, Paradowska-Dogan A, Kodariah R, et al: Expression of the Bcl-2 family genes and complexes involved in the mitochondrial transport in prostate cancer cells. Int J Oncol 45:1489-96, 2014

22. Habermann JK, Bundgen NK, Gemoll T, et al: Genomic instability influences the transcriptome and proteome in endometrial cancer subtypes. Mol Cancer 10:132, 2011
23. Anghileri LJ: Warburg's cancer theory revisited: a fundamentally new approach. Arch Geschwulstforsch 53(1):1-8, 1983
24. Lopez-Lazaro M: The warburg effect: why and how do cancer cells activate glycolysis in the presence of oxygen? Anticancer Agents Med Chem 8(3):305-12, 2008
25. Bedard PL, Hansen AR, Ratain MJ, et al: Tumour heterogeneity in the clinic. Nature 501:355-64, 2013
26. Semenza GL: HIF-1: upstream and downstream of cancer metabolism. Curr Opin Genet Dev 20:51-6, 2010
27. Fukumura D, Xavier R, Sugiura T, et al: Tumor induction of VEGF promoter activity in stromal cells. Cell 94:715-25, 1998
28. Erez N, Truitt M, Olson P, et al: Cancer-Associated Fibroblasts Are Activated in Incipient Neoplasia to Orchestrate Tumor-Promoting Inflammation in an NF-kappaB-Dependent Manner. Cancer Cell 17:135-47, 2010
29. McGowan PM, Kirstein JM, Chambers AF: Micrometastatic disease and metastatic outgrowth: clinical issues and experimental approaches. Future Oncol 5:1083-98, 2009
30. Beacham DA, Cukierman E: Stromagenesis: the changing face of fibroblastic microenvironments during tumor progression. Semin Cancer Biol 15:329-41, 2005
31. Zhang Y, Daquinag AC, Amaya-Manzanares F, et al: Stromal progenitor cells from endogenous adipose tissue contribute to pericytes and adipocytes that populate the tumor microenvironment. Cancer Res 72:5198-208, 2012
32. Bochet L, Lehuede C, Dauvillier S, et al: Adipocyte-derived fibroblasts promote tumor progression and contribute to the desmoplastic reaction in breast cancer. Cancer Res 73:5657-68, 2013
33. Nieman KM, Kenny HA, Penicka CV, et al: Adipocytes promote ovarian cancer metastasis and provide energy for rapid tumor growth. Nat Med 17:1498-503, 2011
34. Karnoub AE, Dash AB, Vo AP, et al: Mesenchymal stem cells within tumour stroma promote breast cancer metastasis. Nature 449:557-63, 2007
35. He J, Hu Y, Hu M, et al: Development of PD-1/PD-L1 Pathway in Tumor Immune Microenvironment and Treatment for Non-Small Cell Lung Cancer. Sci Rep 5:13110, 2015
36. Bandola-Simon J, Roche PA: Dysfunction of antigen processing and presentation by dendritic cells in cancer. Mol Immunol 113:31-37, 2019
37. Tringale KR, Pang J, Nguyen QT: Image-guided surgery in cancer: A strategy to reduce incidence of positive surgical margins. Wiley Interdiscip Rev Syst Biol Med 10:e1412, 2018
38. Prashad A, Mitchell M, Argent-Katwala M, et al: Pan-Canadian standards for cancer surgery. Can J Surg 62:S171-S183, 2019
39. Allen C, Her S, Jaffray DA: Radiotherapy for Cancer: Present and Future. Adv Drug Deliv Rev 109:1-2, 2017
40. Jarosz-Biej M, Smolarczyk R, Cichon T, et al: Tumor Microenvironment as A "Game Changer" in Cancer Radiotherapy. Int J Mol Sci 20(13):3212, 2019
41. Workman P, Kaye SB: Translating basic cancer research into new cancer therapeutics. Trends Mol Med 8:S1-9, 2002
42. Shin SH, Bode AM, Dong Z: Precision medicine: the foundation of future cancer therapeutics. NPJ Precis Oncol 1:12, 2017
43. Falzone L, Salomone S, Libra M: Evolution of Cancer Pharmacological Treatments at the Turn of the Third Millennium. Front Pharmacol 9:1300, 2018

44. Florian S, Mitchison TJ: Anti-Microtubule Drugs. Methods Mol Biol 1413:403-21, 2016
45. Dilruba S, Kalayda GV: Platinum-based drugs: past, present and future. Cancer Chemother Pharmacol 77:1103-24, 2016
46. Rixe O, Fojo T: Is cell death a critical end point for anticancer therapies or is cytostasis sufficient? Clin Cancer Res 13:7280-7, 2007
47. Robinson SP, Langan-Fahey SM, Johnson DA, et al: Metabolites, pharmacodynamics, and pharmacokinetics of tamoxifen in rats and mice compared to the breast cancer patient. Drug Metab Dispos 19:36-43, 1991
48. Hudis CA: Trastuzumab--mechanism of action and use in clinical practice. N Engl J Med 357:39-51, 2007
49. Garbe C, Eigentler TK: Vemurafenib. Recent Results Cancer Res 211:77-89, 2018
50. Somlyai G, Collins TQ, Meuillet EJ, et al: Structural homologies between phenformin, lipitor and gleevec aim the same metabolic oncotarget in leukemia and melanoma. Oncotarget 8:50187-50192, 2017
51. Franzese E, Centonze S, Diana A, et al: PARP inhibitors in ovarian cancer. Cancer Treat Rev 73:1-9, 2019
52. Kim G, Ison G, McKee AE, et al: FDA Approval Summary: Olaparib Monotherapy in Patients with Deleterious Germline BRCA-Mutated Advanced Ovarian Cancer Treated with Three or More Lines of Chemotherapy. Clin Cancer Res 21:4257-61, 2015
53. Kaufman B, Shapira-Frommer R, Schmutzler RK, et al: Olaparib monotherapy in patients with advanced cancer and a germline BRCA1/2 mutation. J Clin Oncol 33:244-50, 2015
54. Nijman SM: Synthetic lethality: general principles, utility and detection using genetic screens in human cells. FEBS Lett 585:1-6, 2011
55. Dziadkowiec KN, Gasiorowska E, Nowak-Markwitz E, et al: PARP inhibitors: review of mechanisms of action and BRCA1/2 mutation targeting. Prz Menopauzalny 15:215-219, 2016
56. Ricci MS, Zong WX: Chemotherapeutic approaches for targeting cell death pathways. Oncologist 11:342-57, 2006
57. Luong KV, Wang L, Roberts BJ, et al: Cell fate determination in cisplatin resistance and chemosensitization. Oncotarget 7:23383-94, 2016
58. Parrish AB, Freel CD, Kornbluth S: Cellular mechanisms controlling caspase activation and function. Cold Spring Harb Perspect Biol 5(60): a008672, 2013
59. Liu PF, Hu YC, Kang BH, et al: Expression levels of cleaved caspase-3 and caspase-3 in tumorigenesis and prognosis of oral tongue squamous cell carcinoma. PLoS One 12:e0180620, 2017
60. Fleury H, Carmona E, Morin VG, et al: Cumulative defects in DNA repair pathways drive the PARP inhibitor response in high-grade serous epithelial ovarian cancer cell lines. Oncotarget 8:40152-40168, 2017
61. Fleury H, Malaquin N, Tu V, et al: Exploiting interconnected synthetic lethal interactions between PARP inhibition and cancer cell reversible senescence. Nat Commun 10:2556, 2019
62. Liao C, Xiao Y, Liu L: The Dynamic Process and Its Dual Effects on Tumors of Therapy-Induced Senescence. Cancer Manag Res 12:13553-13566, 2020
63. Tan P: Divide and conquer: progress in the molecular stratification of cancer. Yonsei Med J 50:464-73, 2009

64. Gnanapragasam VJ, Lophatananon A, Wright KA, et al: Improving Clinical Risk Stratification at Diagnosis in Primary Prostate Cancer: A Prognostic Modelling Study. PLoS Med 13:e1002063, 2016
65. Brierley J, Gospodarowicz M, O'Sullivan B: The principles of cancer staging. Ecancermedicalscience 10:ed61, 2016
66. Committee CCSA: Canadian Cancer Statistics 2019. Toronto, ON: Canadian Cancer Society, 2019
67. Souhami RL, Tobias JS: Cancer and its management (ed 5th). Malden, Mass., Blackwell Pub, 2005
68. Golub TR, Slonim DK, Tamayo P, et al: Molecular classification of cancer: class discovery and class prediction by gene expression monitoring. Science 286:531-7, 1999
69. DiMasi JA: The value of improving the productivity of the drug development process: faster times and better decisions. Pharmacoeconomics 20 Suppl 3:1-10, 2002
70. Early Breast Cancer Trialists' Collaborative G: Effects of chemotherapy and hormonal therapy for early breast cancer on recurrence and 15-year survival: an overview of the randomised trials. Lancet 365:1687-717, 2005
71. Joseph A diMasi RWHHGG: The price of innovation: new estimates of drug development costs, Journal of Health Economics, Elsevier, 2003, pp 151-185
72. Zahreddine H, Borden KL: Mechanisms and insights into drug resistance in cancer. Front Pharmacol 4:28, 2013
73. Shortt J, Johnstone RW: Oncogenes in cell survival and cell death. Cold Spring Harb Perspect Biol 4(12):a009829, 2012
74. Lheureux S, Gourley C, Vergote I, et al: Epithelial ovarian cancer. Lancet 393:1240-1253, 2019
75. Desai A, Xu J, Aysola K, et al: Epithelial ovarian cancer: An overview. World J Transl Med 3:1-8, 2014
76. Committee CCSA: Ovarian Cancer Statistics 2019. Toronto, ON, Canadian Cancer Society, 2019
77. Toss A, Tomasello C, Razzaboni E, et al: Hereditary ovarian cancer: not only BRCA 1 and 2 genes. Biomed Res Int 2015:341723, 2015
78. Purdie DM, Bain CJ, Siskind V, et al: Ovulation and risk of epithelial ovarian cancer. Int J Cancer 104:228-32, 2003
79. Casagrande JT, Louie EW, Pike MC, et al: "Incessant ovulation" and ovarian cancer. Lancet 2:170-3, 1979
80. Reid BM, Permuth JB, Sellers TA: Epidemiology of ovarian cancer: a review. Cancer Biol Med 14:9-32, 2017
81. Tung KH, Wilkens LR, Wu AH, et al: Effect of anovulation factors on pre- and postmenopausal ovarian cancer risk: revisiting the incessant ovulation hypothesis. Am J Epidemiol 161:321-9, 2005
82. Lew R: Natural history of ovarian function including assessment of ovarian reserve and premature ovarian failure. Best Pract Res Clin Obstet Gynaecol 55:2-13, 2019
83. Kurman RJ, Shih Ie M: The origin and pathogenesis of epithelial ovarian cancer: a proposed unifying theory. Am J Surg Pathol 34:433-43, 2010
84. Al Bakir M, Gabra H: The molecular genetics of hereditary and sporadic ovarian cancer: implications for the future. Br Med Bull 112:57-69, 2014
85. Lheureux S, Braunstein M, Oza AM: Epithelial ovarian cancer: Evolution of management in the era of precision medicine. CA Cancer J Clin 69:280-304, 2019

86. Prat J: Ovarian carcinomas: five distinct diseases with different origins, genetic alterations, and clinicopathological features. Virchows Arch 460:237-49, 2012
87. Lisio MA, Fu L, Goyeneche A, et al: High-Grade Serous Ovarian Cancer: Basic Sciences, Clinical and Therapeutic Standpoints. Int J Mol Sci 20, 2019
88. Ahn G, Folkins AK, McKenney JK, et al: Low-grade Serous Carcinoma of the Ovary: Clinicopathologic Analysis of 52 Invasive Cases and Identification of a Possible Noninvasive Intermediate Lesion. Am J Surg Pathol 40:1165-76, 2016
89. Brown J, Frumovitz M: Mucinous tumors of the ovary: current thoughts on diagnosis and management. Curr Oncol Rep 16:389, 2014
90. Lim D, Murali R, Murray MP, et al: Morphological and Immunohistochemical Reevaluation of Tumors Initially Diagnosed as Ovarian Endometrioid Carcinoma With Emphasis on High-grade Tumors. Am J Surg Pathol 40:302-12, 2016
91. del Carmen MG, Birrer M, Schorge JO: Clear cell carcinoma of the ovary: a review of the literature. Gynecol Oncol 126:481-90, 2012
92. Tothill RW, Tinker AV, George J, et al: Novel molecular subtypes of serous and endometrioid ovarian cancer linked to clinical outcome. Clin Cancer Res 14:5198-208, 2008
93. Ducatman ESCaBS: Cytology: Diagnostic principles and clinical coorelated (ed 3rd), ELSEVIER, 2009 pp. 433-450
94. Kobel M, Bak J, Bertelsen BI, et al: Ovarian carcinoma histotype determination is highly reproducible, and is improved through the use of immunohistochemistry. Histopathology 64:1004-13, 2014
95. Kim J, Park EY, Kim O, et al: Cell Origins of High-Grade Serous Ovarian Cancer. Cancers (Basel) 10(11):433, 2018
96. International Collaborative Ovarian Neoplasm G: Paclitaxel plus carboplatin versus standard chemotherapy with either single-agent carboplatin or cyclophosphamide, doxorubicin, and cisplatin in women with ovarian cancer: the ICON3 randomised trial. Lancet 360:505-15, 2002
97. Montemorano L, Lightfoot MD, Bixel K: Role of Olaparib as Maintenance Treatment for Ovarian Cancer: The Evidence to Date. Onco Targets Ther 12:11497-11506, 2019
98. Tew WP, Lacchetti C, Ellis A, et al: PARP Inhibitors in the Management of Ovarian Cancer: ASCO Guideline. J Clin Oncol 38:3468-3493, 2020
99. Chen A: PARP inhibitors: its role in treatment of cancer. Chin J Cancer 30:463-71, 2011
100. Rustin GJ, Vergote I, Eisenhauer E, et al: Definitions for response and progression in ovarian cancer clinical trials incorporating RECIST 1.1 and CA 125 agreed by the Gynecological Cancer Intergroup (GCIG). Int J Gynecol Cancer 21:419-23, 2011
101. Schwartz LH, Litiere S, de Vries E, et al: RECIST 1.1-Update and clarification: From the RECIST committee. Eur J Cancer 62:132-7, 2016
102. Society CC: Prostate Cancer Statistics
103. Zhang D, Zhao S, Li X, et al: Prostate Luminal Progenitor Cells in Development and Cancer. Trends Cancer 4:769-783, 2018
104. Schrecengost R, Knudsen KE: Molecular pathogenesis and progression of prostate cancer. Semin Oncol 40:244-58, 2013
105. Mohler JL, Antonarakis ES, Armstrong AJ, et al: Prostate Cancer, Version 2.2019, NCCN Clinical Practice Guidelines in Oncology. J Natl Compr Canc Netw 17:479-505, 2019
106. Mohler JL, Antonarakis ES: NCCN Guidelines Updates: Management of Prostate Cancer. J Natl Compr Canc Netw 17:583-586, 2019

107. Carreira S, Romanel A, Goodall J, et al: Tumor clone dynamics in lethal prostate cancer. Sci Transl Med 6(254):254ra125, 2014

108. Lozano R, Castro E, Aragon IM, et al: Genetic aberrations in DNA repair pathways: a cornerstone of precision oncology in prostate cancer. Br J Cancer 124:552-563, 2021

109. Mateo J, Carreira S, Sandhu S, et al: DNA-Repair Defects and Olaparib in Metastatic Prostate Cancer. N Engl J Med 373:1697-708, 2015

110. Martin GA, Chen AH, Parikh K: A Novel Use of Olaparib for the Treatment of Metastatic Castration-Recurrent Prostate Cancer. Pharmacotherapy 37:1406-1414, 2017

111. Zhen JT, Syed J, Nguyen KA, et al: Genetic testing for hereditary prostate cancer: Current status and limitations. Cancer 124:3105-3117, 2018

112. Venditti JM, Wesley RA, Plowman J: Current NCI preclinical antitumor screening in vivo: results of tumor panel screening, 1976-1982, and future directions. Adv Pharmacol Chemother 20:1-20, 1984

113. Fleury H, Communal L, Carmona E, et al: Novel high-grade serous epithelial ovarian cancer cell lines that reflect the molecular diversity of both the sporadic and hereditary disease. Genes Cancer 6:378-98, 2015

114. Weiswald LB, Bellet D, Dangles-Marie V: Spherical cancer models in tumor biology. Neoplasia 17:1-15, 2015

115. Torisawa YS, Takagi A, Nashimoto Y, et al: A multicellular spheroid array to realize spheroid formation, culture, and viability assay on a chip. Biomaterials 28:559-66, 2007

116. Johnson JI, Decker S, Zaharevitz D, et al: Relationships between drug activity in NCI preclinical in vitro and in vivo models and early clinical trials. Br J Cancer 84:1424-31, 2001

117. Richmond A, Su Y: Mouse xenograft models vs GEM models for human cancer therapeutics. Dis Model Mech 1:78-82, 2008

118. De Wever O, Mareel M: Role of tissue stroma in cancer cell invasion. J Pathol 200:429-47, 2003

119. Junttila MR, de Sauvage FJ: Influence of tumour micro-environment heterogeneity on therapeutic response. Nature 501:346-54, 2013

120. Sachs N, Clevers H: Organoid cultures for the analysis of cancer phenotypes. Curr Opin Genet Dev 24:68-73, 2014

121. Fan H, Demirci U, Chen P: Emerging organoid models: leaping forward in cancer research. J Hematol Oncol 12:142, 2019

122. Justice BA, Badr NA, Felder RA: 3D cell culture opens new dimensions in cell-based assays. Drug Discov Today 14:102-7, 2009

123. Hirschhaeuser F, Menne H, Dittfeld C, et al: Multicellular tumor spheroids: an underestimated tool is catching up again. J Biotechnol 148:3-15, 2010

124. Morgan MM, Johnson BP, Livingston MK, et al: Personalized in vitro cancer models to predict therapeutic response: Challenges and a framework for improvement. Pharmacol Ther 165:79-92, 2016

125. Bounaix Morand du Puch C, Nouaille M, Giraud S, et al: Chemotherapy outcome predictive effectiveness by the Oncogramme: pilot trial on stage-IV colorectal cancer. J Transl Med 14:10, 2016

126. Huh D, Hamilton GA, Ingber DE: From 3D cell culture to organs-on-chips. Trends Cell Biol 21:745-54, 2011

127. Gencoglu MF, Barney LE, Hall CL, et al: Comparative Study of Multicellular Tumor Spheroid Formation Methods and Implications for Drug Screening. ACS Biomater Sci Eng 4:410-420, 2018

128. Sarisozen C, Abouzeid AH, Torchilin VP: The effect of co-delivery of paclitaxel and curcumin by transferrin-targeted PEG-PE-based mixed micelles on resistant ovarian cancer in 3-D spheroids and in vivo tumors. Eur J Pharm Biopharm 88:539-50, 2014

129. Reyal F, Guyader C, Decraene C, et al: Molecular profiling of patient-derived breast cancer xenografts. Breast Cancer Res 14:R11, 2012

130. Izumchenko E, Paz K, Ciznadija D, et al: Patient-derived xenografts effectively capture responses to oncology therapy in a heterogeneous cohort of patients with solid tumors. Ann Oncol 28:2595-2605, 2017

131. Shuford S, Wilhelm C, Rayner M, et al: Prospective Validation of an Ex Vivo, Patient-Derived 3D Spheroid Model for Response Predictions in Newly Diagnosed Ovarian Cancer. Sci Rep 9:11153, 2019

132. Maenhoudt N, Defraye C, Boretto M, et al: Developing Organoids from Ovarian Cancer as Experimental and Preclinical Models. Stem Cell Reports 14:717-729, 2020

133. Nero C, Vizzielli G, Lorusso D, et al: Patient-derived organoids and high grade serous ovarian cancer: from disease modeling to personalized medicine. J Exp Clin Cancer Res 40:116, 2021

134. Nanki Y, Chiyoda T, Hirasawa A, et al: Patient-derived ovarian cancer organoids capture the genomic profiles of primary tumours applicable for drug sensitivity and resistance testing. Sci Rep 10:12581, 2020

135. Black MM, Kleiner IS, Speer FD: Effects of enzyme inhibitors on in vitro dehydrogenase activity of cancer tissue slices. Proc Soc Exp Biol Med 77:611-5, 1951

136. Thomlinson RH, Gray LH: The histological structure of some human lung cancers and the possible implications for radiotherapy. Br J Cancer 9:539-49, 1955

137. Rambani K, Vukasinovic J, Glezer A, et al: Culturing thick brain slices: an interstitial 3D microperfusion system for enhanced viability. J Neurosci Methods 180:243-54, 2009

138. Misra S, Moro CF, Del Chiaro M, et al: Ex vivo organotypic culture system of precision-cut slices of human pancreatic ductal adenocarcinoma. Sci Rep 9:2133, 2019

139. Gahwiler BH, Capogna M, Debanne D, et al: Organotypic slice cultures: a technique has come of age. Trends Neurosci 20:471-7, 1997

140. Davies EJ, Dong M, Gutekunst M, et al: Capturing complex tumour biology in vitro: histological and molecular characterisation of precision cut slices. Sci Rep 5:17187, 2015

141. Zhang W, van Weerden WM, de Ridder CMA, et al: Ex vivo treatment of prostate tumor tissue recapitulates in vivo therapy response. Prostate 79:390-402, 2019

142. van de Merbel AF, van der Horst G, van der Mark MH, et al: An ex vivo Tissue Culture Model for the Assessment of Individualized Drug Responses in Prostate and Bladder Cancer. Front Oncol 8:400, 2018

143. Roelants C, Pillet C, Franquet Q, et al: Ex-Vivo Treatment of Tumor Tissue Slices as a Predictive Preclinical Method to Evaluate Targeted Therapies for Patients with Renal Carcinoma. Cancers (Basel) 12(1):232, 2020

144. Majumder B, Baraneedharan U, Thiyagarajan S, et al: Predicting clinical response to anticancer drugs using an ex vivo platform that captures tumour heterogeneity. Nat Commun 6:6169, 2015

145. Meijer TG, Naipal KA, Jager A, et al: Ex vivo tumor culture systems for functional drug testing and therapy response prediction. Future Sci OA 3:FSO190, 2017

146. Powley IR, Patel M, Miles G, et al: Patient-derived explants (PDEs) as a powerful preclinical platform for anti-cancer drug and biomarker discovery. Br J Cancer 122:735-744, 2020

147. Rousset N, Monet F, Gervais T: Simulation-assisted design of microfluidic sample traps for optimal trapping and culture of non-adherent single cells, tissues, and spheroids. Sci Rep 7:245, 2017
148. Nagaraj AS, Bao J, Hemmes A, et al: Establishment and Analysis of Tumor Slice Explants As a Prerequisite for Diagnostic Testing. J Vis Exp, 141, 2018
149. Elliott AD: Confocal Microscopy: Principles and Modern Practices. Curr Protoc Cytom 92:e68, 2020
150. Sanders CK, Mourant JR: Advantages of full spectrum flow cytometry. J Biomed Opt 18:037004, 2013
151. Simeone K, Guay-Lord R, Lateef MA, et al: Paraffin-embedding lithography and micro-dissected tissue micro-arrays: tools for biological and pharmacological analysis of ex vivo solid tumors. Lab Chip 19:693-705, 2019
152. Kang J, Lee DW, Hwang HJ, et al: Mini-pillar array for hydrogel-supported 3D culture and high-content histologic analysis of human tumor spheroids. Lab Chip 16:2265-76, 2016
153. Erlichman C, Vidgen D: Cytotoxicity of adriamycin in MGH-U1 cells grown as monolayer cultures, spheroids, and xenografts in immune-deprived mice. Cancer Res 44:5369-75, 1984
154. Ricci F, Bizzaro F, Cesca M, et al: Patient-derived ovarian tumor xenografts recapitulate human clinicopathology and genetic alterations. Cancer Res 74:6980-90, 2014
155. Scott CL, Becker MA, Haluska P, et al: Patient-derived xenograft models to improve targeted therapy in epithelial ovarian cancer treatment. Front Oncol 3:295, 2013
156. Ooft SN, Weeber F, Dijkstra KK, et al: Patient-derived organoids can predict response to chemotherapy in metastatic colorectal cancer patients. Sci Transl Med 11, 2019
157. Peduzzi P, Concato J, Kemper E, et al: A simulation study of the number of events per variable in logistic regression analysis. J Clin Epidemiol 49:1373-9, 1996
158. Protocols O: Paraffin Processing of Tissue, 2016
159. Webster JD, Miller MA, Dusold D, et al: Effects of prolonged formalin fixation on diagnostic immunohistochemistry in domestic animals. J Histochem Cytochem 57:753-61, 2009
160. Arnold MM, Srivastava S, Fredenburgh J, et al: Effects of fixation and tissue processing on immunohistochemical demonstration of specific antigens. Biotech Histochem 71:224-30, 1996
161. Ramos-Vara JA: Technical aspects of immunohistochemistry. Vet Pathol 42:405-26, 2005
162. Zhanmu O, Yang X, Gong H, et al: Paraffin-embedding for large volume bio-tissue. Sci Rep 10:12639, 2020
163. Haka AS, Shafer-Peltier KE, Fitzmaurice M, et al: Diagnosing breast cancer by using Raman spectroscopy. Proc Natl Acad Sci U S A 102:12371-6, 2005
164. Dereli-Korkut Z, Akaydin HD, Ahmed AH, et al: Three dimensional microfluidic cell arrays for ex vivo drug screening with mimicked vascular flow. Anal Chem 86:2997-3004, 2014
165. Santamaria R, Gonzalez-Alvarez M, Delgado R, et al: Remodeling of the Microvasculature: May the Blood Flow Be With You. Front Physiol 11:586852, 2020
166. Shim S, Belanger MC, Harris AR, et al: Two-way communication between ex vivo tissues on a microfluidic chip: application to tumor-lymph node interaction. Lab Chip 19:1013-1026, 2019
167. Kashaninejad N, Nikmaneshi MR, Moghadas H, et al: Organ-Tumor-on-a-Chip for Chemosensitivity Assay: A Critical Review. Micromachines (Basel) 7(8):130, 2016

168. Schmitt E, Steyaert A, Cimoli G, et al: Bax-alpha promotes apoptosis induced by cancer chemotherapy and accelerates the activation of caspase 3-like cysteine proteases in p53 double mutant B lymphoma Namalwa cells. Cell Death Differ 5:506-16, 1998

169. Guillon J, Petit C, Toutain B, et al: Chemotherapy-induced senescence, an adaptive mechanism driving resistance and tumor heterogeneity. Cell Cycle 18:2385-2397, 2019

170. Zhou Y, Sun K, Ma Y, et al: Autophagy inhibits chemotherapy-induced apoptosis through downregulating Bad and Bim in hepatocellular carcinoma cells. Sci Rep 4:5382, 2014

171. Jiang Y, Ji F, Liu Y, et al: Cisplatin-induced autophagy protects breast cancer cells from apoptosis by regulating yes-associated protein. Oncol Rep 38:3668-3676, 2017

172. Crowe EP, Nacarelli T, Bitto A, et al: Detecting senescence: methods and approaches. Methods Mol Biol 1170:425-45, 2014

173. Ting HJ, Hsu J, Bao BY, et al: Docetaxel-induced growth inhibition and apoptosis in androgen independent prostate cancer cells are enhanced by 1alpha,25-dihydroxyvitamin D3. Cancer Lett 247:122-9, 2007

174. Das T, Meunier L, Barbe L, et al: Empirical chemosensitivity testing in a spheroid model of ovarian cancer using a microfluidics-based multiplex platform. Biomicrofluidics 7:11805, 2013

175. Patra B, Lateef MA, Brodeur MN, et al: Carboplatin sensitivity in epithelial ovarian cancer cell lines: The impact of model systems. PLoS One 15:e0244549, 2020

176. Schmitt E, Sane AT, Steyaert A, et al: The Bcl-xL and Bax-alpha control points: modulation of apoptosis induced by cancer chemotherapy and relation to TPCK-sensitive protease and caspase activation. Biochem Cell Biol 75:301-14, 1997

177. O'Neil NJ, Bailey ML, Hieter P: Synthetic lethality and cancer. Nat Rev Genet 18:613-623, 2017

178. Jones ML, Cifu DX, Backus D, et al: Instilling a research culture in an applied clinical setting. Arch Phys Med Rehabil 94:S49-54, 2013

179. Parlato S, De Ninno A, Molfetta R, et al: 3D Microfluidic model for evaluating immunotherapy efficacy by tracking dendritic cell behaviour toward tumor cells. Sci Rep 7:1093, 2017

180. Parlato S, Grisanti G, Sinibaldi G, et al: Tumor-on-a-chip platforms to study cancer-immune system crosstalk in the era of immunotherapy. Lab Chip 21:234-253, 2021

181. Zhao Z, McGill J, Gamero-Kubota P, et al: Microfluidic on-demand engineering of exosomes towards cancer immunotherapy. Lab Chip 19:1877-1886, 2019

5 APPENDICES

5.1 List of Publications and Contributions

Published Articles:

Simeone K*, Guay-Lord R*, Lateef AM*, Péant B, Carmona E, Kendall-Dupont J, Orimoto AM, Provencher D, Mes-Masson AM, Gervais T, Saad F. 2018. Chapitre 7: Microfluidic devices and micro-dissected tissue to predict therapeutic response inpatients with prostate cancer. Huifang CHEN and Paulo N. Martins. Advances in Experimental Surgery Volume 2. Nova Science Publishers, Inc. New York, United States. * These authors contributed equally to the work. (1)

Simeone K*, Guay-Lord R*, Lateef AM, Péant B, Kendall-Dupont J, Orimoto AM, Carmona E, Provencher D, Saad F, Gervais T†, Mes-Masson A-M†. Paraffin-embedding lithography and micro-dissected tissue micro-arrays: tools for biological and pharmacological analysis of *ex vivo* solid tumors. 2019. Lab on a Chip. 19(4): 693-705. * These authors contributed equally to the work. (2)

Sauriol A*, **Simeone K***, Portelance L, Meunier L, Leclerc-Desaulniers K, De Ladurantaye M, Chergui M, Kendall-Dupont J, Rahimi K, Carmona E, Provencher D, Mes-Masson AM. Modeling the diversity of epithelial ovarian cancer through ten novel well characterized cell lines covering multiple subtypes of the disease. 2020. Cancer. 12(8):2222. * These authors contributed equally to the work. (3)

Brodeur M.N*, **Simeone K***, Leclerc-Deslauniers K, Fleury H, Carmona E, Provencher D, Mes-Masson AM. Carboplatin response in preclinical models for ovarian cancer: comparison of 2D monolayers, spheroids, *ex vivo* tumors and *in vivo* models. 2021. Scientific Reports. * These authors contributed equally to the work. (4)

Dorrigiv D, **Simeone K**, Communal L, Kendall-Dupont J, St-Georges-Robillard A, Péant B, Euridice C, Mes-Masson AM and Gervais T. Microdissected tissue vs tissue slices – A comparative study of tumor explant models cultured on-chip and off-chip. 2021. Cancers. 13(6): 4208. (5)

Article in Preparation:

Simeone K, Kendall-Dupont J, Peant B, Carmona E, Gervais T, Saad F, Provencher D, Mes-Masson AM. *Ex vivo* model preserves natural tumor microenvironment to accurately predict patient response to chemotherapy. 2021. In preparation. (6)

5.2 Unpublished Direct Passage to Doctorate Program Manuscript

Validation of *ex vivo* patient derived model for predicting patient response to therapeutic agents.

Kayla Simeone

**** Collaboration with Robin Guay-Lord at Polytechnique Montréal**

**** Device fabrication and design**

Director: Anne-Marie Mes-Masson, PhD

Co-Director: Fred Saad, MD, FRCSC

Admission into Doctoral program by Direct Passage (Regular)

Molecular Biology Department

July 14, 2017

5.2.1 Introduction

Cancer remains the most lethal disease worldwide. Approximately two in five Canadians will develop cancer in their lifetime, and about one in four diagnosed with cancer will die each year[1]. It is known that individuals respond differently to the same therapeutic agent due to their individual genetic and tumor specific characteristics[2]. This response variability makes it difficult to impose standard of care treatment regimens to cure diseases, making it a public health concern. To address this problem, research has focused on developing a personalized medicine approach, which dictates that each cancer patient be matched to the most appropriate treatment. This not only results in superior medical care, by improving effectiveness while diminishing toxicities, but it also directly impacts health economics and patient quality of life.

Cancer research has based their fundamental and preclinical findings on classical two-dimensional (2D) and three-dimensional (3D) models. These models include 2D monolayer cell cultures[3,4], 3D spheroids[5,6], cell line xenografts[7,8] and patient-derived xenografts (PDX)[9,10]. They are well suited for evaluating key phenotypic and genotypic characteristics of cancer cells as well as evaluating the pharmacodynamics and pharmacokinetics of newly developed treatments. However, common disadvantages such as the lack of cell population heterogeneity as well as the non-representative selection of cancer clones[11] seen in these models limits their usability in predicting patient specific responses. Various components of the tumor microenvironment, including immune, stromal and endothelial cell components, have been shown to play a crucial role in cancer progression, thus, the loss of such factors in the model systems may modulate the effect of the therapeutic agents[12,13]. In addition, in vitro 2D tumor cell lines grown in an artificial environment may be open to potential irreversible genetic changes, altering their genotypic and phenotypic characteristics[14,15]. Moreover, in 3D cell line xenograft models, the stromal infiltration from the mouse-host impedes the evaluation of treatment induction. The 3D PDX models may be beneficial for putative resistance analysis, however it takes approximately 6-10 months to produce a first generation PDX from a particular donor tumor, thus making it a costly model to maintain and impossible to determine the chemosensitivity of a patient before the first treatment is initiated. While these models allow for empirical

testing of therapeutic agents, they remain incapable in predicting patient response to treatment in a clinical relevant timeframe and with sufficient accuracy as to be practically applicable.

There remains a strong clinical interest in developing assays that allow for direct testing of therapeutic agents on patient tumor samples. To answer to this need, our group has developed a novel 3D ex-vivo model implementing a personalized medicine strategy to identify the most suitable treatment regimen for a particular cancer patient. The novelty of the presented model relies on the micro-dissection of the surgically resected patient's tumor into sub-microliter sized tissue samples using a 500 µm biopsy punch[16] (figure 1A-B). These micro-dissected tissues (MDTs) are further loaded and cultured in specifically designed microfluidic devices, enabling precise spatiotemporal control of the MDTs[16]. These microfluidic devices are fabricated through the plasma bonding of two polydimethylsiloxane (PDMS) layers, where the bottom layer contains the channels and gravitational traps that hold the MDTs allowing for proper culturing and induction using various pharmacological agents. The original design of these microfluidic devices consisted of five serpent channels holding a total of 25 MDTs (figure 2A), thus enabling the analysis of five different conditions in a single chip[16].

Our ex-vivo 3D organotypic model has the potential to predict patients' response to treatment. A major advantage of our model is its ability to maintain a variety of cell subtypes (endothelial, stromal, epithelial and immune cells) within the primary tumor microenvironment. Moreover, the micro-size of the tissues eliminates the need for continuous perfusion of the system; a simple diffusion of oxygen through the gas permeable PDMS matrix is enough to prevent hypoxia in the sample core[16]. Also, the viability of the MDTs can be sustained for up to 15 days in the microfluidic devices, which allows them to be introduced to numerous cycles of therapeutic agents. Moreover, patient samples can be introduced to various treatments and analyzed in a 3-week time frame, thus representing the perfect model to predict the patients' response in a time frame suitable for clinical decision-making.

Confocal microscopy and flow cytometry techniques were commonly used to assess the viability of the MDTs in the presence or absence of various therapeutic agents (figure 1A). However, each technique has disadvantages. The confocal microscopy generally underestimates the mortality due to washing out of

dead cells during medium changes and staining protocols as well as the staining of early apoptotic cells by "live" dyes. Additionally, there is a limit in imaging depth (around 100 μm) creating a "black" unanalyzed region in the center of the MDTs thus impeding the evaluation of cancer cell survival at the core of the MDTs. In addition, the flow cytometry protocol requires complete digestion of the sample in order to analyze protein-specific characteristics of single cells, and therefore, can only be used as a one-time analysis tool. In addition, the digestion of tissue prevents the preservation of tissue architecture and morphology. The disadvantages presented suggest that these techniques are inefficient to answer all the biologically fundamental questions that may arise.

In pathology, predictive biomarkers in combination with immunohistochemical (IHC) assays are widely used for diagnostic purposes and clinical decision-making. The predictive potential of patient outcome using these biomarkers rely on computed statistical analysis, in which clinicians may over-estimate the likelihood of response. For this, we opted to develop an innovative tool, Micro-Dissected Tissue Array (MDTA), merging the standard paraffin embedding protocol with microfluidic technologies to empirically test the patients' response to therapeutic agents through the use of proliferative and viability biomarkers. MDTAs takes advantage of the high-throughput nature of microfluidics and Tissue Micro-Arrays (TMAs) to handle, probe and analyze large quantity of patient samples with simple manipulations and clinically available techniques.

5.2.2 Hypothesis

We hypothesis that our 3D *ex vivo* patient-derived model maintains its primary tumor characteristics over time.

5.2.3 Objectives

1. **Evaluate MDT evolution over time from high-grade serous ovarian cancer patients in an *ex vivo* culture platform by transcriptome analysis.**

   We will analyze the evolution of MDTs from high-grade serous ovarian cancer (HGSOC) patients in the microfluidic culture platform. We will characterize the transcriptome of MDTs at different

time points by DNA microarray and compare these results to the transcriptome profile of the parental HGSOC as well as to primary cell cultures.

2. **Develop a new histological tool that preserves the tissue architecture and cell morphology: the Micro-Dissected Tissue Array (MDTA)**

   We will develop a method appropriate for fixing and embedding tissue samples within the microfluidic devices, thereby making the amenable to classical histologic examination. This FFPE fixed tissue will be further characterized to interrogate tissue architecture and cell content of tumor tissues over time.

Model systems

1. **Patient sample Inquiries**

Taking advantage of our active PC and OC tissue-banking infrastructure at the CRCHUM in association with the CHUM's Urologic and Gynecologic Oncology division it will be possible to obtain post-surgery biopsy samples as well as clinical follow-up of response to therapy.

2. **Cell Line Xenografts**

Different human carcinoma cell lines derived from prostate cancer tumors (LNCaP and PC-3 Manassas, USA) and ovarian cancer tumors and ascites (TOV112D, OV90, OV2295, OV1946) were used to produce mouse xenografts. All protocols involving animals were reviewed and approved by the Comité institutionnel de protection des animaux (CIPA) at the CRCHUM.

5.2.4 Experimental Study

Evaluate MDT evolution over time from high-grade serous ovarian cancer patients in an ex vivo culture platform by transcriptome analysis.

For this aim, we have recruited and collected six HGSOC post-surgical tumor samples. From single tumor fragments, we have established primary cell cultures and produced over 200 MDTs, which were loaded in 25-well microfluidic devices. Total RNA was derived from the primary tumors, fifteen MDTs at day 0, 8 and 15 and primary cell cultures at various passage states. To do so, we established an RNA

extraction method specifically for MDTs that allow us to obtain a sufficient quantity of RNA with suitable quality and purity. From the transcriptome analysis of these model types we will determine the epigenetic stability of the MDTs over time. From these results, we expect that the MDTs produced from our HGSOC patients maintain similar genetic properties as the primary tumor.

RNA extraction protocol for transcriptome analysis

The extraction protocol has been optimized specifically for MDTs. All the reagents used for our protocol are from Qiagen. The primary tumor used had a maximum volume of 24 mm^3, required flash freezing in liquid nitrogen, and storage at -80˚C. The extraction proceeded after mechanical disruption using the TissueRuptor. The primary cell cultures take approximately one to four months for the first series to obtain optimal confluence. Once obtained, a standard lysis buffer extraction protocol is performed. Furthermore, the MDTs are harvested at different time points, at day 0, after 8 days and 15 days of cultivation. They were first rinsed with RNase-free phosphate buffered saline (PBS) to remove the culture medium and were placed in a tube with RNAlater solution to diminish potential RNAse contamination. They were further stored at -80˚C and once ready to be processed; the RNAlater solution was properly removed. Keeping the MDTs on dry ice, they were crushed into small debris using a plastic piston and further incubated for several minutes in RLT lysis buffer. The RNeasy Micro Kit was used to facilitate the RNA extraction of the samples.

The RNA was quantified and analyzed for suitable quality and purity by the NanoDrop and Bioanalyzer. The RNA extracted from two patient samples were sent to Genome Quebec for an Affymetrix HumanGene ST 2.0 gene expression analysis. A normalization of the results as well as control probe verification was performed using a publically available expression analysis software to ensure high quality and reliability of results. The results were further analyzed by hierarchal cluster analysis (transcriptome analysis consoleTM) where we compared the MDTs at various time points to the primary tumor tissue independently as well as compared the primary cell cultures to each of the other sample groups. From these

results, we performed a cluster analysis taking into account the 44 000 probes to identify the genes that were differentially expressed between each group.

Preliminary results of transcriptome analysis of MDTs over time and discussion

We initially sent all the samples from an endometrioid carcinoma patient and our first HGSOC patient to Genome Quebec for gene expression analysis. We performed a cluster gene analysis for each patient and observed distinctly different results. The endometrioid carcinoma patients' cluster shows a genetic similarity between the day 0 MDTs and the primary tumor. However, the MDTs cultured for 8 and 15 days seem fairly more genetically similar to the primary cell cultures than the primary tumor (figure 3A). We postulate that for this particular patient, there is a similar selection of cancer cell clones within the MDTs as the primary cell cultures. On the other hand, the cluster gene analysis of our HGSOC patient suggests that the MDTs maintain their epigenetic integrity through time as opposed to primary cell cultures (figure 3B). We cannot conclude that the results obtained were due to low sample size or cancer subtype. To validate these results, we must perform the expression analysis on the remaining five HGSOC patient samples.

Develop a new histological and high-throughput tool that preserves the tissue architecture and cell morphology: Micro-Dissected Tissue Array

Our goal was to define a method for formalin fixed paraffin-embedding (FFPE) MDTs within microfluidic devices in a high-density MDTA. Architecture, viability and proliferation are characterized using MDTA, an adaptation of the standard FFPE technique currently used in pathology, allowing on-chip fixation and direct casting of all samples in a unique paraffin block. This paraffin-embedding protocol of micro-scaled tissue samples is the core aspect of this methodology that has not been reported to date. Previous work using standard FFPE protocol was unsuccessful in maintaining tissue architecture and cell morphology further orienting my goal to optimize the FFPE conditions for the MDTs.

Optimization of the methodology

Dehydration process

The initial dehydration procedure (direct 70% to 100% ethanol) produced MDTAs showing ghost-like structured cells with no nucleus or cellular components (figure 4A). In comparison to paraffin-embedding protocols, our optimization revealed that the most crucial step to preserving the morphology of the cells was to introduce incremental concentrations (50, 70, 80, 90, 95, 100%) of ethanol for a 20-minute incubation period. The results obtained from this dehydration process with MDTAs showed better morphological and architectural preservation with well-defined cell representation and distinction between cell types (Figure 4B).

Formalin fixation and phloxine staining

Formalin is widely used in pathology to preserve the tissue from decay, preventing autolysis[17]. It is an ideal fixation agent for tissue specimens as well as for MDTs. We examined if it was possible to diminish the incubation period (4 hours) with the fixative agent to favour a high-throughput potential. We produced MDTs from our ovarian cell line (OV1946) xenograft models and proceeded with an on-chip formalin fixation using various time points (5 to 60 minutes) (figure 5A). With the help of a pathologist, we determined that the best results were obtained with a fixation period of 30 minutes, thus reducing the traditional fixation time (24 to 48 hour incubation) of tissue specimen by 98%. We validated this step by using various epithelial ovarian cancer (EOC) and prostate cancer (PC) cell line xenografts (figure 5B). Theoretically, the tissue diffusion rate of formalin is 1 mm per hour[17]. Therefore, a tissue section of approximately 400 µm in thickness and 500 µm in diameter would require fixation for approximately 30 minutes and this observed time correlated well with the theoretical time.

The size of the MDTs and their opaque coloration makes them obscure in the paraffin. To facilitate the visibility of the MDTs in the paraffin block, we elected to stain the cell cytoplasm and connective tissue regions of the MDTs with a red biological stain, phloxine B. This unique step, not part of standard FFPE,

successfully allowed MDTs to be visualized within the paraffin block. Importantly, this biological stain does not interfere with further IHC, immunofluorescence (IF) or Hematoxylin & Eosin (H&E) colorations.

Paraffin-embedding and MDT alignment

In general, the MDTs were fixed with formalin, stained with phloxine and dehydrated (figure 6A, table 1). The next step in the procedure is the addition of a xylene substitute solution that was less volatile and of low toxicity in the inlets of the device. This slowly removed all traces of the dehydrant, further curving the device and facilitating the separation of the two PDMS layers. Once separated (figure 6B), the bottom layer containing the MDTs was placed in a stainless steel base mold and embedded in liquid paraffin (figure 6C) at 60˚C for 90 minutes, allowing full infiltration of the embedding agent into the MDTs. The paraffin block was then solidified at 4˚C to allow proper removal of the remaining PDMS layer (figure 6D), leaving the MDTs upright in the paraffin block. The exposed MDTs were then covered with a second layer of liquid paraffin (figure 6E). This step resulted in misalignment of the MDTs within the paraffin block thus requiring a large number of slides to integrate MDTs within the block. This greatly affected the high-throughput potential of our approach. To circumvent this problem, we re-liquefied the paraffin block in an oven at 60°C (figure 6F), thus allowing the sedimentation of the MDTs to the bottom of the block, while keeping the microfluidic device alignment (figure 6G). This step allowed all the MDTs in the block to be on the same cutting plane, which is a crucial step to forming high-density MDTA slides.

Changes in the microfluidic device

Advantages and disadvantages of three different microfluidic devices

We tested several microfluidic device designs in order to favor the generation of a high-density array of tissue samples as well as to increase the number of MDTs that can be treated on a single chip (summary of device specifications in table 2). The original 25-well device (figure 2A), allowed for analysis of five MDTs per condition. However, the heterogeneity of the tumor imposes that the number of MDTs analyzed per condition must be high. This device requires the production of a large number of blocks per

patient (3-4 blocks), reducing the high-throughput ability and high-density capability of MDTA. In order to increase capacity, a seven vertical channel device design holding a total of 70 MDTs was produced, thus allowing seven different conditions to be analyzed at the same time (figure 2B). Advantageously, this design doubled the number of samples per condition and greatly reduced the number of blocks (1-2 blocks). We also noted that the stability of the MDTs within the wells increased as the reservoir channel increased in width. However, these devices were prone to trapping air bubbles, required a lot of time to operate and relatively large amount of reagents, and had a low resistance factor to reagent flow. To compensate for these disadvantages, a 32-well serpent-like device (figure 2C) was produced, holding four channels that each contained eight wells allowing analysis of four different conditions. This compromise makes it the most practical device to work with.

Reproducibility and medium change variability of each device

The operation of a microfluidic device is diffusion-driven[16,18], therefore, it is important to properly remove previously introduced medium in order to maintain the viability of MDTs. This was equally important for the MDTA and required rinsing the devices thoroughly before starting the required incubation periods for optimal fixation and dehydration. For this, the procedure required a minimum of two rinsing intervals of 5-minutes before initiating the required incubation periods.

Each device was thoroughly inspected for usage potential. The incubation period with the fixative for the MDTA procedure was tested on each device to optimize the conditions. The results suggested a minimal incubation of 20 and 30 minutes for the 70-well (figure 7A) and 32-well devices (figure 7B), respectively. Moreover, a coloration test using culture medium was performed on each device (figure 8A). Our results suggested that the 25-well and 32-well devices required a minimum of 3 medium changes in order to sufficiently remove enough of the former medium in both the channels and wells. However, the 70-well device required a minimum of 7 medium changes, correlating to the COMSOL Multiphysics® modeling software analysis (figure 8B). Finally, the alignment step has been optimized for each device and

slight adjustments have been made in the device design in order to perfect the reproducibility of this step (figure 9). Together, the results show that the 32-well device is most suitable for our future experiments.

5.2.5 Results

In FFPE, evaluation of tissue architecture, viability and proliferation can be carried out through IHC/IF analysis. The approach is simple, robust, and provides a whole new framework for using conventional IHC/IF to study post-treated ex vivo tissue specimens. In order to validate the MDTA tool, we used cell line xenograft models.

The PC cell line, LNCaP, generates heterogeneous tumors such that we performed our micro-dissection procedure on the harvested tumor to show that our MDTs were representative of the different tissue architectures found in tumors. By visually selecting various tissue regions of the tumor, which were characterized as brittle (brownish coloration), vascularized (red coloration) or hard textured (whitish coloration), MDTs produced from these heterogeneous regions of the tumor were placed in indicated devices for proper analysis. In comparing the different types of MDTs produced at day 0 to the FFPE tumor xenograft specimen, we were able to correlate the tissue characteristics of the MDTs to the various tumor regions. This demonstrated that the MDTs maintained an architecture specific to selected tumor regions (figure 10).

We then examined the evolution of the MDTs over time to determine if we were able to maintain tissue viability and sustain epithelial cells within the MDTs. For this, we produced xenografts from an ovarian cancer cell line, OV2295, which generated a more homogeneous tumor. The MDTs were analyzed at day 0, day 3/5 and day 8. Flow cytometry analysis was used to validate the results observed with the MDTA. The tumor epithelial cells were identified using a human anti-mitochondrial antibody. Various other biomarkers were used to assess the viability for flow cytometry (Annexin V, DRAQ 7 for detection of apoptotic and dead cells and cleaved caspase-3 for MDTA) and proliferation (Ki-67 for MDTA) potential of the type of cells within the MDTs. As we have previously reported, the MDTs at day 0 showed lower levels of proliferation and viability than the MDTs that had been cultivated for 3 and 8 days (figure 11A).

We suspect this occurs to mechanical stress induced by the MDT procedure. We also observed an increase in the number of epithelial cells as well as an increase in their proliferating ability as the days of culture progressed (figure 11B-C). We speculate that the initial culture period of the MDTs, within the microfluidic device, allowed for them to recover from the micro-dissection procedure and the medium supplied them with sufficient nutrients for viability. We did observe a slight reduction in epithelial cells in day 8 MDTs; however, the cells were viable and proliferating (figure 11D). From this, we show that the epithelial cells remain viable and in a proliferative state within the MDTs over time.

Going from xenograft models to patient samples and recognizing that there is a higher degree of heterogeneity in human tumors, we expected to obtain a larger amount of patient-derived MDTs to show stronger stromal components rather than epithelial components. This heterogeneity imposed the need to produce 2 or 3 MDTAs per condition, in order to obtain a sufficient number of MDTs expressing epithelial markers. Moreover, we optimized various biomarker conditions in order to look at the expression of certain well-known biomarkers (figure 12). These results suggest that there is need for improvement in identifying the proper antibody concentration condition for our MDTs, however we are able to use this MDTA protocol on patient samples, maintaining high quality cell morphology.

5.2.6 Conclusion

Many research groups have reported using paraffin-embedding techniques as therapeutic read-outs to their organotypic chemosensitivity and resistance assay[19,20]. However, these techniques remain incompatible with microfluidic technology. For instance, Hattersley et al. used histology combined with "off-chip" analysis of a cell viability biomarker (cytochrome c) to demonstrate that head and neck squamous cancer biopsies cultured in their microfluidic device remains viable for up to 8 days[19]. Similarly, Vaira et al. showed sustained 3D architecture, viability and proliferation for up to 120 hours using IHC in their organotypic slice model[20]. However, these assays require removal of individually cultured samples from the culture platform for processing, yielding poor throughput potential, a lot of manual labor and risk of experimental and biomarker variability.

Due to the micro-size of the tissue samples and the use of microfluidic chips, the MDTA procedure takes advantage of the fast reagent-reaction time and low reagent consumption, reducing total procedure time. The procedure relies on the direct and systematic transfer of the MDTs from the microfluidic matrix to the paraffin block while maintaining tissue alignment further allowing all the sample conditions are analyzed on the same slide. This incorporates a high number of replicated that may provide a superior read-out. Favorably, MDTA preserves the tissue architecture and cell morphology, in which will provide in-depth characterization of therapeutic response as well as following biological mechanisms or pathways using standard HP/IHC/IF techniques. In conclusion, we must further optimize IHC techniques and characterize the evolution of the MDTs over time. This will form the basis of a first author article that is now under preparation, mainly focusing on the methodology and MDTA approach potential.

5.2.7 Proposed Doctorate Project

Rational for investigation and Hypothesis

We will proceed with the expression analysis of the remaining five HGSOC patient samples to validate that the primary tumor characteristics are maintained in our 3D ex vivo patient-derived model over time. In addition to my masters project, we postulate that the treatment response of the MDTs correlate to the clinical patient outcome thus making the viable model effective in empirically predicting drug response in patients. This specific aim will be answered in two parts. First, we will compare the response to treatment of micro-dissected xenograft tissues (ex vivo model) in microfluidic devices with matched mouse xenografts (in vivo model). We will follow, on-chip and in mice, the impact of chemotherapies (docetaxel) and hormonal therapy (enzalutamide) on the survival and growth of hormone-sensitive and castrate-resistant PC xenografts. Secondly, we will validate the prognostic potential of our patient-derived ex vivo model system on a large cohort of high-grade serous ovarian cancer (HGSOC) patients.

As previously mentioned, each patient will respond differently to the same therapeutic agent. In particular, 96% of PC patients that relapse after surgery and treated with the standard androgen deprivation therapy (ADT) and 80% of HGSOC patients treated with standard platinum-paclitaxel-based chemotherapy

will develop a resistance [21-24]. The pathways by which innate and acquired resistance mechanisms develop remain a major clinical challenge for both CRPC and HGSOC patients. This novel model system in combination with MDTA and transcriptome analysis will permit us to study such mechanisms. My doctoral research proposal will be based on depicting and further studying fundamental molecular pathways of resistance development to standard therapies in CRPC and HGSOC patients. We postulate that treatment-dependent molecular signature of unresponsive patients correlate with the occurrence of innate or acquired resistance mechanisms.

Research Objectives

1. Evaluate MDT evolution over time from high-grade serous ovarian cancer patients in an ex vivo culture platform by transcriptome analysis.
2. Determine the prognostic potential of the ex vivo patient-derived model in a clinical context.
3. Characterization of molecular and pathological responses of CRPC and HGSOC tumor tissues to treatment to study innate and acquired resistance.

Study/Experimental design

Evaluate MDT evolution over time from high-grade serous ovarian cancer patients in an ex vivo culture platform by transcriptome analysis.

We will complete the transcriptome analysis of the remaining five HGSOC patients. From the compilation of the six patient complete transcriptome we will do a thorough analysis of the cell composition in the two model systems (MDTs over 15 day period and primary cell culture) and compare it to the primary tumor. We will be able to look at the proliferative potential of the MDTs over time and examine the evolution of the tumor microenvironment in the MDTs. In addition, we will perform a thorough investigation of the various pathways activated and suppressed significantly determining the differences between each model type as well as within each ex vivo time-point.

Determine the prognostic potential of the ex vivo patient-derived model in a clinical context.

Correlation between ex vivo and in vivo cultured PC tissue responses to ADT and chemotherapy

To validate our ex vivo model as a surrogate for chemotherapeutic response in vivo, we will determine whether the chemosensitivity of MDTs reflect the sensitivity of matched PC xenografts: PC-3 (castrate-resistant) and LNCaP (hormone-sensitive). We will compare the response of MDTs in microfluidic devices and of xenografts in mice to different therapies: chemotherapy (docetaxel) and hormonotherapy (enzalutamide), either alone, in combination, or sequential administration (table 3). Previously, we have shown that 3D culture models demonstrate a higher IC50 to drugs than 2D monolayer cultures[25]. Consequently, the drug concentrations used in this study will be adjusted to a 10-fold increase of the 2D IC50.

Chemotherapeutic intra-tumoral injections at cell line-specific doses (10X IC_{50}) will begin for the first group (64 mice) when tumor size reaches 1000 mm3 and will be administered once a week for 3 weeks. Tumors will be measured every 3 days for 15 days at which time mice will be sacrificed. The second group (12 mice) will be sacrificed when tumor size reaches 1000 mm3, which will be immediately processed to produce multiple MDTs (table 4) that will be exposed to 2 cycles of 24-hour drug treatment followed by a 48-hour recovery. MDT samples and xenografts will be collected at the end of experiments to analyze cancer cell survival and growth by flow cytometry (AnnexinV) and by MDTA using antibodies against Ki-67, Caspase-3, p16, and p21.

Statistical analyses will be performed using SPSS software, version 20 (SPPS, Inc., Chicago). Pearson correlations will be used to measure the association between drug sensitivity of MDTs and the xenograft response to treatment in mice. We expect to validate the potential of MDTs in association with microfluidic devices for empirical prediction of primary tumor sensitivity that will improve the sequence of treatment to various chemotherapeutic agents. Moreover, as sequence of treatments using these specific compounds and combinations in the xenograft models has not been described, our mouse studies themselves will provide valuable results for future experimentation.

Correlation of HGSOC patient ex vivo model to clinical outcome.

We will continue working on the validation of our ex vivo patient-derived 3D model for the study of patient response to treatment on a larger cohort of HGSOC patients. We will continue to recruit HGSOC patients from the CHUM clinic and obtain specimens for treatment response analysis using MDTA and flow cytometry techniques. The newly developed MDTA tool will give a visualization of the change in cell morphology in the presence of treatment. For example, cells may have acquired characteristics allowing them to induce an epithelial to mesenchyme transition. The viability (cleaved caspase-3) and proliferative (Ki-67) capability of the cells will further be defined by using IHC or IF techniques. Flow cytometry techniques will be used in parallel to assess the viability of the epithelial and immune cells using specific apoptotic (Annexin V) and dead (DRAQ7) cell markers. In comparison with the patients' clinical outcome we can validate the precise prediction utility of our ex vivo patient-derived 3D model.

Preliminary results of treatment response analysis for prediction of clinical outcome

We obtained a tumor specimen from a HGSOC patient diagnosed with a stage IIb (FIGO) to generate MDTs and performed a two-cycle chemotherapy regimen that consisted of a combination of carboplatin (300 μM) and paclitaxel (80 nM). Each treatment cycle consisted of a 24-hour induction with the combinatorial treatment followed by a 48-hour recovery period. At the end of the experiment, the MDTs were fixed and embedded in paraffin to produce MDTAs. In parallel, the viability of another set of MDTs from the same patient sample was analyzed using flow cytometry. The preliminary results obtained from MDTA showed tissue distortion as well as increased expression of cleaved caspase-3 and drastic reduction in cell proliferative biomarker, Ki-67, in the treated MDTs compared to the controls (figure 13B). The viability assessment by flow cytometry showed a 40% increase in cell death in the treated MDTs compared to the controls (figure 13C), further confirming the results observed with the MDTA and, thus, predicting the response to the combinatorial treatment regimen. The clinical follow-up of this patient's progression showed a major decrease of her CA-125 levels from 2935 U/ml to 13 U/ml (figure 13D) within the first 6

months after the initial treatment cycle, resulting in full remission. We are extending these results to a larger cohort of cancer patients.

Characterization of molecular and pathological responses of CRPC and HGSOC tumor tissues to treatment to study innate and acquired resistance.

For this aim, we will recruit four treatment naïve high-grade PC patients as well as four treatment naïve HGSOC patients treated at the CHUM clinic to obtain post-surgery tumor tissues. In particular, our PC patient samples will preferentially come from relapse patients undergoing a transurethral resection of the prostate (TURP) procedure or a metastatic tissue biopsy (from the bone or liver) to study acquired resistance. For HGSOC patients, we will obtain either a laparoscopy biopsy specimen or a full tumor resection to study the innate resistance mechanisms.

Using these tumor specimens, we will generate more than 300 MDTs in which every 30 MDTs will be exposed to a different drug or combination of drugs for a period of 24 hours and then immediately processed (table 5). A portion of the MDTs (approximately 112 MDTs) will be fixed and embedded in paraffin to produce MDTAs. The remaining (approximately 210 MDTs) will be used for RNA extraction in order to characterize the transcriptome of each treatment group of samples from the same patient. This will allow us to identify the molecular signature induced in response to one drug alone or in combination. We aim to validate the signature using IF co-staining of biomarkers representing cancer cell fates such as proliferative biomarker, Ki-67; apoptosis biomarker, cleaved caspase-3; senescence biomarkers, p16 and p21; and necrosis biomarkers, FK18 and RIP1. We will include epithelial specific proteins such as epithelium-specific EPCAM and cytokeratins 8 and 18 proteins to enable a targeted analysis of the predominant cancer cells. We will quantify the presence of each biomarker using a quantitative analysis system (Visiomoph software, Visiopharm) that allows subcellular localization of signals and fluorescence multi-labeling on the same MDTA slide. Multiple monochromatic and high-resolution images of MDTA spots are obtained using an Olympus VS110 epifluorescence microscope (Olympus). These results in

combination with viability assessment using flow cytometry will confirm if MDTs respond or are resistant to each treatment.

Furthermore, the compilation of DNA micro-array results from these four patients will help generate a list of genes preferentially expressed in response to each treatment that we would call the treatment response signature. By combining the specific molecular response signatures from the four patients, we will be able to identify and determine a set of proteins within molecular pathways of interest that are involved in chemo-sensitivity. Furthermore, we will analyze the prevalence of these proteins of interest in the cancer genome atlas (TCGA) dataset for each cancer type and correlate them with the cancer progression (staging) and response to treatment to which will be further developed during this thesis. This will further allow us to focus our fundamental research on the most important molecular resistance pathways.

Conclusion

We are developing a novel model system suitable to address a range of biological questions in cancer. We have currently demonstrated the feasibility of our model and we will begin to determine the predictive potential of MDT model system for personalized medicine. Having developed our new MDTA tool, we can include published or emerging predictive and prognostic IHC/IF based biomarkers in decision-making monogram. In addition, we will provide a model system to dissect innate and acquired resistance.

5.2.8 References

1. Statistics CCSsACoC: Canadian Cancer Statistics 2016. Toronto, ON: Canadian Cancer Society, 2016
2. James Ritter RF, Graeme Henderson, Humphrey Rang: Rang & Dale's Pharmacology (ed 7th), Elsevier, 2011
3. Venditti JM, Wesley RA, Plowman J: Current NCI preclinical antitumor screening in vivo: results of tumor panel screening, 1976-1982, and future directions. Adv Pharmacol Chemother 20:1-20, 1984
4. Fleury H, Communal L, Carmona E, et al: Novel high-grade serous epithelial ovarian cancer cell lines that reflect the molecular diversity of both the sporadic and hereditary disease. Genes Cancer 6:378-98, 2015
5. Weiswald LB, Bellet D, Dangles-Marie V: Spherical cancer models in tumor biology. Neoplasia 17:1-15, 2015
6. Torisawa YS, Takagi A, Nashimoto Y, et al: A multicellular spheroid array to realize spheroid formation, culture, and viability assay on a chip. Biomaterials 28:559-66, 2007

7. Johnson JI, Decker S, Zaharevitz D, et al: Relationships between drug activity in NCI preclinical in vitro and in vivo models and early clinical trials. Br J Cancer 84:1424-31, 2001
8. Richmond A, Su Y: Mouse xenograft models vs GEM models for human cancer therapeutics. Dis Model Mech 1:78-82, 2008
9. De Wever O, Mareel M: Role of tissue stroma in cancer cell invasion. J Pathol 200:429-47, 2003
10. Junttila MR, de Sauvage FJ: Influence of tumour micro-environment heterogeneity on therapeutic response. Nature 501:346-54, 2013
11. Justice BA, Badr NA, Felder RA: 3D cell culture opens new dimensions in cell-based assays. Drug Discov Today 14:102-7, 2009
12. Hirschhaeuser F, Menne H, Dittfeld C, et al: Multicellular tumor spheroids: an underestimated tool is catching up again. J Biotechnol 148:3-15, 2010
13. Morgan MM, Johnson BP, Livingston MK, et al: Personalized in vitro cancer models to predict therapeutic response: Challenges and a framework for improvement. Pharmacol Ther 165:79-92, 2016
14. Bounaix Morand du Puch C, Nouaille M, Giraud S, et al: Chemotherapy outcome predictive effectiveness by the Oncogramme: pilot trial on stage-IV colorectal cancer. J Transl Med 14:10, 2016
15. Huh D, Hamilton GA, Ingber DE: From 3D cell culture to organs-on-chips. Trends Cell Biol 21:745-54, 2011
16. Astolfi M, Peant B, Lateef MA, et al: Micro-dissected tumor tissues on chip: an ex vivo method for drug testing and personalized therapy. Lab Chip 16:312-25, 2016
17. Protocols O: Paraffin Processing of Tissue, 2016
18. Nassim Rousset FMTG: Simulation-assisted design of microfluidic sample traps for optimal trapping and culture of non-adherent single cells, tissues, and spheroids. Scientific reports 7, 2017
19. Hattersley SM, Sylvester DC, Dyer CE, et al: A microfluidic system for testing the responses of head and neck squamous cell carcinoma tissue biopsies to treatment with chemotherapy drugs. Ann Biomed Eng 40:1277-88, 2012
20. Vaira V, Fedele G, Pyne S, et al: Preclinical model of organotypic culture for pharmacodynamic profiling of human tumors. Proc Natl Acad Sci U S A 107:8352-6, 2010
21. Coutinho I, Day TK, Tilley WD, et al: Androgen receptor signaling in castration-resistant prostate cancer: a lesson in persistence. Endocr Relat Cancer 23:T179-T197, 2016
22. Armstrong DK: Relapsed ovarian cancer: challenges and management strategies for a chronic disease. Oncologist 7 Suppl 5:20-8, 2002
23. Luvero D, Milani A, Ledermann JA: Treatment options in recurrent ovarian cancer: latest evidence and clinical potential. Ther Adv Med Oncol 6:229-39, 2014
24. Staropoli N, Ciliberto D, Chiellino S, et al: Is ovarian cancer a targetable disease? A systematic review and meta-analysis and genomic data investigation. Oncotarget 7:82741-82756, 2016
25. Das T, Meunier L, Barbe L, et al: Empirical chemosensitivity testing in a spheroid model of ovarian cancer using a microfluidics-based multiplex platform. Biomicrofluidics 7, 2013

5.2.9 Figures and Tables

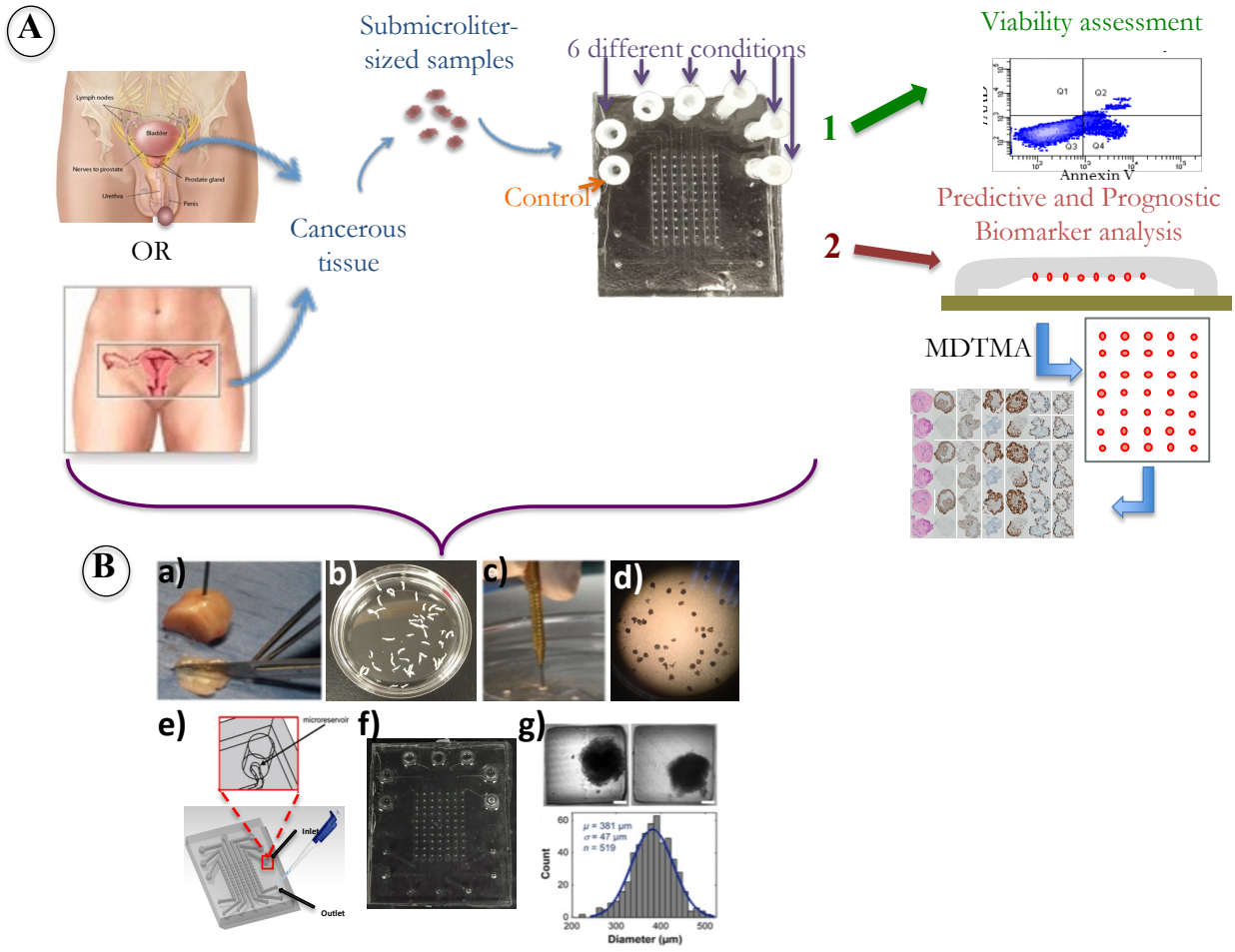

Figure 1. Novel 3D ex vivo model using microfluidic technologies. A) General Concept. The tumor is surgically resected and micro-dissected into a sub-microliter size as micro-dissected tissues (MDTs). They are cultured for several days in microfluidic devices fabricated with two layers of polydimethylsiloxane (PDMS). Viability assessment of samples is achieved by using flow cytometry and predictive and prognostic biomarker analysis with Micro- Dissected Tissue Array (MDTA) using immunohistochemistry (IHC) techniques. B) Micro-dissection procedure of patient-derived 3D ex-vivo model to study patient response to treatment. a. Slicing of tumor specimen. b. Sliced sections of the tissue. c. Micro-dissection of sectioned tissue sample using a 500 µm biopsy punch. d. Microscopic view of the MDTs. e. Microfluidic device of 7 channels, each holding 10 wells and inlets with a micro-reservoir to hold medium. f. Overview of a filled device. g. Microscopy imaging of MDTs and histogram (grey) with normal fit (blue) representing average diameter of MDTs from cell line xenograft tumor samples.

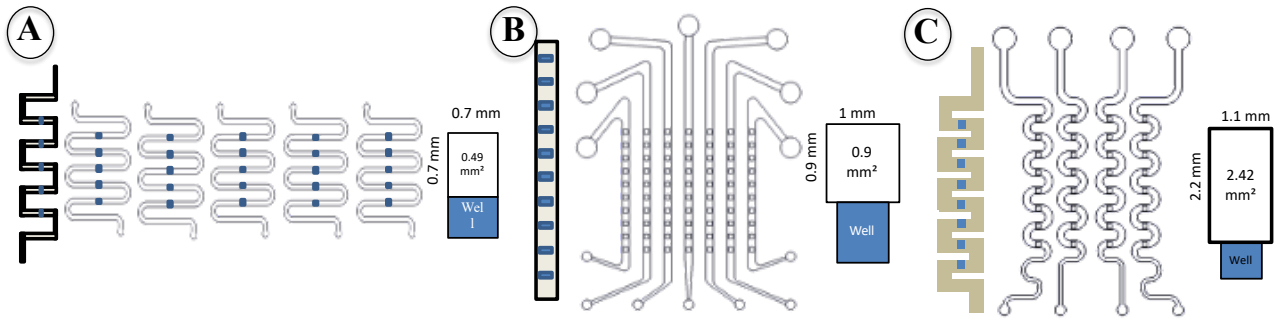

Figure 2. A Schematic representation of microfluidic device designs. A) 25-well device B) 70-well device C) 32-well device.

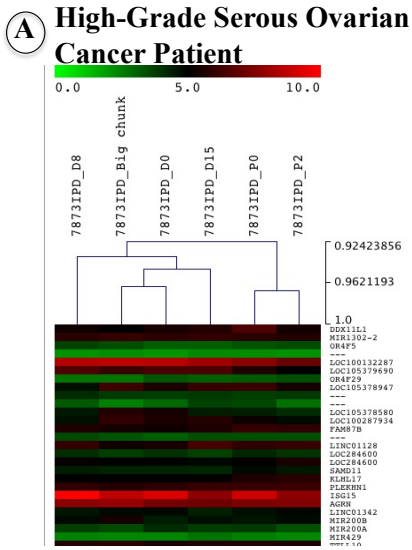

	Gene	Primary Tumor	MDTs at Day 0	MDTs at Day 8	MDTs at Day 15	Primary culture P0	Primary culture P2
Epithelial Cell components	E-cadherin	11.10	11.33	11.02	10.88	6.66	7.20
	Desmoplakin	10.22	9.93	9.85	9.31	6.61	8.62
	Cytokeratin 19	6.29	6.73	6.04	6.69	6.91	6.46
	Secreted phosphoprotein 1	10.82	10.68	11.26	9.11	7.70	9.64
Mesenchymal component	Vimentin	6.53	6.84	6.92	5.90	8.31	7.16
	N-cadherin	2.37	2.36	2.41	2.45	2.65	3.12
	Matrix Metallopeptidase 3	4.08	4.96	9.28	5.47	5.51	10.56
	Secreted Protein Acidic And Cysteine Rich	8.23	8.19	8.13	6.21	9.85	9.54

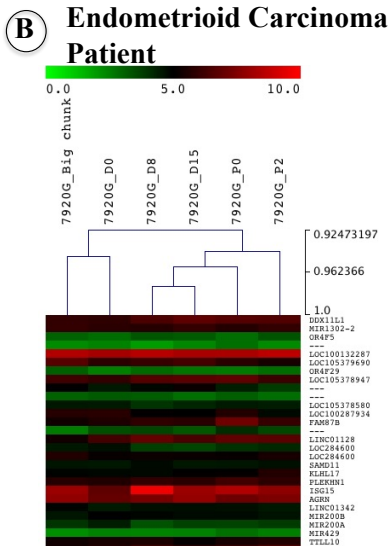

	Gene	Primary Tumor	MDTs at Day 0	MDTs at Day 8	MDTs at Day 15	Primary culture P0	Primary culture P2
Epithelial Cell components	E-cadherin	11.50	11.50	11.53	11.94	10.74	5.93
	Desmoplakin	9.27	8.86	9.14	9.22	8.58	8.72
	Cytokeratin 19	6.62	5.47	6.70	6.69	6.68	6.98
	Secreted phosphoprotein 1	10.38	10.55	8.90	10.72	9.19	9.09
Mesenchymal component	Vimentin	6.46	6.87	6.39	5.90	7.33	7.97
	N-cadherin	2.09	2.33	2.55	2.35	3.75	2.77
	Matrix Metallopeptidase 3	4.71	4.37	7.67	6.34	5.72	6.95
	Secreted Protein Acidic And Cysteine Rich	8.64	8.47	7.55	7.64	8.65	9.35

Figure 3. HGSEOC and Endometrioid Carcinoma patient HumanGene ST 2.0 gene expression analysis. Cropped image of a cluster analysis of the 44, 000 genes. A) HGSEOC patient cluster and epithelial-mesenchyme transition gene analysis (log2 of the level of expression). B) Endometrioid carcinoma patient cluster and epithelial mesenchyme transition gene analysis (log2 of the level of expression).

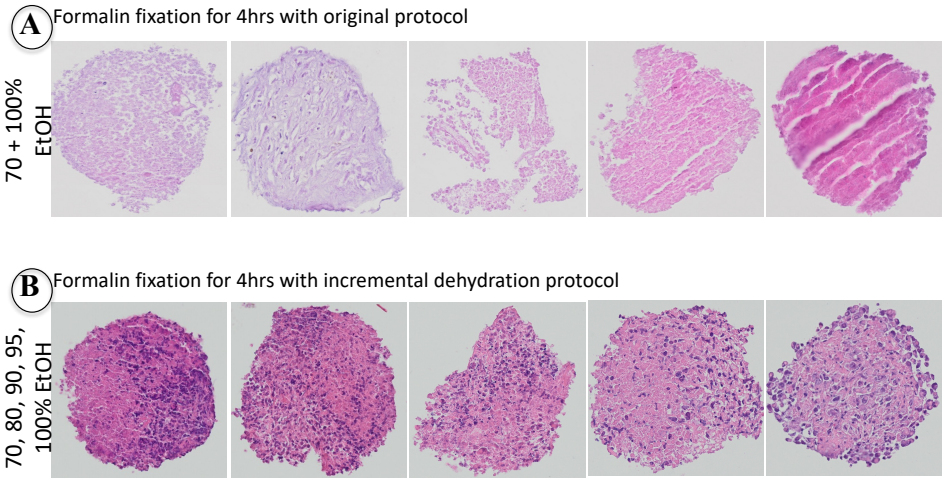

Figure 4. Optimization of the dehydration process in a 25-well device. A) MDTs of OV90 cell line xenografts exposed to a 4-hour treatment with formalin following a 70% ethanol incubation and direct 100% ethanol incubation before embedding in paraffin. B) MDTs of TOV1946 cell line xenografts exposed to a 4-hour formalin incubation which is proceeded with incremental incubations of ethanol (70, 80, 90, 95, 100%), with enlarged regions of two MDTs. ** Incremental increases of ethanol concentration maintains cell morphology of great quality.

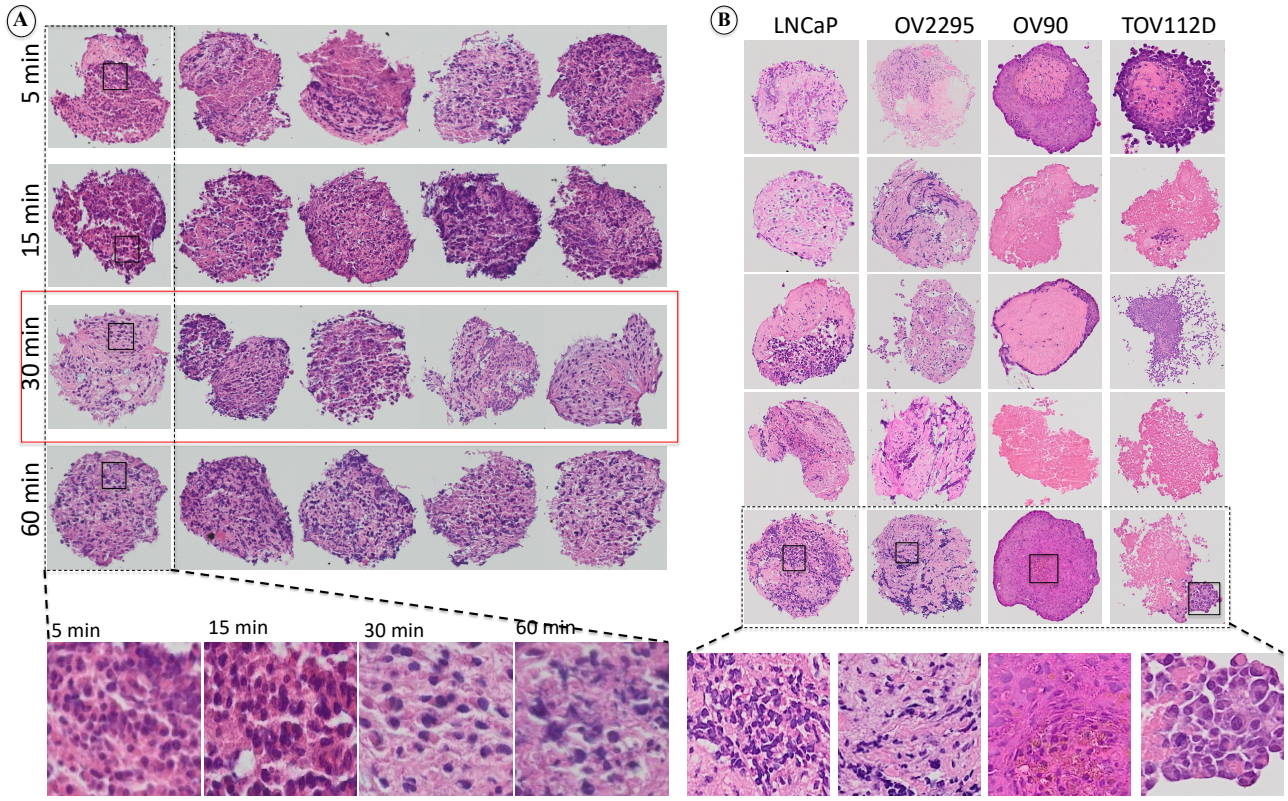

Figure 5. Optimisation of formalin fixation conditions. A) The EOC cell line, TOV1946, was used to optimize these conditions in the 25-well device. Each system was exposed to formalin for a period of either 5, 15, 30 or 60 minutes. A 30-minute incubation period shows a better preservation of tissue architecture and cell morphology as seen in the enlarged regions of chosen MDTs in each incubation condition. B) Validation of the 30 minute incubation period in a 25-well device using PC (PC3) and other EOC (OV2295, OV90, TOV112D) cell line xenografts. Although the component composition varies between each MDT and cell line, the morphology of the cells within each MDT is preserved using these conditions.

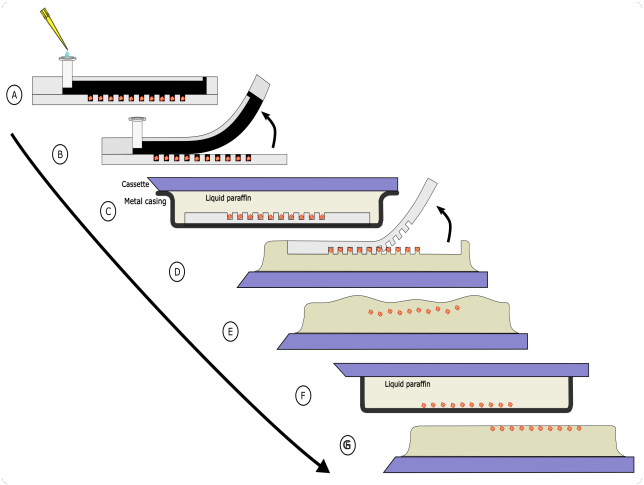

Figure 6. Paraffin embedding protocol to produce Micro-Dissected Tissue Micro-Array (Paraffin-Embedding Lithography). A) Formalin fixation and dehydration of the MDTs directly in the microfluidic device. B) Peeling apart of the two PDMS layers. C) Replica molding of the channel layer by immersion in liquid paraffin followed by solidification. D) Removing the remaining PDMS layer from the solid paraffin block. E) Covering the exposed MDTs with liquid paraffin and solidification. F) Re-melting of the block to align the MDTs on the same plan. G) Solidification of block with MDTs perfectly aligned on the surface plane.

Table 1. Summary of MDTA procedure in which formalin fixation incubation is dependent on device type.

Time of incubation (min)	25-well Device	70-well Device	32-well Device
Formalin Fixation	30	20	25
50% Ethanol	3x5	4x5	3x5
70% Ethanol	20	20	20
Phloxine	20	20	20
80% - 100% Ethanol	20	20	20
Xylene Substitute	3x5	3x5	3x5
Paraffin embedding	120	120	120
Solidification	40	40	40
Peeling off PDMS & covering up	15	15	15
Re-melting & solidification	120	120	120
TOTAL TIME: ~ 11 hours if done on the same day			

Fixation time depended on the device type as a function of the amount of volume the channel unit could hold (for more details see table 2). For every ethanol step the systems were rinsed with 2 intervals of 5-minute incubations before starting the real incubation time, allowing removal of previous solution from the wells and channels. This procedure was usually done over a 3-day period; the steps highlighted in green were primarily done at the end of the experimental time point at which time the samples were stored for a couple weeks in 70% ethanol at 4˚C. The orange highlighted steps were done all on the same day and finally the blue highlighted steps could be done the day following paraffin embedding if needed.

Table 2. Particularities of each device type fabricated with all important specifications.

	25-well Device	70-well Device	32-well Device
Channel Dimensions	0.7mm by 0.7mm	1.1mm by 2.2mm	1mm by 0.9mm
Well dimensions	0.7mm by 0.7mm	0.7mm by 0.7mm	0.7mm by 0.7mm
Assembly of device	Channel and wells on same layer	Channel and well on separate PDMS layers	Channels and wells on same layer
Volume of medium channel can hold	45 µl	100 µl	80 µl
Time for glucose to diffuse out of well (rate of diffusion $9x10^{-6}cm^2/sec$)	5 min	18 min	8 min
Time for phloxine to diffuse out of well (rate of diffusion $5x10^{-6}$ cm^2/sec)	7 min	25 min	12 min

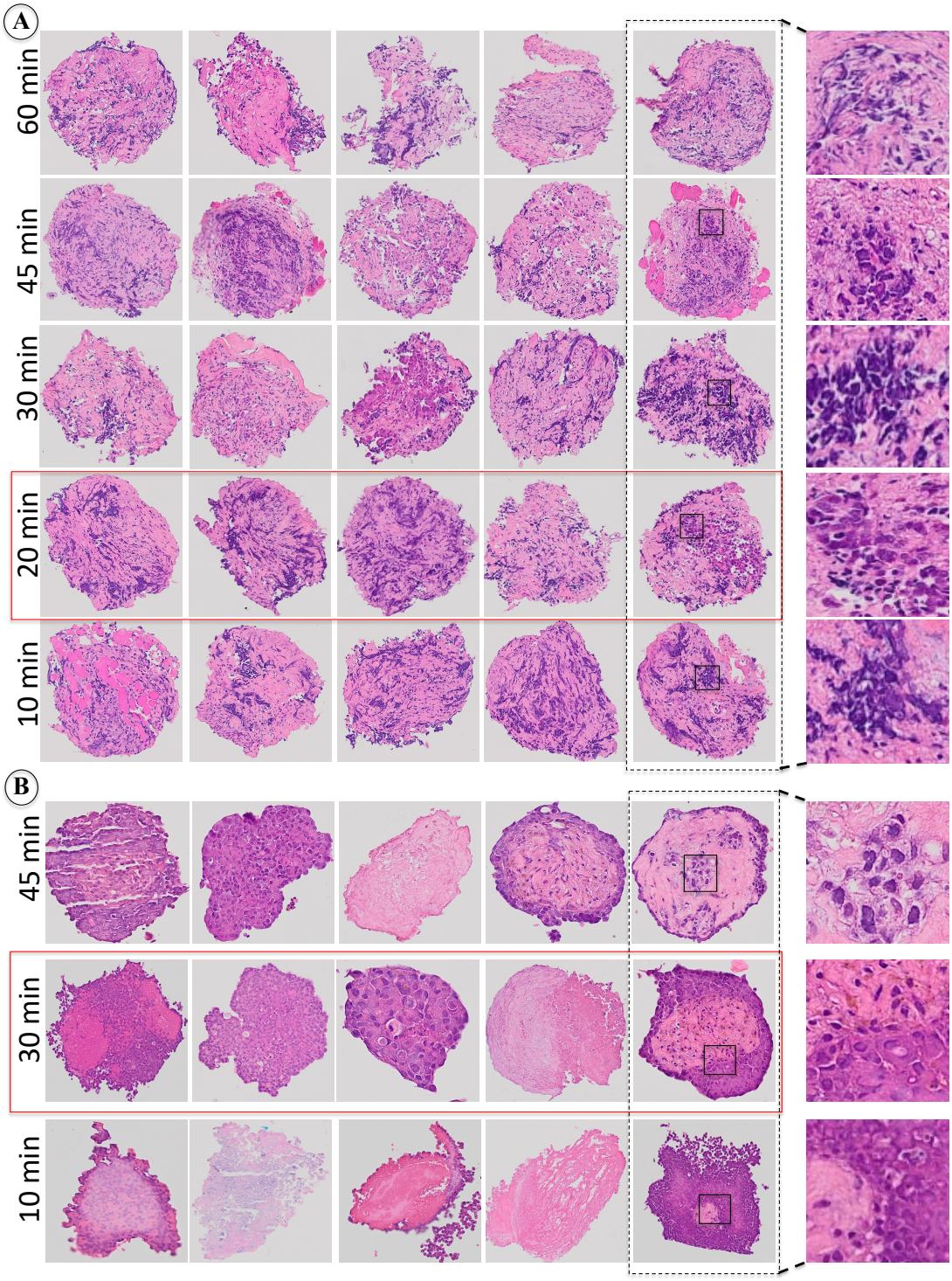

Figure 7. Optimization of formalin fixation of the 70-well and 32-well device. A) Xenograft MDTs of the epithelial EOC cell line, OV2295, exposed to formalin during different incubation time points (10, 20, 30, 45 and 60 minutes) in a 70-well device. B) Xenograft MDTs of the epithelial EOC cell line, OV90, exposed to formalin during different incubation time points (10, 30 and 45 minutes) in 32-well device.

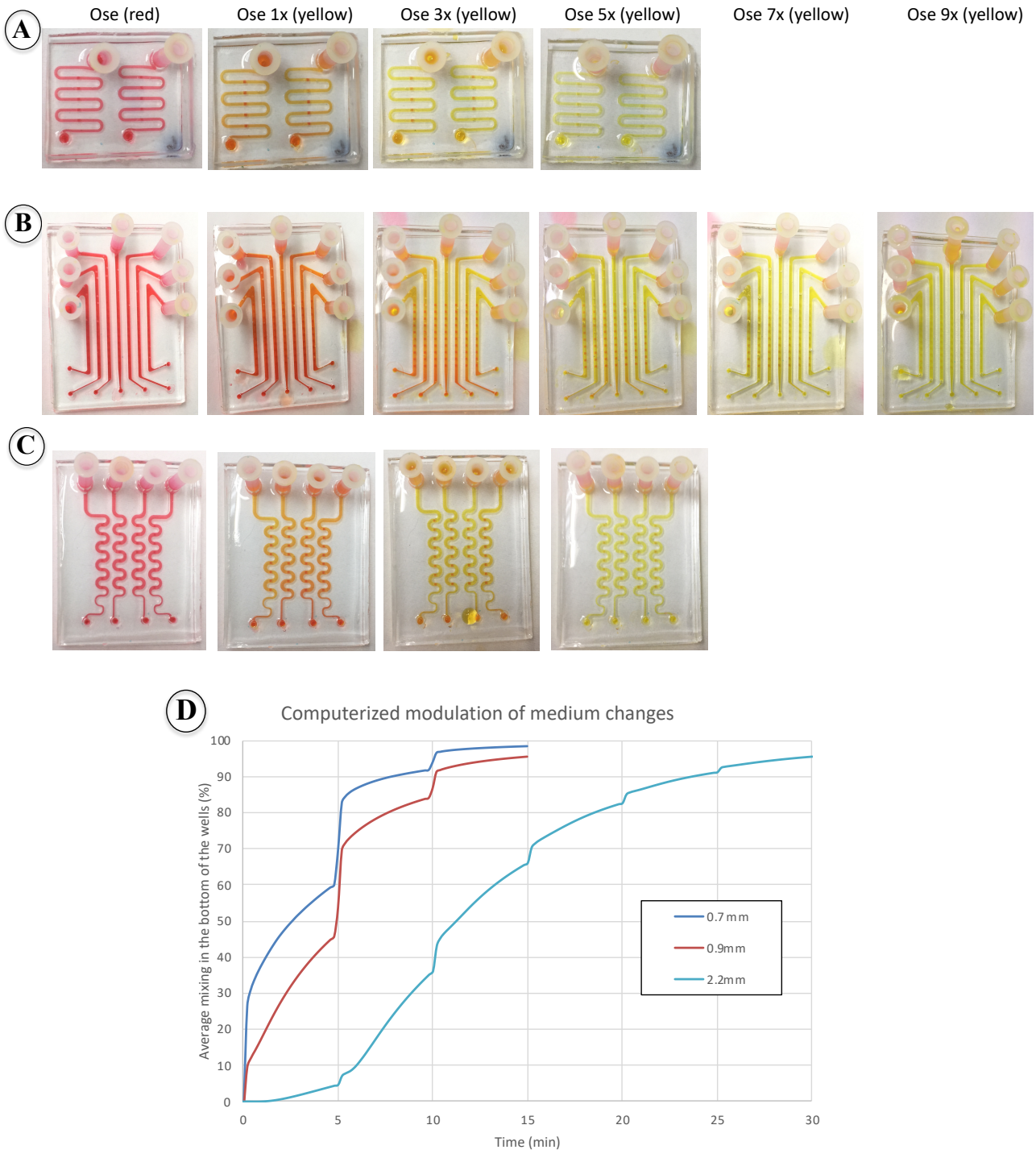

Figure 8. Medium change variability and usage potential of each device type. Culture medium coloration test using OSE medium of different colors (red and yellow). *The device wells did not contain any MDTs during testing procedures. A) 25-well device B) 70-well device C) 32-well device. Each device was initially rinsed with 100% ethanol to remove possible air bubbles that may have been trapped within the channels or wells, and then rinsed first with red medium and then with yellow medium. Between each medium change, 5 minutes of diffusion time was given before adding the next rinsing change. D) Computer stimulations using COMSOL Multiphysics® modeling software was

performed for establishing rinsing procedure as a function of diffusion rate of glucose. * In the graph legend 0.7 mm refers to the 25-well device, 0.9 mm refers to the 32-well device and 2.2 mm refers to the 70-well device.

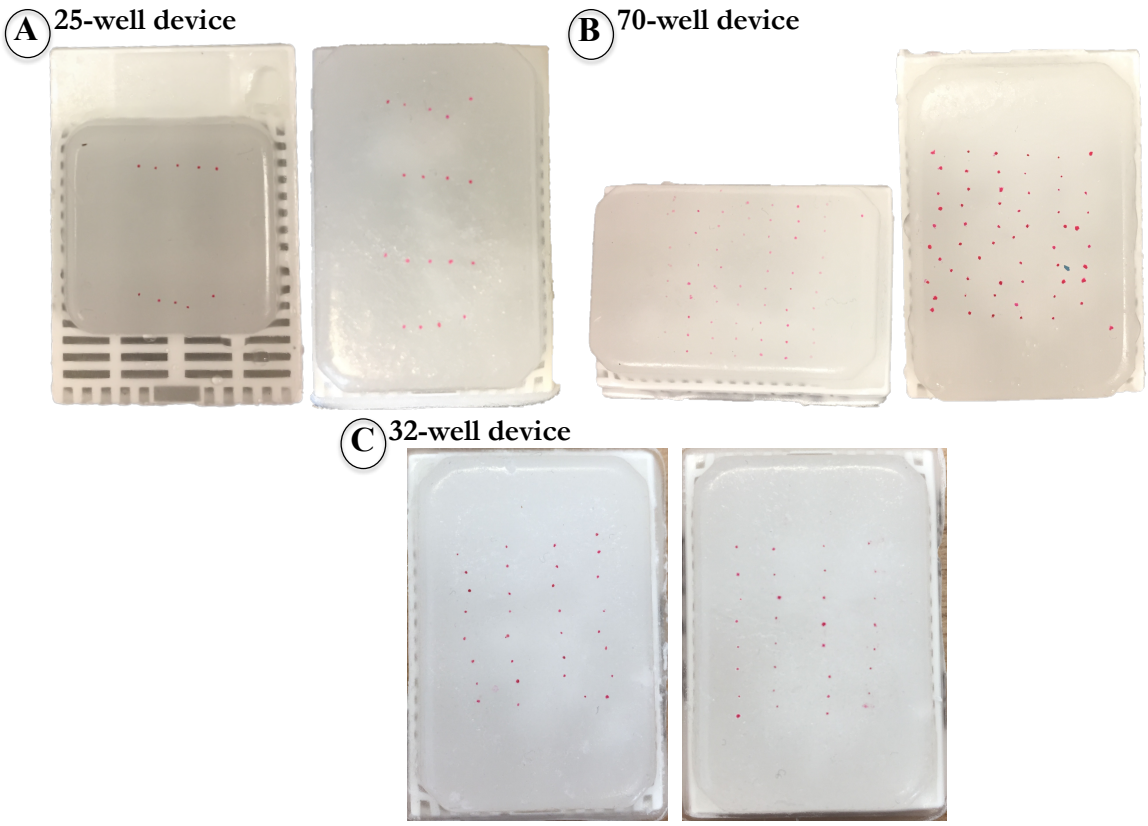

Figure 9. Reproducibility of MDTA alignment using different device types. A) 25-well device B) 70-well device C) 32-well device * More than ten blocks were produced and analyzed for this part of the procedure.

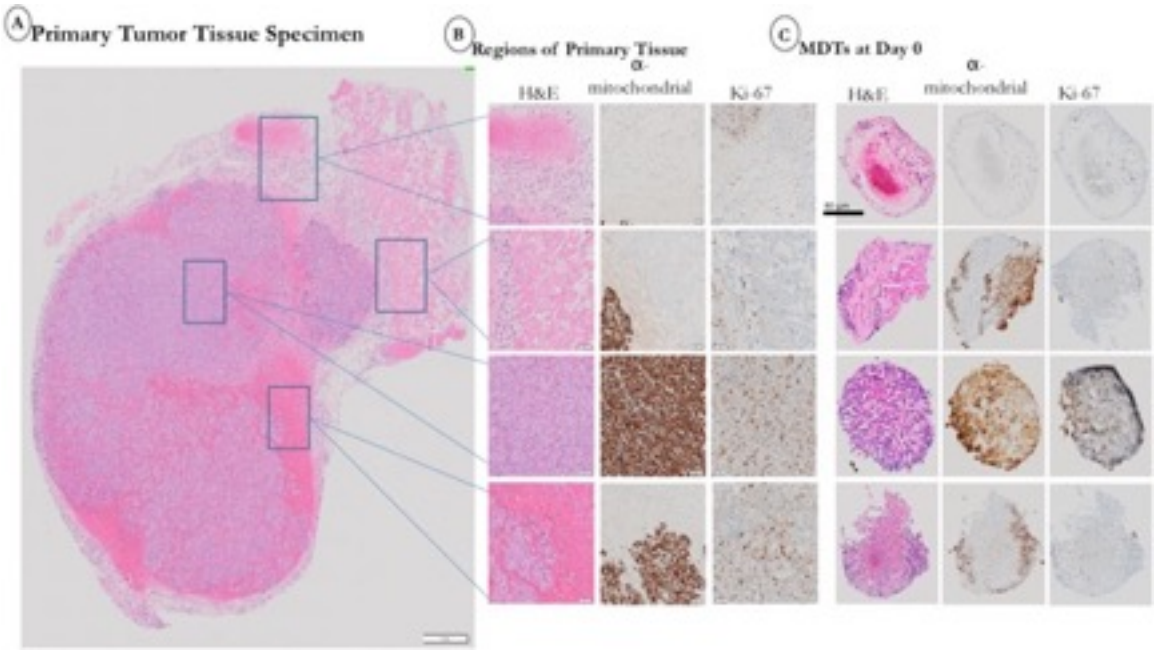

Figure 10. Heterogeneity preserved in prostate cancer cell line xenograft model (LNCaP). Each primary tissue region and MDTs were stained with H&E, a human mitochondrial antibody staining human epithelial cells and the cell proliferative marker Ki-67. A) Primary tumor tissue sectioning stained with Hematoxylin and Eosin (H&E). B) Closeup of different regions showing heterogeneity of the tumor C) Representative MDTs corresponding to the different tumor regions of the primary tissue.

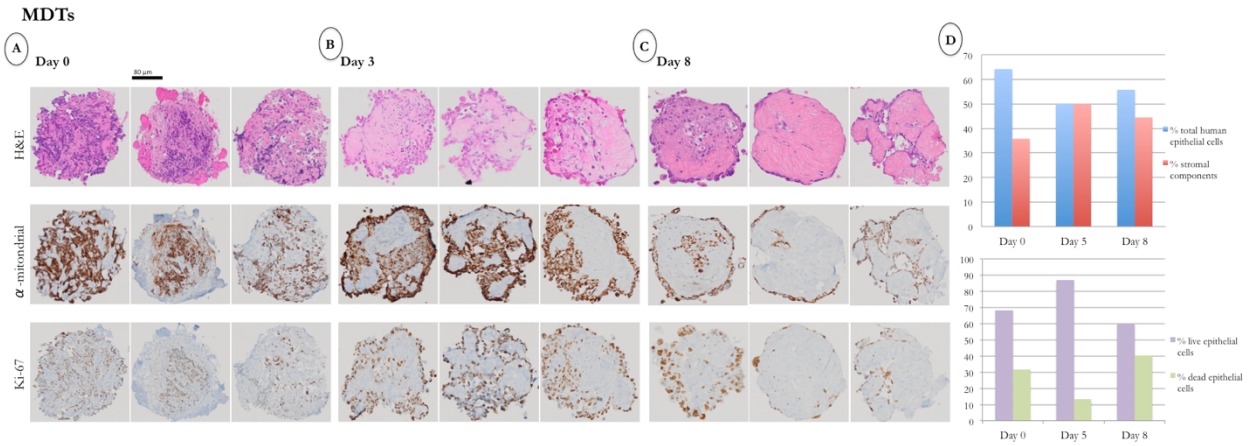

Figure 11. Evolution of the MDTs over time in ovarian cancer xenograft model (OV2295). IHC analysis (A-C) of randomly selected MDTs at different time-points stained with H&E, human mitochondrial antibody and cell proliferative biomarker, Ki-67, showing sustained proliferation of human epithelial cells over time A) MDTs fixed on primary tissue harvest day (Day 0). B) Fixation after 3 days of culturing. C) Fixation of MDTs after 8 days of culturing. D) Flow cytometry analysis of 15 MDTs at Day 0, 5 and 8 stained with human mitochondrial antibody identifying the percentage of human epithelial cells and showing tissue viability using combination of Annexin V (detection of apoptotic cells) and DRAQ7 (detection of dead cells) antibodies.

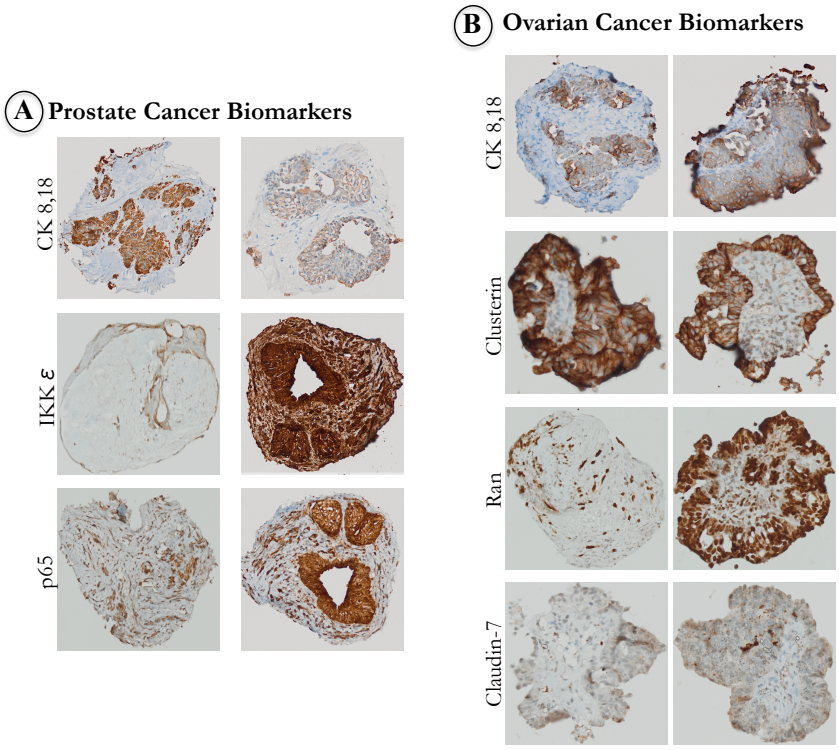

Figure 12. MDTA procedure on prostate cancer and epithelial ovarian cancer patient samples. A) Hematoxylin and Eosin (H&E) coloration of three PC patient sample MDTs. B) H&E staining of three EOC patient sample MDTs. C) Same PC patient samples exposed to different biomarkers such as epithelial cell identifier, CK8/18; IκB kinase, IKKε; and the p65 subunit of NF-κB. D) Same EOC patient MDTs exposed to various biomarkers such as epithelial cell identifier, CK8/18; molecular chaperone, clusterin; GTPase, Ran; and tight junction membrane protein, claudin-7. * Optimizations of antibody concentration conditions are on going however from these results we show we can convey this protocol onto patient samples maintaining high quality cell morphology.

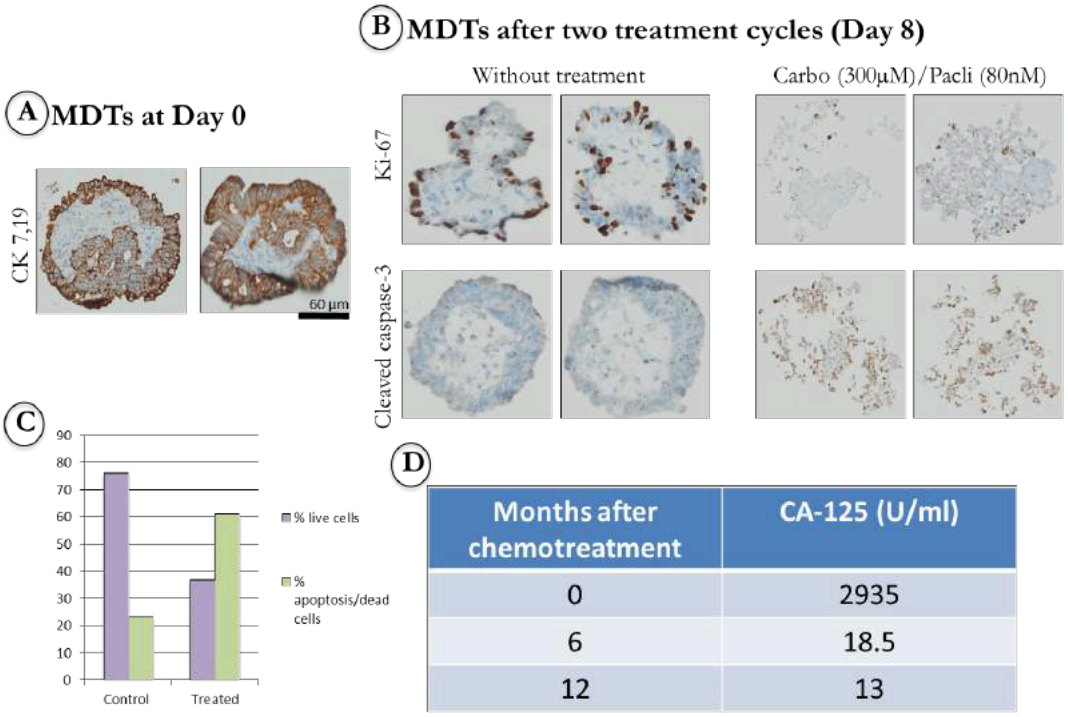

Months after chemotreatment	CA-125 (U/ml)
0	2935
6	18.5
12	13

Figure 13. Chemo-treatment response analysis of a high-grade serous ovarian cancer patient sample. A) MDTs at day of tumor resection (Day 0) stained for epithelial cell markers, cytokeratin 7,19. B) Day 8 MDTs treated with two cycles of a combinatorial chemotherapy treatment of carboplatin (300 µM) and paclitaxel (80 nM). Viability and proliferative analysis through the use of cleaved caspase-3 and Ki-67, respectively. C) Viability assessment of treatment response validated using flow cytometry. Fifteen MDTs were analyzed per condition (control and treated) and stained with Annexin V (detection of apoptotic cells) and DRAQ7 (detection of dead cells) antibodies taking into account a combination of stromal and epithelial survival. D) Patients' clinical outcome. Patient was diagnosed with stage IIB (FIGO) HGSEOC and underwent six cycles of chemotherapy (combination of carboplatin and paclitaxel) and showed complete remission after 12 months of observation based on the CA-125 levels in the blood.

5.3 Unpublished MDT Data

5.3.1 Figures

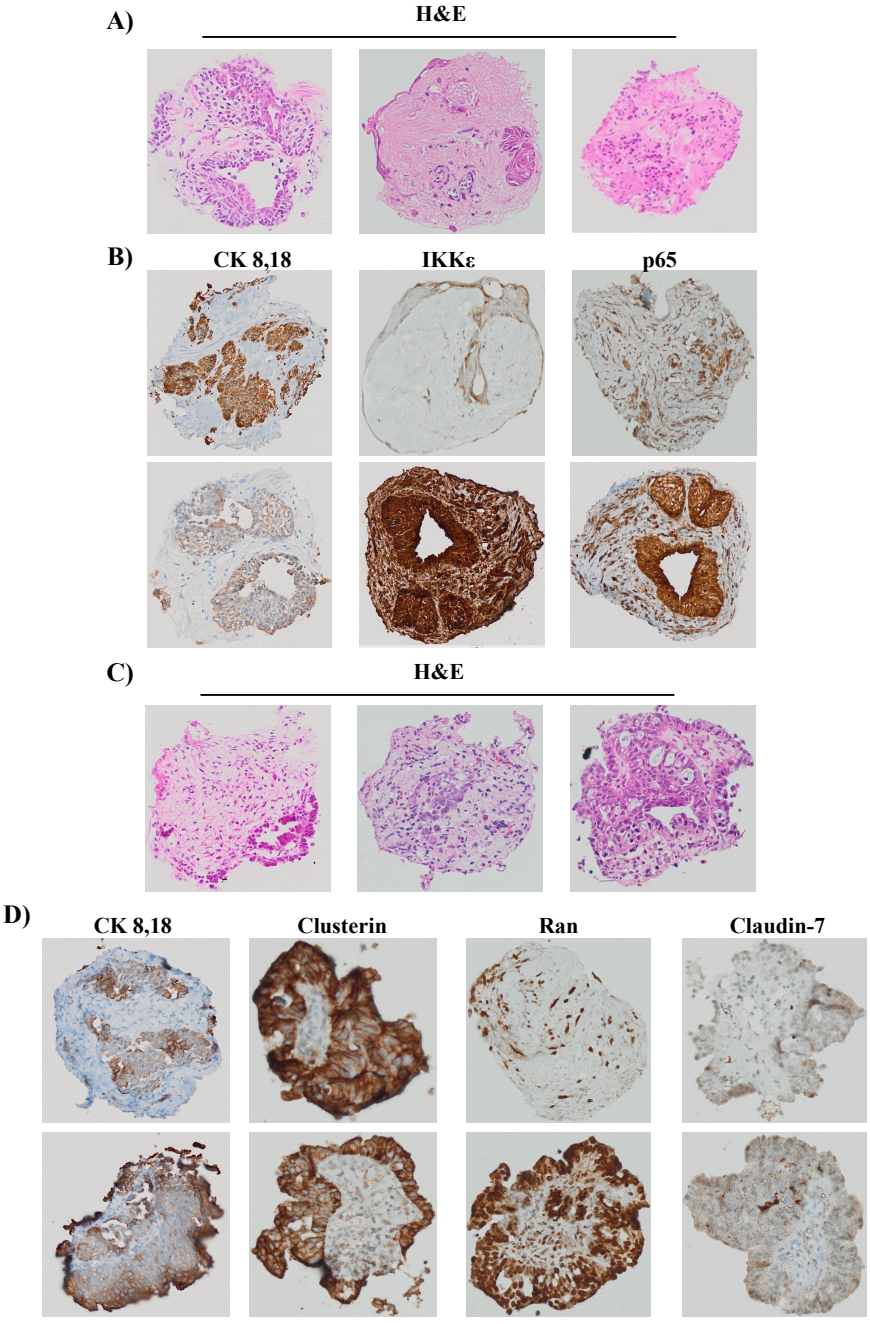

Figure 1. MDTMA procedure on PC and EOC patient samples. A) H&E staining of three PC patient-derived MDTs. B) Immunohistochemical staining for different biomarkers such as epithelial cell identifier, CK8/18; IκB kinase, IKKε; and the p65 subunit of NF-κB. On PC patient-derived MDTs. C) H&E staining of three EOC patient-derived MDTs D) Immunohistochemical staining for biomarkers such as EOC identifier, CK8/18; molecular

chaperone, clusterin; GTPase, Ran; and tight junction membrane protein, claudin-7 on EOC patient-derived MDTs. *Preliminary optimizations of antibody concentration conditions show patient samples maintain cell morphology, generating high quality stained images for analyses.

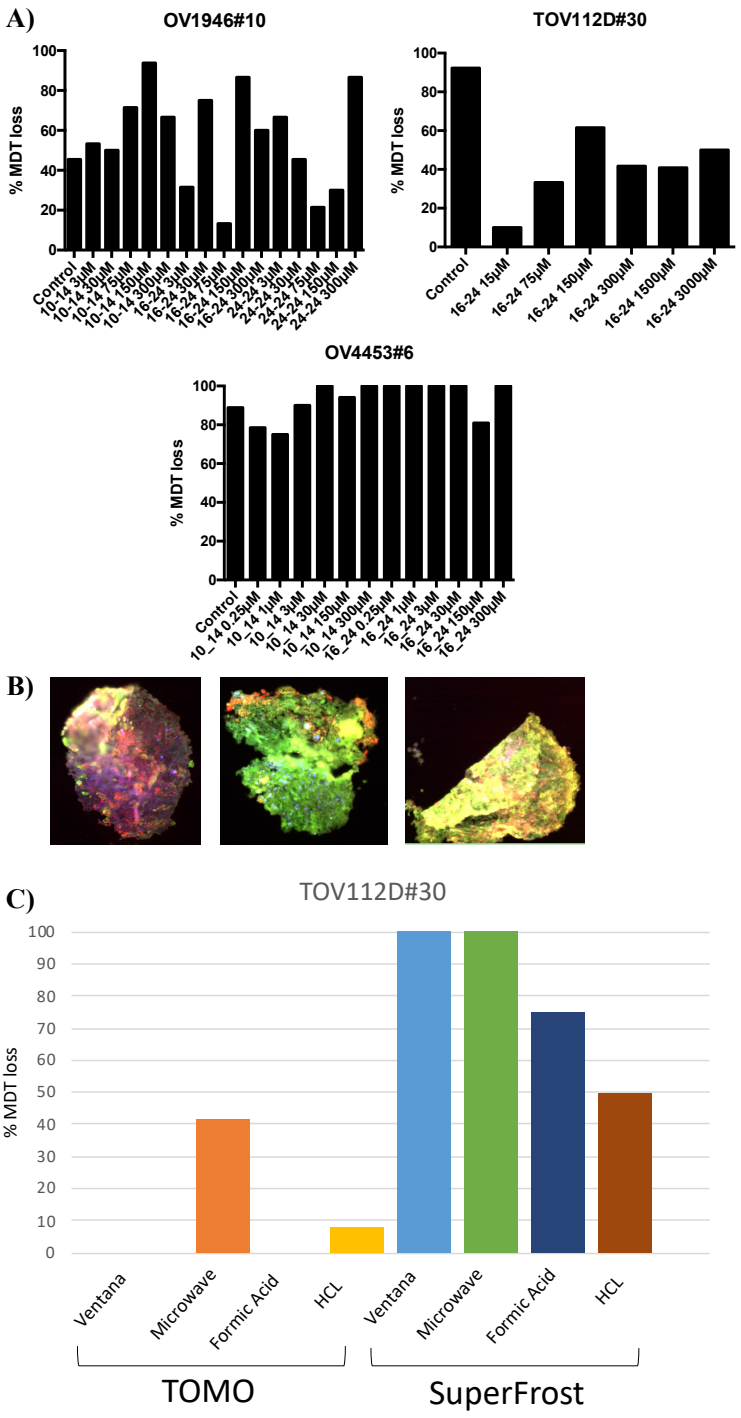

Figure 2. TOMO microscope slides highly retain MDTs during histological staining. A) Bar graph showing percentage of MDT loss after IF staining for three different cell line xenograft derived tumors placed on superfrost microscope slides. B) representative images of MDTs stained on superfrost microscope slides. C) Bar graph comparison percentage of MDTs lost when comparing MDTs placed on TOMO and superfrost slides.

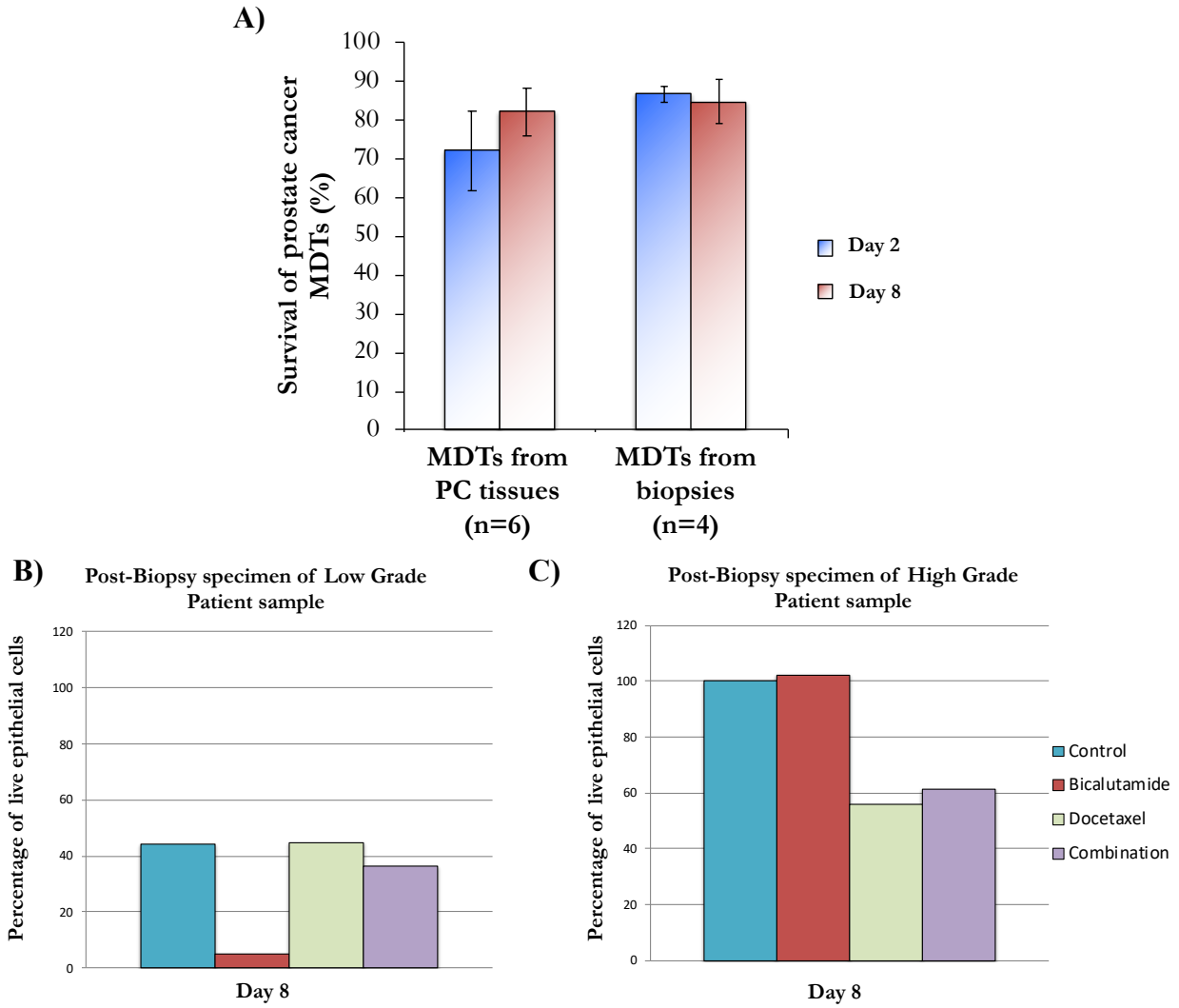

Figure 3. Viability and treatment response analysis of PC tissue and biopsy specimen as MDTs. A) Cell viability of MDTs derived from either PC tissue or biopsy samples after 2 and 8 days of culture in microfluidic device. Flow cytometry analysis of MDTs derived from B) low grade C) high grade PC patient samples in RPMI medium and treated with Bicalutamide (100μM), Docetaxel (10nM) or combination therapy.

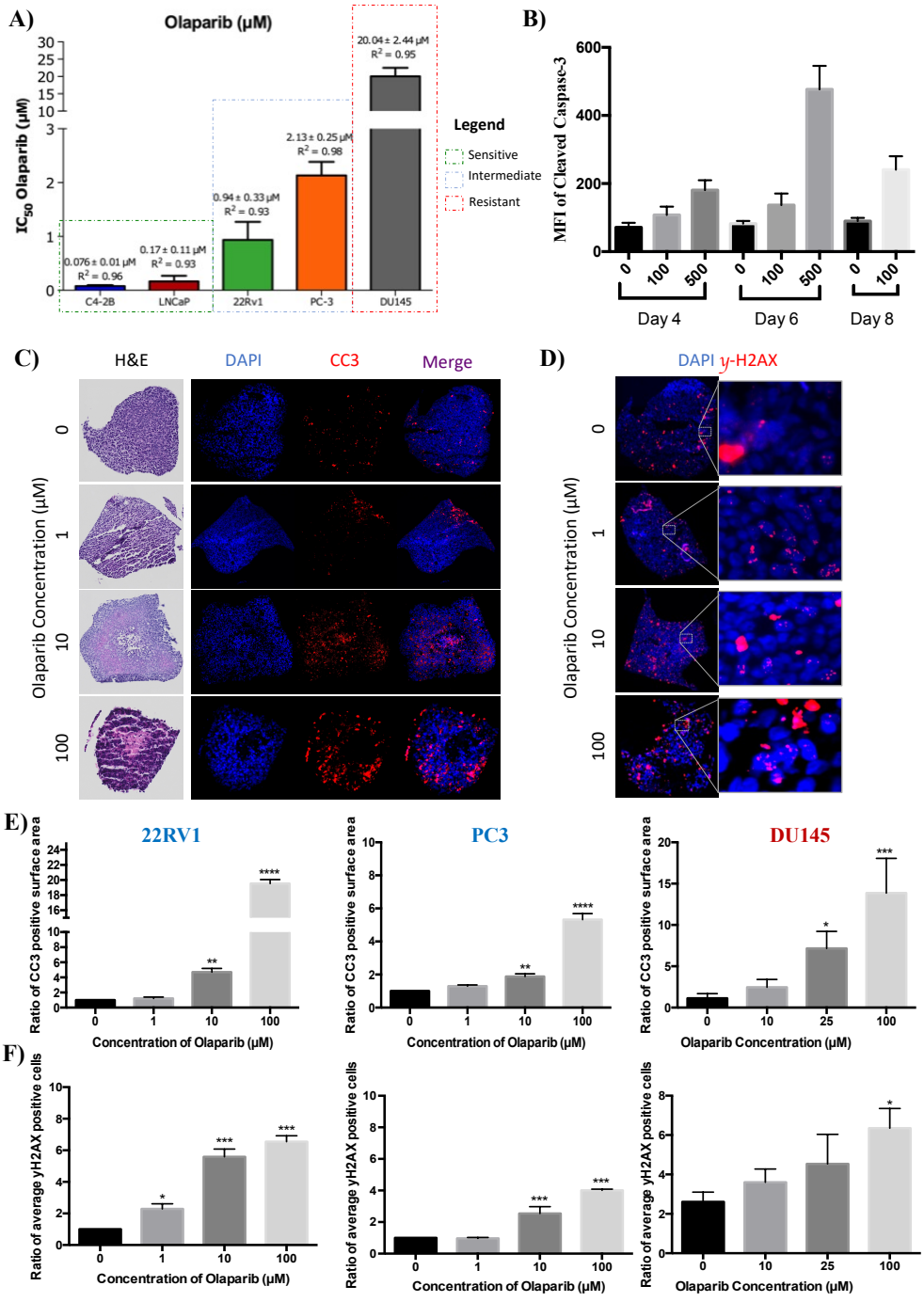

Figure 4. Optimization of Olaparib on PC cell line models. A) Calculation of the 2D response to Olaparib calculating (IC_{50}) in PC cell lines. B) Optimization of treatment response in MDTs derived from PC3 cell-line xenograft tumors using three Olaparib concentrations (0, 100, 500 μM) and three different treatment regimens (4,6, 8 days of induction). Representative images of 22RV1 MDTs stained forr C) cleaved caspase-3 and D) y-H2AX staining at increasing concentrations of Olaparib. Bar graphs of ratio of E) cleaved caspase-3 and F) y-H2AX normalized to control for MDTs derived from 22RV1, PC3 and DU145 cell line xenograft tumors. Error = S.E.M. $p<0.05$ is significant.